Integral-Abutment Bridges: Problems and Innovative Solutions Using EPS Geofoam and Other Geosynthetics

by

John S. Horvath, Ph.D., P.E.
Professor of Civil Engineering

Manhattan College
School of Engineering
Civil Engineering Department
Bronx, New York, U.S.A.

May 2000

Prof. John S. Horvath, Ph.D., P.E.
Manhattan College
Civil Engineering Department
Bronx, New York 10471-4098
U.S.A.

e-mail: <jhorvath@manhattan.edu>

Limitations

   The information contained in this document is the result of original research and is made available solely as a contribution to the general state of civil engineering knowledge. As such, this document does not constitute a design manual or standard, and should not be interpreted, used or referred to as such. The author assumes no liability for the performance of any structure constructed using the methodologies discussed in this document.
   In addition, any reference, either direct or indirect, to a specific geosynthetic material or product is made solely for the purposes of the study documented in this report and does not constitute an endorsement or promotion of that material or product by the author.

Distribution and Use

   Authorization is hereby granted to copy, distribute and print this document without restriction provided that this document is copied, distributed and printed in its entirety, at no cost and used for individual reference purposes only. This document may not be sold or used in whole or in part in any manner for commercial purposes of any type, including manufacturer's product or marketing literature, without prior written consent of the copyright holder.

Printing

   Those wishing to make a paper copy of this document are advised that it is formatted for double-sided printing. A gutter has been provided in the page formatting to allow space for binding along the side if desired. It is suggested that the printer settings in Adobe® Acrobat® be set to "Print as image" for optimum readability.

References

   This report plus several of the author's earlier reports in the Manhattan College Civil Engineering Department geotechnical engineering program (CE/GE) research report series are available in PDF format via the Internet at <web1.manhattan.edu/jhorvath/pubs.html>.

Contents

Section 4 - Conclusions and Recommendations

Section 5 - References

Section 6 - Notation

Section 7 - Bibliography

Appendix A - Reduced Earth Pressure (REP) Wall Analysis: Version 2.0

This page intentionally left blank.

List of Figures

This page intentionally left blank.

List of Tables

This page intentionally left blank.

EXECUTIVE SUMMARY

Background

The most common design concept for a road bridge traditionally consists of some type of superstructure resting on an abutment at each end as shown in Figure ES.1. There may also be one or more intermediate piers but they are incidental to the focus of this report. Because of natural, seasonal variations in air temperature, the bridge superstructure will change in temperature and tend to change dimension in its longitudinal direction as shown in Figure ES.1. However, the supporting abutments are relatively insensitive to air temperature so remain spatially fixed year 'round. To accommodate the seasonal relative movement between superstructure and abutments and prevent temperature-induced stresses from developing within the superstructure, the traditional solution has been to provide expansion joints and bearings at each end of the superstructure as shown in Figure ES.1. These joints and bearings typically must accommodate movements of the order of several tens of millimetres (one inch).

expansion joints

primary direction of
thermally induced movement

superstructure

bearings

abutments
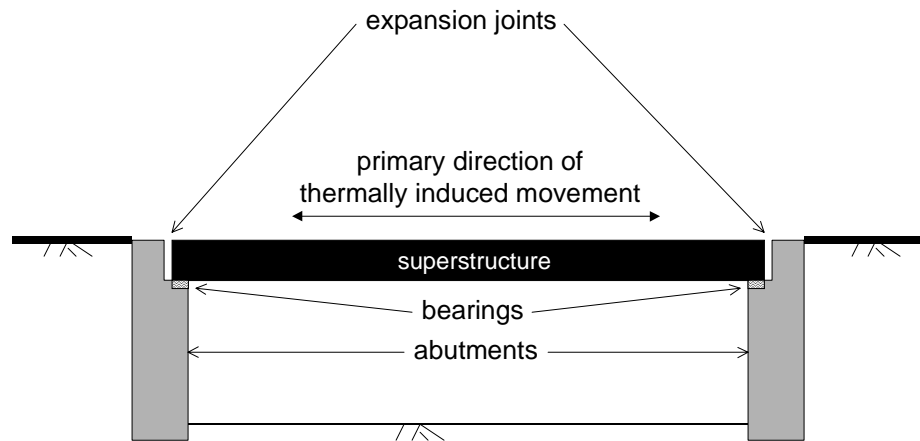
Figure ES.1. Conventional Bridge Design

Although the design shown in Figure ES.1 works well in concept, experience indicates that the expansion joint/bearing detail can be a significant post-construction maintenance item and thus expense during the in-service life of a bridge. Therefore, the concept was developed to physically and structurally connect the superstructure and abutments as shown in Figure ES.2 to create what is referred to as an *integral-abutment bridge* (IAB). In doing so, the troublesome and costly expansion joint/bearing detail is eliminated. IABs have been used for roads since at least the early 1930s in the U.S.A. However, they have seen more extensive use worldwide in recent years because of their economy of construction in a wide range of conditions. Over the years and in different countries IABs have also been called *integral bridges*, *integral bridge abutments*, *jointless bridges*, *rigid-frame bridges* and *U-frame bridges*. There is also a design variant called the *semi-integral-abutment bridge.*

approach slab

(a)

(b)
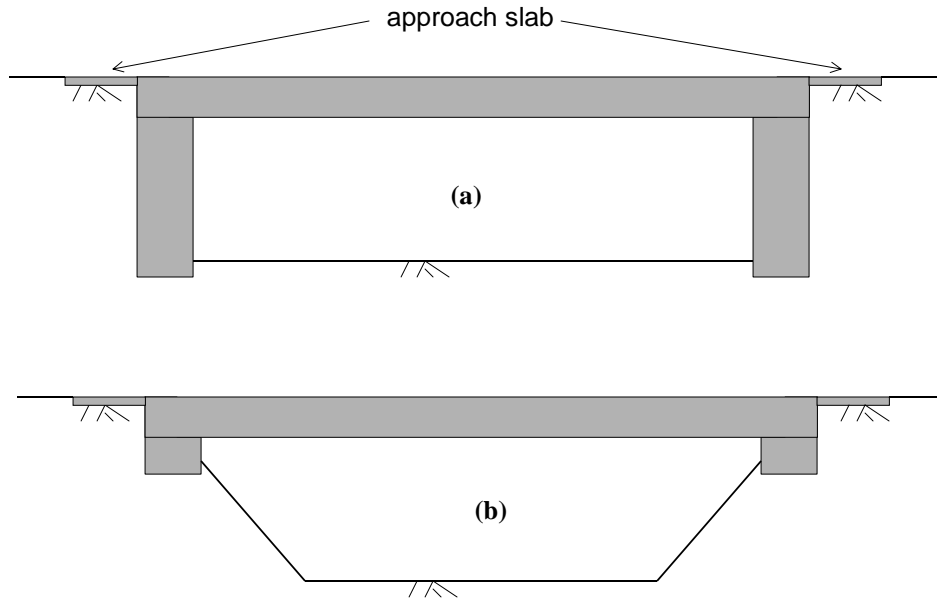
Figure ES.2. Integral-Abutment Bridge Variations

The Problem

Although the IAB concept has proven to be economical in initial construction for a wide range of span lengths as well as technically successful in eliminating expansion joint/bearing problems, it is not problem free overall in service. In retrospect, this is not surprising and perhaps should have been expected. This is because the IAB concept does nothing to fundamentally alter nature and physics and the tendency of a bridge superstructure to undergo seasonal temperature and concomitant length changes. All that has changed are the details of how this movement occurs and the fact that the problems that result from this movement are primarily geotechnical and not structural in nature.

Because of the increased use of IABs, there is now greater awareness of and interest in their post-construction, in-service problems. Fundamentally, these problems are due to a complex soil-structure interaction mechanism involving relative movement between the bridge (more specifically, its abutments) and adjacent retained soil. Because this movement is the result of natural, seasonal thermal variations, it is inherent in all IABs. Although these problems turn out to be primarily geotechnical in their cause, they can result in significant damage to structural components of the bridge. In addition, on the approach to an IAB there can be pavement ride-quality problems for motor vehicles due to development of the "bump at the end of the bridge". Overall, these post-construction problems, and the maintenance and/or remedial costs they generate, inflate the true life-cycle cost of an IAB. In essence, IABs still have maintenance costs as did their jointed predecessors. Only the nature of the maintenance has changed.

The primary cause of post-construction, in-service problems for IABs is shown in Figure ES.3. As the bridge superstructure goes through its seasonal length changes, it causes the structurally connected abutments to move away from the soil they retain in the winter and into the soil during the summer. The mode of abutment movement is primarily rotation about their bottom although there is a component of translation (horizontal displacement) as well. As expected, the total horizontal displacements are greatest at the top of each abutment and can have a maximum magnitude of the order of several tens of millimetres (one inch).
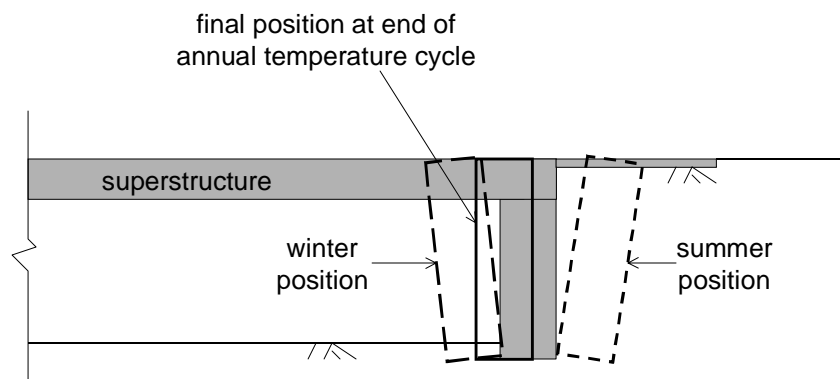
Note: Initial abutment position at start of annual temperature cycle
shown by shaded area.

Figure ES.3. Thermally Induced IAB Abutment Movement

At the end of each annual thermal cycle, there is often a net movement of each abutment away from the retained soil as shown in Figure ES.3. This net movement is exacerbated when the bridge superstructure is composed primarily of portland cement concrete (PCC) because PCC undergoes inherent post-construction shrinkage that causes the bridge superstructure to shorten permanently and pull the abutments away from the retained soil in the process.

There are at least two important consequences of this annual thermal movement cycle of IABs. It appears that the first one was recognized at least as far back as the 1960s and is the large horizontal earth stresses ("lateral earth pressures") that develop between the back of each abutment and retained soil during the annual summer expansion of the superstructure. As each abutment is rotated and translated into the soil mass that it retains these lateral earth pressures can approach the theoretical passive state, especially along the upper portion of the abutment where horizontal displacements are largest. This means that the horizontal resultant earth force on each abutment can be more than an order of magnitude greater than that for which an abutment would typically be designed. This far exceeds any normal structural safety factors and thus can result in a structural failure of an abutment.

Recent (circa 1990s) research has indicated that this seasonal increase in lateral earth pressures may actually be a bigger problem than initially thought. The reason is related to the net movement of the abutments away from the retained soil as shown in Figure ES.3. The explanation of the cause of this net movement (in addition to any post-construction superstructure shrinkage) begins with the fact that a wedge-shaped portion of the retained soil moves toward each abutment during the annual winter contraction of the bridge superstructure and concomitant movement of an abutment away from the soil. When the superstructure expands towards its next summer maximum, this soil wedge does not return to its original position. This is due to the inherent non-linear behavior of soil and can thus occur with any type of soil and no matter how properly it was placed during original construction. In any event, as a result of this soil movement the summer lateral earth pressures tend to increase over time as the soil immediately adjacent to each abutment becomes increasingly wedged in. Because each summer's lateral earth pressures are somewhat greater in magnitude than those from the preceding year it

means that structural failure may take years to develop, a phenomenon that has been observed in practice for other types of earth retaining structures where thermally induced cyclic movements and soil wedging also occurs. Overall, this phenomenon of soil wedging and long-term buildup of lateral earth pressures is referred to as *ratcheting*. Given the relatively long (100-plus years) design lives of IABs, ratcheting behavior represents a potentially serious long-term source of IAB problems, primarily structural failure of the abutments.

The second important consequence of the annual thermal cycle movement of IABs is also related to the net inward movement of the abutments and has become fully appreciated only recently circa the 1990s. This is the development of a settlement trough adjacent to each abutment as shown in Figure ES.4. This settlement trough is the result of the above-described soil wedge slumping downward and toward the back of each abutment. The consequences of this settlement depend on whether or not an approach slab was constructed as part of the bridge. If there is no slab, there will be a difference in road surface elevation occurring over a short distance creating the classical "bump-at-the-end-of-the-bridge" condition. If there is a slab, initially it will span over the void created underneath it by the settled soil. However, with time and traffic the slab will likely fail in flexure. The development of a settlement trough behind IAB abutments has received much more interest than the lateral earth pressure problem in recent years, apparently because settlement tends to develop and become problematic relatively soon (a few years at most) after an IAB is placed into service whereas the ratcheting buildup of lateral earth pressures might not create problems for decades. Note that even a very small magnitude of settlement beneath an approach slab will cause a void and result in the slab's losing contact with the underlying ground.
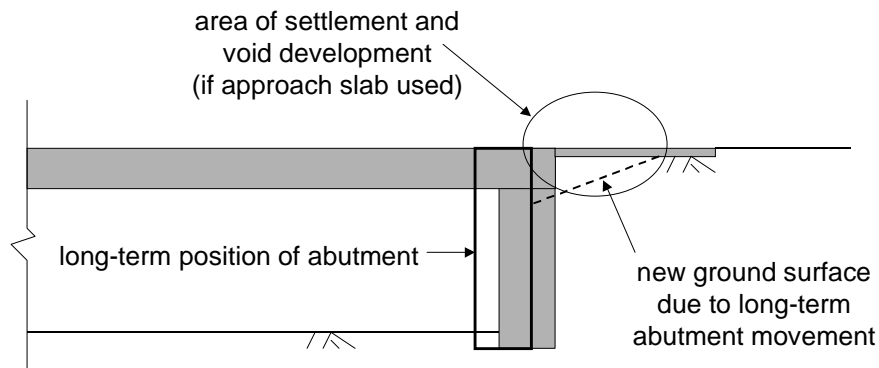
Figure ES.4. Settlement Trough and Void Development behind IAB Abutments

Proposed Solutions

Because of the current extensive use of IABs, there is a critical need to develop improved designs to correct the behavioral deficiencies inherent in all IABs as they are designed currently. The study documented in this report used a conceptual framework for developing improved IAB designs that was based on a fundamental understanding of knowledge gained from both

conventional bridges as well as observed problems with IABs. The key concepts and considerations used in developing the solutions presented in this report are as follows:

- A bridge should be allowed to move freely with seasonal temperature variations to prevent the development of thermally induced forces within its components. With IABs, this means that both the superstructure and abutment should be allowed to move.

- The retained soil adjacent to a bridge abutment is not directly affected by seasonal temperature variations. Therefore, it can and should remain spatially and temporally fixed to prevent pavement settlement on the approach embankment or void formation under approach slabs. With conventional bridges, the necessary soil fixity is provided by the abutments. With IABs, the necessary fixity must be developed from within the retained soil itself as the abutments move seasonally and no longer provide this function. Because soil with a vertical slope is not inherently self stable, this suggests that geosynthetics could be useful.

- Relative movement between a bridge and adjacent ground should be accommodated in an orderly predictable manner. With conventional bridges, this is provided by expansion joints and bearings. With IABs, no such detail exists with current designs so a new type of expansion joint should be developed. Leaving a void between IAB abutments and the retained soil as a de facto expansion joint is not considered an acceptable option. Experience indicates that a void is difficult to construct routinely and reliably, and cannot be depended on to remain for the life of the bridge.

- The seasonal increase in lateral earth pressures on IAB abutments and the related tendency for permanent long-term increases due to ratcheting behavior should be addressed. Although this could be handled structurally by designing more-robust abutments this may not be the most economical solution. Other, more-innovative solutions may exist. Again, leaving a void between IAB abutments and retained soil is not considered an acceptable option.

This report presents the results of a preliminary study conducted to investigate potential design alternatives that have as their primary component expanded polystyrene (EPS) geofoam. The use of other types of geosynthetics, principally geogrids and geotextiles as tensile reinforcement, in synergistic combination with EPS geofoam was also investigated. Although revised design strategies that make use of geosynthetics will increase the construction cost of an IAB, the anticipated superior post-construction, in-service performance of such IABs should more than make up for the increase by reducing future maintenance and repair costs.

This report has identified two different designs that each appear to address all the issues enumerated above. They are shown schematically in Figure ES.5. The one likely to be more cost effective in most applications is shown in Figure ES.5(a). It utilizes tensile reinforcement (likely geogrid or geotextile) to create a *mechanically stabilized earth* (MSE) mass within the retained soil adjacent to each abutment. This will provide a soil mass that is inherently self-stable for the design life of the bridge. In addition, a resilient-EPS geofoam compressible inclusion would be used between the abutment and MSE mass. This inclusion is designed to be highly compressible and thus functions as the desired expansion joint between IAB and retained soil. It will also thermally insulate the retained soil and can be designed to serve as the always necessary drainage layer. This inclusion simultaneously allows the reinforcement within the soil to function as well as the abutments to move seasonally. Summer increases in lateral earth pressures would be reduced to relatively small magnitudes. Overall, lateral earth pressures acting on the abutments

would be significantly reduced from current design levels which would achieve a cost savings in the structural design of the abutment.
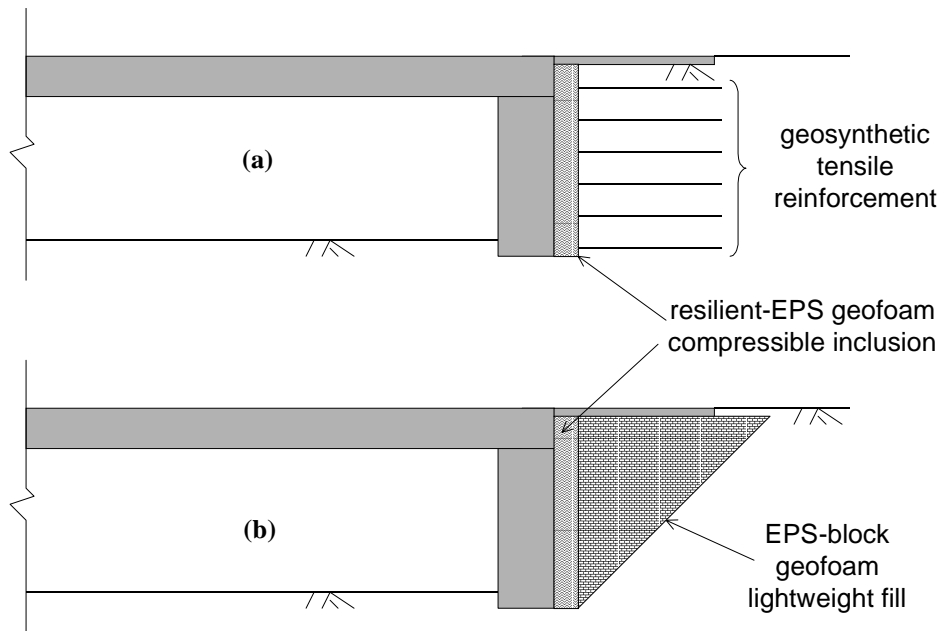
Figure ES.5. Proposed New IAB Design Alternatives

The other design alternative is shown in Figure ES.5(b). A self-stable wedge of EPS-block geofoam is used in lieu of the reinforced soil of the first alternative. A layer of highly compressible resilient-EPS geofoam is again used to function as an expansion joint. This alternative is expected to be the one of choice for sites where the underlying soils are soft and compressible. The extraordinarily low density of the EPS-block geofoam (approximately 1% of that of soil) would function as a lightweight fill to minimize settlements and enhance stability of the ground adjacent to the bridge as well as greatly reduce the loads acting on the abutment and the deep foundations that would likely be supporting it in such soil conditions.

The Future

The numerical analyses documented in this report indicate that the proposed design alternatives shown in Figure ES.5 will achieve the desired goals. Both alternatives utilize proven geosynthetic products. In addition, the principal components of both alternatives (MSE and EPS-block geofoam lightweight fill behind bridge abutments) have already seen successful use on several projects involving conventional bridges. In addition, EPS-block geofoam is known to have been used as lightweight fill on at least one IAB project. Thus the only novel or unverified aspects of the proposed new designs are the particular combinations of geosynthetic products shown in Figure ES.5. Therefore, the probability is high that the design alternatives shown in Figure ES.5 will in fact provide the desired solutions to problems experienced with current IAB designs. Consequently, future research should focus on both instrumented applications of actual IABs as well as further research to develop relatively simple analysis and design algorithms for use in routine practice. Fundamental research into the behavior of the proposed design alternatives under seismic loading and with fine-grain soils is also required.

Section 1
Background and Overview of Study

1.1 INTRODUCTION

This report documents a research study performed by Prof. John S. Horvath, Ph.D., P.E. of the Manhattan College Civil Engineering Department. Background information concerning the genesis and scope of this study is presented in this section of the report.

1.2 BACKGROUND

1.2.1 Soil-Structure Interaction

1.2.1.1 Definition. An important category of civil engineering problems that straddles the boundary between the specialties of geotechnical and structural engineering is the *soil-structure interaction* (SSI) problem. SSI problems involve situations where a sufficiently accurate analysis of the forces within and displacements of some structure (building, bridge, etc.) must explicitly model the structure and adjacent ground acting together. Thus neither the structural nor geotechnical component of the problem can be satisfactorily analyzed as if the other were not present. This generally requires a single, combined analysis of both the structural and geotechnical components of the problem although it is sometimes feasible to iteratively perform separate analyses of the structural and geotechnical components (Ulrich 1991). Note that SSI problems are distinct from problems where the behavior of the structure and ground can be analyzed, with sufficient accuracy for routine practice, as being independent of one another.

It is worth noting that some civil engineers restrict the use of the term soil-structure interaction to problems involving seismic loading. In the author's opinion, this narrower definition is needlessly restrictive. The broader definition described above is adopted in this report.

1.2.1.2 Application to Bridges. Bridges are a type of structure for which SSI can often be an important analysis or design consideration. There are several different SSI mechanisms that affect bridges. They are discussed in more detail in Section 2 of this report. Depending on the specific project (type and span length of bridge, geologic conditions, geographic location), any one these mechanisms can have a significant effect on the analysis or design of a bridge.

1.2.2 Integral-Abutment Bridges

A type of bridge that is used extensively in road applications in particular is the *integral-abutment bridge* (IAB). Depending on geographic location and time period, other terms such as *integral bridge*, *integral bridge abutments*, *jointless bridge*, *rigid-frame bridge* or *U-frame bridge* have been or are used to refer to this type of structure. Although IABs have apparently been used since at least the early 1930s in the U.S.A. (Card and Carder 1993), the 1990s saw growing interest and use of this type of bridge worldwide.

The design details of IABs that are relevant to this study are discussed in Section 2 of this report. Also discussed in Section 2 is the fact that IABs involve a unique SSI issue that is not encountered with other types of bridges. This SSI issue has resulted in significant post-

construction, in-service problems with the performance of IABs that was the motivating factor for the study covered by this report.

1.2.3 Geofoam

On a separate but parallel track, the use of *geofoam* also saw a dramatic increase during the 1990s although geofoam usage actually dates back at least to the early 1960s (Horvath 1995b). For those unfamiliar with the term or its correct definition, geofoam is the generic term applied to any closed-cell foam material or product used in a geotechnical application. Geofoam is now recognized worldwide as a category or type of geosynthetic product in the same way as the more conventional, planar types of geosynthetics (geogrids, geomembranes, geotextiles, etc.).

The greater awareness and use of geofoams throughout the 1990s has been accompanied by significant research into new and varied applications. This is especially true for expanded polystyrene (EPS), a polymeric (plastic) foam which is the most commonly used geofoam material worldwide. One reason why EPS geofoam is the material of choice for recent geofoam research is that there is no other proven geofoam material that can match the cost effectiveness and range in geotechnically relevant properties of EPS. Therefore, EPS geofoam offers great diversity in the ways that it can function in the ground (Horvath 1995b).

This report presumes a basic working knowledge of both EPS geofoam as well as other types of geosynthetics (primarily geogrids and geotextiles) used for tensile reinforcement. For those unfamiliar with either geofoam geosynthetic or reinforcement geosynthetics, the necessary background information can be found in Horvath (1995b) for geofoam and Koerner (1998) for all other types of geosynthetics.

1.3 PRESENT STUDY

1.3.1 Purpose and Objectives

As noted in Section 1.2.2, the use of IABs has not been without significant post-construction in-service problems. This implies that there is an inherent defect in current IAB designs that requires correction. As a result, much of the geotechnical research interest in IABs throughout the 1990s has focused on developing preventive or remedial design strategies.

This same time period also saw significant research into numerous aspects of EPS geofoam to extend its traditional geosynthetic functions and applications. Therefore, it occurred to the author that a useful research project would be to combine these two areas of research to see if EPS geofoam could be useful in overcoming some of the problems experienced with IABs. Although the possible use of geofoams in general to eliminate or at least reduce problems with IABs has been noted previously both by the author and others (Briaud et al. 1997; Carder and Card 1997; Horvath 1995b, 1996, 1998a), there is no published study known to the author that focuses on the use of geofoam in this application and, more specifically, the different functional ways in which geofoam, specifically EPS geofoam, can potentially act beneficially. Therefore, it was felt that such a study would be a useful contribution to the state of knowledge.

This study was conducted by the author as the principal and sole investigator. There was no external financial support for this study so the scope was determined solely by the author based on an independent and objective assessment of IAB problems and the feasibility of potential solutions involving geosynthetics. In addition, there was no support or resources of any kind provided for any part of this study by Manhattan College. This report was issued under the auspices of Manhattan College solely as a venue for publication. All resources necessary to produce this report were provided by Horvath Engineering, P.C. of Scarsdale, New York, U.S.A.

1.3.2 Scope

Because of the restrictions imposed by available resources, this study was limited to a numerical and theoretical investigation of one relatively simple, hypothetical problem that included what were felt to be key components of a typical IAB with respect to the objectives of this study. Therefore, this study was not intended to provide final answers and comprehensive design guidelines for all IABs. However, it was felt that the results of this study would provide useful preliminary conclusions and guidance for interim use in practice as an improvement over the status quo. It was also believed that this study would serve as a logical precursor for more-detailed research that would include physical modeling using large-scale 1-g models and/or a geotechnical centrifuge as well as instrumented observations of actual IABs. Thus it is hoped that the results of this study will serve as both a catalyst and resource for improving the current state of practice as well as future research.

1.3.3 Organization of Report

This report contains all published results of the study outlined in Section 1.3.2. In addition to this introductory section, this report is organized as follows:

- Section 2 describes the phenomena and mechanisms of SSI problems for IABs.

- Section 3 presents and discusses the results of all analyses performed for the present study.

- Section 4 presents the conclusions drawn from the results of this study as well as recommendations for future study.

- Section 5 contains a list of all references cited in this report.

- Section 6 contains a definition list of all notation used in this report.

- Section 7 contains a limited, selective bibliography of publications related to IABs as well as several other areas of lateral earth pressure theory and application that the author has found of particular relevance or interest. The intention of this bibliography is to serve as a resource for future research by others.

- Appendix A contains the theoretical derivation of an improved analytical method for what the author terms the Reduced Earth Pressure (REP) Wall concept. The REP-Wall concept is related to certain behavioral aspects of IABs.

This page intentionally left blank.

Section 2
Soil-Structure Interaction and Bridges

2.1 OVERVIEW

As noted in Section 1.2.1.2, the analysis and design of bridges often involves consideration of one or more categories of SSI involving the bridge superstructure, the superstructure support elements (abutments and intermediate piers, if any, and their foundations) and the ground supporting the foundations of the abutments and piers. The SSI categories most commonly encountered and considered in bridge-engineering practice are:

- total and differential settlement of the abutments and piers under gravity and live loads, and the effect that differential settlements in particular have on the performance (both the *Serviceability Limit State* (SLS) and *Ultimate Limit State* (ULS))[1] of the bridge superstructure; and

- total and relative displacements of, as well as forces in, the various bridge components under seismic loading, usually as they relate to the ULS.

Note that wind-induced displacements of and forces within a bridge superstructure, which can be of significant importance, are usually not an SSI problem as the ground typically has relatively less influence over how a bridge superstructure behaves under wind loading.

An additional SSI category, and the one of primary interest in this study, is thermal loading. Simply stated, the issue here is that a bridge superstructure is exposed to annual, seasonal variations in air temperature that can be of the order of 50°C (90°F) or more in temperate climates. The temperature of the structural elements that comprise the bridge superstructure will, more or less, reflect this variation. As a result, the bridge superstructure will, in the theoretical limiting cases, either:

- freely expand and contract longitudinally to the maximum extent theoretically possible (if unconstrained against movement) or

- develop the maximum theoretically possible thermally induced compression and tension stresses within its members (if fully constrained against movement).

There can also be intermediate conditions of constraint in which the bridge superstructure will experience some combination of thermally induced displacement and internal stresses.

On the other hand, although the ground that supports the bridge will see some near-surface seasonal temperature variation most soils and rocks do not change volume with temperature, at least for the temperature ranges of interest with regard to bridges[2]. This means that, for all

---

[1] For those unfamiliar with the limit states (failure) concepts of SLS and ULS for structures, SLS involves issues that relate to the serviceability (intended use and maintenance) of the structure while ULS refers to a physical collapse of all or part of the structure.
[2] This statement relates only to behavior of the dry soil-particle skeleton. Not considered here are phenomena such as frost heave, thaw settlement or swelling/shrinking which involve interaction between the soil skeleton and ground water within the voids of the soil skeleton.

practical purposes, the ground and the support it provides to the bridge foundations (abutments and intermediate piers if any) is spatially and temporally fixed with respect to any changes in temperature that occur to the ground.

This relatively dissimilar behavior under temperature changes between the thermally active bridge superstructure and thermally inactive ground is what creates a SSI problem for bridges. The conflict is that the bridge superstructure wants to deform with temperature; the ground does not; yet the two are linked together through the foundations so the bridge and ground must react as one in some fashion. Thus the SSI challenge here is to find a way to accommodate the tendency of a bridge superstructure to move with temperature changes yet still provide a sufficiently smooth transition to the adjacent ground which is relatively temperature stable. This SSI challenge as it applies to IABs was the focus of the study covered by this report.

2.2 DESIGN FOR TEMPERATURE-INDUCED SOIL-STRUCTURE INTERACTION

2.2.1 Conventional Bridges

2.2.1.1 Concept and Details. The traditional design concept used to address the temperature-related SSI problem discussed in Section 2.1 is shown schematically in Figure 2.1 for the basic case of a single-span bridge. Note that the details of the bridge superstructure are incidental to the discussion here.

expansion joints

primary direction of
thermally induced displacement

superstructure

bearings

abutments
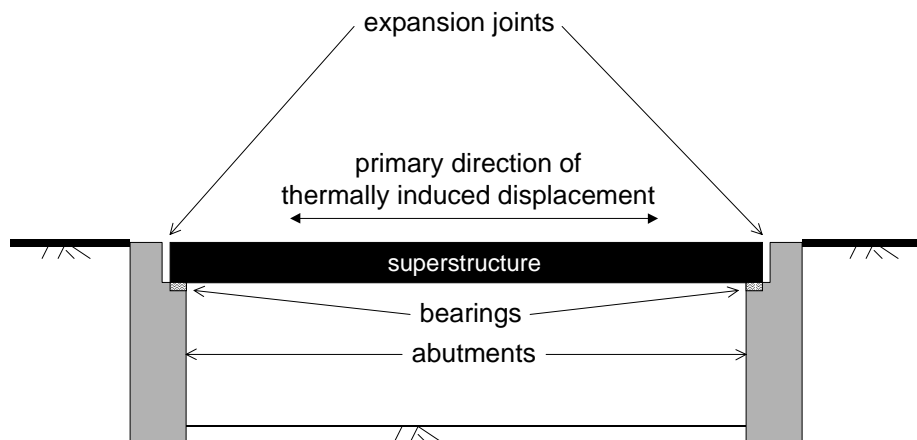
**Figure 2.1. Traditional Design Concept to Allow
Thermally Induced Bridge-Superstructure Movement**

The overall design philosophy on which this design concept is based is to make the bridge superstructure as unconstrained as practicable to minimize thermally induced loads from developing within the superstructure. However, the bridge abutments are spatially and temporally fixed, at least as far as thermal issues are concerned. This means that longitudinal displacement of the superstructure (i.e. in the direction indicated in the figure) between the fixed abutments must be accommodated. This is done by creating a physical gap, called an *expansion joint*, that is placed between each end of the superstructure and its adjacent abutment as shown in Figure 2.1. Each abutment is then designed as a more or less conventional rigid retaining wall of either the

gravity or cantilever type (modern alternatives using geosynthetics can also be used) to retain the soil behind the abutment.

With regard to the horizontal soil stresses (referred to colloquially as *lateral earth pressures*) for which the abutments are designed, although the active earth pressure state within the retained soil is often assumed the author's opinion is that the normally consolidated at-rest state is more appropriate because structural and geometric restraints imposed on abutments generally prevent their movement. An allowance for additional compaction-induced lateral earth pressures should always be made (Duncan et al. 1991) although this is not always done in practice.

To allow the bridge superstructure to move as freely as possible with respect to its abutments, structural *bearings* are placed between the superstructure and abutments as shown in Figure 2.1. The bearings typically rest on a ledge (*bridge seat*) that is formed into the top of the abutment as shown schematically in Figure 2.1. Traditionally, these bearings were constructed entirely of metal. Later designs utilized other materials as well to make the bearing as close to frictionless as any real material can be.

For the case of a bridge with multiple spans, there are typically additional intermediate expansion joints placed between each adjacent pair of spans with bearings placed on the top of each intermediate pier and supporting each span as shown in Figure 2.2.
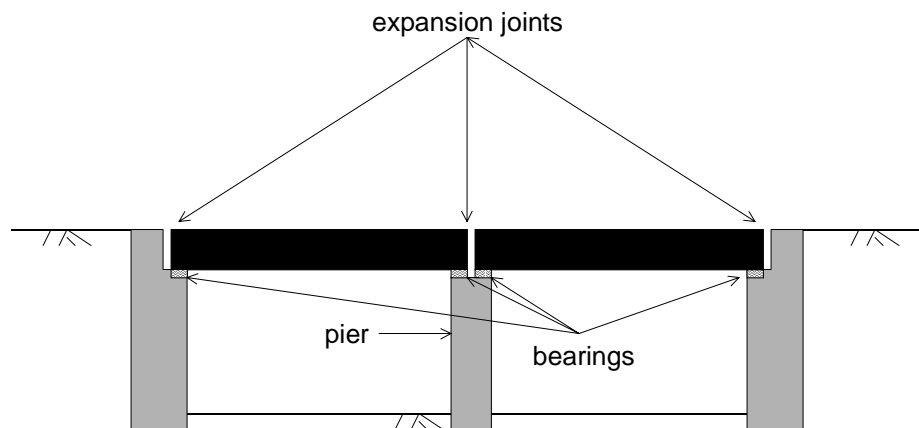
Figure 2.2. Traditional Design Concept as Applied to Multi-Span Bridges

The expansion joints and bearings must accommodate all anticipated longitudinal displacement of the superstructure during the design life of the bridge which is often 100 years or more. To understand the magnitude of this movement, it is useful to state here the basic solid mechanics equation (Timoshenko and Gere 1972) defining the idealized limiting case of unconstrained movement of a solid structural element (called the *free-bar solution*) under thermal loading:

$$\Delta L = L_o \cdot \alpha \cdot \Delta T \tag{2.1}$$

where:

L_o = original length of the structural element,

α = coefficient of thermal expansion of the material comprising the structural element,

ΔL = change in length of the structural element and

ΔT = change in temperature of the structural element.

As information, the other limiting case is that of full constraint and no movement, and is called the *fixed-bar solution*. The governing equation is (Timoshenko and Gere 1972):

$$P_s = A_s \cdot E_s \cdot \alpha \cdot \Delta T \tag{2.2}$$

where:

A_s = cross-sectional area of the structural element,

E_s = Young's modulus of the material comprising the structural element,

P_s = temperature-induced force in the structural element and

the other parameters are as defined previously for Equation 2.1.

From a practical perspective with respect to bridges in general, the only real variables in Equation 2.1 are the bridge span length, L_o, and annual range in air temperature[3], ΔT, at the site of the bridge[4] as the coefficients of thermal expansion for the most common bridge materials (steel and portland-cement concrete (PCC)) are of the same order of magnitude (Timoshenko and Gere 1972).

To provide orders of magnitude for typical superstructure movements to aid in visualizing the issue at hand, a relatively short-span bridge (say 30 metres (100 feet) long) in a temperate climate might have an annual (summer to winter or vice versa) superstructure length change of several tens of millimetres (one inch). On the other hand, a long-span suspension or cable-stayed bridge in the same climate might have a range in superstructure length change of the order of several hundred millimetres (one foot).

In view of the relatively large range in movements that must be accommodated with different bridges, the detail for how the expansion joint gap is actually created is handled in different ways. For relatively short-span bridges, the presumption is that a vehicle tire can cross the relatively small gap of perhaps a few tens of millimetres (one inch) maximum without creating excessive discomfort to the occupants of the vehicle. Therefore, the edge of the abutment or superstructure road surface on either side of the gap typically has a hard, smooth, straight corner created by a special product developed for this purpose (traditionally metal but nowadays possibly some type of hard plastic or rubber). In some cases, there may be a relatively compressible, elastic joint filler used as part of the overall expansion joint detail. On the other hand, the joints for long spans typically have an interlocking-steel-finger geometry to provide a reasonably continuous and smooth traveling surface for vehicles yet accommodate the relatively large superstructure movements typical of such structures.

2.2.1.2 Problems. The traditional expansion joint/bearing system has been found to perform more or less as intended conceptually but at the cost of being a high maintenance item, especially for relatively short-span bridges. The primary problem is the corrosion and other physical

---

[3] It is assumed here for simplicity that the average temperature of the bridge superstructure is the same as the air temperature which is not necessarily the case.

[4] Note that there is no one value for ΔT even at a given geographic location because different return periods (e.g. 10 year, 50 year, 100 year, etc.) of measured air temperatures could be chosen for design.

deterioration of the bridge bearings that occurs with time[5]. Corrosion is exacerbated in areas with seasonal below-freezing air temperatures where salts of various composition are placed on the road surface for pavement deicing purposes. These salts can be washed down onto the bearings where they accelerate corrosion and deterioration of the bearings. Thus bridge bearings, especially in some climates, require relatively expensive periodic maintenance, repair or even replacement to maintain their function.

The structural materials used to create the expansion joint itself also suffer physical deterioration and require periodic maintenance, repair or replacement due to the repetitive impact by vehicle tires. There can also be deterioration of any material used as a joint filler. In addition, there is the issue of how to accommodate subsequent pavement overlays on either side of the expansion joint. Obviously the joint itself should not be paved over but adhering to this rule will result in a local depression in the pavement surface at the expansion joint which remains at his original elevation.

2.2.2 The Integral-Abutment Bridge Alternative and Related Concepts

2.2.2.1 Introduction. The maintenance problems and costs associated with conventional jointed bridges, especially for relatively short spans, has created an opportunity to develop more-economical alternative designs for this application. It is beyond the scope of this study to discuss all the alternatives that have been or might be considered, both actual and theoretical. This study focuses only on IABs for the reasons discussed in Section 1.

2.2.2.2 Concept. Because the expansion joint/bearing detail is the primary point of weakness with conventional short-span bridge designs, it is no surprise that the basic element of IABs is to eliminate this detail entirely. This is done by creating a physical and structural connection between the bridge superstructure and abutments as shown schematically in Figure 2.3(a). The details of the structural connection between superstructure and abutments vary depending on the structural materials (steel or reinforced PCC) used as well as preferences or policy of the designer or owning agency. In addition, the abutments may be supported on shallow foundations (spread footings) or deep foundations (driven piles or drilled shafts) depending on technical need. However, these details are not important for the purposes of this study and it is sufficient to visualize an IAB simply as a rigid-frame structure that, from a behavioral and analytical perspective, acts as a single structural element.

A reinforced PCC slab, generally called an *approach slab*, that is structurally connected to the bridge appears to be used quite often with IABs. This detail is also shown schematically in Figure 2.3(a). The function of the approach slab is to provide a smooth transition between the IAB and adjacent approach embankment. Various approach-slab designs are discussed in detail by Briaud et al. (1997).

Not considered in this study but noted here for the sake of completeness is a variation of the IAB concept that the author refers to as a *semi-integral-abutment bridge* (SIAB). Such a structure is shown schematically in Figure 2.4. In an SIAB, only the expansion joint is eliminated by extending the bridge superstructure over the top of the abutment. The bearing between deck and abutment is still present. Bearing maintenance is presumably reduced with this type of design because surface water no longer has direct access to the bearing.

---

[5] Bearing corrosion is often referred to as *freezing* which, in this context, has nothing to do directly with the physical phenomenon of the liquid-to-solid phase change of water. Rather, in this context freezing means that the bearing components corrode and cease to move, and thus the bearing ceases to perform its intended function of allowing relatively unrestrained displacement of the bridge superstructure.

approach slab

(a)

(b)
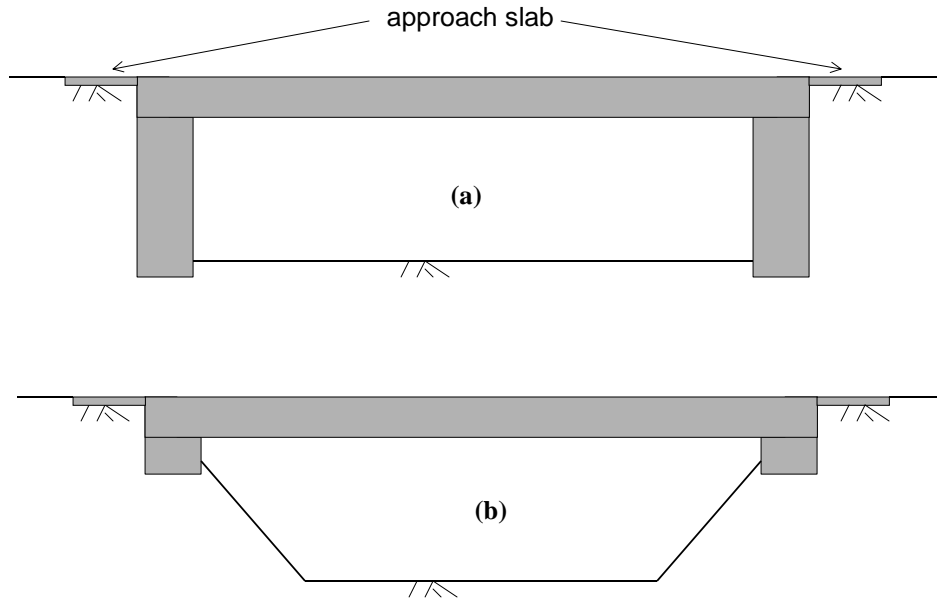
Figure 2.3. Integral-Abutment Bridge Variations

superstructure

bearings
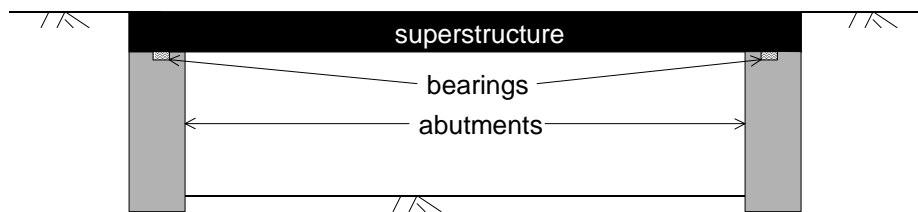
abutments

Figure 2.4. Semi-Integral-Abutment Bridge

   2.2.2.3 Problems. In retrospect, it is no surprise that post-construction, in-service problems
(there are two major ones but they are related) have been experienced with IABs. The reason is
that the fundamental phenomenon of a bridge superstructure that is thermally active and in
contact with the thermally inactive ground still exists. The use of an IAB does not and cannot
change nature nor alter the basic laws of physics. Rather, the use of IABs simply shifts the
location of where the bridge-ground interaction takes place and, as a result, shifts the locations,

symptoms and underlying causes of the problems that develop. What is most noteworthy to recognize is that the root cause of problems has shifted from being primarily structural to geotechnical in nature. This is important to appreciate as it suggests that an efficient solutions to the problems should likewise be primarily geotechnical and not structural.

Of the two major problems observed with IABs, the one noted and discussed earlier in the literature (e.g. Broms and Ingleson 1971, Card and Carder 1993, Sandford and Elgaaly 1993) is the development of lateral earth pressures against the abutments that go above the at-rest state and approach, or even reach, the passive state (at least along the upper portion of the abutments). Such conditions occur each summer when expansion of the bridge superstructure reaches a maximum. Referring to Figure 2.5, as the bridge superstructure expands during the summer it causes each abutment to rotate about its bottom as well as translate (displace horizontally) into the retained soil. The magnitude of displacement relative to the original (shaded) position of the abutment is exaggerated in this figure for clarity and is typically of the order of tens of millimetres (one inch) at the top of each abutment. It is well known that displacements of this magnitude will develop lateral earth pressures that tend toward the passive state (Clough and Duncan 1991). The problem with passive earth pressures is that they are relatively very large in magnitude, typically at least an order of magnitude larger than the normally consolidated at-rest state for which an abutment should normally be designed.
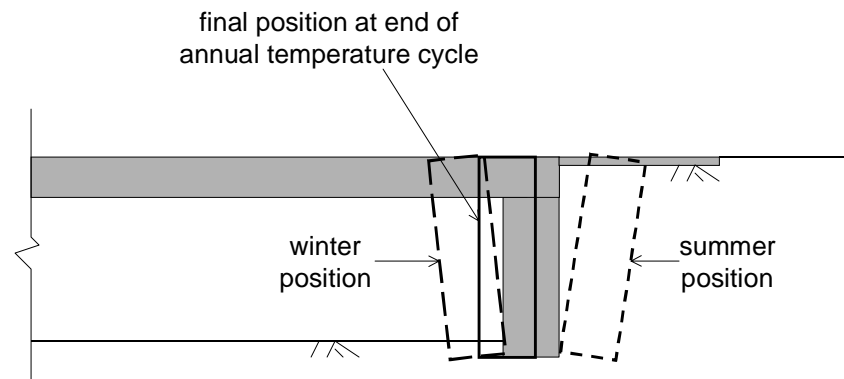
Note: Initial abutment position at start of annual temperature cycle shown by shaded area.

Figure 2.5. Thermally Induced IAB Abutment Movement

As a consequence of these large summer lateral earth pressures:

- structural damage to the abutment will likely occur if it has not been designed properly for the larger pressures or

- the cost of the abutment will increase significantly if it is designed properly to accommodate the larger pressures.

As a corollary to this seasonal summer increase in lateral earth pressures acting on the abutments, there will be a concomitant winter decrease as the contracting superstructure pulls

each abutment away from the retained soil, also as shown in Figure 2.5. As a result, the lateral earth pressures will tend to decrease to the active state. In at least one case in a cold climate, it was found that the earth pressures dropped to zero as the retained soil behind the abutment froze and the abutment pulled away leaving a gap (Broms and Ingleson 1971).

Although this problem of seasonal variations in lateral earth pressures has apparently been recognized for decades, recent research has refined the understanding of the nature and potential severity of this problem. Specifically, it is now appreciated that the higher summer pressures are not constant during the life of an IAB but will tend to increase with time as seasonal cycles of expansion and contraction occur. The reason for this is that after each annual cycle of seasonal expansion and contraction, an abutment does not return to exactly the same position it started from. In most cases, there is a net movement of the abutment away from its initial position and the retained soil as shown schematically in Figure 2.5[6]. This is because soil is inherently non-linear and inelastic in its behavior. During winter contraction of the bridge, a wedge-shaped portion of the soil retained by each abutment moves downward and toward the abutment. As the temperature warms up and an abutment moves toward the soil again the soil wedge does not return to its original position. As a result, a greater lateral earth pressure develops because the soil effectively becomes wedged behind the abutment.

This general phenomenon of a buildup of lateral earth pressures due to cyclic thermal movements of earth retaining structures is referred to as *ratcheting* behavior (England 1994, England and Dunstan 1994, England et al. 1995) and has been found to lead to eventual ULS failure of earth retaining structures (England 1994). The overall concern here is that, because of the relatively long (100-plus years) design life of bridges, long-term problems could develop with many if not most IABs as lateral earth pressures on their abutments build ("ratchet up") with time. This could lead to SLS or even ULS failure decades after an IAB was constructed.

Recent research has also identified a second IAB problem that is essentially caused by the same seasonal cycle of expansion and contraction of the bridge superstructure and the concomitant cyclic displacement of the abutments. This is the development of a settlement trough immediately behind each abutment. This is due largely to the progressive, cumulative outward and downward movement of soil wedges as described above. As a consequence of this settlement, a void develops under the approach slab (if one was used) as shown schematically in Figure 2.6. If there is no approach slab, a noticeable sharp drop would occur on the pavement surface of the approach embankment in the area immediately behind the abutment.

Although void development under approach slabs or settlement of the pavement surface is a common problem with road bridges in general for a number of reasons unrelated to thermal movement of IABs (Briaud et al. 1997), it is apparently a chronic, inherent problem with IABs in particular. For example, Reid et al. (1998a, 1998b) noted that a survey of 140 IABs in the State of South Dakota in the U.S.A. found a void under virtually every approach slab. The void depths ranged from 13 mm (0.5 in) to 360 mm (14 in), and the voids extended as much as 3 m (10 ft) behind the abutment. The surface settlement that results in voids under approach slabs was also found in physical model testing, both in a geotechnical centrifuge (Ng et al. 1998) and a large-scale 1-g retaining wall test facility (Reeves and Filz 2000).

As noted by Reid et al. (1998b), the primary problem resulting from void development is physical damage due to ULS structural failure of approach slabs. This is because the slabs are forced to span over the void, a function for which they are typically not designed. Note that a void does not have to be very deep in order for it to produce damage to an approach slab. All that is required is for the underside of the slab to lose contact with the ground surface.

---

[6] Another factor that contributes to permanent abutment displacement for IABs with a PCC superstructure is the inherent post-construction shrinkage of PCC.

area of settlement and
void development

long-term position of abutment →

new ground surface
due to long-term
abutment movement
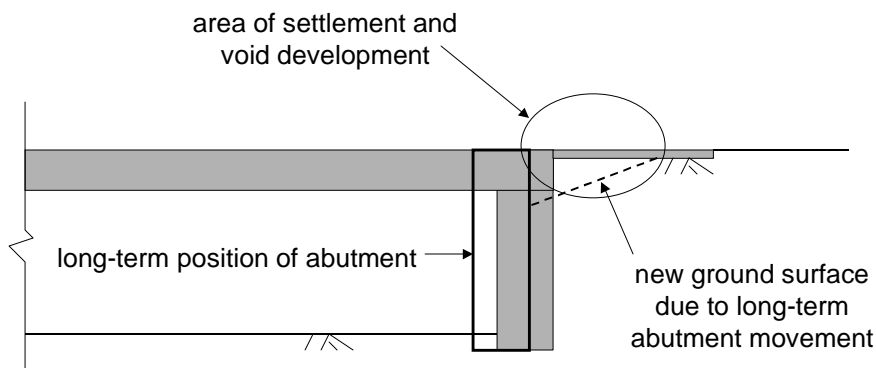
Figure 2.6. Settlement and Void Development Adjacent to IAB Abutments

If there is no approach slab, the settlement of the paved road surface on the approach embankment produces the classic "bump at the end of the bridge" that causes discomfort to vehicle occupants and possible damage to both vehicles and pavement and is thus an SLS failure that requires periodic pavement maintenance. The author has received personal communication that such pavement problems have indeed occurred with IABs without approach slabs.

The severity of void development/pavement settlement appears to be somewhat dependent on the quality of the soil used to backfill/fill behind the abutment. Void development is apparently relatively less if "high quality" material is used (this is generally interpreted to mean a predominantly coarse-grain soil that is relatively free of fine-grain particles) and placed in a well-compacted condition. This is consistent with general observations for all types of bridges as discussed by Briaud et al. (1997).

2.2.2.4 Potential Solutions: Present. The potential solutions to the IAB problems discussed in Section 2.2.2.3 are still evolving. This is because the understanding that there are really two problems to address (summer lateral earth pressure increases on abutments with long-term ratcheting buildup and surface settlement behind abutments) instead of just one (summer lateral earth pressures) have become more clearly identified, appreciated and conceptually understood only relatively recently during the 1990s. In fact, the evolutionary state of solving IAB problems was the primary motivation to undertake the study covered by this report.

Not surprisingly, the solutions to IAB problems proposed initially focused on the summer increase in lateral earth pressures on abutments simply because this problem was identified earlier. A purely structural approach is to shorten the height of each abutment considerably as shown conceptually in Figure 2.3(b). The abutments in this configuration can still be supported on either shallow or deep foundations. Although the lateral earth pressures acting on the abutments will still increase every summer, the total resultant force and flexural stresses that the abutment must be designed for will be considerably less because the effective span length (i.e. the abutment height) is markedly reduced. As an observation, it would appear that the SIAB

design shown in Figure 2.4 is a variation of this concept as only the ends of the bridge deck bearing against the ground are subjected to higher summer lateral earth pressures.

A more-geotechnical solution to dealing with the lateral earth pressure issue is to leave the full-height abutment as shown in Figure 2.3(a) but take preemptive measures so that the abutment does not have to be designed for lateral earth pressures in excess of those for which a bridge abutment is normally designed. The basic concept employed to achieve this is using what the author calls a *compressible inclusion*. In general, a compressible inclusion is any material placed in the ground (in any application, not just with IABs) that is significantly more compressible than the materials adjacent to it. Thus under a given magnitude of stress, the compressible inclusion will always deform (typically the mode is one-dimensional compression) much more than the adjacent materials. This sacrificial deformation will generally result in an overall localized reduction in stresses due to any one of several geotechnical mechanisms depending on the particular application (Horvath 1995b, 1996, 1998a).

The concept of a compressible inclusion in geotechnical applications in general is not new. It has been used at least since early in the 20th century with pipes and culverts (referred to collectively as *underground conduits*). In the original application of this concept, bales of hay or straw were placed above a conduit as a compressible inclusion to compress and create vertical soil arching that results in lower vertical stresses on the conduit (McCarthy 1988, Spangler and Handy 1982). In addition, cardboard void formers have been and are used in a variety of applications beneath structural (supported) slabs and behind earth retaining structures, especially in expansive-ground conditions. What is new in recent years with compressible inclusions is the significantly increased diversity of applications (Horvath 1995b, 1996, 1997, 1998a, 1998b) as well as the use of materials that offer advantages over bales of hay/straw, cardboard and other organic materials in terms of predictability and controllability of behavior and durability in the ground[7]. In particular, EPS geofoam has become the compressible inclusion material of choice in many applications worldwide. However, other factors sometimes influence the decision as to which material is used for a compressible inclusion. In particular, recycled tire fragments have enjoyed favor at different times and geographic locations for political and legislative reasons as well as their relatively low (often governmentally subsidized) cost. However, experience with tire fragments as a geotechnical fill material in general indicates that they can be variable in composition; variable and unpredictable in their behavior; and environmentally problematic.

The specific manner in which a compressible inclusion is applied to IABs is shown conceptually in Figure 2.7. This is an extension of what the author terms the *Reduced Earth Pressure* (REP) *Wall* concept for reducing lateral earth pressures due to gravity and live loading on any type of rigid, non-yielding (non-moving) earth retaining structure (Horvath 1990, 1991a, 1991b, 1995b). Depending on the specific material used and other design requirements, the thickness of the compressible inclusion in a direction perpendicular to the back of the abutment can be quite variable, ranging from tens of millimetres (a few inches) to hundreds of millimetres (a foot or more).

The most extensive and comprehensive formal research to date into the use of compressible inclusions with IABs to reduce the summer increase in lateral earth pressures has been performed in the U.K. (Carder and Card 1997). In the U.S.A., most of the work to date has been more material-specific and focused on using recycled tire fragments (Humphrey et al. 1998, Reid et al. 1998b).

---

[7] Any organic material will, with time and the moisture that exists naturally in the ground, decompose anaerobically. Some of the natural byproducts of anaerobic organic decomposition such as methane gas are potentially hazardous because of their inherent toxic and explosive nature.
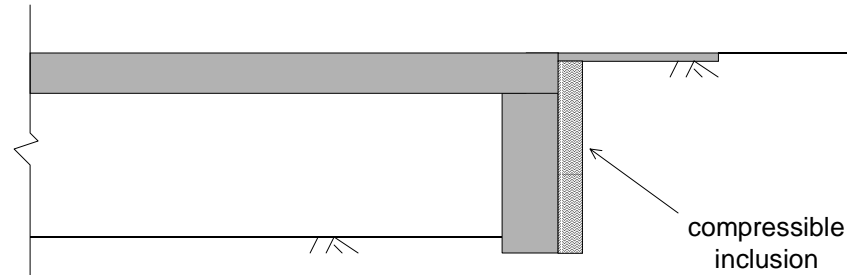
Figure 2.7. Compressible Inclusion Application with Integral-Abutment Bridges

Research to date indicates that an appropriate compressible inclusion can be effective in reducing the summer increase in lateral earth pressure on IAB abutments to acceptable levels but is ineffective in controlling settlement behind the abutment. This is because the highly compressible nature of a compressible inclusion that is so desirable under summer expansion of the bridge superstructure becomes a detriment when winter contraction of the superstructure occurs. As the superstructure contracts and pulls each abutment away from the retained soil, the compressible inclusion is unable to restrain the soil from slumping outward (toward the abutment) and downward which results in surface settlement behind the abutment. This has been observed for an actual IAB where a compressible inclusion consisting of recycled tire fragments was used with an approach slab (Reid et al. 1998b). It has also been observed in large-scale 1-g physical model testing where a compressible inclusion composed of resilient block-molded EPS geofoam was used with a coarse-grain backfill (Reeves and Filz 2000). It is of relevance to note that the presence of an inherently highly compressible inclusion may even exacerbate the settlement problem behind IABs even as it solves the summer lateral earth pressure problem.

2.2.2.5 Potential Solutions: Future. Although the use of a compressible inclusion is an answer to part of the overall IAB problems and thus a step in the right direction, a complete solution to all IAB problems needs to address both the lateral earth pressure and settlement issues simultaneously. To develop a concept to achieve this, one needs to revisit the way a conventional jointed bridge is designed as discussed in Section 2.2.1.1. In a conventional bridge, a relatively massive, rigid and non-yielding abutment keeps the retained soil stable year 'round while the bridge superstructure is allowed to move relatively freely with temperature. Effectively, the abutment is part of the ground, not the bridge. The expansion joint/bearing detail provides for a smooth, deformable transition between the two components (superstructure and abutment/soil).

What changes, of course, with an IAB is that the abutment is now inherently a part of the bridge superstructure and not the ground. Thus it is clear that with an IAB:

- the retained soil must be kept stable year 'round while the structurally integral bridge superstructure/abutment is allowed to move and

- there must be some design detail between the retained soil and superstructure/abutment to accommodate the relative movement between the two components. This detail must conceptually replace the expansion joint/bearing detail of a conventional bridge.

There are possibly several different design concepts that might be used to achieve these goals. Only two are considered in this study. The first design alternative is shown in Figure 2.8(a). The mass of retained soil can be kept stable by using geosynthetic tensile reinforcement (geogrid, geotextile or metallic elements) and building a *mechanically stabilized earth* (MSE) mass within the soil. In essence, the MSE mass becomes its own wall (called a *mechanically stabilized earth wall*, MSEW) although no facing panel would be used in this application as would be necessary in conventional MSEW construction. If polymeric reinforcements were used with IABs (as would be likely), one would just use a wrapped face.
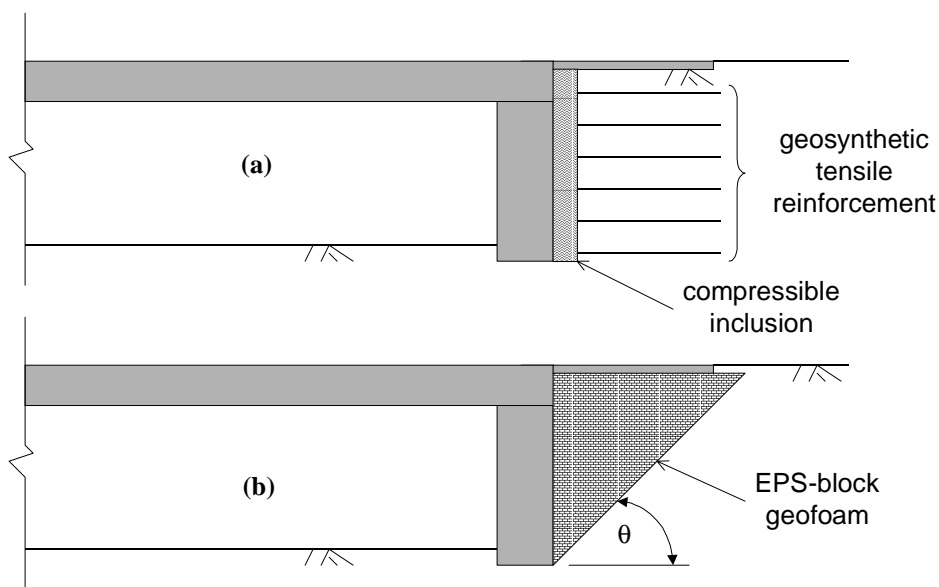
**Figure 2.8. IAB Design Alternatives to Simultaneously Reduce
Lateral Earth Pressures on and Control Settlement Adjacent to Abutments**

As shown by Monley and Wu (1993), the MSE concept can be very effective in an application similar to that shown in Figure 2.8(a). To accommodate the movement between an IAB abutment and adjacent MSE mass, some have suggested and used a physical gap of the order of 100 mm (4 in) or more (Edgar et al. 1989, Reid et al. 1998a). Although such gaps appear to be effective in their performance, at least in the short term (Reid et al. 1998a), they can be difficult to construct reliably and repeatedly (Edgar et al. 1989). This suggests that using a gap is not practicable in routine practice from a constructability perspective.

Actually, the more-serious problem with leaving a gap is that there is no guarantee that it will not become filled with soil or other material washed into it by infiltrating precipitation with time (the gap will serve as a de facto drainage layer behind the abutment), especially considering the long (100-plus year) design life of bridges. Therefore, the author believes that a compressible inclusion should always be used to provide the necessary joint filler between an IAB abutment and adjacent MSE mass. This is an extension of what the author terms the *Zero Earth Pressure* (ZEP) *Wall* concept for virtually eliminating lateral earth pressures due to gravity and live loading on any type of rigid, non-yielding earth retaining structure (Horvath 1990, 1991a, 1991b,

1995b). Furthermore, the author believes that only a geofoam compressible inclusion (most likely composed of resilient block-molded EPS) offers the necessary reliability, predictability and ease of use for this application. A geofoam compressible inclusion can also be designed to be multifunctional and cost effectively provide the necessary drainage behind the abutment as well as year 'round thermal insulation of the MSE mass. The detrimental effect of high summer temperatures on the creep of polymeric geosynthetic tensile reinforcement such as geogrids and geotextiles used as part of MSEW is perhaps not fully appreciated and considered in design (Murray and Farrar 1988, Segrestin and Jailloux 1988). During the winter, the geofoam compressible inclusion would prevent seasonal freezing of both the abutment drainage system and the retained soil.

The second design alternative is shown in Figure 2.8(b). A wedge-shaped mass of EPS-block geofoam can be used in a completely different function (role), that of lightweight fill. In this case, the geofoam mass is inherently self stable and creates what is called a *geofoam wall*. Therefore, as the abutment is pulled away from the geofoam by the contracting bridge superstructure in the winter no settlement behind the abutment would occur even though a gap between the back of the abutment and face of the geofoam mass would likely develop. This alternative is particularly attractive for sites underlain by soft, compressible soils. The extraordinarily low density of the EPS blocks (only about 1% of the density of soil) would minimize settlements overall as well as significantly reduce loads on the abutments and their foundations, both directly and indirectly (e.g. the potential for lateral squeeze within the soft underlying soil, which can buckle a pile-supported abutment, would be greatly reduced).

Note that the EPS geofoam used in this case would not be the same as that used as the compressible inclusion in Figure 2.8(a). The EPS geofoam in Figure 2.8(b) would have to be significantly stiffer to be able to support the vertical stresses imposed on it without excessive deformation. This highlights the fact that geofoam in general, and EPS geofoam in particular, can be used for both "large strain" and "small strain" applications depending on the geofoam function utilized in a given application (compressible inclusion and lightweight fill in this case). This also highlights the fact that there is no "universal" geofoam material or product. The appropriate material and product must be engineered and used in a given application.

The primary design issue with this second alternative of using EPS-block geofoam as a lightweight fill is what angle θ (see Figure 2.8(b)) is desirable for the assumed planar interface[8] between the geofoam wedge and soil. Theoretically, if θ equals the Mohr-Coulomb strength parameter ϕ ("angle of internal friction")[9] of the soil then the soil would exert no earth pressure on the geofoam mass and, therefore, no lateral earth pressure would be transmitted through the geofoam mass to the abutment. An angle θ greater than ϕ would require a smaller volume of geofoam but, theoretically, result in some earth pressure being applied to the geofoam from the soil and transmitted through the geofoam and onto the back of the abutment. Regardless of the value of θ used, a design question with the second design alternative shown in Figure 2.8(b) is whether or not a gap is necessary between the face of the geofoam mass and the back of the abutment (or possibly even a compressible inclusion used between the two as with the first design alternative using MSE shown in Figure 2.8(a)) to accommodate the movement between the abutment and geofoam.

---

[8] In reality, this interface is not planar but stepped because of the shape of the EPS blocks. However, this interface is generally assumed, with sufficient accuracy for practice, to be planar for analytical purposes.

[9] In this particular application, the angle ϕ is often referred to, especially in older literature, as the *angle of repose* of the soil.

This page intentionally left blank.

Section 3
Details and Results of Study

3.1 INTRODUCTION

This section first describes the details of the analyses performed for the study covered by this report. The results of the analyses are then presented and the factual observations deduced from the results are discussed. The overall conclusions drawn from this study are presented separately in Section 4.

3.2 DETAILS OF STUDY

3.2.1 Introduction and Overview

This study was limited to theoretical work, primarily using numerical analysis of an arbitrary but realistic problem of an IAB with a single span. This hypothetical bridge was subjected to several cycles of thermal change to induce movement and loads within the bridge superstructure and abutment. To focus on the effect of the thermal loading, the dead load of the bridge superstructure was ignored (the mass of the abutment was modeled however) and no live loads from vehicles were included. In addition, other phenomena that might induce load in the bridge, such as long-term shrinkage of PCC members, were also omitted from consideration. The overall details of the assumed problem are discussed in detail in Section 3.2.2.

The primary focus of this study was evaluating the efficacy of using different materials or combinations of materials as backfill/fill behind the abutment. To achieve this goal, 12 different backfill/fill designs were evaluated. A detailed discussion of the different designs is presented in Section 3.2.3.

The primary analytical tool utilized in this study was a continuum model of the key structural and geotechnical components of the problem. The forces and displacements within this continuum, and the estimated stresses and strains they produced, were calculated numerically using the finite element method (FEM) at various stages of simulated construction and subsequent thermal loading. The details of the FEM mesh and input parameters used are discussed in detail in Section 3.2.4.

Where possible and appropriate, hand-calculated theoretical results as well as the use of previously published solutions and simplified analytical methods were also compared against the FEM results. The specific supplemental analyses performed are discussed on a case-by-case basis together with the presentation and discussion of results in Section 3.3.

3.2.2 Overall Problem Details

3.2.2.1 Geometry. Figure 3.1 shows the assumed geometry of the overall structure. Values of the parameters in Equation 2.1, which defines the theoretical unconstrained movement of the bridge superstructure, were chosen so that the total change in length of the 50 m (164 ft) long superstructure under the full 60°C (108°F) temperature range assumed in this problem was 36 mm (1.4 in) which was judged to be realistic. Assuming symmetric movement, this means that the theoretical maximum range of unrestrained displacement at each end of the superstructure

and top of the adjacent abutment was 18 mm (0.7 in), or 9 mm (0.35 in) in either direction from the as-built neutral temperature position.
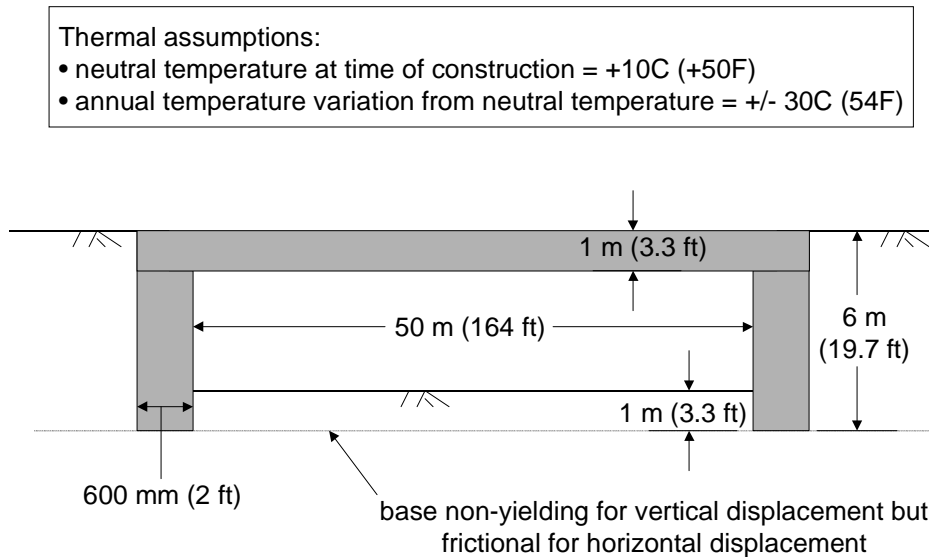
Figure 3.1. Overall Geometry and Thermal Assumptions of Problem Studied

It is relevant to note that although the problem used in this study was hypothetical, broad guidance for the assumed overall geometry and bridge superstructure parameters was obtained from an actual IAB, The Forks Bridge in the State of Maine U.S.A., that was the focus of a detailed geotechnical study by Sandford and Elgaaly (1993). That bridge had a span of 50.3 m (165 ft) and abutment height of approximately 7 m (23 ft). The primary structural components (both superstructure and abutment) were steel so that, from a structural perspective, the bridge looked like a classical rigid steel frame with tapered members. However, the columns (legs) of the frame, which served as the primary structural elements of the abutment, were encased in PCC so gave the appearance of a traditional reinforced PCC abutment.

The ground underlying each abutment in the problem assumed for this study was taken to be non-yielding (rigid) for vertical displacement meaning that the abutments could not move downward, i.e. settle. It also meant that the soil behind and in front of each abutment could not settle although vertical compression within the soil masses could occur. However, the horizontal interface between the bottom of each abutment and underlying rigid support layer was assumed to be frictional in nature so that horizontal displacement could occur. The same was true of the interface between the soil on either side of the abutment and the underlying rigid base (most geotechnical FEM analyses assume either a perfectly fixed or free horizontal bottom boundary condition).

The no-settlement boundary assumption may appear to be somewhat restrictive. However, the desire here was to remove any influence of foundation behavior from the problem as this would complicate interpretation of the results. The desire in this study was to focus on interaction between abutments and adjacent ground. Furthermore, the no-settlement bottom boundary condition is not totally unrealistic as it could occur in practice for an IAB with abutments founded on rock.

3.2.2.2 Thermal Environment. The assumptions regarding the thermal environment of the bridge were:

- The bridge was constructed at a neutral (force- and displacement-free) temperature of +10°C (+50°F).

- The annual air temperature range was 60°C (108°F), between a summer maximum of +40°C (+104°F) and winter minimum of -20°C (-4°F). This was judged to be representative of conditions that might occur in many temperate climates during the 100-plus year design life of an IAB.

- The temperature of the bridge superstructure is at all times the same as the air temperature.

- Four complete cycles of temperature variation were applied, starting at the neutral temperature and initially reducing to the first winter minimum. The number of cycles was arbitrary but dictated largely by limitations of the computer software used.

3.2.3 Abutment Backfill/Fill Variables Considered

The primary goal of this study was to evaluate the effect of varying the material used to backfill/fill behind the abutment of an IAB. The analyses performed were separated into three broad cases as follows:

- Case 1. This case focused on three subcases that did not incorporate the use geofoam in any way. A soil backfill/fill was assumed in all subcases with no other material between the back of the abutment and retained soil. The first subcase (Case 1a) was the basic, conventional solution of an unreinforced soil as shown conceptually in Figure 2.3(a). This subcase provided baseline results against which all other results obtained for this study were compared and evaluated. Thus Case 1a served as the reference for judging the benefit(s), if any, of using geosynthetics with IABs. Also included in Case 1 were two subcases (Case 1bi and Case 1bii) in which horizontal layers of geosynthetic tensile reinforcement were embedded within the retained soil. The two subcases differed solely in the type of reinforcement, polymeric (Case 1bi) and metallic (Case 1bii), simulated to make a first-order assessment of the effect of reinforcement stiffness on calculated results. Although geosynthetic tensile reinforcement would not normally be used alone behind a relatively rigid, non-yielding earth retaining structure such as a bridge abutment, these two subcases were included for the sake of completeness in the combination of problem variables considered.

- Case 2. This case focused on the strategy for solving IAB problems that is based primarily on using geofoam as a compressible inclusion between the abutment and retained soil. In each of the five separate analyses (subcases) performed for Case 2 the geofoam was assumed to be resilient[10] EPS-block geofoam. This is currently the most-efficient geofoam material to use whenever maximum compressibility (technically a minimum Young's modulus) is desired under relatively low stress (< ~100 kPa (2 kips/ft^2)) conditions. Figure 3.2 shows a comparison between normal and resilient block-molded EPS under strain-controlled,

---

[10] *Resilient* EPS is the term currently preferred for what was formerly called *elasticized* or *elastified* EPS as it more accurately describes the behavior of the material.

unconfined, axial compression[11]. The first group (Case 2a) of three analyses assumed the use of a compressible inclusion alone as shown in Figure 2.7. Collectively, the Case 2a analyses (referred to as cases 2ai, 2aii and 2aiii respectively) represent the solution to the IAB problem of increased summer lateral earth pressures that has already been proposed and used to date as discussed in Section 2.2.2.4. The three Case 2a subcases differed only in the thickness of geofoam assumed to evaluate the sensitivity of results to the inclusion thickness. Also included in Case 2 was a group (Case 2b) of two subcases (2bi and 2bii) where the retained soil was assumed to be reinforced as shown conceptually in Figure 2.8(a). This combination of a geofoam compressible inclusion plus MSE was one of the improved IAB design concepts suggested by the author in Section 2.2.2.5. Note that only one compressible inclusion thickness was considered in Case 2b to eliminate this parameter as a variable. The two Case 2b subcases differed only in the type of geosynthetic tensile reinforcement that was assumed within the retained soil. Polymeric (Case 2bi) and metallic (Case 2bii) reinforcement were considered separately to evaluate the effect of reinforcement stiffness.
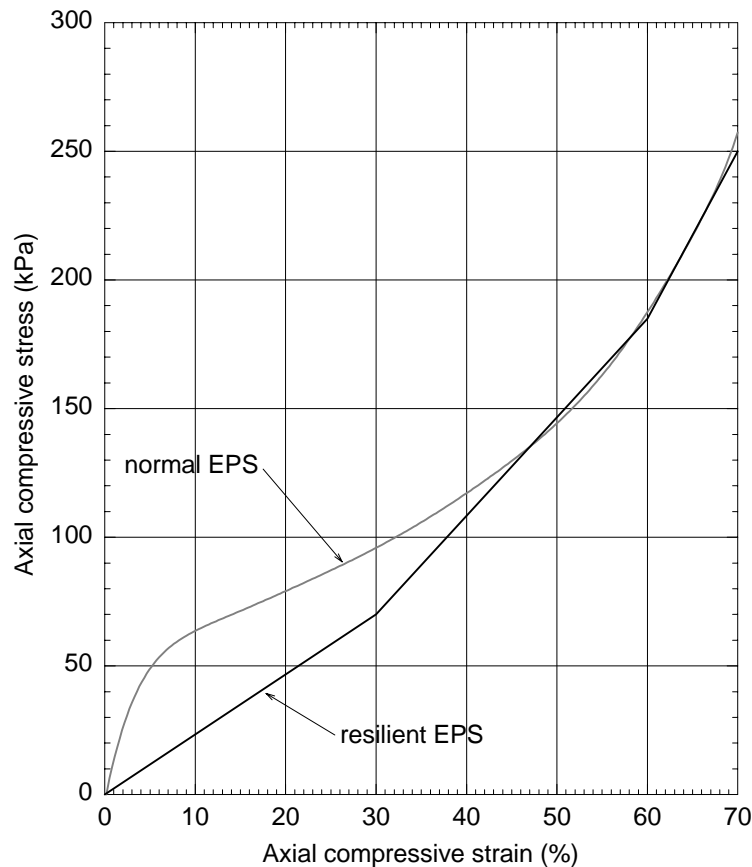
Figure 3.2. Normal versus Resilient Block-Molded EPS
(density = 12 kg/m^3 (0.75 lb/ft^3))
[data courtesy of GeoTech Systems Corporation]

---

[11] A discussion of the process for manufacturing resilient EPS and its effect on stress-strain properties can be found in Horvath (1995b) with summaries in Horvath (1997, 1998b).

- Case 3. This case included four subcases that focused on the use of EPS-block geofoam as a lightweight fill material in partial replacement of soil as shown conceptually in Figure 2.8(b). This was the second of two improved IAB design concepts suggested by the author in Section 2.2.2.5. The primary variable considered in Case 3 was the angle, θ, defining the assumed planar geofoam-soil interface. Two different magnitudes of θ were considered:

  - $\theta = 45° + \phi/2$ where ϕ = the peak Mohr-Coulomb shear strength parameter for the soil replaced by the geofoam[12]. This is the angle of the planar intra-soil failure surface assumed in Coulomb's classical solution for the active earth pressure state. Thus this was called the "active wedge" alternative.
  - $\theta = \phi$ which results in the minimum horizontal stress on the back of the abutment as discussed in Section 2.2.2.5. This was called the "full wedge" alternative.

Two analyses (cases 3ai and 3aii) were performed assuming the EPS blocks were in direct contact with the back of the abutment. The difference between these two subcases was in the assumed magnitude of θ (active versus full wedge). Two additional analyses (cases 3bi and 3bii) were performed assuming that a compressible inclusion consisting of resilient-EPS geofoam as in Case 2 and aligned as shown in Figure 2.7 was placed between the back of the abutment and the EPS blocks acting as a lightweight fill. Only one thickness of the compressible inclusion was considered. These two subcases varied only in the assumed magnitude of θ (active versus full wedge).

Table 3.1 summarizes in matrix format the combination of variables considered in this study with the designations used for each of the 12 subcases considered. The baseline Case 1a is shaded in gray for reference.

Table 3.1. Combinations of Primary Variables in Analyses Performed for Present Study

material between back of abutment and backfill/fill material used behind abutment		backfill/fill material used behind abutment				
		soil			EPS-block geofoam as lightweight fill	
		unreinforced	reinforced		active wedge	full wedge
			polymeric	metallic		
none		Case 1a	Case 1bi	Case 1bii	Case 3ai	Case 3aii
resilient-EPS geofoam	100 mm (4 in)	Case 2ai	-	-	-	-
	200 mm (8 in)	Case 2aii	Case 2bi	Case 2bii	Case 3bi	Case 3bii
	400 mm (16 in)	Case 2aiii	-	-	-	-

3.2.4 Numerical Analysis Details

3.2.4.1 Computer Software. The problem shown in Figure 3.1 was modeled utilizing the symmetry of the IAB so only one abutment was incorporated into the continuum model. The

---

[12] This report uses SI units as the primary system of units with imperial units secondary. However, angular measurements are in expressed only in degrees even though this is an imperial unit. This is because the SI unit of angular measurement, the *grad*, is used rarely if at all in geotechnical engineering practice. The alternative of expressing angular measurements nondimensionally as fractions or multiples of π, while conceptually correct, was deemed too clumsy.

ground on either side of the abutment was modeled for a finite horizontal distance considering rules of thumb established by others from more than 30 years of performing similar FEM analyses of earth retaining structures.

Due to the limitations of the computer software available for this study, only a two-dimensional, plane-strain model could be analyzed. The resulting model continuum of abutment plus ground was then discretized for numerical solution using the FEM. The basic FEM mesh used for all parts of this study is shown in Figure 3.3. Note that the vertical Y axis shown in this figure was required by the software used for this study for internal program purposes (input preparation, etc.). A new vertical z axis, also shown in Figure 3.3 and defined as having $z = 0$ at the top of the abutment ($Y = 6$ metres), was actually used for all plots in this study.
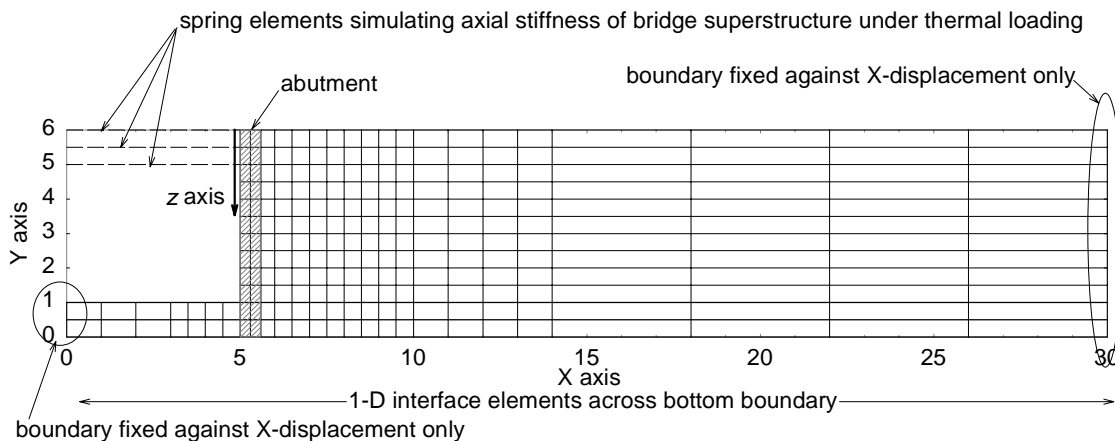
Note: Both axes scaled in metres (1 m = 0.305 ft).

Figure 3.3. Finite Element Mesh Used for Present Study

The FEM software used for this study is named *SSTIPNH*™. It is the author's proprietary microcomputer version of the mainframe program *SSTIPN* that was developed and subsequently modified over a period of many years first at the University of California at Berkeley and later at The Virginia Polytechnic Institute and State University at Blacksburg under the overall direction of Prof. J. Michael Duncan. Although *SSTIPNH* does not have the graphical interfaces typical of current commercially available software, the analytical logic incorporated into *SSTIPNH* is still representative of the state of practice in such software.

3.2.4.2 Solid Material Model Parameters. Two-dimensional (2-D) "solid" finite elements were used to model the materials comprising the abutment, soil and geofoam (if any). The only constitutive model for solid material elements in *SSTIPNH* is the well known non-linear hyperbolic model although by appropriate choice of the model parameters either an elasto-plastic or linear-elastic material can also be simulated with this model.

It should be noted at the outset that the hyperbolic model has some significant shortcomings with particular regard to modeling the way soil is loaded in the IAB problem. Specifically, cyclic loads are known to be an important aspect of soil behavior in IAB problems. An important rheological aspect of cyclic soil loading is the accumulation of plastic (non-recoverable) strains due to the inherent hysteretic behavior of soil (England 1994, England and Dunstan 1994, England et al. 1995). The hyperbolic model does not do a good job of replicating hysteretic behavior. Therefore, from the beginning of this study it was known that certain aspects of the anticipated soil behavior would not be well modeled. However, it was felt that this would not detract from the overall qualitative and quantitative correctness of the results of this study.

Only one type of soil was used for both sides of the abutment throughout the entire study. An actual soil, one of those included in a study reported by Boscardin et al. (1990), was chosen. The soil was classified as SW and A-1-a(0) in the Unified Soil Classification System (USCS) and American Association of State Highway and Transportation Officials (AASHTO) system respectively. From a practical perspective, this is about as good a soil as would be used as a general backfill and fill in actual highway earthwork. Parameters for the soil in a fairly loose condition (85% relative compaction using the "Standard Proctor" compaction energy as the reference standard) were assumed. The peak value of the Mohr-Coulomb friction angle, ϕ, was used and no correction in magnitude (typically a 10% increase) was made for the plane-strain conditions that existed in this problem simulated in this study.

The PCC comprising the abutment was assumed to have a compressive strength, f_c', of 27600 kPa (4000 lb/in^2). Linear-elastic behavior was assumed with a Young's modulus (approximately 25 GN/m^2 (3600 kips/in^2)) that was consistent with empirical correlation to compressive strength.

The geofoam parameters varied depending on the way (function) in which the geofoam was used, but in all cases the geofoam material was assumed to be EPS manufactured by the block-molding process. The resilient EPS used as a compressible inclusion for the Case 2 and Case 3b analyses was assumed to be made from EPS with an initial (molded) density[13] of 12 kg/m^3 (0.75 lb/ft^3) that increased 15% in magnitude to 13.8 kg/m^3 (0.86 lb/ft^3) due to the post-molding resiliency (elasticization) process. Linear-elastic stress-strain behavior was assumed for the resilient EPS with a Young's modulus of 250 kN/m^2 (5200 lb/ft^2). This corresponds to the *de facto* standard rapid loading conditions used for EPS geofoam testing and normal compressive stresses up to approximately 75 kPa (1500 lb/ft^2; see Figure 3-2) which was not expected to be exceeded in the analyses performed for this study. This modulus is conservative for this application as creep of resilient-EPS geofoam of the density assumed in this study is relatively significant throughout all stress ranges (see Figure 3.4). As a result, the Young's modulus of this material in an actual application would decrease significantly with time, of the order of 50% after one year. The effect of creep on the behavior of a geofoam compressible inclusion adjacent to an earth retaining structure was explored by Murphy (1997).

EPS-block geofoam used as lightweight fill was assumed to have a density of 20 kg/m^3 (1.25 lb/ft^3). It was assumed that normal stresses applied to and within the geofoam mass would be within the elastic-limit stress of the geofoam (approximately 50 kPa (1000 lb/ft^2) in this case) for all analyses so creep would be expected to be negligible (Horvath 1995b). Therefore, linear-elastic behavior was assumed for the geofoam with a Young's modulus of 6000 kN/m^2 (125 kips/ft^2) that was equal to the initial tangent Young's modulus of EPS-block geofoam of this density based on empirical correlations given by Horvath (1995b).

---

[13] Consistent with practice worldwide, in SI units geofoam *density*, with units of kilograms per cubic metre, as opposed to *unit weight* in Newtons per cubic metre is normally stated. However, in imperial units geofoam *unit weight*, with units of pounds per cubic foot, is given as the equivalent even though density and unit weight are not strictly equivalent (although they are, of course, linearly related).
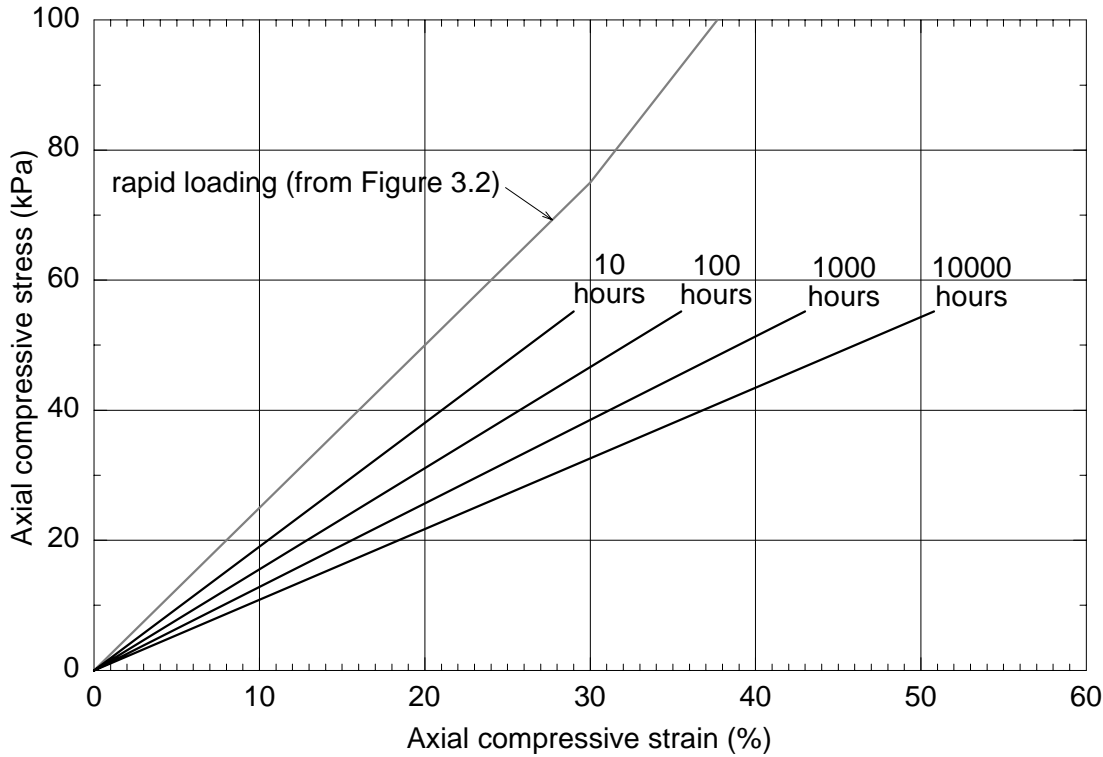
Figure 3.4. Isochronous Stress-Strain Curves for Resilient Block-Molded EPS (initial molded density = 12 kg/m^3 (0.75 lb/ft^3)) [data courtesy of GeoTech Systems Corporation]

Table 3.2 summarizes the specific values of the hyperbolic constitutive model parameters used in this study for solid materials. The parameter notation for this constitutive model is consistent with that appearing in the literature for many years. However, the relevant equations for this model are given in Section 6.2.1 for ease of reference and the sake of completeness.

Table 3.2. Hyperbolic Constitutive Model Parameters for 2-D (Solid) Element Materials

material		parameters									
		γ_t (N/m^3)	K	n	R_f	K_b	m	c (kN/m^2)	ϕ_1 (°)	$\Delta\phi$ (°)	K_o
soil		19800	450	0.35	0.8	110	0.1	0	38	0	1.0
PCC		23500	250000	0	0	119000	0	13800	0	0	0.18
geofoam	resilient	140	2.5	0	0	0.83	0	100	0	0	0
	normal	200	59	0	0	26	0	60	0	0	0.13

One comment is made concerning the coefficient of earth pressure at rest, K_o, for soil given in Table 3.2. An arbitrary value of this parameter (= 1.0), somewhat higher than the normally consolidated value (= 0.38), was chosen to reflect the lateral stresses locked into a layer of soil immediately after simulated placement with compaction equipment. While this simple approximation does not begin to reflect the complexity of soil behavior during the compaction

process (see, for example, Duncan et al. (1991) for a state-of-art discussion of this topic), it was used to at least approximate, albeit in a crude way, the temporarily higher lateral stresses that result from the compaction process.

3.2.4.3 Interface Model Parameters. Interfaces between dissimilar materials can be modeled in *SSTIPNH* using the familiar one-dimensional (1-D), zero-thickness elements that can have hyperbolic, elasto-plastic or linear-elastic stress-strain behavior in shear. The particular interface model incorporated into *SSTIPNH* allowed for shear stiffnesses that differ between initial loading (K_{si}) and unloading/reloading (K_{su}).

To minimize the size and complexity of the FEM mesh, not all interfaces between dissimilar materials were modeled using interface elements. In general, interface elements were employed only where it was judged beforehand that it was important to accommodate inter-material slippage. This included both sides of the abutment and the horizontal surface across the entire bottom of the mesh where soil-on-soil (except for poured-in-place-PCC-on-soil beneath the abutment) contact was assumed (see Figure 3.3). In addition, whenever a compressible inclusion was modeled (all parts of Case 2 plus cases 3bi and 3bii) the vertical interface between the compressible inclusion and retained material (soil in Case 2 and EPS-block geofoam lightweight fill in Case 3b) 1-D interface elements were employed as well.

Table 3.3 summarizes the specific values of the interface element model parameters used in this study. The values used were based on an assessment of realistic δ/ϕ ratios for the materials involved as well as an assessment of the magnitude of displacement required to fully mobilize the peak shear resistance under average values of normal stresses encountered in this problem. Relevant equations for the interface constitutive model are given in Section 6.2.2 for ease of reference and the sake of completeness.

Table 3.3. Constitutive Model Parameters for 1-D (Interface) Elements

materials in contact	parameters							
	$K_{s,i}$	$K_{s,u}$	n	R_f	K_n	c_a (kN/m²)	δ_1 (°)	$\Delta\delta$ (°)
soil-soil (also soil-geofoam)	1000	2000	0.5	0.9	100000000	0	38	0
soil-poured PCC	3000	6000	0.5	0.9	100000000	0	34	0
soil-formed PCC	800	1600	0.5	0.9	100000000	0	23	0
formed PCC-geofoam	300	600	1.0	1.0	100000000	0	18	0
geofoam-geofoam	300	600	1.0	1.0	100000000	0	30	0

3.2.4.4 Reinforcement Modeling. The way in which the geosynthetic tensile reinforcement was modeled in this study requires some discussion. The traditional method of incorporating reinforcement into a FEM analysis is to model each layer of reinforcement explicitly, typically using a chain of one-dimensional spring elements to simulate the reinforcement product (the spring stiffness represents the tensile stiffness of the reinforcement) with one-dimensional interface elements above and below the spring elements to simulate the shearing between the reinforcement and the soil on either side of it. Such modeling can be realistic and successful (Horvath 1991a, 1991b) but tedious to work with. In particular, this modeling methodology is inflexible when it comes to making any changes in reinforcement geometry during the course of a study as it requires substantive revisions of the FEM mesh and input file each time.

In analyses where it is necessary only to model the overall effect of reinforcement for stiffening a soil mass (as opposed to being able to replicate slippage or pullout of an individual reinforcement layer for example), a useful modeling technique was suggested and verified by Ebeling et al. (1992). In their technique, the reinforced soil mass, shown conceptually in Figure 3.5(a), is modeled as an unreinforced soil mass with a spring (linear and elastic in most practical cases) connecting the soil elements at the horizontal limits of the reinforcement as shown conceptually in Figure 3.5(b). The stiffness of the spring is equal to $A_r E_r / L_r$, where A_r = total cross-sectional area of the reinforcement, E_r = Young's modulus of the reinforcement material and L_r = overall length of the reinforced zone as shown in Figure 3.5. In actuality, several springs in parallel as opposed to one spring would be used to enhance the accuracy of this approximate technique, with the sum of the individual spring stiffnesses equaling the desired overall stiffness.
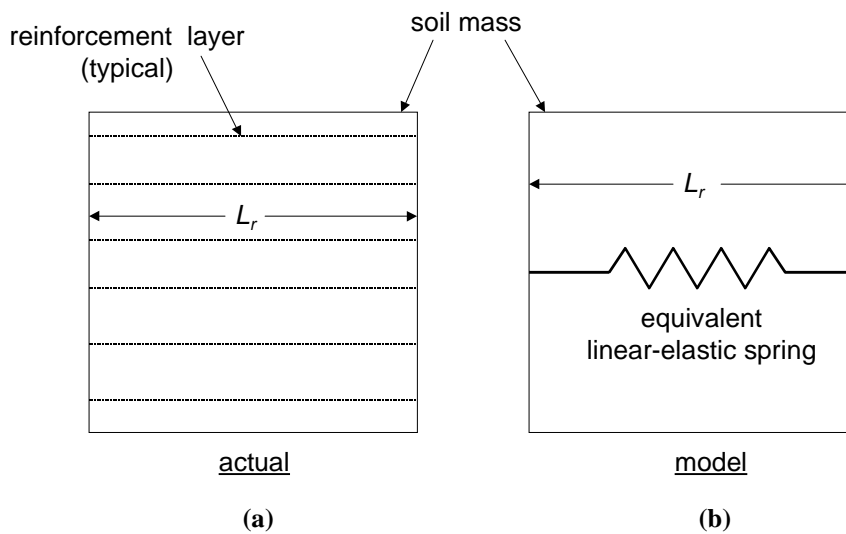
Figure 3.5. Approximate FEM Modeling of Geosynthetic Tensile Reinforcement

The utility of this modeling technique is that it is relatively easy to add, delete or modify the reinforcement spring elements so that various layouts and stiffnesses of reinforcement can be studied easily. Most FEM software has a category of elements that can be used for this purpose. In the program *SOILSTRUCT*[14] used by Ebeling et al. (1992), such an element is called an *overlay* element. In the *SSTIPNH* program used for this study, it is called a *nodal link*. However, care must be taken in problems such as considered in this study when there are changes in the direction of movement of reinforced soil masses. That is because geosynthetic reinforcements are presumed to have zero stiffness when loaded in compression. Fortunately, *SSTIPNH* has a provision wherein nodal links can be "turned off" at any given step in a simulation although this did not produce wholly satisfactory results as discussed in Section 3.3.

The two types of reinforcements considered in the various subcases of this study were broadly categorized as polymeric (intended to represent as a group primarily geogrids but high-strength geotextiles as well) and metallic (intended to represent as a group steel strips and related products). It was assumed that one layer of reinforcement, where used, would be placed with each soil layer (i.e. layer of 2-D elements in Figure 3.3) which would give a 500 mm (20 in)

---

[14] This program has many attributes and capabilities in common with *SSTIPNH* that was used in this study.

vertical spacing between reinforcement layers. Referring to the FEM mesh in Figure 3.3, the lowest reinforcement layer was at a vertical (*Y*) axis coordinate of 0 and the uppermost was at *Y* = 5.5 m.

The assumed stiffness, A_rE_r/L_r, of each layer of reinforcement was 400 kN/m (27 kips/ft) for polymeric reinforcement and 20000 kN/m (1400 kips/ft) for metallic reinforcement. It should be kept in mind that because of the plane-strain model used, each of these values (including the imperial-unit equivalents) is per the implied unit width (one metre) of the model and FEM mesh.

3.2.4.5 Bridge Superstructure Modeling. The bridge superstructure was modeled using what are called *bar elements* in *SSTIPNH*. These are linear-elastic springs for analytical purposes. The superstructure was modeled using three bar elements that covered its assumed 1 m (3.3 ft) thickness as shown in Figure 3.3. Conceptually, the combined stiffnesses of these bar elements represents the total longitudinal stiffness of the superstructure to a thermal-induced length change. From equations 2.1 and 2.2, it can be shown that the deck stiffness equals A_sE_s/L_o where the parameters are as defined previously in Section 2.2.1.1. Here, L_o = 25 m (82 ft) which is one half of the span length in the assumed problem geometry. Note that the actual areas, A_s, of the bar elements input were adjusted to reflect the fact that the bar elements in the FEM mesh (Figure 3.3) were only 5 m (16.4 ft) long. However, the overall stiffness A_sE_s/L_o was the same as the actual problem which is all that was important.

3.2.4.6 Simulation of Construction and Thermal Load Application. Each of the 12 analyses performed for this study as summarized in Table 3.1 began with no pre-existing elements in the mesh shown in Figure 3.3. Abutment construction was then simulated in 12 steps, including placement of the bridge superstructure as well. This was followed by backfilling/filling on both sides of the abutment in 14 steps for a total of 26 construction steps. As noted in Section 3.2.2.2, construction was assumed to occur at a neutral temperature of +10°C (+50°F).

After the construction simulation, thermal loading was simulated by applying a horizontal stress over the top 1 metre (3.3 feet) of the abutment where the bridge superstructure was assumed to be connected to the abutment. The stress was applied in decrements or increments representing temperature changes of 10°C (18°F). Thus an entire simulated annual temperature cycle of 60°C (108°F) (from the neutral temperature of +10°C (+50°F); down to -20°C (-4°F); up to +40°C (+104°F); and back down to the neutral temperature) required 12 steps. This was not intended to explicitly reflect the number of months in a year. Rather, the number of cycles was arrived at by happenstance as a result of dividing the total simulated temperature change of 120°C (216°F) into relatively small increments of 10°C (18°F).

The magnitude of the thermal-induced horizontal stress applied in each thermal-load step was calculated using Equation 2.2 and was 2400 kPa (50 kips/ft^2). Note that at any given load application step, the actual resultant force within the bridge superstructure is the sum of the applied force (applied stress times 1 metre height) minus the total force in the bar elements used to model the structure. Conceptually, then, the applied stress represents the potential for thermal-induced forces to develop in the bridge superstructure whereas the total stiffness of the bar elements used to model the superstructure represents the ability of the superstructure to relieve thermal forces by changing length.

For the reasons discussed in Section 3.2.4.4, care was taken to temporarily inactivate the nodal links representing any soil reinforcements whenever the applied thermal load was such that it tended to push the abutment into the retained soil which would tend to induce compression in the reinforcements. Although this does not produce entirely correct results (not all levels of reinforcement will necessarily shift from tension to compression at the same time) it was the best approximation that could be accommodated within the capabilities of the software used.

3.3 RESULTS AND DISCUSSION

3.3.1 Plotting and Interpretation of Results

3.3.1.1 Introduction. Before proceeding with the presentation and evaluation of the results of the various numerical simulations performed for this study, it is useful to discuss various details that are common to the numerous plots of lateral pressures[15] acting on the abutment that are contained in this report as well as interpretation of the results shown on these plots. To illustrate these items, the basic template used to create these plots is shown in Figure 3.6.
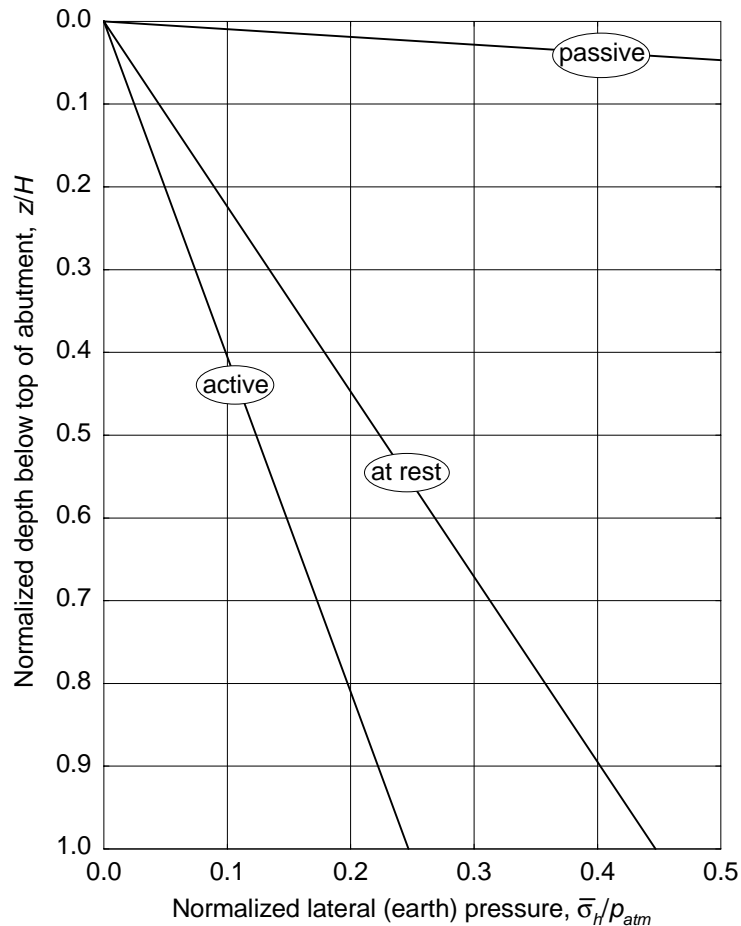
Figure 3.6. Template for Lateral (Earth) Pressure Plots

3.3.1.2 Classical Earth Pressure Theory. The first item to discuss is the theoretical lateral earth pressures[16] for various earth pressure states. These classical solutions, which are

---

[15] Which may or may not be earth pressures depending on the material in contact with the abutment.

[16] In correct civil engineering terminology, the term *pressure* should only be used for a normal stress (normal force per unit area) exerted by a fluid (gas or liquid). In solid materials (or quasi-solids such as soil), a normal force per unit area should be called a *stress*. In addition, the term *horizontal* is more precise and correct in civil engineering usage than *lateral*. However, the expression *lateral earth pressure*, not

easily obtained by manual calculation, are always useful reference conditions for any plot of lateral earth pressure. In particular, the following are shown in Figure 3.6:

- The normally consolidated (NC) at-rest state based on the well-known relationship

$$K_{onc} = 1 - \sin \phi \qquad (3.1)$$

  where $K_{onc} =$ the coefficient of lateral earth pressure at rest for the NC state. Equation 3.1 resulted in $K_{onc} = 0.38$ in this study.

- The horizontal component of earth pressure for the active state based on the "exact" solution[17] given on Page 7.2-67 of *Foundations and Earth Structures* (1982) which resulted in a coefficient of active earth pressure, K_a, = 0.23 in this case.

- The horizontal component of earth pressure for the passive state based on the exact solution[18] page 7.2-67 of *Foundations and Earth Structures* (1982) which resulted in a value of the coefficient of passive earth pressure, K_p, = 9.9.

Note that in none of these cases was an empirical adjustment for compaction-induced stresses made to the earth pressure diagrams shown in Figure 3.6 as suggested most recently by Duncan et al. (1991) and others before that.

3.3.1.3 Plot Axes. Next considered are the plot axes used. To enhance the generality of all plots (not just those for lateral pressures), for the vertical axis the depth variable, z, is normalized by dividing it by the abutment height, H. For the horizontal axis, the lateral (earth) pressure, $\overline{\sigma}_h$, is normalized by dividing it by the atmospheric pressure, p_{atm}. Note that this does not imply that atmospheric pressure per se influences lateral pressures. Atmospheric pressure is simply a convenient stress parameter whose magnitude is well known or easily calculated in any system of units.

It is worth noting that lateral (earth) pressure plots are usually normalized by dividing $\overline{\sigma}_h$ by the product of the total soil unit weight, γ_t, and the "geotechnical" wall height[19] (see, for example,

---

horizontal earth stress, has been used traditionally in geotechnical engineering. Although this report adheres to this traditional colloquial terminology, the correct notation for normal stress, σ, is used, not the usual notation for pressure, p. Also, *horizontal* is used to indicate direction in all cases except when the term *lateral earth pressure* is used.

[17] "Exact" in the sense that it was based on a curved intra-soil failure surface as opposed to the incorrect planar surface assumed by Coulomb in his classical solution. As discussed by Tschebotarioff (1973), for the more-common case of positive relative soil-wall friction, as was assumed and verified by inspection of calculated results in this study, the difference in results between exact solutions (there are several) and Coulomb's solution is generally negligible in any practical context. That was confirmed here as the calculated Coulomb value for $K_a = 0.22$.

[18] Exact theories for the passive state are also based on a curved intra-soil failure surface as opposed to the incorrect planar surface assumed by Coulomb. However, in the passive state Coulomb's theory is almost always in error on the unconservative side and thus should never be used in practice.

[19] *Geotechnical wall height* is defined as the vertical distance from the base of a wall to the point where the retained soil contacts the back of a wall. This height, upon which lateral earth pressure theories and calculations are based, may be less than the actual wall height in applications where some additional free-standing height (freeboard) must be provided for safety. However in this study the geotechnical and actual wall heights are the same as is typical for bridge abutments.

Karpurapu and Bathurst (1992)), not atmospheric pressure as used in this study. However, because backfill/fill materials of different composition and widely varying unit weights were considered in this study atmospheric pressure was used as the normalization parameter to prevent any ambiguity or confusion.

3.3.1.4 Comparison of Results. The final issue to discuss is the methodology for the overall interpretation and assessment of results. Because comparison of results between various subcases is a significant aspect of this study, a succinct and insightful methodology for characterizing results is of critical importance and deserving of careful consideration.

In terms of lateral (earth) pressures, the primary issue is the magnitude of pressures relative or normalized to some reference value. In general,

$$P_h = \int_0^H \overline{\sigma}_h \, dz \qquad (3.2)$$

where P_h = the horizontal resultant (earth) force acting on an earth retaining structure and the other terms have been defined previously.

Assuming a soil backfill/fill with all material parameters constant in magnitude with depth, Equation 3.2 can be extended to yield:

$$\int_0^H \overline{\sigma}_h \, dz = \int_0^H \left(K_h \cdot \overline{\sigma}_{vo} \right) dz = K_h \int_0^H \overline{\sigma}_{vo} \, dz = K_h \int_0^H \left(\gamma_t \cdot z \right) dz = \left(K_h \cdot \gamma_t \right) \int_0^H z \, dz = \frac{K_h \cdot \gamma_t \cdot H^2}{2} \qquad (3.3)$$

which, when rearranged, yields:

$$K_h = \frac{2}{\gamma_t \cdot H^2} \int_0^H \overline{\sigma}_h \, dz \qquad (3.4)$$

where:

K_h = the coefficient of lateral earth pressure in general,

$\overline{\sigma}_{vo}$ = the effective vertical stress under gravity (overburden) conditions

and the other terms have been defined previously.

In a study performed by Karpurapu and Bathurst (1992), they found it convenient to:

- normalize results using the active earth pressure state (K_a) as the reference condition;
- calculate K_h using Equation 3.4 and the FEM results for each case they analyzed; and
- compare results based on dimensionless K_h/K_a ratios.

While this was effective for their purposes, an alternative approach was used in this study:

- The resultant force P_h, as opposed to the earth pressure coefficient K_h, was calculated using Equation 3.2 for each subcase. This was to remove any ambiguity or error from dealing with backfills/fills of different composition having different material unit weights.

- The normally consolidated (NC) at-rest, not active, earth pressure state was used as the reference condition for normalization. The NC at-rest earth pressure state is the line in Figure 3.6 labeled "at rest". It was felt that the at-rest state was a more representative baseline for a relatively rigid and non-yielding earth retaining structure such as a bridge abutment. The resultant force, P_h, for this reference condition was given the special notation P_o^*.

- A new dimensionless parameter, β, called the *normalized horizontal resultant (earth) force* was used to reflect the relative results between analysis subcases by defining

$$\beta = \frac{P_h}{P_o^*} \tag{3.5}$$

This means that $\beta = 1$ represents the baseline condition of the NC at-rest earth pressure state.

Conceptually, the approach used in this study to portray and compare lateral pressures achieves the same goal as the approach used by Karpurapu and Bathurst (1992). It is simply more general and better suited to the specific elements and requirements of this study.

Using the concept defined by Equation 3.5, it is of interest to note that the other classical earth pressure theories discussed in Section 3.3.1.2 and shown in Figure 3.6 yield values of $\beta = 0.55$ and 24 for the active and passive states respectively.

It is important to note that both this study as well as that of Karpurapu and Bathurst (1992) focus only on the magnitudes of resultant forces applied to an earth retaining structure. The point of application of the resultant force, which affects bending moments in and global stability of (if it is free to move) the structure, is not considered. Therefore, care is required when interpreting the results of this study as two different subcases might happen to produce the same value of β but might not affect the abutment structurally in the same way due to different points of application of the resultant forces.

3.3.2 Case 1: No Geofoam

3.3.2.1 Introduction. The primary focus of Case 1 was the baseline condition of traditional IAB construction with an unreinforced soil backfill/fill and no geofoam (Case 1a). This baseline condition yielded results against which all other results in this study were compared for their effectiveness in addressing the most critical IAB problems, i.e. reducing lateral earth pressures on the abutment and settlement of the ground surface behind the abutment.

Also included in Case 1 were two other subcases (1bi and 1bii) in which tensile reinforcement was embedded within the retained soil. The simulated zone of reinforcement is shown in Figure 3.7. The length of the reinforcements, L_r, in both subcases was 3.9 m (12.8 ft). This resulted in a reinforcement-length-to-wall-height ratio, L_r/H, = 0.65 which is within the range of typical values for MSEW under gravity loads. It was assumed that this reinforcement length would be sufficient to make reinforcement pullout, which is not possible using the modeling technique described in Section 3.2.4.4 that was used in this study, unlikely under service load conditions.

34
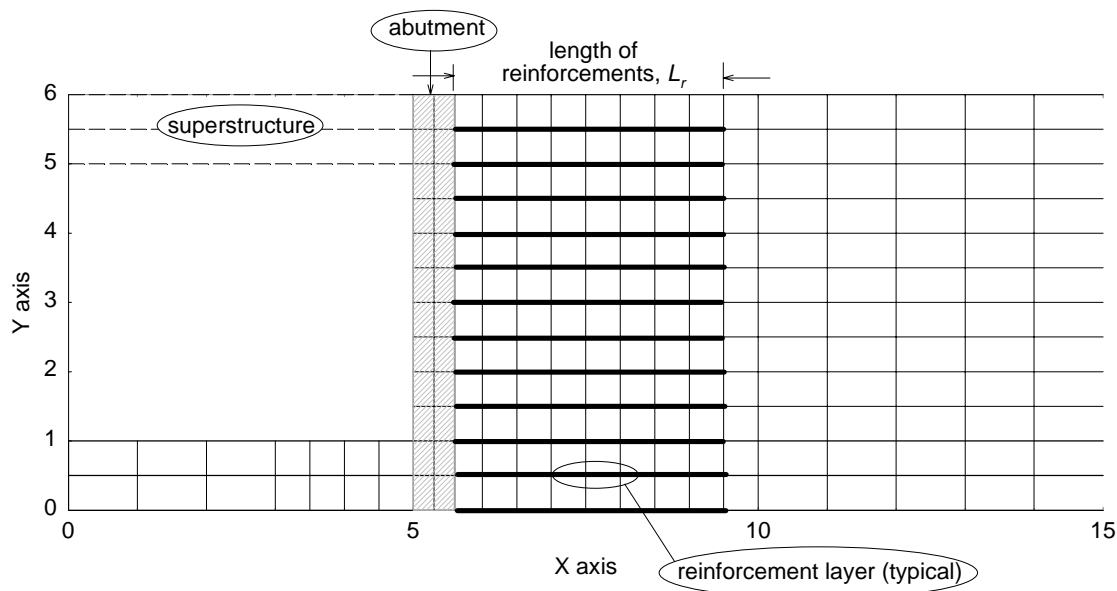
Figure 3.7. Case 1b: FEM Mesh (partial)

3.3.2.2 End of Construction. The lateral earth pressures acting on the back of the abutment at the end of construction are shown in Figure 3.8. Note that this also represents the initial neutral temperature condition before the thermally induced forces are applied.

As might be expected, the baseline unreinforced soil subcase (Case 1a) essentially reflects the NC at-rest state ($\beta = 0.99$) with a slight increase in stress near the top of the abutment due to residual compaction effects there (qualitatively similar to what would be predicted by the method in Duncan et al. (1991) for example) and a slight decrease in stress near the bottom of the abutment. This localized reduction is due to the fact that during backfilling/filling, the abutment exhibited a slight tendency to rotate clockwise about its top where it is effectively restrained against movement by the bridge superstructure. The bottom of the abutment, which is restrained only by one metre of soil and friction along its base, moved approximately 2 mm (0.1 in) outward (toward the left in Figure 3.7). As a result, an early stage of horizontal arching in the mode of "rotation about top" was created within the retained soil (Handy 1985, Harrop-Williams 1989). The observed pressure distribution shown in Figure 3.8 is qualitatively consistent with results from both physical testing using 1-g models reported by Fang and Ishibashi (1986) as well as theoretical work by Harrop-Williams (1989).

As expected based on past work (Horvath 1990, 1991a, 1991b), the presence of geosynthetic tensile reinforcement within the retained soil had little benefit ($\beta = 0.92$) in the case of the polymeric reinforcement (Case 1bi) and only modest benefit ($\beta = 0.82$) in the case of the metallic reinforcement (Case 1bii) as the slight outward movement of the bottom of the abutment allowed the lower levels of the relatively stiff metallic reinforcements to mobilize some tensile resistance.
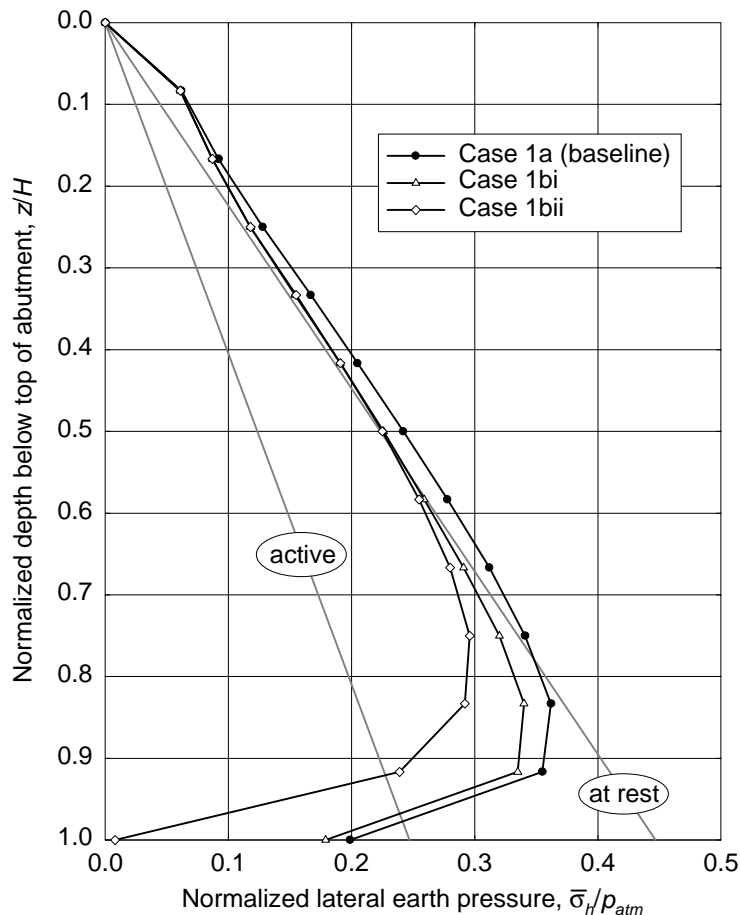
Figure 3.8. Case 1:
Lateral Earth Pressures at End of Construction

Elaborating on a point implied in the preceding paragraphs, it has been known from the beginning of modern soil mechanics that the classical triangular distributions of lateral earth pressure for the active and passive states (as shown in Figure 3.6 for example) are simplistic idealizations that are rarely if ever observed in practice. This is because horizontal displacement of an earth retaining structure does not cause simple soil wedges to develop and slide along the intra-soil failure surfaces assumed by classical theories. Such displacements actually mobilize a complex pattern of arching that results in lateral earth pressure distributions that are more parabolic in shape (Handy 1985, Harrop-Williams 1989). Even the basic at-rest state is more complex than normally assumed in practice with phenomena such as the existence of significant vertical shear stresses along the interface between the earth retaining structure and retained soil, even in the absence of horizontal movement of the wall (Duncan et al. 1990). Nevertheless, the classical triangular distributions have remained in use up to the present as they are easy to work with in terms of calculating pressures, resultant forces and points of resultant application, and produce acceptable designs in routine practice for most earth retaining structures. It is for this reason that the classical lateral earth pressure distributions for the active and at-rest states (and passive state where appropriate) are shown in Figure 3.8 and many others throughout this report.

However, in a study such as this it is important to understand the actual, more complex lateral earth pressure distributions that develop. A useful tool for the purpose of gaining insight into the calculated results of FEM analyses is to contour values of the dimensionless *stress level*, *S*,

within the soil. This is one of many quantities calculated by *SSTIPNH* and similar FEM software. Stress level at some point is defined as:

$$S = \frac{\left(\overline{\sigma}_1 - \overline{\sigma}_3\right)}{\left(\overline{\sigma}_1 - \overline{\sigma}_3\right)_f} \tag{3.6}$$

where:

$\left(\overline{\sigma}_1 - \overline{\sigma}_3\right)$ = calculated principal effective stress difference at that point and

$\left(\overline{\sigma}_1 - \overline{\sigma}_3\right)_f$ = theoretical principal effective stress difference at failure at that point.

Essentially, this is the ratio of actual shear stress to that required to cause failure. For 2-D solid elements, stress level is typically calculated based on the average stress state existing at the geometric centroid of an element.

Inspection of Equation 3.6 indicates that $S = 0$ defines the isotropic stress state; $S = 1$ soil "failure", i.e. full mobilization of shear strength; and $0 < S < 1$ intermediate conditions. Thus contours of stress levels equal to or approaching one indicate zones where soil failure occurs or is tending to occur. Furthermore, patterns formed by the stress level contours illustrate actual or potential failure zones (or approximately one-dimensional failure surfaces if the contours are closely spaced) within the soil. However, care is required to properly interpret contoured stress levels in lateral earth pressure problems as there is nothing to distinguish a soil failure in the active or passive state. Which is occurring will be clarified in the text of this report.
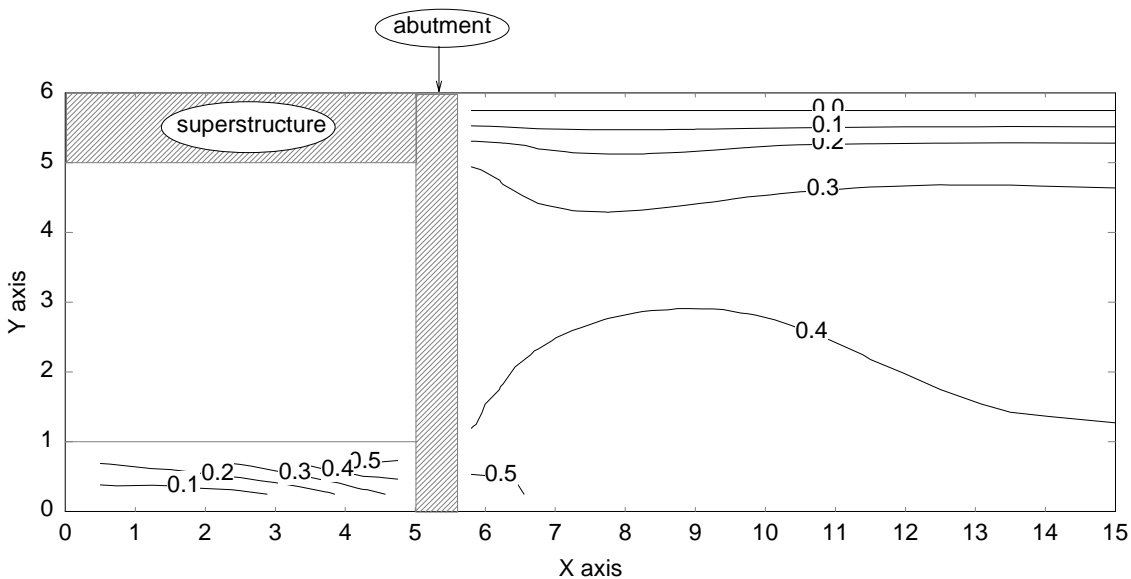
Note: Both axes scaled in metres (1 m = 0.305 ft).

Figure 3.9. Case 1a: Stress Levels at End of Construction

A plot of the stress levels for Case 1a only[20] at the end of construction is shown in Figure 3.9. Much of the retained soil is close to the NC at-rest state ($S \cong 0.4$ for the soil parameters used in this study) except for residual compaction effects near the surface ($S = 0$ for the as-compacted soil in this study) and a slight increase in mobilized strength ($S > 0.4$) on both sides of the abutment near its bottom as a result of the slight outward movement in that area.

3.3.2.3 First Thermal Contraction Peak. The initial post-construction thermal load simulation consisted of a temperature reduction from the post-construction neutral temperature of +10°C (+50°F) to -20°C (-4°F) in three equal decrements of 10°C (18°F). This resulted in the first thermal contraction peak of the bridge. The lateral earth pressures corresponding to this would be expected to be minimum and approach the theoretical active state ($\beta = 0.55$ for the soil parameters assumed in this study). Thus the primary concern for this load case would not be lateral earth pressures *per se* but the development of an active soil "wedge" that would have a downward component of displacement that would result in settlement of the ground surface immediately behind the abutment.
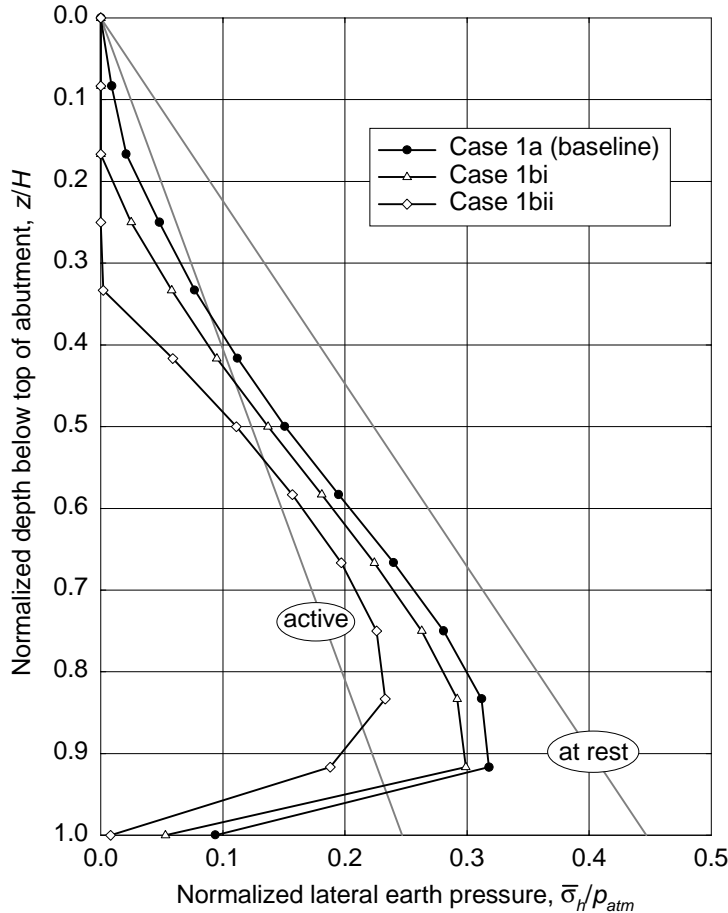
Figure 3.10. Case 1:
Lateral Earth Pressures at First Thermal Contraction Peak

---

[20] Because of the approximate way in which geosynthetic tensile reinforcement was modeled in this study, stress-level contours within the reinforced soil mass for cases 1bi and 1bii were felt to be unreliable so are not shown.

The lateral earth pressures acting on the back of the abutment at this first thermal contraction peak are shown in Figure 3.10. Addressing first the results for the baseline all-soil subcase (1a), the horizontal resultant earth force is reduced significantly ($\beta = 0.68$) from the post-construction at-rest state ($\beta = 0.99$) but did not achieve the theoretical active state ($\beta = 0.55$). The reduction in lateral earth force is due to the fact that contraction of the bridge superstructure pulled the top of the abutment outward (toward the left in Figure 3.7) approximately 9 mm (0.4 in), which is exactly that expected based on theoretical calculations, with a slight (approximately 2 mm (0.1 in)) additional outward translation of the bottom of the abutment. Thus the mode of abutment displacement is primarily rotation about its bottom with a minor translation component. The calculated lateral earth pressure distribution shown in Figure 3.10 is qualitatively consistent with that expected based on prior experimental and theoretical work into the mechanism of arching when the primary displacement mode is rotation about the bottom of an earth retaining structure (Fang and Ishibashi 1986, Harrop-Williams 1989).

The contoured stress levels for Case 1a are shown in Figure 3.11 and give further insight into what is occurring. A zone of active soil failure ($S = 1$) is clearly evident along the upper portion of the abutment due to the relatively large horizontal displacement (toward the left in the figure) in that area. The location of the theoretical planar failure surface for the classical Coulomb active state is also shown in Figure 3.10 for information and broad comparison only.
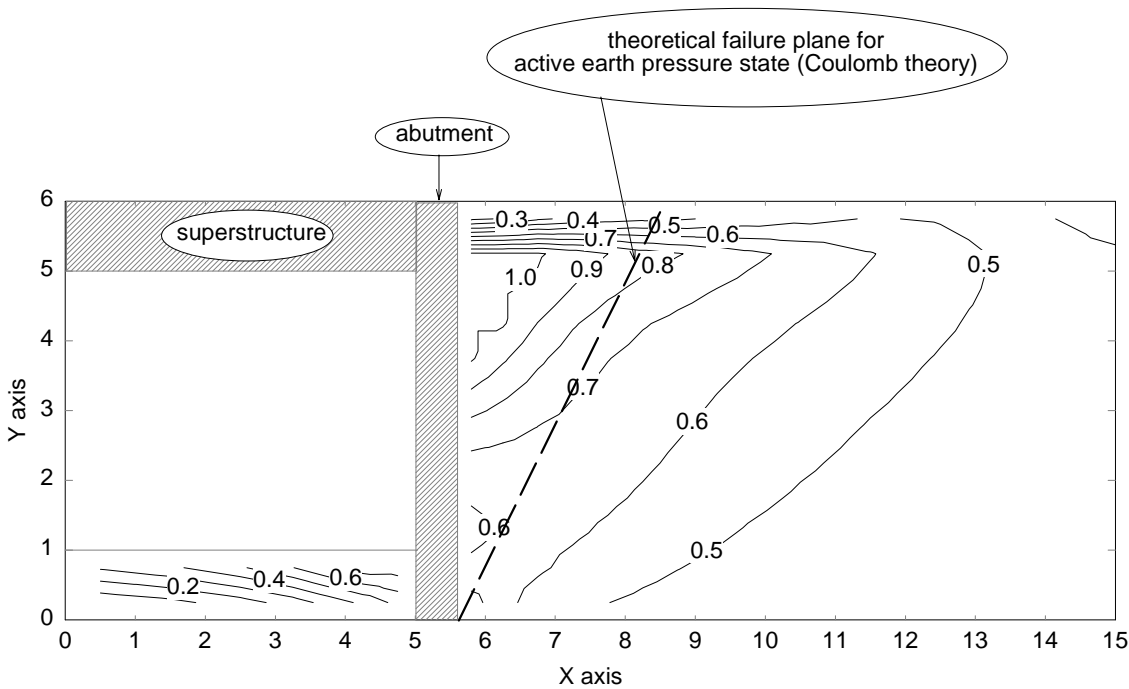
Note: Both axes scaled in metres (1 m = 0.305 ft).

Figure 3.11. Case 1a: Stress Levels at First Thermal Contraction Peak

The lateral earth pressures for the two subcases with reinforcement (1bi and 1bii) are also shown in Figure 3.10. For these subcases, $\beta = 0.60$ and 0.44 respectively. Thus each is less than the soil-only Case 1a ($\beta = 0.68$) indicating that the presence of the reinforcement is somewhat

effective in further reducing lateral earth pressures. This is because the outward movement of the abutment, especially its upper part, allows the reinforcements to strain in tension and develop their intended load carrying capacity. Along the upper portion of the abutment, the horizontal displacement is sufficient for the reinforcement to support all soil loads, especially for the stiffer metallic reinforcements. This suggests that there would likely be some physical separation (gap) between the back of the abutment and reinforced soil mass, assuming the reinforcement was constructed with a wrapped face to contain the soil. In the absence of wrapping, soil particles would tend to fall into this gap. However, the 1-D interface elements in *SSTIPNH* that are used along the vertical abutment-soil interface are not numerically reliable in tension for calculating the exact magnitude of this separation although the calculated results indicated some separation developed.

The settlement of the ground surface immediately behind the abutment is small, approximately 6 mm (0.2 in) for Case 1a and somewhat less for the two subcases with reinforcement. This is consistent with what would be expected based on research by Monley and Wu (1993).

For all three Case 1 subcases there was indication of a slight (of the order of 1 mm) net upward movement of the abutment out of the ground. Whether this was simply a happenstance peculiar to the numerical model used in this study or an actual behavioral characteristic of IABs is not known at this time. If such behavior does indeed occur in actual IABs (it would likely be highly dependent on the type of foundation used among other variables) the combination of upward movement of the abutment and downward movement of the soil immediately behind it would exacerbate the observed problem of void development beneath approach slabs or, in the absence of an approach slab, settlement of the pavement surface behind the abutment.

3.3.2.4 First Thermal Expansion Peak. After the first thermal contraction peak, six equal load increments of 10°C (18°F) each were applied to bring the structure to +40°C (+104°F) and its first thermal expansion peak. As discussed in Section 2.2.2.3, the primary concern when this thermal condition occurs is that lateral earth pressures could approach or even equal the passive state, at least along a portion of the abutment.

The calculated lateral earth pressures at the first thermal expansion peak are shown in Figure 3.12 together with the theoretical active, normally consolidated at-rest and passive states. The results in Figure 3.12 indicate that the calculated lateral earth pressures are above the at-rest state over most of the abutment height but approach the passive state only near the top of the abutment where horizontal displacements are the largest. Overall, $\beta = 1.5, 1.4$ and 1.3 for cases 1a, 1bi and 1bii respectively. These are all above the theoretical at-rest state ($\beta = 1$) but well below the theoretical full passive state ($\beta = 24$).

The increase in β is not surprising as the thermally induced expansion of the bridge superstructure pushed the top of the abutment approximately 20 mm (0.8 in) toward the retained soil relative to the first contraction peak. This is an approximately 10 mm (0.4 in) net inward movement from the initial post-construction position of the abutment top and approximately the maximum expected based on theoretical considerations. This indicates that, from a practical perspective, the retained soil effectively offers no resistance to the tendency of an IAB superstructure to expand thermally and maintain a thermal-stress-free condition. The bottom of the abutment also moved approximately 5 mm (0.1 in) inward toward the retained soil which returned it roughly to its post-construction position. It was of interest to note that this first cycle of superstructure expansion caused the top of the abutment to move further slightly upward and out of the ground, continuing the trend noted previously.
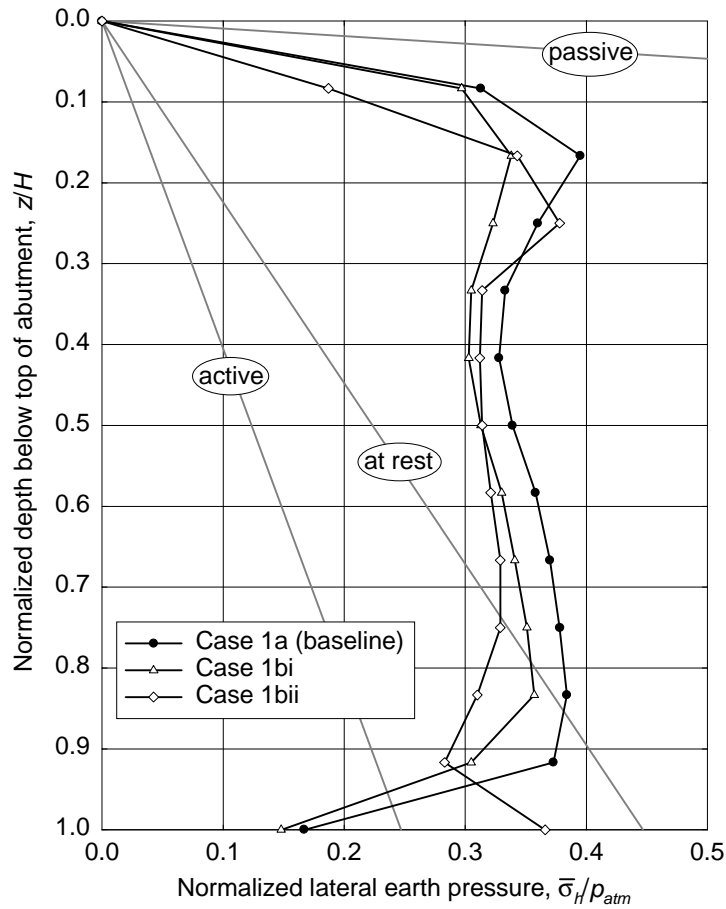
Figure 3.12. Case 1:
Lateral Earth Pressures at First Thermal Expansion Peak

The stress-level contours for Case 1a are shown in Figure 3.13 and illustrate the complex developments reflected in Figure 3.12. Along the upper portion of the abutment, stress reversal has occurred so the horizontal stresses exceed the vertical and the soil is tending toward a passive failure ($S = 1$). With increasing depth, stress reversal is still developing so the stresses tend toward isotropic ($S = 0$). Finally, near the bottom the vertical stresses still exceed the horizontal and conditions are close to the NC at-rest state ($S \cong 0.4$). The location of the theoretical planar failure surface for the classical Coulomb passive state is also shown in Figure 3.13 for broad comparison only.
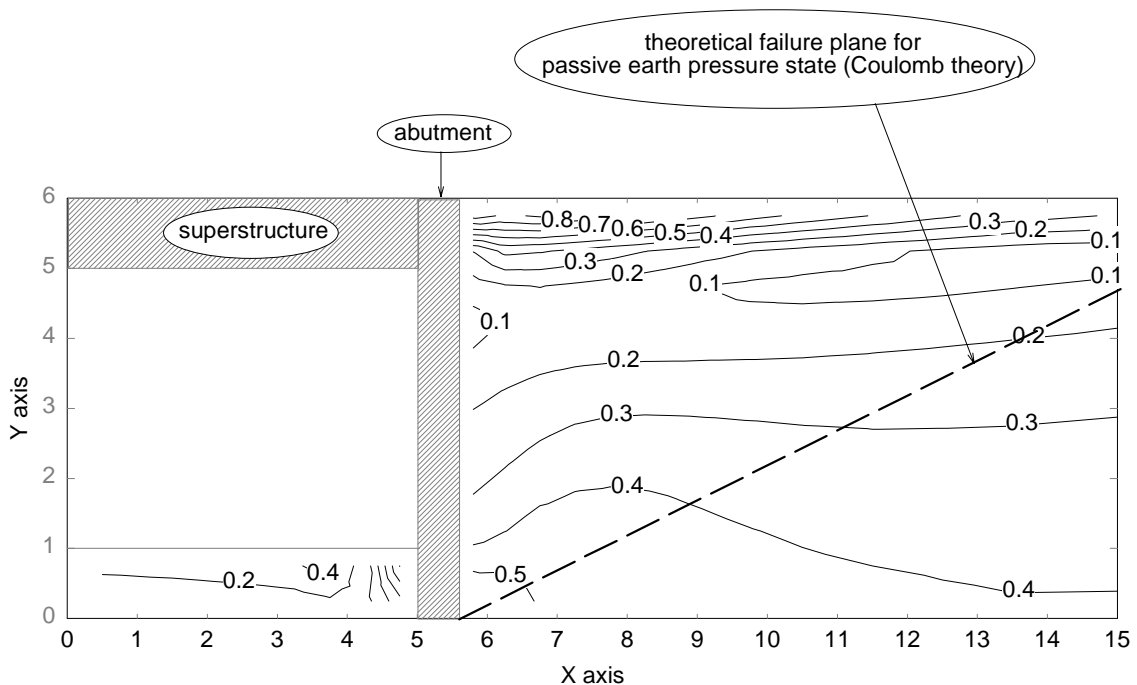
Note: Both axes scaled in metres (1 m = 0.305 ft).

Figure 3.13. Case 1a: Stress Levels at First Thermal Expansion Peak

3.3.2.5 End of First Thermal Cycle. After the first thermal expansion peak, three load decrements of 10°C (18°F) each were applied to bring the structure back down to its neutral temperature of +10°C (+50°F) and complete one full thermal cycle. The calculated lateral earth pressures for this condition are shown in Figure 3.14. The results for Case 1bii with metallic reinforcement are not shown as they were of questionable accuracy based on visual inspection of the plotted results. This suggests that the procedure of activating and deactivating the nodal-link elements, which model the geosynthetic reinforcement, depending on the loading step to prevent compressive forces from developing within the reinforcements is not totally successful in meeting its intended objectives, at least for this particular analysis. Also shown in Figure 3.14 for comparative purposes are the end-of-construction results for the baseline Case 1a (the end-of-construction results for Case 1bi were similar) and the usual theoretical earth pressure states.
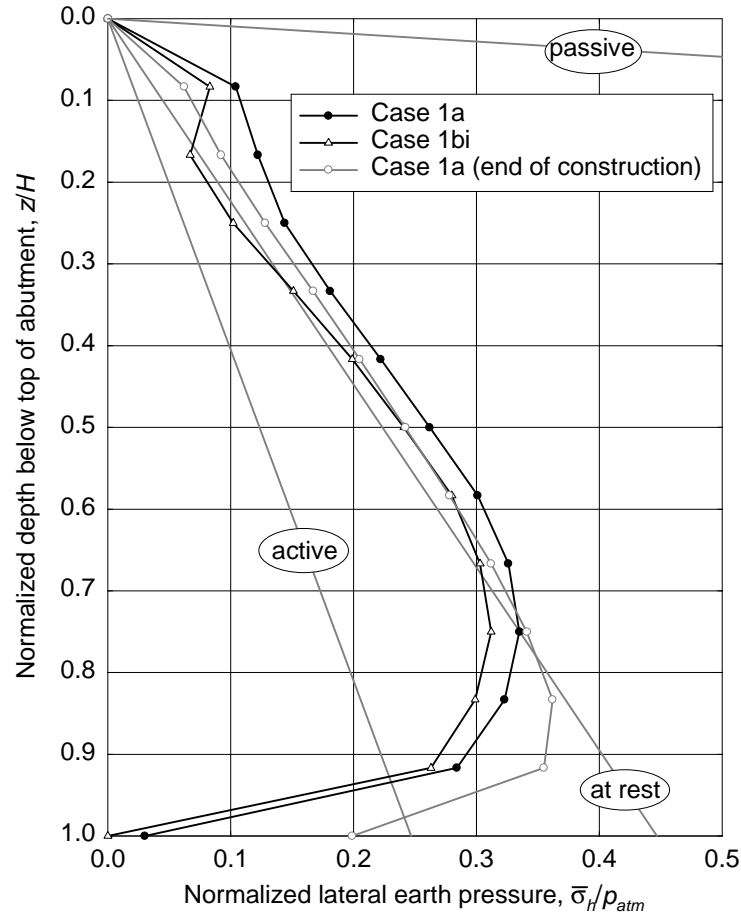
Figure 3.14. Case 1:
Lateral Earth Pressures at End of First Thermal Cycle

Overall, after one complete thermal cycle the horizontal resultant forces were actually slightly lower compared to the end of construction (Case 1a decreased marginally from $\beta = 0.99$ to 0.98, Case 1bi slightly from $\beta = 0.92$ to 0.86) although this is somewhat misleading as there was a noticeable redistribution of the lateral earth pressures. The slight reductions in resultant force were due solely to the fact that the bottom of the abutment moved a few millimetres outward (5 mm (0.2 in) for Case 1a) from its original position and relieved pressures locally near the bottom of the abutment. On the other hand, even though the top of the abutment returned to its post-construction position lateral earth pressures remained somewhat above their post-construction magnitudes in that area suggesting a tendency to build lateral earth pressures, at least along the upper portion of the abutment adjacent to the superstructure, due to thermal cycling.

The stress-level contours for Case 1a are shown in Figure 3.15 and illustrate the very complex conditions reflected in Figure 3.14. At the top of the abutment, stress reversal has occurred such that horizontal stresses still exceed the vertical and the soil is tending toward a passive failure ($S = 1$) even though the top of the abutment has essentially returned to its as-built position. Slightly below that, stress reversal is still developing so the stresses tend toward isotropic ($S = 0$). At a point that is approximately mid-height of the abutment, the vertical stresses still exceed the horizontal and conditions are close to the NC at-rest state ($S \cong 0.4$). Then at the very bottom of the abutment the stress levels increase again but this time reflecting the net outward movement of

the bottom of the abutment and the localized development of the active state. Consistent with this, the stress levels along the outside face of the abutment are increasing toward a passive failure ($S = 1$).
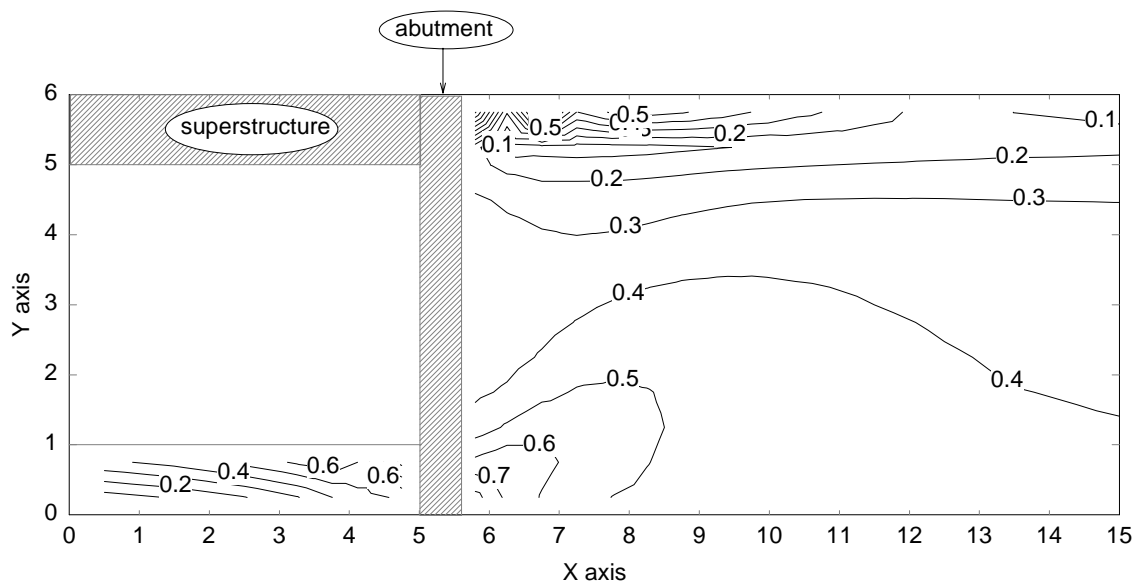
Note: Both axes scaled in metres (1 m = 0.305 ft).

Figure 3.15. Case 1a: Stress Levels at End of First Thermal Cycle

The complexity of the stress patterns within the soil are even more apparent when Figure 3.15 is compared to Figure 3.9 which shows the stress levels at the end of construction and beginning of the first thermal cycle. Although the bridge is at the neutral temperature in both figures, the tendency for even one thermal cycle to lock in higher lateral earth pressures near the top of the abutment where the horizontal displacement range is greatest is quite evident.

The entire abutment continued to move upward as it had from the very first thermal-load application. At this point, the abutment was approximately 1 mm (0.04 in) higher than its post-construction position. Again, whether this reflects only some aspect peculiar to this numerical model or an actual behavioral pattern of IABs is not known at this time.

3.3.2.6 Fourth (Final) Thermal Expansion Peak. After the first full thermal cycle, additional load decrements and increments of 10°C (18°F) each were applied to bring the structure down to -20°C (-4°F), up to +40°C (+104°F) and back to the neutral temperature through three complete thermal cycles. The results for these intermediate loadings were judged not to be significant for the objectives of this report so are neither presented nor discussed further. The next load of interest was judged to be toward the end of the fourth (and final in this study) thermal cycle when the fourth and final thermal expansion peak was reached. The primary interest here was to see if there was a net buildup of lateral earth pressures with loading cycles for the critical summer expansion condition.
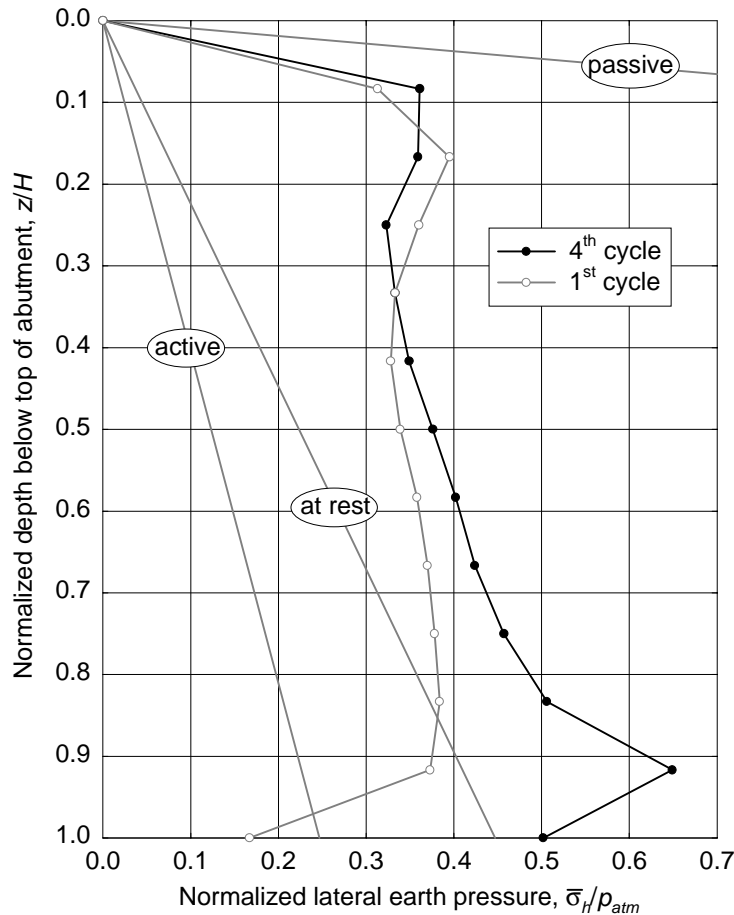
Figure 3.16. Case 1a:
Lateral Earth Pressures at Thermal Expansion Peaks

The calculated lateral earth pressures for this load are shown in Figure 3.16 for Case 1a only. The results for Case 1bi with polymeric reinforcement were of questionable accuracy and those for Case 1bii with metallic reinforcement were clearly incorrect. Again, this was believed due to the approximate way in which the reinforcement stiffness was modeled during load cycles that would tend to produce compression in the reinforcements. Also shown in Figure 3.16 for comparative purposes are the results of the first expansion peak for Case 1a and the usual theoretical earth pressure states.

Overall, from the first to the fourth cycles there was a buildup of lateral earth pressure within the lower half of the abutment, the result of net inward movement of this portion of the abutment. As a result, the value of β for the baseline Case 1a went from 1.5 (first peak) to 1.8 (fourth peak). The contoured stress levels are shown in Figure 3.17 and reflect the trend toward a localized passive failure along the upper portion of the abutment.

As discussed in Section 2.2.2.3, the issue of and problems resulting from increased lateral earth pressures during annual thermal expansion of an IAB superstructure have been recognized since at least the 1960s. Therefore, it is not surprising that some instrumentation and observation of actual IABs have been made and lateral earth pressure design procedures derived from these observations. At this point, it is of interest to compare the calculated results obtained in this study to some of these other observations and design methods. Figure 3.18 shows the following:
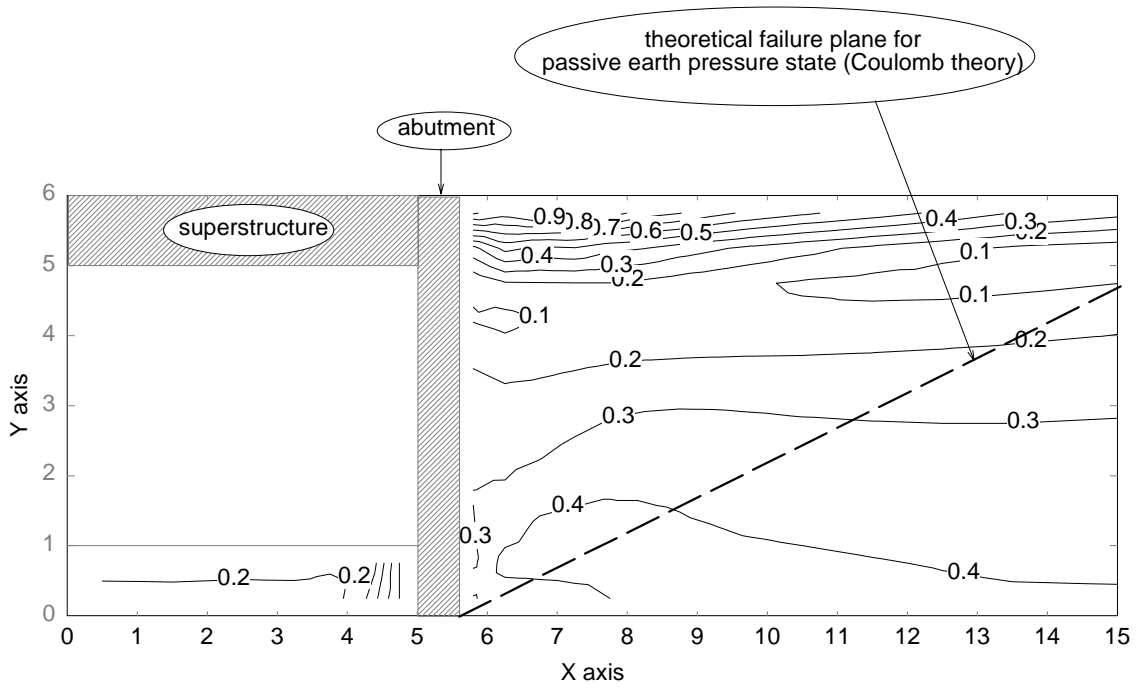
Note: Both axes scaled in metres (1 m = 0.305 ft).

Figure 3.17. Case 1a: Stress Levels at Fourth Thermal Expansion Peak
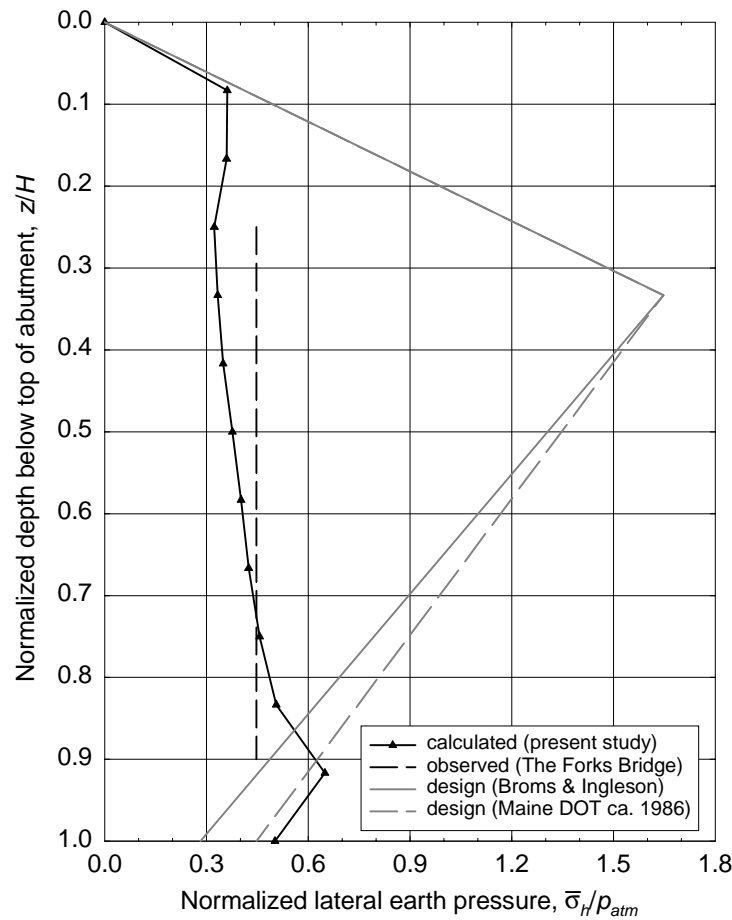
Figure 3.18. Case 1a:
Comparison of Lateral Earth Pressures at Peak Conditions

- The results calculated in this study for the fourth and final thermal peak of baseline Case 1a.

- A trend of observations from The Forks Bridge studied by Sandford and Elgaaly (1993). As discussed in Section 3.2.2.1, the hypothetical bridge used in this study is loosely patterned after this actual IAB. Although the somewhat different variables between The Forks Bridge and the one assumed in this study preclude a direct comparison of results, there are sufficient similarities to at least infer a trend from the results observed for The Forks Bridge. As background information, the trend shown in Figure 3.18 for The Forks Bridge reflects data for the third summer expansion peak experienced by that structure. At that point in time, the bridge had experienced a maximum seasonal temperature variation of approximately 48°C (86°F). This compares to the 60°C (108°F) maximum variation assumed in this study.

- Maximum lateral earth pressure design envelopes proposed by Broms and Ingleson (1971) and a slightly modified version of it as used by the State of Maine Department of Transportation (DOT) circa 1986 (Sandford and Elgaaly 1993). In each method, the lateral

earth pressure is assumed to peak at the theoretical Rankine[21] passive state at a relative depth of H/3 below the top of the abutment. The only difference between the methods is that the original Broms and Ingleson method assumed that below the peak, the lateral earth pressures decreased to the theoretical Rankine active state. On the other hand, the 1986 Maine DOT design envelope assumed a decrease to the normally consolidated at-rest state.

As can be seen, the observed trend inferred from the measured results for The Forks Bridge given by Sandford and Elgaaly (1993) shows remarkable similarity to the calculated results for Case 1a in the present study. Both the Broms and Ingleson and 1986 Maine DOT design envelopes appear to give conservative results overall. However, it should be kept in mind that these design envelopes are presumably intended to cover a 100-plus year design life (which implies 100-plus load cycles) of an IAB whereas both the calculated and observed results are for far fewer load cycles and, therefore, a far shorter period of time. In addition, both design envelopes are significantly less conservative than using the theoretical passive pressure over the full height of the abutment. This can be seen in Table 3.4 using the concept of normalized horizontal resultant earth force, β, that was developed for use in this study.

Table 3.4. Case 1a: Comparison of β Values for Unreinforced Soil Backfill/Fill

method		β
calculated (baseline Case 1a - 4th cycle expansion peak)		1.8
simplified design envelopes	Broms and Ingleson (1971)	4.1
	State of Maine DOT (1986)	4.8
theoretical (full passive from "exact" theory)		24

With regard to displacements, the entire abutment continued to move upward as it had from the very first load application. At this point the abutment was approximately 5 mm (0.2 in) higher than its post-construction position. No importance is placed on this calculated result until observation of actual IABs and/or realistic physical modeling (e.g. in a geotechnical centrifuge) at least qualitatively confirms or refutes this behavior.

3.3.2.7 End of Fourth (Final) Thermal Cycle. The thermal loading simulation for Case 1 ended with the application of three additional load decrements to complete four full cycles of thermally induced contraction and expansion and return the problem to the +10°C (+50°F) neutral condition it started from after construction. The final distribution of calculated lateral earth pressures is shown in Figure 3.19, again for Case 1a only as the results from both Case 1b subcases were clearly in error. For comparison, also shown are the pressures immediately after construction as well as after one full thermal load cycle.

---

[21] Theoretically, the classical Rankine solutions for lateral earth pressures in the active and passive states should never be used in earth retaining structure problems. This is because Rankine's solutions were developed assuming free-field conditions so that complementary planar failure surfaces could develop without interference from the presence of an earth retaining structure. However, most geotechnical engineers (practitioners and academicians alike) routinely ignore this fact and use Rankine's solutions in earth retaining structure problems. The fact that Rankine's solutions yield the same numerical results as Coulomb's solutions (a "true" retaining wall solution) with a zero soil-wall friction angle, δ, further adds to the confusion.
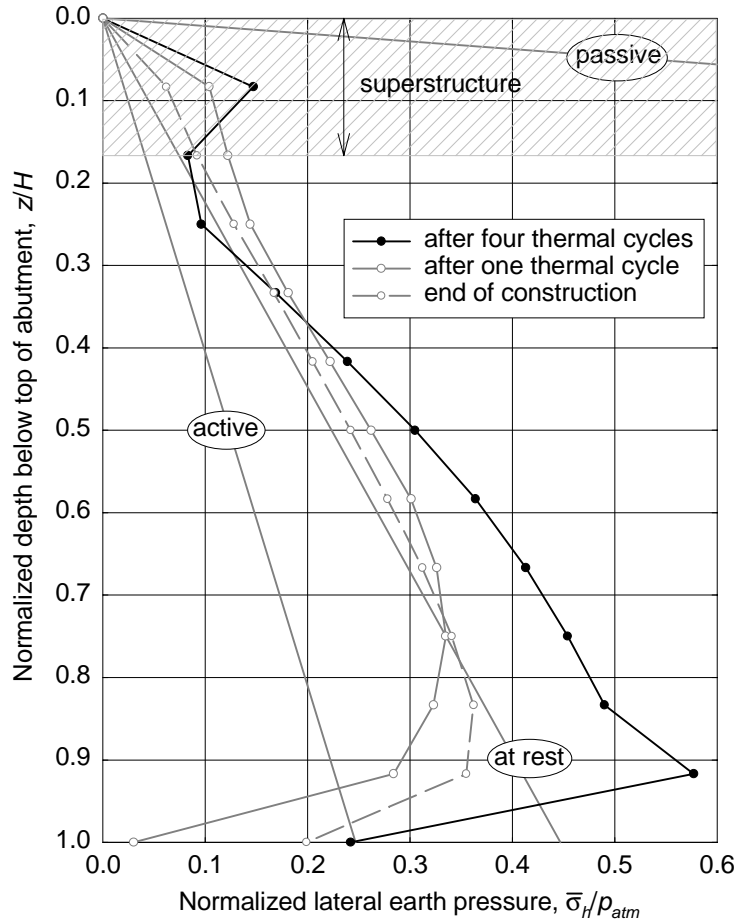
Figure 3.19. Case 1a:
Comparison of Lateral Earth Pressures at Neutral Temperature

As can be seen in this figure, after four thermal cycles lateral earth pressures increased over most of the abutment compared to earlier stages, including continued development of a peak near the top is where it appears the soil has become wedged behind the relatively stiff superstructure. The contoured stress levels in Figure 3.20 clearly show the development of relatively large lateral earth pressures near the top of the abutment that approach the passive state ($S = 1$). Overall, β went from 0.99 before any thermal loading to 1.3 after four thermal cycles indicating a net increase of resultant earth force of approximately 30% from the end of construction.
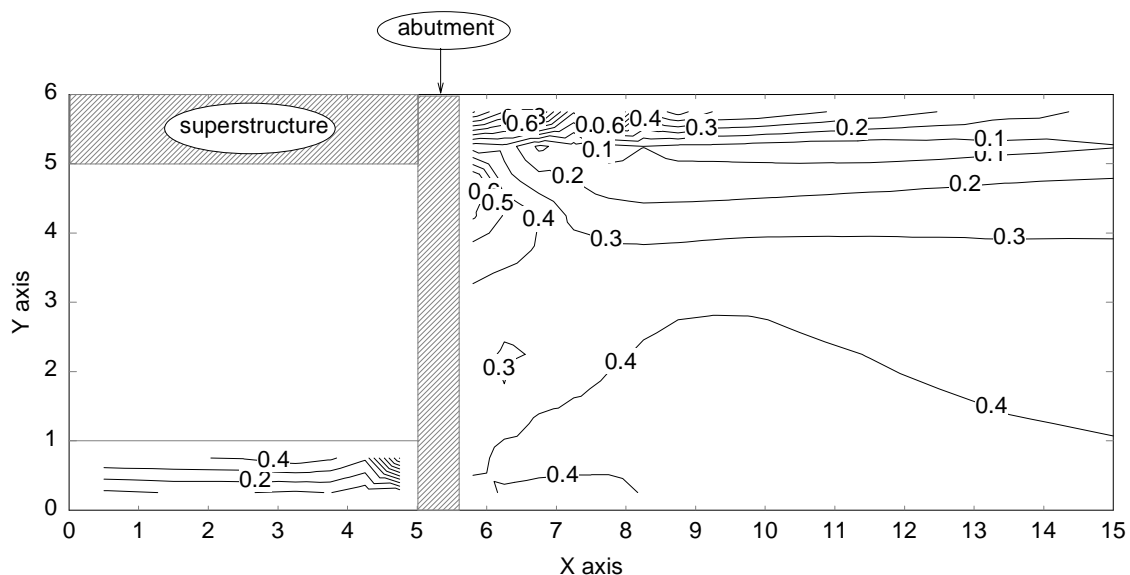
Note: Both axes scaled in metres (1 m = 0.305 ft).

Figure 3.20. Case 1a: Stress Levels at End of Fourth Thermal Cycle

With regard to displacements, at the top of the abutment there was a residual net horizontal movement of approximately 4 mm (0.2 in) into the retained soil (toward the right in Figure 3.20) compared to the initial post-construction position. This is the opposite of what has often been observed in practice where the abutment permanently moves away from the retained soil as shown qualitatively in figures 2.5 and 2.6. This may have been at least partially due to the fact that long-term shrinkage of PCC members was not simulated in this study. Another factor may be the inability of the hyperbolic soil model used to properly model the hysteretic soil behavior under cyclic loading and/or the tendency of the soil retained by the abutment to slump downward with each thermal contraction cycle. The bottom of the abutment had no net movement, essentially returning to its initial post-construction location.

The top of the abutment exhibited a net upward movement of approximately 4 mm (0.2 in) and the surface of the soil immediately behind the abutment had a net settlement of 3 mm (0.1 in) for a total difference in elevation (which would appear as a void under an approach slab or pavement settlement in the absence of a slab) of approximately 7 mm (0.3 in). While at the lower end of the magnitude of voids actually measured in practice, the qualitative development of a void was nonetheless observed.

3.3.3 Case 2: Resilient EPS-Block Geofoam as a Compressible Inclusion

3.3.3.1 Introduction. The primary focus of Case 2 was evaluating the benefit(s) of using a resilient-EPS geofoam compressible inclusion behind the abutment as shown in Figure 3.21. Note that the inclusion was intentionally extended to the ground surface. As noted by Murphy (1997), it is generally desirable to use a compressible inclusion for as much of a wall's height as is practicable to derive maximum benefit from the use of the inclusion. However, in practice it is sometimes necessary to terminate the compressible inclusion short of the surface to allow for a road pavement, etc. In the case of an IAB, it was assumed that the area immediately behind the abutment would be spanned by an approach slab which would allow the compressible inclusion to be extended to the surface.

Note: Both axes scaled in metres (1 m = 0.305 ft).
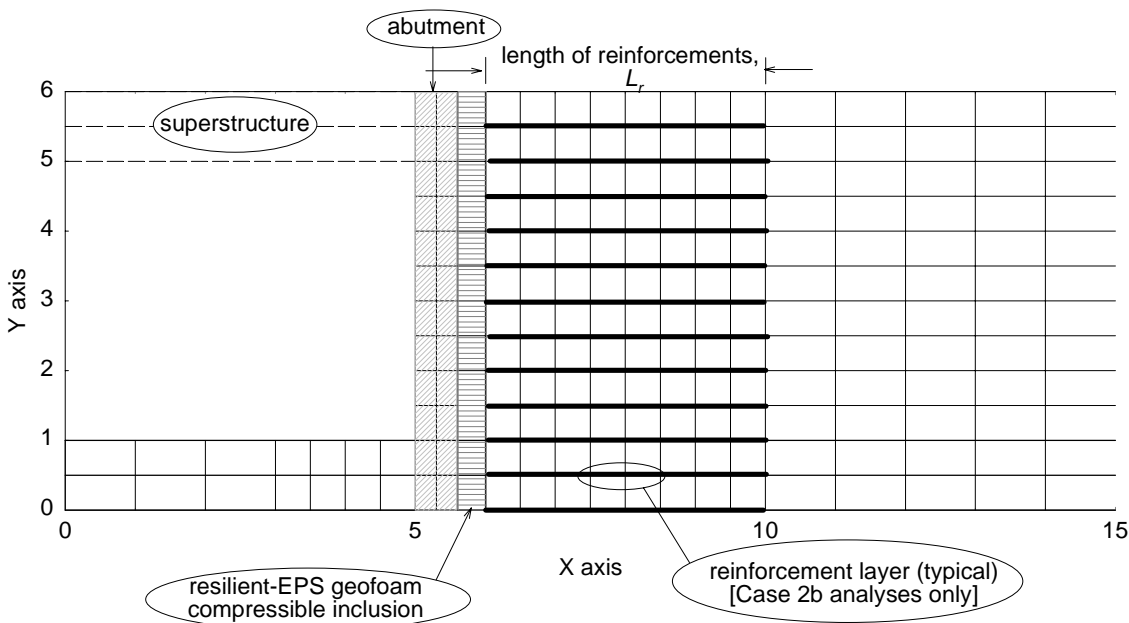
Figure 3.21. Case 2: FEM Mesh (partial)

There were two groups of analyses performed for Case 2, cases 2a and 2b. Case 2a consisted of three subcases (2ai, 2aii and 2aiii) to evaluate the effect of the compressible inclusion thickness, t_{ci}, on the results. The assumed thicknesses were 100 mm (4 in), 200 mm (8 in) and 400 mm (16 in) respectively. These reflect dimensionless thickness-to-wall-height ratios, t_{ci}/H, of 0.017, 0.033 and 0.067 respectively. These values are within the range typically used in earth retaining structure applications for a compressible inclusion material with a Young's modulus as assumed in this study (Karpurapu and Bathurst 1992).

Note, however, that in the FEM analyses the actual width of the elements that comprised the compressible inclusion was fixed at 400 mm (16 in) for all Case 2a analyses as shown to scale in Figure 3.21 to avoid having to revise the FEM mesh for each change in compressible inclusion thickness. The desired variation in inclusion thickness was simulated by varying the Young's modulus of the geofoam material. This makes use of the fact that a parameter more insightful

than either the Young's modulus of the inclusion material or the inclusion thickness taken individually is the *stiffness* of the inclusion. This stiffness is defined as E_{ci}/t_{ci}, the ratio of the Young's modulus of the inclusion material to its thickness. This stiffness parameter has dimensions of force per length cubed, better interpreted as force per unit length (an equivalent spring stiffness) per unit area. Thus to simulate a 100 mm (4 in) thick inclusion, for example, within the actual 400 mm (16 in) width of the elements the actual value of E_{ci} (reflected in the values of K and K_b in Table 3.2) was multiplied by four.

While the stiffness ratio, E_{ci}/t_{ci}, is a useful parameter it is even more useful to define a dimensionless stiffness parameter. As discussed in Section 3.3.1, dimensionless parameters can be powerful tools for portraying results provided they incorporate the key individual parameters that affect a particular problem. For compressible inclusions used behind earth retaining structures, the key parameters of interest are the Young's modulus and thickness of the compressible inclusion, and geotechnical height of the wall. Therefore, the author proposes using a dimensionless parameter, λ, called *normalized compressible inclusion stiffness* defined as

$$\lambda = \frac{E_{ci} \cdot H}{t_{ci} \cdot p_{atm}} \qquad \textbf{(3.7)}$$

where all terms are as defined previously. Note that atmospheric pressure is used here solely as a tool to non-dimensionalize the parameter and has no physical significance per se.

For the three subcases performed for Case 2a, λ = 149, 74 and 37 for inclusion thicknesses of 100 mm (4 in), 200 mm (8 in) and 400 mm (16 in) respectively. Thus the interpretation of λ is that the smaller its magnitude the more compressible the inclusion. The limiting conditions of incompressibility (perfect rigidity) and infinite compressibility (perfect compressibility) are seen as λ = ∞ and λ = 0 respectively. Hopefully, use of the λ parameter will facilitate comparison in the future between compressible inclusions constructed of different materials and thicknesses and applied to earth retaining structures of different types and heights.

Case 2b consisted of two subcases (2bi and 2bii) in which tensile reinforcement was embedded within the retained soil as shown in Figure 3.21 in addition to using a compressible inclusion. Conceptually, the Case 2b analyses were a combination of Case 1b (reinforced soil only) and Case 2a (geofoam compressible inclusion only) to investigate the author's hypothesis that synergistic results would derive from the combination of these two already proven concepts. The two Case 2b subcases differed only in the reinforcement stiffness assumed, polymeric and metallic respectively. The compressible inclusion thickness was fixed at 200 mm (8 in) to focus on the effect of the reinforcement. The length, L_r, of the reinforcements in both subcases was 4.0 m (13.1 ft). This was slightly (100 mm (4 in)) longer than that assumed in Case 1b due to the geometry of the FEM mesh used. However, the overall stiffness of the nodal-link elements used to simulate the reinforcements was kept the same as in Case 1b. The reinforcement length to wall height ratio, L_r/H, = 0.67 which again is within the range of typical values for MSEW and was assumed to be sufficient so that reinforcement pullout would not occur.

The various stages of the analyses at which the calculated Case 2 results were evaluated are the same as used previously for Case 1 and discussed in the following sections. However, for clarity separate presentations are made for cases 2a and 2b. Comparisons between the Case 2a and Case 2b results are contained within the Case 2b sections.

Note that in all Case 2 plots of lateral pressure[22] acting on the abutment the values for the horizontal component of the theoretical active state were assumed to be the same as for Case 1.

---

[22] Technically not earth pressures as it is the geofoam compressible inclusion, not soil, that is in direct contact with the back of the abutment.

Strictly speaking, this is not correct as the friction angle between the abutment and retained material was not the same due to the presence of the geofoam compressible inclusion. However, choosing the correct friction angle for the Case 2 analyses is complicated by the fact that the friction angles assumed for the soil-geofoam and geofoam-abutment interfaces were different. Consequently, the author chose to use the same results as for Case 1 as being acceptably correct for the purposes of this report.

3.3.3.2 End of Construction (Case 2a). The first set of results examined is at the completion of the simulated construction of the bridge and associated earthwork. The calculated lateral pressures acting on the back of the abutment are shown in Figure 3.22. Also shown for absolute comparative purposes are the theoretical active and normally consolidated at-rest state pressures for a soil backfill/fill (from Case 1) as well as the calculated results from the baseline Case 1a. Note that the theoretical at-rest state ($\beta = 1$) represents an idealized, perfectly rigid inclusion ($\lambda = \infty$) as does Case 1a ($\beta = 0.99$) for all practical purposes although the lateral pressure distributions are somewhat different. Also, a vertical line drawn through zero normalized lateral pressure (the left vertical axis in Figure 3.22) represents an infinitely compressible inclusion ($\lambda = 0$).
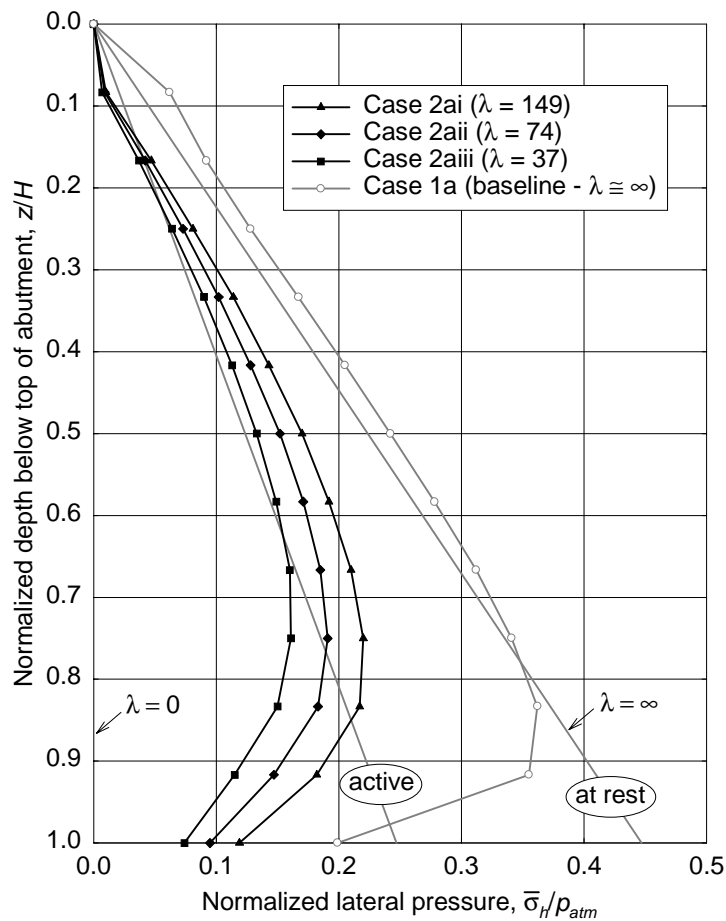
Figure 3.22. Case 2a:
Lateral Pressures at End of Construction

The Case 2a results are qualitatively consistent with those determined numerically in the past by Horvath (1991a) and Karpurapu and Bathurst (1992) for the basic, generic application of a geofoam compressible inclusion against a rigid, non-yielding wall (the Reduced Earth Pressure (REP) Wall concept). The results are also consistent qualitatively with what would be predicted theoretically for arching induced by the translation mode (Harrop-Williams 1989). Note that the normalized depth, z/H, at which the peak lateral pressure occurs is approximately 0.75, not 1.0, as theoretical classical earth pressure solutions with their simple triangular distributions always predict.

In all cases, the lateral pressures are reduced significantly from the baseline Case 1a ($\beta = 0.99$) reflecting the expected beneficial result from using a compressible inclusion with a rigid, non-yielding earth retaining structure. Quantitatively, $\beta = 0.61$, 0.53 and 0.45 for cases 2ai, 2aii and 2aiii respectively. By linear interpolation, the implication is that a compressible inclusion 175 mm (7 in) thick would be sufficient to mobilize the active state. Note that for the purposes of this study, achieving the active state is taken to be satisfied by simply matching the β value for the active state ($\beta = 0.55$) and not necessarily matching the classical triangular distribution of earth pressure. This is consistent with the criterion used in a related study by Karpurapu and Bathurst (1992) that was discussed in Section 3.3.1.4.
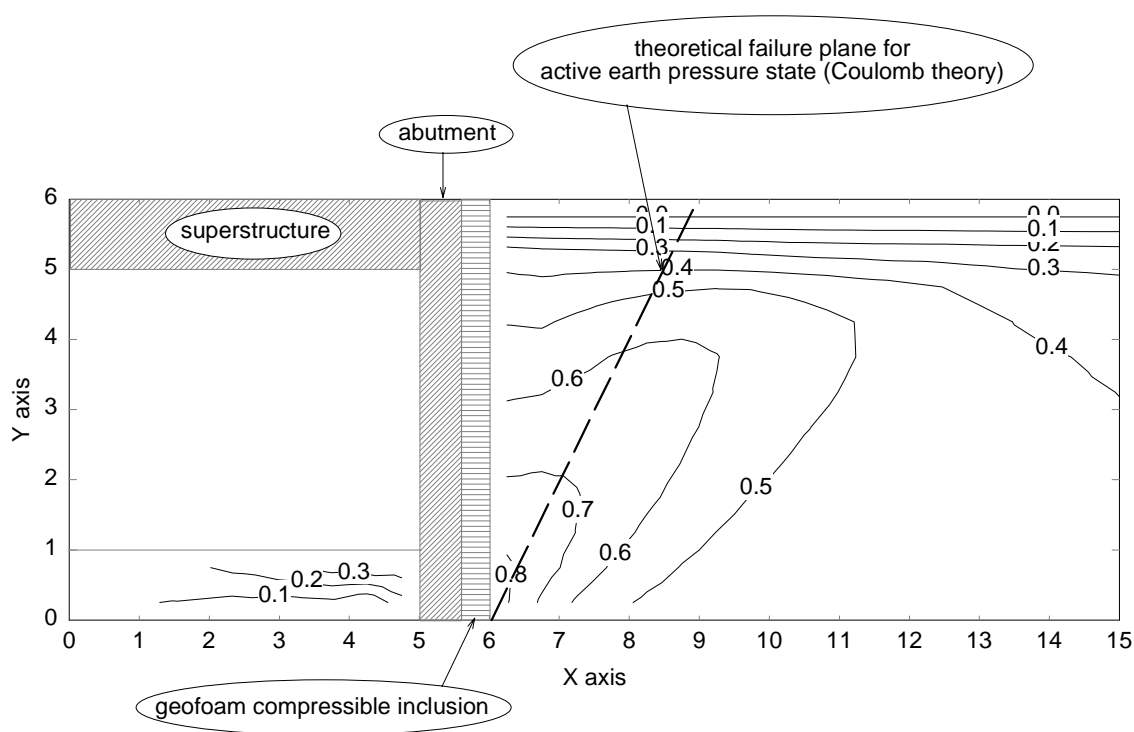
Note: Both axes scaled in metres (1 m = 0.305 ft).

Figure 3.23. Case 2aii: Stress Levels at End of Construction

Figure 3.23 shows the contoured stress levels for Case 2aii (200 mm (8 in) compressible inclusion) only. This subcase had a $\beta = 0.53$ that was, for all practical purposes, the same as the classical active state ($\beta = 0.55$). The contours suggest development of a failure zone that resembles that assumed by Coulomb's classical theory for the active state.

Whenever a compressible inclusion is used, it is of interest to investigate both the pattern and magnitude of deformation (horizontal in this application) of the compressible inclusion. As shown in Figure 3.24, there are two dimensionless interpretations of this. Figure 3.24(a) shows the horizontal normal strain, ε_h, within the geofoam. As can be seen, strain decreases with increasing thickness of the inclusion. However, the magnitude of horizontal compression (strain times inclusion thickness), Δ_{ci}, increases with increasing geofoam thickness, ranging from 10 mm (0.4 in) to 29 mm (1.1 in). In all cases the strain is well within the limits of the material[23] and consistent with the stress-strain range over which the chosen Young's modulus of the geofoam is applicable (see figures 3.2 and 3.4).
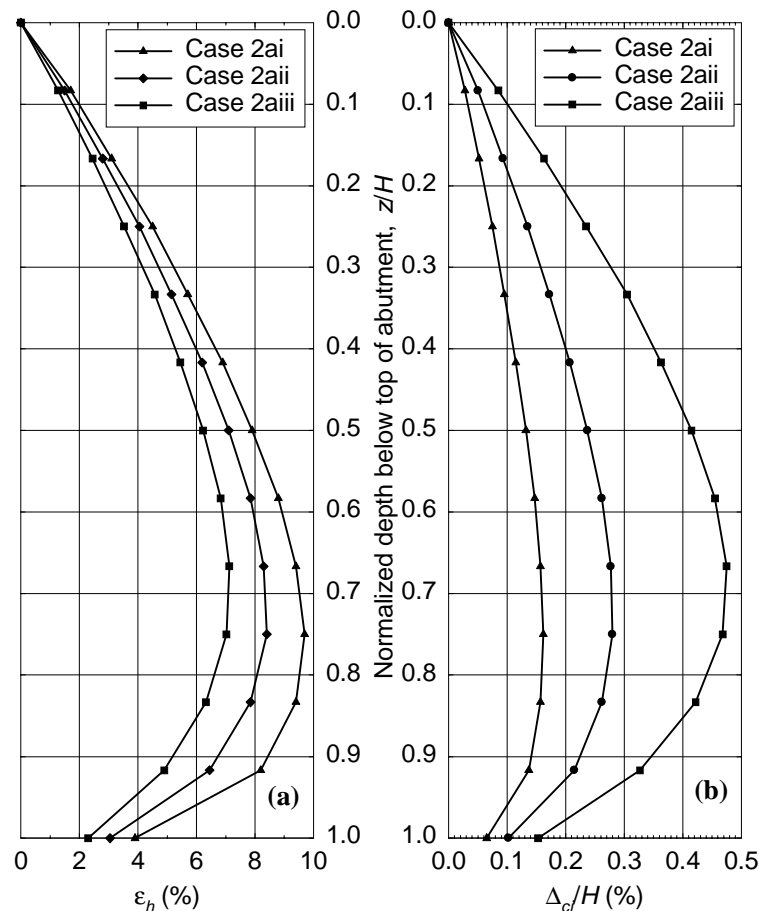
**Figure 3.24. Case 2a: Horizontal Deformation of
Geofoam Compressible Inclusion at End of Construction**

Figure 3.24(b) shows the horizontal compression of the geofoam normalized to abutment height, expressed as a percent (the decimal form could be used alternatively). This ratio increases

---

[23] Compressive strains up to approximately 50% in the long term are generally considered to be an acceptable working range for EPS geofoam (either normal or resilient) in compressible inclusion applications. The reason for this approximate upper strain limit is that as compressive strains approach 60 to 70%, the stress required to compress the EPS further begins to increase rapidly and non-linearly which reduces the effectiveness of the material as a compressible inclusion (see Figure 3.2).

with increasing inclusion thickness. This plot is of interest as it allows comparison with the $(\Delta_s/H)_a$ ratios discussed in the following section that deals with alternative calculation methods.

Regardless of the parameter chosen, the deformation patterns of the compressible inclusion reflect the lateral pressure distributions shown in Figure 3.22. This is to be expected as the geofoam that comprises the compressible inclusion in this study has linear stress-strain behavior within the stress range in this problem.

3.3.3.3 Discussion of Simplified Methods for REP-Wall Analysis. Using a geofoam compressible inclusion with a rigid, non-yielding earth retaining structure in what is called the Reduced Earth Pressure (REP) Wall concept is one geofoam application for which analytical methods other than a FEM numerical analysis have been developed. This is because the broad applicability of the REP-Wall concept makes simplified analytical methods very attractive for use in practice.

The abutment of an IAB with a compressible inclusion at the end of construction and prior to any post-construction thermal loading is an example of a REP-Wall application. Thus before continuing with a discussion of the results of this study, it is of interest to digress and compare results obtained from simpler, alternative analytical methods with the rigorous results from the FEM analyses performed for this study.

First considered are chart solutions developed by Karpurapu and Bathurst (1992). Using either Figure 9 or 11 in their paper and assuming a compressible inclusion with a Young's modulus = 250 kN/m^2 (5200 lb/ft^2) to match the resilient-EPS geofoam modeled in this study, a compressible inclusion approximately 150 mm (6 in) thick would be required to mobilize the active earth pressure state. The agreement with the 175 mm (7 in) thickness inferred from the FEM analyses performed for this study is very good. However, it should be noted that Karpurapu and Bathurst used the same soil parameters as in this study (from the work of Boscardin et al. (1990)). Thus the agreement may reflect the fact that the same soil was assumed in both the present study and that of Karpurapu and Bathurst. Nevertheless, the agreement is reassuring.

It is also of interest to explore a simple manual calculation method (referred to herein as Version 1.1) suggested by the author (Horvath 1997, 1998b) that is a modified version of a procedure suggested originally (referred to herein as Version 1.0) by Partos and Kazaniwsky (1987). The general equation for this method is:

$$t_{ci} = \frac{E_{ci} \cdot \left(\Delta_s / H\right)_a}{K_{hh} \cdot \gamma_t} \qquad \textbf{(3.8)}$$

where:

K_{hh} = the horizontal component of the coefficient of lateral earth pressure,

$(\Delta_s/H)_a$ = dimensionless ratio of minimum horizontal displacement, Δ_s, of soil to geotechnical wall height, H, necessary to achieve the active earth pressure state

and the other terms were defined previously.

For historical interest, Version 1.0 of Equation 3.8 suggested by Partos and Kazaniwsky (1987) assumed $K_{hh} = K_{onc}$, the coefficient of lateral earth pressure at rest for the normally consolidated condition, which results in the following equation:

$$t_{ci} = \frac{E_{ci} \cdot \left(\Delta_s / H\right)_a}{K_{onc} \cdot \gamma_t} \qquad \textbf{(3.9)}$$

The author believes assuming $K_{hh} = K_{onc}$ is conceptually incorrect for the reasons discussed in Horvath (1987, 1988b). This led to development of the author's Version 1.1, first published in Horvath (1987, 1988b), in which $K_{hh} = (K_a \cdot \cos \delta)$ was assumed where K_a = the active earth pressure coefficient from either exact or Coulomb (but never Rankine) theory and δ = the soil-geofoam friction angle. This results in the following equation for the author's Version 1.1:

$$t_{ci} = \frac{E_{ci} \cdot \left(\Delta_s / H \right)_a}{K_a \cdot \cos\delta \cdot \gamma_t} \tag{3.10}$$

It is of interest to note that Partos and Kazaniwsky's Version 1.0 produces a significantly smaller value for t_{ci} than the author's Version 1.1. Nevertheless, Partos and Kazaniwsky's bold and innovative actual project use of geofoam in the early 1980s for what is now known as the REP-Wall concept was successful in achieving the desired goal due both to their arbitrary increase, based on engineering judgement, of the t_{ci} actually used (Partos and Kazaniwsky 1987) as well as the subsequent creep of the geofoam material (Murphy 1997).

The primary element of subjectivity when using Equation 3.8 in general is the value chosen for $(\Delta_s/H)_a$. Guidance can be obtained from a number of sources with Clough and Duncan (1991) being typical and the reference used by the author for this study. Using their value of $(\Delta_s/H)_a$ = 0.002 for medium-dense sand (which implies that a displacement of 12 mm (0.5 in) is necessary to mobilize the active state for the IAB problem considered in this study) and the author's Version 1.1 (Equation 3.10), the calculated value of the required geofoam thickness, t_{ci}, = 140 mm (5.5 in). This is in fair agreement with the results inferred from the FEM analyses for this study (t_{ci} = 175 mm (7 in)) but, more importantly, unconservative. Note that using Version 1.0 of Partos and Kazaniwsky (Equation 3.9), the required geofoam thickness, t_{ci}, = 66 mm (2.6 in) which is in even poorer agreement with the FEM results and more unconservative.

As an aside, the assumed value of $(\Delta_s/H)_a$ = 0.002 = 0.2% can be compared to the FEM results plotted in Figure 3.24(b). Note that it is consistent with a result intermediate (t_{ci} = 175 mm (7 in)) between cases 2ai and 2aii (200 mm (4 in) and 200 mm (8 in), respectively) which is the inferred thickness of geofoam necessary to mobilize the active earth force in this problem.

Returning to the discussion of simplified analytical methods, it is clear that the author's current Version 1.1 (Equation 3.10) should be improved. It is of interest to note that both versions 1.0 and 1.1 are based on the assumption from classical earth pressure theories that the maximum lateral earth pressure, whether for the at-rest state (Version 1.0) or active state (Version 1.1), occurs at z/H = 1.0. This is based on the assumption that the distribution of the horizontal component of lateral earth pressure always has the classical triangular distribution. The results obtained in this study as well as numerous other studies involving theoretical work based on arching concepts, numerical analyses and physical testing consistently show that the actual distribution of lateral (earth) pressures is curved and qualitatively identical to those shown in Figure 3.22. The only variation observed between different studies is the depth at which the peak pressure occurs. This appears to be dependent on the boundary condition imposed at the bottom, i.e. perfectly smooth, perfectly fixed or some intermediate case such as the frictional boundary used in this study.

Because the frictional boundary used in this study is believed to be realistic, to develop an improved Version 1.2 of this methodology a lateral stress peak at z/H = 0.75 which is consistent with that shown in Figure 3.22 is used. The resulting equation is:

$$t_{ci} = \frac{E_{ci} \cdot \left(\Delta_s / H \right)_a}{0.75 \cdot K_a \cdot \cos\delta \cdot \gamma_t} \tag{3.11}$$

Using this equation, the calculated required compressible inclusion thickness for the problem considered in this study increases to 185 mm (7.3 in) which is in much better agreement with the results (175 mm (7 in)) inferred from the FEM analyses performed for this study. Therefore, the author suggests that the procedure suggested previously in Horvath (1997, 1998b) be modified and Equation 3.11 used in lieu of Equation 3.10. Table 3.5 summarizes the results presented in the foregoing paragraphs.

Table 3.5. Comparison of Required Thickness of Compressible Inclusion, t_{ci}, to Achieve the Active Earth Pressure State (REP-Wall Concept)

analytical method		t_{ci}, mm (inches)
inferred from FEM analysis (present study)		175 (7)
charts based on parametric FEM analyses (Karpurapu and Bathurst 1992)		150 (6)
simplified analytical method	Version 1.0 (Partos and Kazaniwsky 1987)	66 (2.6)
	Version 1.1 (Horvath 1997, 1998b)	140 (5.5)
	Versions 1.2 and 2.0 (Horvath, present study)	185 (7.3)

The latest Version 1.2 of this simplified REP-Wall analysis appears to yield reasonably accurate results and can be used in routine practice. The advantage of this method over the charts contained in Karpurapu and Bathurst (1992) is that it can be used with any type of soil by using the appropriate value for $(\Delta_s/H)_a$ from a reference such as Clough and Duncan (1991).

As a final comment, the above sequence of theoretical development ending with Equation 3.11 is based on equating the assumed maximum lateral (earth) pressure with the stiffness of the compressible inclusion. It is of interest to note that an alternative path of theoretical development can be based on using horizontal resultant forces and the dimensionless β parameter that was introduced in Section 3.3.1.4. Such a resultant force approach is used subsequently in Section 3.3.3.10 to develop a simplified analytical method for the Zero Earth Pressure (ZEP) Wall problem involving both a compressible inclusion and tensile reinforcement. Applying a resultant-force approach to the REP-Wall problem produces a result identical to Equation 3.11. Derivation of this resultant-based alternative, which the author calls Version 2.0 of simplified REP-Wall analysis, is presented in Appendix A of this report. The benefit of using Version 2.0 in lieu of the Version 1.X methods discussed in this section is that Version 2.0 provides a unified conceptual approach with the ZEP-Wall analytical method presented subsequently in Section 3.3.3.10.

3.3.3.4 First Thermal Contraction Peak (Case 2a). Returning now to the presentation and discussion of FEM analyses performed for the present study, the lateral pressures at the first thermal contraction peak are shown in Figure 3.25. Corresponding results from the baseline Case 1a are shown together with the theoretical pressures. Modest additional reductions overall from the end of construction condition occur ($\beta = 0.46$ to 0.37 with increasing inclusion thickness), especially along the upper portion of the abutment where pressures drop to zero and a small separation between the abutment and geofoam was calculated. This is due to the fact that contraction of the superstructure pulled the top of the abutment outward approximately 9 mm (0.4 in) as expected from theoretical calculations. As in Case 1, the mode of abutment displacement during thermal contraction is primarily rotation about its bottom with a small translation component. Additional shear strength mobilization within the retained soil from the end of construction condition occurs as depicted by the contoured stress levels shown in Figure 3.26 for Case 2aii only.
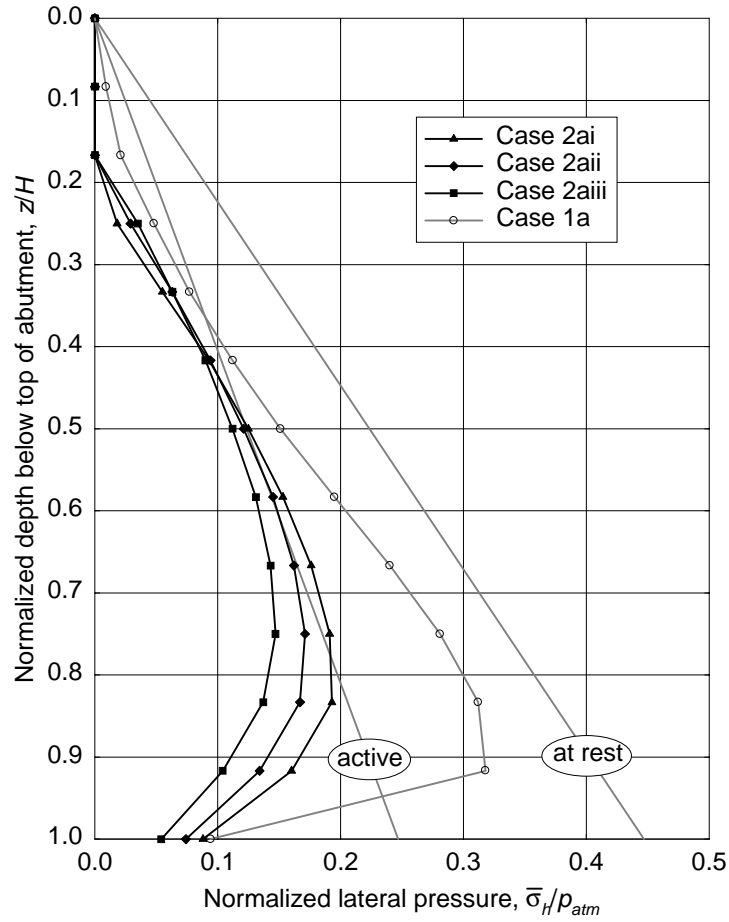
Figure 3.25. Case 2a:
Lateral Pressures at First Thermal Contraction Peak
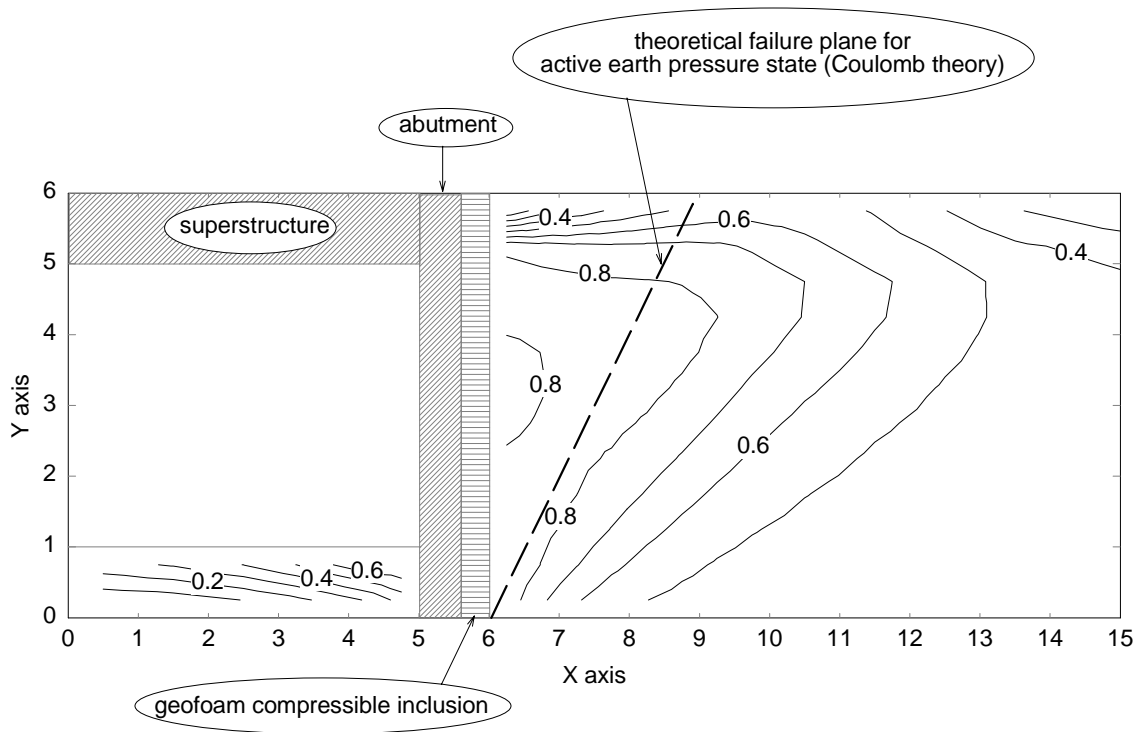
Note: Both axes scaled in metres (1 m = 0.305 ft).

Figure 3.26. Case 2aii: Stress Levels at First Thermal Contraction Peak

Horizontal deformation of the compressible inclusion is shown in Figure 3.27. Not surprisingly, the compressible inclusion expanded somewhat from the end of construction (Figure 3.24), especially along the upper portion of the abutment.
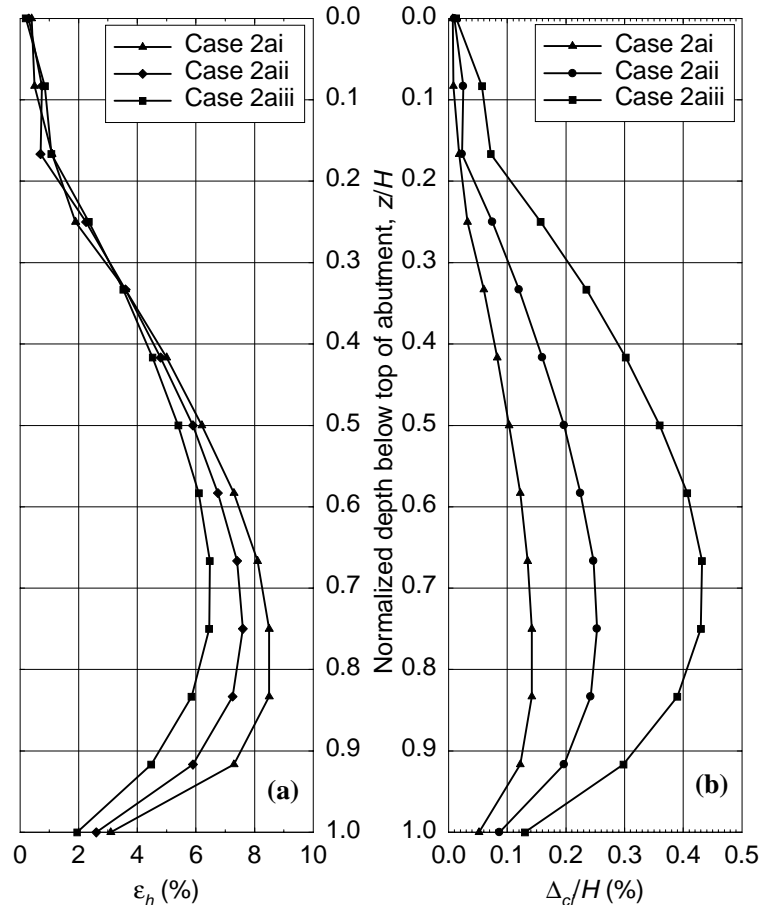
Figure 3.27. Case 2a: Horizontal Deformation of Geofoam Compressible Inclusion at First Thermal Contraction Peak

The settlement of the ground surface immediately behind the abutment was small (approximately 2 mm (0.1 in)) for all Case 2a subcases. This is less than that calculated in Case 1. For all three Case 2a subcases there was again indication of a slight (of the order of 1 mm) net upward movement of the abutment out of the ground as calculated in Case 1.

3.3.3.5 First Thermal Expansion Peak (Case 2a). The calculated lateral pressures at the first thermal expansion peak are shown in Figure 3.28 together with the results from the baseline Case 1a and the theoretical active, normally consolidated at-rest and passive states. Note in this figure that the lateral pressures acting on the abutment can realistically be, and in fact are, calculated to be, non-zero at the ground surface. This is because the geofoam compressible inclusion, not soil, is in contact with the abutment. Because resilient-EPS geofoam is a solid material with inherent, stress-independent material strength (cohesion in the context of the Mohr-Coulomb failure criterion), it has strength even when the total stress is zero (as it is at the surface). This is not the case with a particulate material such as soil.
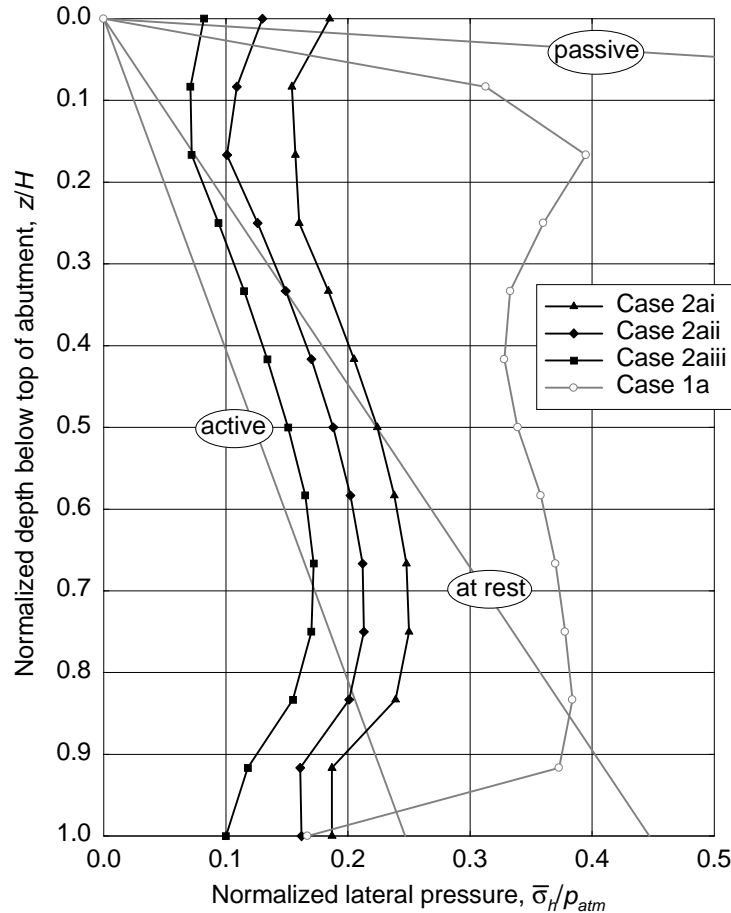
Figure 3.28. Case 2a:
Lateral Pressures at First Thermal Expansion Peak

Overall, the normalized horizontal resultant forces are $\beta = 0.94$, 0.76 and 0.58 for cases 2ai, 2aii and 2aiii respectively. They are all below the theoretical at-rest value ($\beta = 1$) and well below the Case 1a baseline value ($\beta = 1.5$) indicating that the geofoam compressible inclusion is quite effective in its primary intended purpose. However, the values of β are somewhat misleading as the distributions of lateral pressures are significantly different than earlier load steps, being nearly uniformly distributed with depth. This suggests a complex pattern of earth pressure states within the retained soil which is reflected in the contoured stress levels shown in Figure 3.29 for Case 2aii (chosen as being representative). Near the top of the abutment, stress reversals have occurred with horizontal stresses exceeding vertical and stress levels increasing toward a passive failure ($S = 1$). This is not surprising as the thermally induced expansion of the superstructure pushed the top of the abutment approximately 10 mm (0.4 in) inward from its initial post-construction position, the same as in the Case 1 analyses and the maximum expected based on theoretical considerations. Mid-height along the abutment stresses are close to the NC at-rest state ($S \cong 0.4$). Toward the bottom of the abutment, pressures actually decrease toward the active state ($S = 1$) and the increased stress levels in this area reflect this. This tendency toward the active state occurs even though the bottom of the abutment moved inward toward the retained soil and returned approximately to its post-construction position. This apparent contradiction in

behavior occurred because compression of the compressible inclusion allowed simultaneous inward movement of the abutment and outward movement of the retained soil.
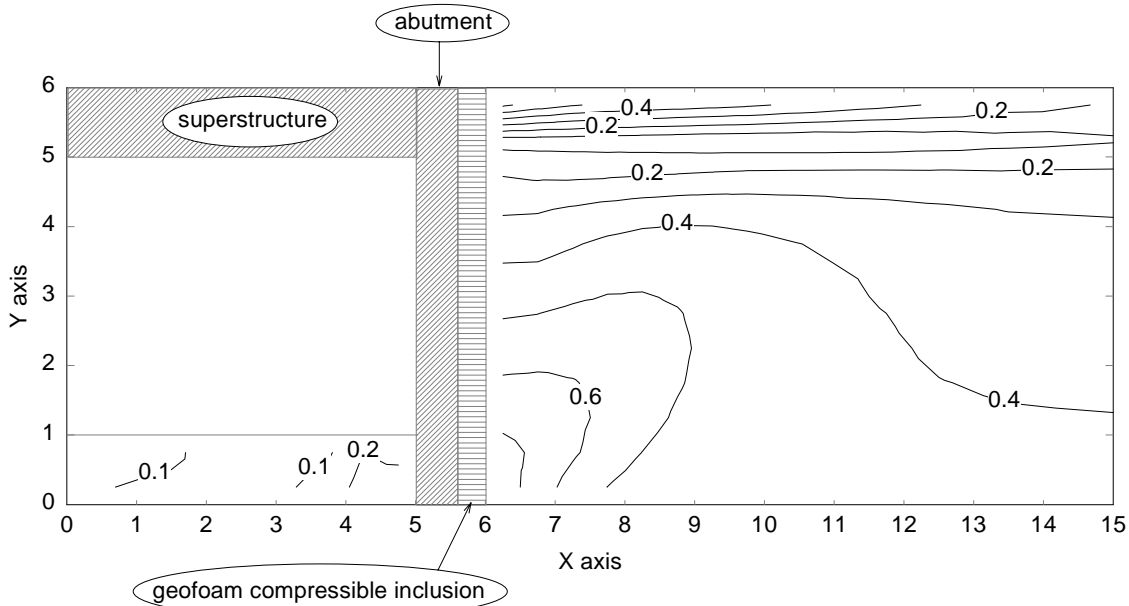
Note: Both axes scaled in metres (1 m = 0.305 ft).

Figure 3.29. Case 2aii: Stress Levels at First Thermal Expansion Peak

The patterns of deformation within the compressible inclusion are shown in Figure 3.30 and qualitatively reflect the lateral pressures shown in Figure 3.28. Although not apparent from Figure 3.30, it is of interest to note that virtually all horizontal movement of the abutment as a result of thermal expansion of the bridge superstructure was accommodated by compression within the geofoam. Very little horizontal movement along the vertical geofoam-soil interface occurred and what little that did was concentrated near the top of the abutment.

Also of interest is that this first peak of thermal expansion caused the top of the abutment to further move slightly upward and out of the ground, continuing the trend noted previously.

3.3.3.6 End of First Thermal Cycle (Case 2a). The calculated lateral pressures at completion of the first full thermal cycle are shown in Figure 3.31. The corresponding results from the baseline Case 1a as well as the usual theoretical pressures are shown also for absolute comparison purposes. Overall, the resultant forces increased somewhat from the end of construction, with $\beta = 0.66$, 0.57 and 0.46 for subcases 2ai, 2aii and 2aiii respectively. However, the resultant forces are still substantially less than the baseline Case 1a ($\beta = 0.98$). The results indicate that, even though the geofoam material in this study was perfectly elastic, the soil is not so there was some net lateral pressure increase as the soil did not return to exactly the same position as immediately after construction even though the abutment had essentially returned to the same horizontal position it had occupied after construction.
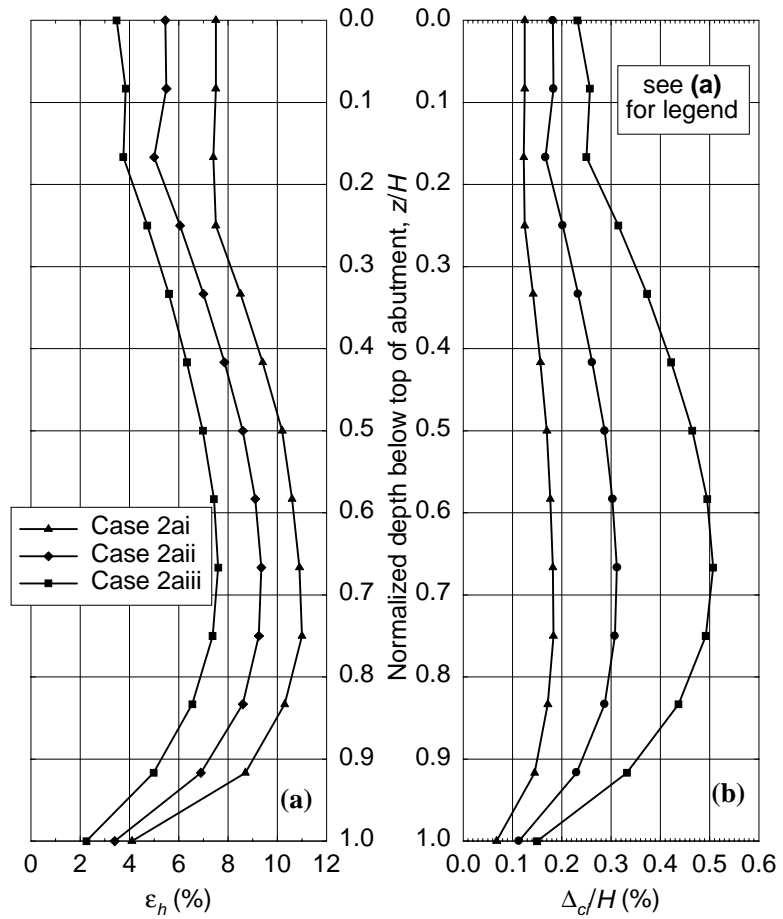
Figure 3.30. Case 2a: Horizontal Deformation of Geofoam Compressible Inclusion at First Thermal Expansion Peak
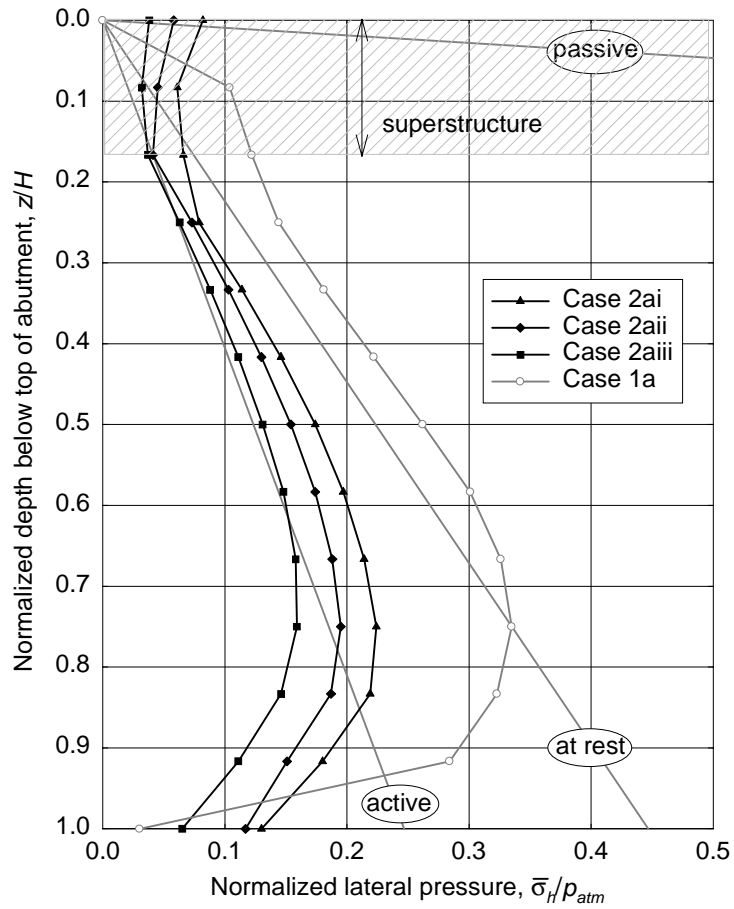
Figure 3.31. Case 2a:
Lateral Pressures at End of First Thermal Cycle

Comparing Figure 3.31 to Figure 3.22 (end of construction), it is apparent that the majority of the increase in the overall resultant force after one full thermal cycle is due to an accumulation of lateral pressures along the upper portion of the abutment, behind the bridge superstructure. This is more clearly understood from the stress-level contours, for Case 2aii only as before, shown in Figure 3.32. Once again, the stress conditions are quite complex. Only at the very top of the abutment do stresses even approach the isotropic condition ($S = 0$). Below that, vertical stresses remain larger than the horizontal. The tendency toward an active failure ($S = 1$) toward the bottom of the abutment is evident.
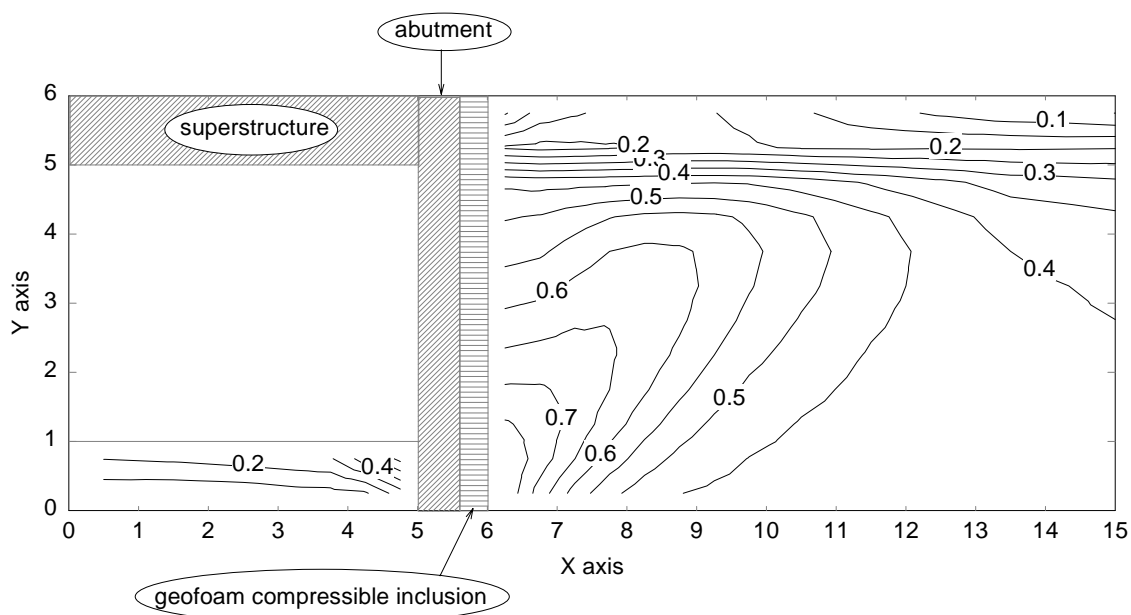
Note: Both axes scaled in metres (1 m = 0.305 ft).

Figure 3.32. Case 2aii: Stress Levels at End of First Thermal Cycle

The patterns of horizontal deformation within the compressible inclusion are shown in Figure 3.33.

3.3.3.7 Fourth (Final) Thermal Expansion Peak (Case 2a). The calculated lateral pressures for this load are shown in Figure 3.34. It is interesting to note that in each of the three subcases they are almost uniform in magnitude with depth. The corresponding results from the baseline Case 1a as well as the usual theoretical pressures are shown also for absolute comparison purposes. Overall, the resultant forces increased somewhat from the first cycle, with $\beta = 1.0$, 0.79 and 0.62 for subcases 2ai, 2aii and 2aiii respectively. This suggests that there is a tendency to increase lateral pressures with load cycling even when a linear-elastic compressible inclusion is used. However, the resultant forces are still substantially less than those for the fourth thermal peak of the baseline Case 1a ($\beta = 1.8$).

66
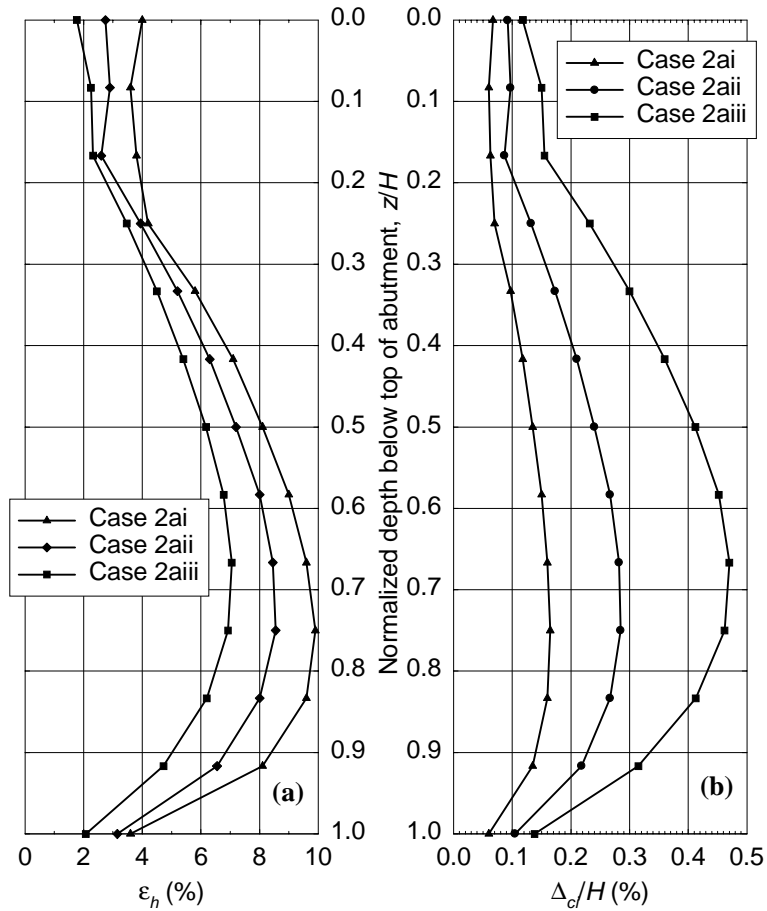
Figure 3.33. Case 2a: Horizontal Deformation of Geofoam Compressible Inclusion at End of First Thermal Cycle
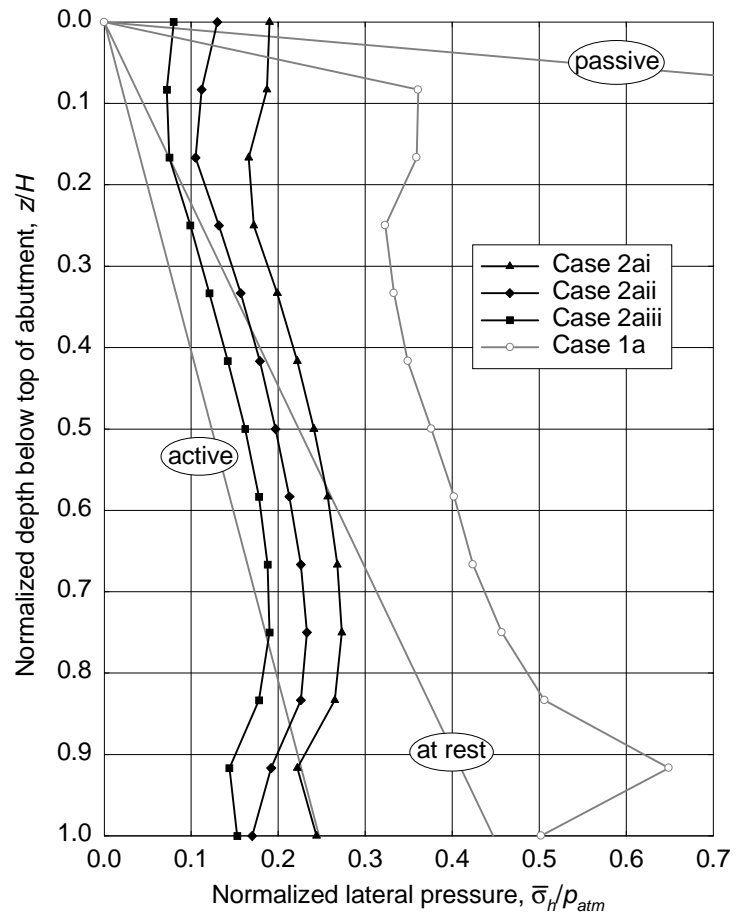
Figure 3.34. Case 2a:
Lateral Pressures at Fourth Thermal Expansion Peak

The contoured stress levels are shown in Figure 3.35. They are complex with some notable differences compared to those observed after one thermal cycle (Figure 3.32). In particular, at the upper portion of the abutment there is a reversal in stresses so that horizontal exceed vertical and the stress level is increasing toward a passive failure ($S = 1$). This means that even with a compressible inclusion larger horizontal stresses are becoming locked in even after just four thermal cycles. With increasing depth behind the abutment, the stress level drops to the isotropic condition ($S = 0$) and then increases again but with the vertical stresses larger than the horizontal. The tendency toward an active failure ($S = 1$) toward the bottom of the abutment is evident.
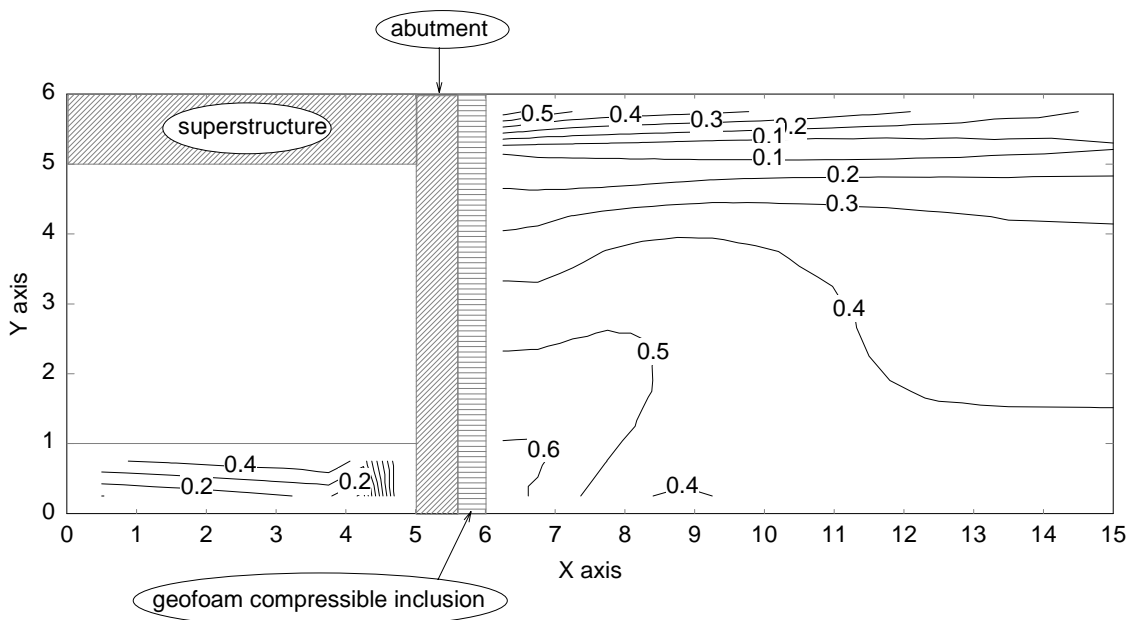
Note: Both axes scaled in metres (1 m = 0.305 ft).

Figure 3.35. Case 2aii: Stress Levels at Fourth Thermal Expansion Peak

The patterns of horizontal deformation within the compressible inclusion are shown in Figure 3.36.

3.3.3.8 End of Fourth (Final) Thermal Cycle (Case 2a). The final distribution of calculated lateral pressures is shown in Figure 3.37 together with the corresponding results from the baseline Case 1a as well as the usual theoretical pressures for absolute comparison purposes. Overall, the resultant forces were essentially unchanged compared to those at the end of one full thermal cycle, with $\beta = 0.65$, 0.56 and 0.49 for subcases 2ai, 2aii and 2aiii, respectively. Interestingly, these represent almost insignificant increases overall from the end of construction. However, the distribution of lateral pressures is noticeably different compared to the end of construction (Figure 3.22). There has been a redistribution of lateral pressures with an increase in pressures near the upper portion of the abutment just behind the bridge superstructure that is compensated by decreases in pressure with depth.
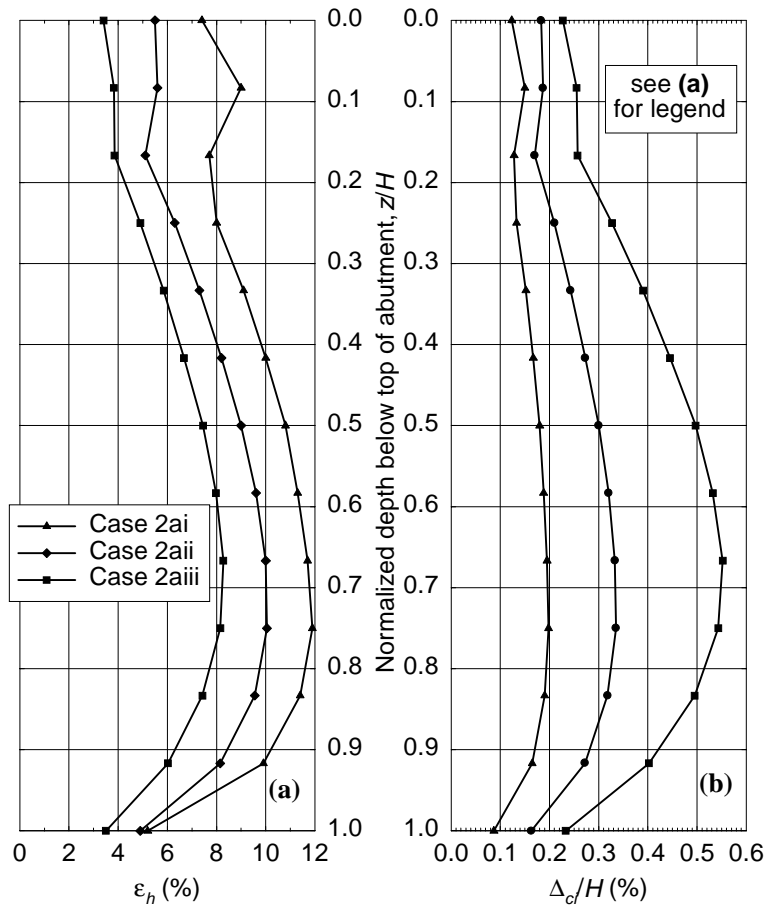
Figure 3.36. Case 2a: Horizontal Deformation of Geofoam Compressible Inclusion at Fourth Thermal Expansion Peak
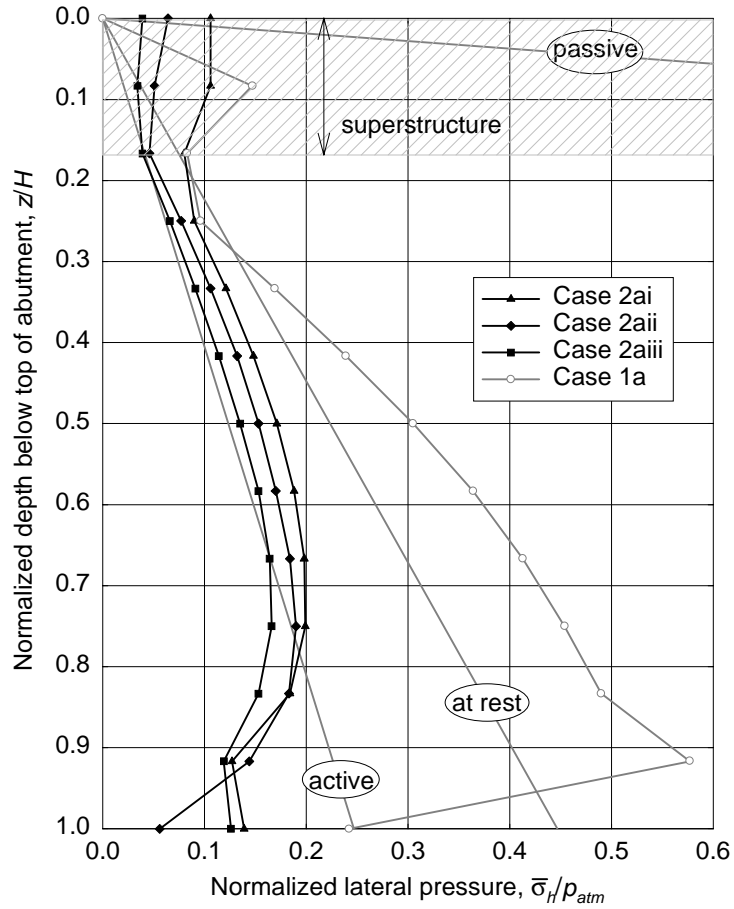
Figure 3.37. Case 2a:
Lateral Pressures at End of Fourth Thermal Cycle

The redistribution of lateral pressures is more clearly understood from the stress-level contours, for Case 2aii only as before, shown in Figure 3.38. As at the end of the first thermal cycle (Figure 3.32), the stress conditions are complex. Only at the very top of the abutment do stresses even approach the isotropic condition ($S = 0$). Below that, vertical stresses remain larger than the horizontal. The tendency toward an active failure ($S = 1$) toward the bottom of the abutment is evident.
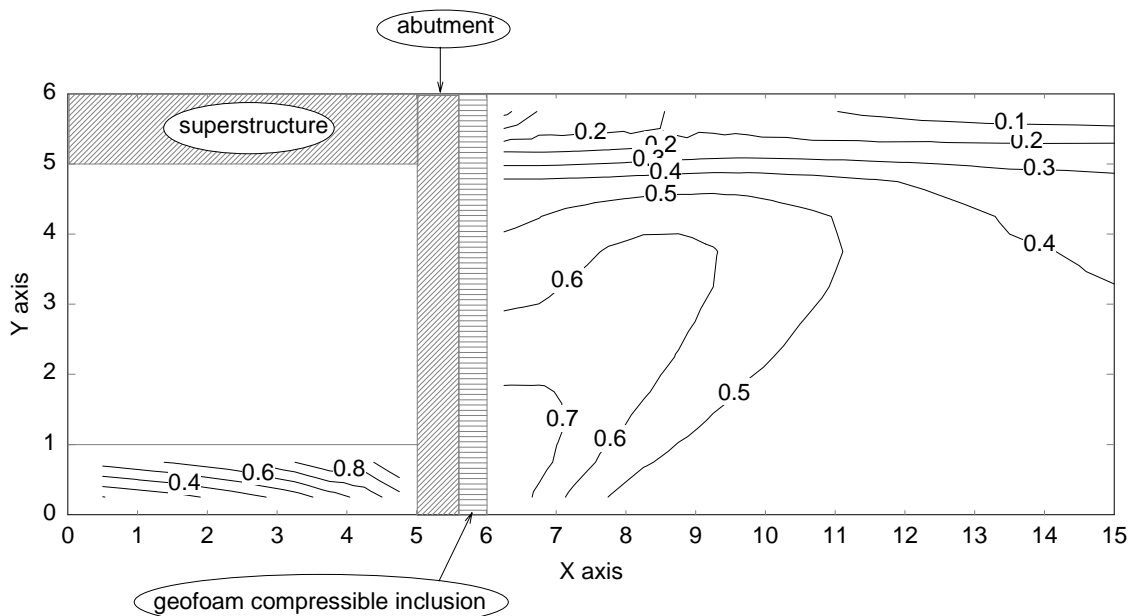
Note: Both axes scaled in metres (1 m = 0.305 ft).

Figure 3.38. Case 2aii: Stress Levels at End of Fourth Thermal Cycle

With regard to displacements, at the top of the abutment there was no net horizontal movement relative to the end of construction position. The abutment exhibited a net upward movement of approximately 5 mm (0.2 in) but the surface of the soil immediately behind the abutment had no net settlement for a total difference in level (which would appear as a void under an approach slab or pavement settlement in the absence of a slab) of approximately 5 mm (0.2 in). Depending on the subcase, the bottom of the abutment had a net outward movement (toward the left in Figure 3.21) that ranged from zero for Case 2aiii to 6 mm (0.2 in) for Case 2ai. The final distribution of deformations within the compression inclusion is shown in Figure 3.39.

3.3.3.9 End of Construction (Case 2b and Case 2a/2b Comparison). The first set of results examined is at the completion of the simulated construction of the bridge and associated earthwork. The calculated lateral pressures are shown in Figure 3.40. Also shown in this figure for relative comparison are the calculated results from Case 2aii (a geofoam compressible inclusion of identical thickness but without reinforcement) and for absolute comparison are the theoretical active and at-rest state pressures for a soil backfill/fill (from Case 1).
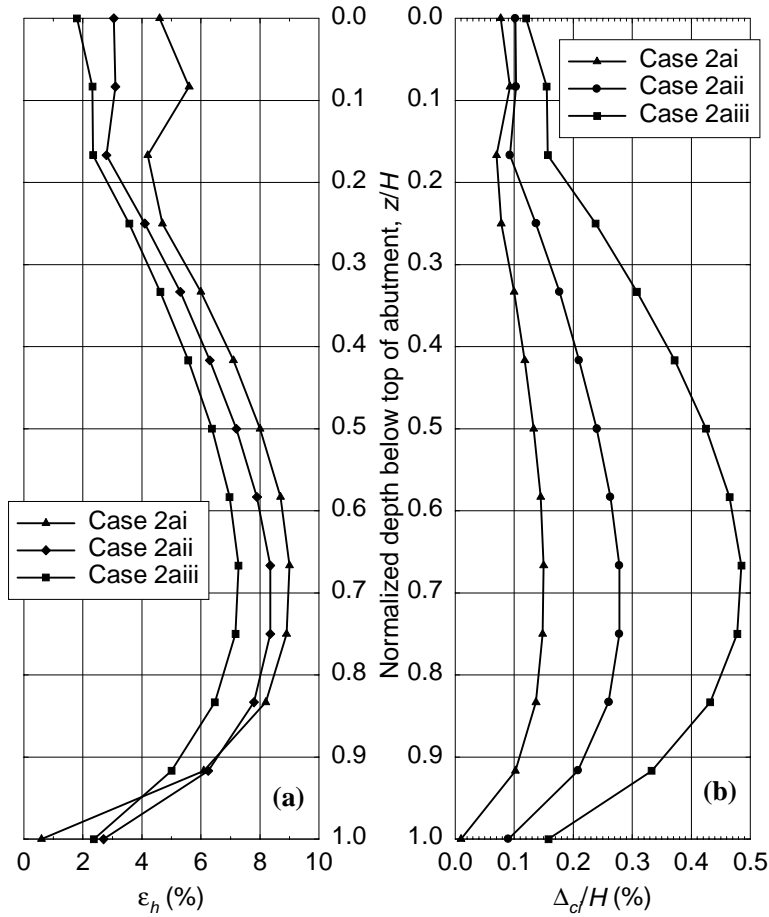
Figure 3.39. Case 2a: Horizontal Deformation of Geofoam Compressible Inclusion at End of Fourth Thermal Cycle
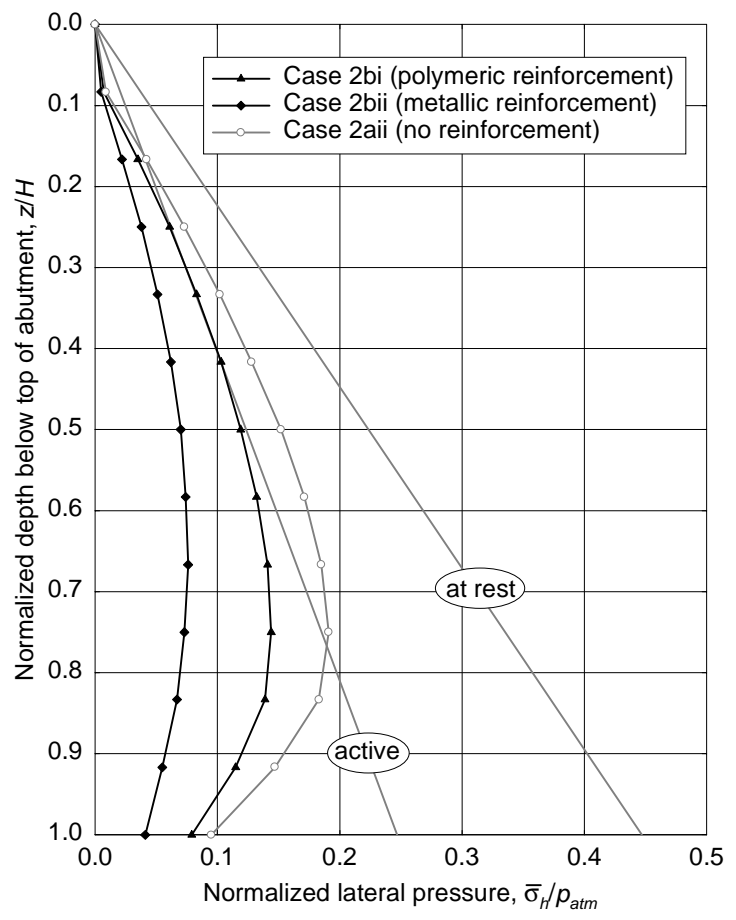
Figure 3.40. Case 2b:
Lateral Pressures at End of Construction

It is of interest to note that the results shown in Figure 3.40 are qualitatively consistent with those determined by the author for the problem of a geofoam compressible inclusion plus tensile reinforcement behind a generic rigid, non-yielding wall (Horvath 1991a). In that earlier study, the reinforcement was modeled explicitly and in detail in accordance with the usual practice for FEM modeling of geosynthetically reinforced soil masses. This qualitative agreement between the results in Horvath (1991a) and Figure 3.40 supports the use in the present study of the simpler procedure for modeling the gross effects of geosynthetic tensile reinforcement.

In both Case 2b subcases, the lateral pressures are reduced from the reference geofoam-compressible-inclusion-only Case 2aii ($\beta = 0.53$) reflecting the expected benefit of using geosynthetic tensile reinforcement to stiffen the retained soil as it deforms horizontally against the compressible inclusion. Quantitatively, $\beta = 0.42$ and 0.23 for cases 2bi (polymeric reinforcement) and 2bii (metallic reinforcement) respectively. Although the baseline Case 1a lateral earth pressures are not shown in Figure 3.40, recall $\beta = 0.99$ for that case so there is a significant reduction in horizontal resultant force compared to using soil backfill/fill alone.

Stress levels were not contoured for any Case 2b analyses. A decision was made beforehand that, due to the approximate technique used to model the reinforcement, stress levels within the 2-D finite elements representing the reinforced soil mass did not reflect actual conditions.

The deformation pattern within the geofoam compressible inclusion is shown in Figure 3.41. Strains are well within the operational range of the assumed resilient-EPS geofoam material.
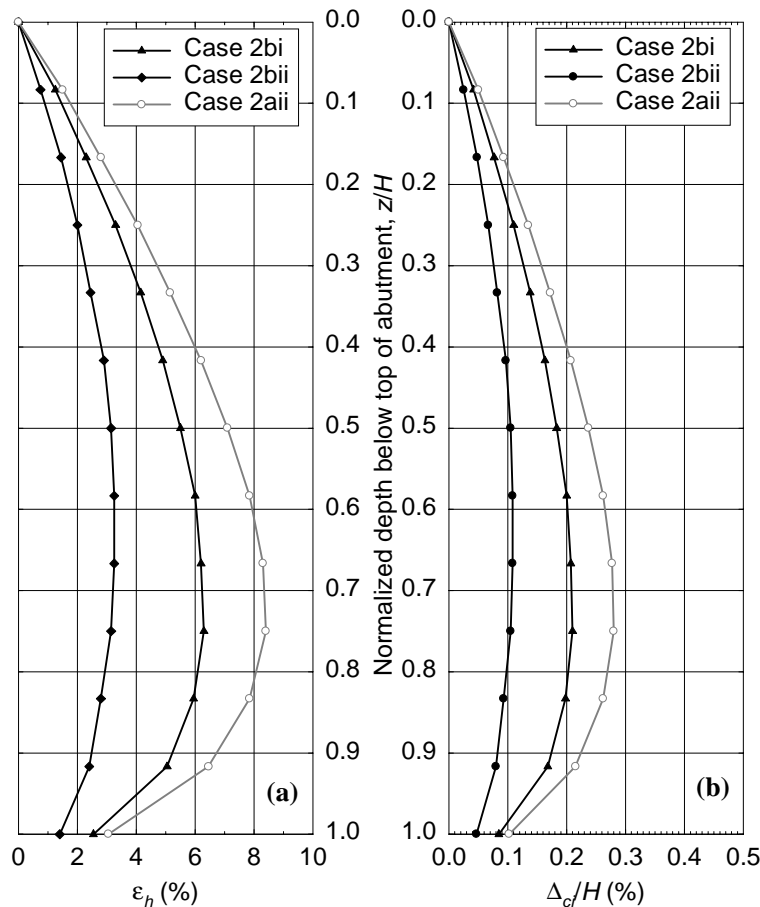
Figure 3.41. Case 2b: Horizontal Deformation of Geofoam Compressible Inclusion at End of Construction

3.3.3.10 Simplified Analytical Method for the ZEP-Wall Concept. As noted in Section 2.2.2.5, using a geofoam compressible inclusion in synergistic combination with tensile reinforcement adjacent to a rigid, non-yielding earth retaining structure is called the Zero Earth Pressure (ZEP) Wall concept[24]. The Case 2b analysis of an IAB abutment at the end of construction and prior to any post-construction thermal loading that was discussed in the preceding section can be viewed as an example application of this concept.

As with the REP-Wall concept that was discussed in detail in Section 3.3.3.3, there is a wide range of potential applications of the ZEP-Wall design concept (Horvath 1995b, 1996, 1998a). In recognition of this, the author previously presented a working hypothesis for an approximate manual calculation method for ZEP-Wall analysis (Horvath 1997, 1998b). The utility of such a method is that it would allow use of the ZEP-Wall concept in routine practice without resorting to the computational effort required by a FEM analysis. Thus it is of interest to digress from the continued discussion of results for the Case 2b analyses and compare the numerical results obtained in the present study to the author's approximate method for ZEP-Wall analysis. The author's originally proposed method (referred to herein as Version 1.0) is outlined here not only for the sake of completeness but to present and discuss modifications developed subsequent to its publication. These modifications (referred to herein as Version 2.0) were also developed by the author with the intention of further simplifying and improving the methodology.
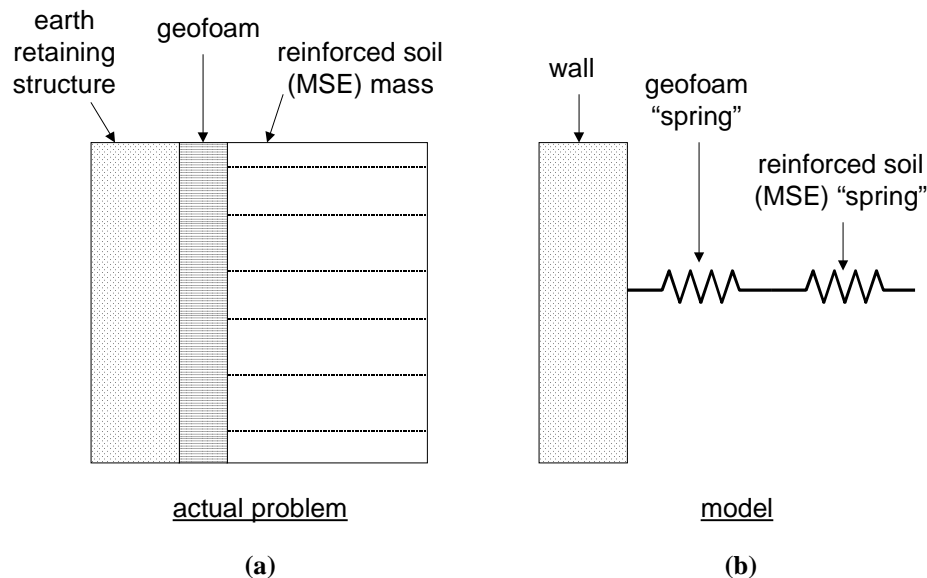
Figure 3.42. Approximate ZEP-Wall Analysis Method: Model Concept

The conceptual framework of the author's simplified methods for ZEP-Wall analysis is illustrated in Figure 3.42. The actual problem solved is shown in Figure 3.42(a) and the model in Figure 3.42(b). The model is based on the assumption that the key behavioral issues to incorporate are the horizontal load-deformation behavior of both the geofoam compressible inclusion and MSE mass (the earth retaining structure is assumed to be both rigid and non-

[24] This term derives from the fact that, with an appropriate combination of compressible inclusion and reinforcement, the lateral pressures acting on an earth retaining structure can be as close to zero as realistically possible. The concept was first identified by the author in Horvath (1990, 1991a).

yielding). Each problem component is modeled as a single spring (not necessarily linear) for this purpose. This implies that only resultant forces are considered, not distributions of lateral pressures. Clearly, these two springs act in parallel and the unique solution to this problem occurs when the force within and displacement of each spring are equal.

Conceptually and qualitatively, the problem and model are very simple. What remains to be done is to define:

- the limiting force-displacement boundary conditions for each spring and

- the spring behavior, linear or nonlinear, between the boundary conditions.

The primary difficulty in application lies in quantifying the spring stiffnesses. There is also the inherent approximation that the behavior of the geofoam compressible inclusion and MSE mass can be reasonably modeled by single values of horizontal resultant force and horizontal displacement. The latter assumption is especially approximate as can be seen from the calculated pattern of horizontal deformation of the geofoam compressible inclusion (the deformation pattern of the MSE mass would have to be qualitatively identical) shown in Figure 3.41. Nevertheless, certain approximations are inevitable if the methodology is to be kept relatively simple.

The geofoam compressible inclusion spring is relatively easy to quantify as the stress-strain-time behavior of the resilient-EPS geofoam that would typically be used for ZEP-Wall applications is satisfactorily known and predictable as shown in figures 3.2 and 3.4. One boundary condition is that the geofoam spring force is initially zero when the geofoam is placed in the ground and its horizontal compression is zero. The spring force increases as the geofoam is compressed by the lateral earth pressure from the MSE mass. Thus the other boundary condition is simply the maximum compression the geofoam compressible inclusion can tolerate. For practical applications this can assumed to be limitless as illustrated subsequently.

The reinforced soil (MSE) spring is more difficult to quantify. One boundary condition is when the MSE spring is fully compressed as would occur if the MSE mass were perfectly confined by a rigid, non-yielding wall in the absence of a compressible inclusion. Under such a condition the force within the spring (which represents the horizontal resultant earth force, P_h) is at its maximum value, $P_{h(MAX)}$. If the MSE spring is allowed to expand horizontally to some magnitude of displacement, $\Delta = \Delta_{MSE}$, the spring force is zero as the reinforcements are fully mobilized with respect to strain necessary to carry all the earth load. This is essentially what happens in a free-standing MSE wall (MSEW). A remaining issue is how the load-deformation behavior of the MSE mass varies between these two limiting conditions, i.e. linearly or non-linearly.

The unique solution to the problem (defined as $P_h = P_h^{'}$, $\Delta = \Delta'$) occurs when horizontal compression of the geofoam compressible inclusion equals the horizontal expansion of the MSE mass, and the horizontal resultant force is the same for both. This is illustrated in Figure 3.43. The following comments are made with regard to understanding this figure:

- The MSE spring is assumed for simplicity and in the absence of more-definitive knowledge to be linear. It is most likely curved concave upward (as shown qualitatively) as unreinforced soil exhibits such curved behavior. Currently available information suggests that the assumption of linearity produces more conservative results compared to the presumed curved behavior shown.

- The geofoam compressible inclusion spring can be linear as shown in the figure or curved depending on the specific material and product used. In the present study, the resilient-EPS geofoam assumed was linear as shown in figures 3.2 and 3.4.
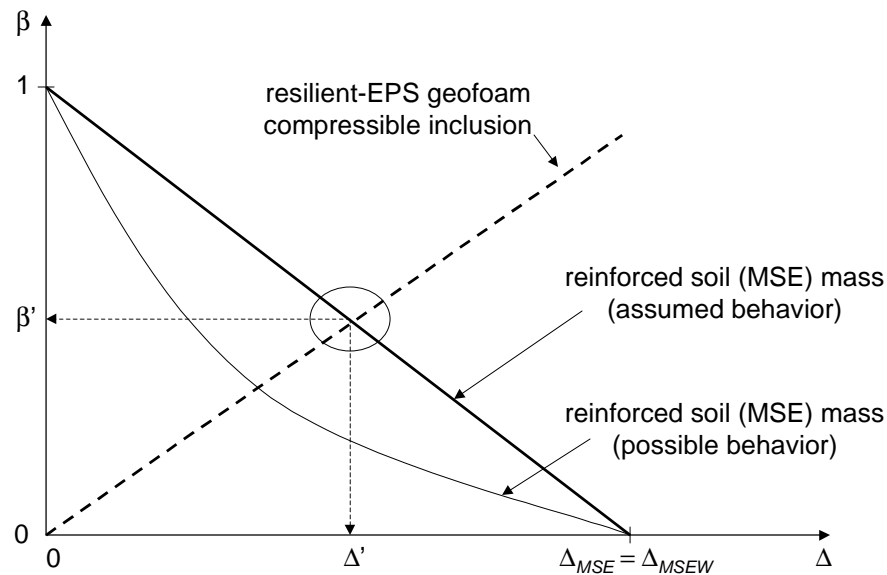
Figure 3.43. Approximate ZEP-Wall Analysis Method: Spring Stiffnesses

- In the original Version 1.0 of the proposed method (Horvath 1997, 1998b), the vertical axis in a figure equivalent to Figure 3.43 was the parameter of lateral pressure, not resultant force. The assumed distribution of lateral pressure was a complex trapezoidal-shaped diagram that was found to be unwieldy to construct in practice because it required assumptions as to the particular compaction equipment that would be used during earthwork operations. In the modified Version 2.0 presented for the first time in this report, the vertical axis has been changed to the horizontal resultant (earth) force, P_h. In addition, it is assumed that the maximum value of P_h, $P_{h(MAX)}$, is equal to that in the normally consolidated at-rest state. This means that $P_{h(MAX)} = P_o^*$. Thus it is possible to use the normalized horizontal resultant (earth) force, β (= P_h / P_o^*), as a variable as shown in Figure 3.43.

- For calculating the horizontal resultant force in the spring representing the geofoam compressible inclusion, it was assumed that the average horizontal strain of the geofoam is two-thirds of the maximum value. This was based on the results of the present study as well as other, similar unpublished analyses by the author which always showed the curved deformation patterns shown in Figure 3.41.

- The magnitude of Δ_{MSE} was taken to be the maximum that would be expected for an MSEW, Δ_{MSEW}. In the absence of more definitive information, Δ_{MSEW} can be estimated using empirical relationships, used previously in Version 1.0 of this method, that were developed from MSEW research and observation. Specifically, for polymeric reinforcement $\Delta_{MSEW} = H/75$ and for metallic reinforcement $\Delta_{MSEW} = H/250$. These relationships assume a reinforcement length to wall height ratio, L_r/H, = 0.7 which was judged to be sufficiently close to the L_r/H = 0.67 used in this study so that no correction was made. These empirical relationships yielded values of Δ_{MSEW} = 80 mm (3.1 in) and 24 mm (0.94 in) for the polymeric and metallic reinforcements respectively.

- The slopes of the two lines shown in Figure 3.43 that define the load-deformation behavior of the MSE mass and geofoam compressible inclusion springs are the spring stiffnesses for the model shown in Figure 3.42(b). These spring stiffnesses are equal to $(1/\Delta_{MSEW})$ and $\left[\left(2 \cdot E_{ci} \cdot H\right)/\left(3 \cdot t_{ci} \cdot P_o^*\right)\right]$ for the MSE mass and geofoam compressible inclusion respectively.

- Using these spring stiffnesses, the following simple algebraic equations can be written to define the force-displacement relationships of the lines shown in Figure 3.43 representing the behavior of the MSE mass and geofoam compressible inclusion:

$$\beta_{MSE} = 1 - \left(\frac{\Delta}{\Delta_{MSEW}}\right) \tag{3.12a}$$

$$\beta_{geofoam} = \frac{2 \cdot E_{ci} H \cdot \Delta}{3 \cdot t_{ci} \cdot P_o^*} \tag{3.12b}$$

- Solution to the problem consists of equating equations 3.12a and 3.12b to solve for either $\beta = \beta'$ or $\Delta = \Delta'$ as shown graphically in Figure 3.43.

- If a lateral pressure distribution is desired for structural analysis of the earth retaining structure, for simplicity the resultant force P_h $(= \beta' \cdot P_o^*)$ can be distributed as a stress over the face of the earth retaining structure using a classical triangular distribution even though the likely distribution is curved as shown in Figure 3.40. Using a triangular lateral pressure distribution means that the resultant force would be applied at a height of $H/3$ above the bottom of the earth retaining structure.

The above procedure was applied using the variables of this study. The calculated results are shown in Table 3.6. As can be seen, the current Version 2.0 of the author's simplified method yields results in this case that are significantly greater than the FEM numerical results which is an error on the conservative side. However, given the tremendous difference in level of effort required between the two methods and the lack of any other alternatives the current version of the author's simplified method is believed to be useful in practice.

Table 3.6. Comparison of Calculated Results for ZEP-Wall Analysis Methods

type of reinforcement	β	
	author's simplified method (Version 2.0)	FEM
polymeric	0.75	0.42
metallic	0.47	0.23

It is of interest to note that the conservatism of the author's simplified analytical method can be reduced by using a less-conservative estimate of the Young's modulus of the geofoam compressible inclusion. For example, in the present study a modulus of 250 kN/m^2 (5200 lb/ft^2) was assumed. This corresponds to the rapid-loading curve shown in Figure 3.4. Some allowance

could be made for the fact that backfilling/filling behind an abutment would take some time in actuality. If a modulus corresponding to say 100 hours (approximately four days) load duration were chosen, a modulus of 150 kN/m^2 (3100 lb/ft^2) could be used. This would reduce the calculated β values to 0.64 and 0.35 for the polymeric and metallic reinforcements respectively. Of course the FEM results using the lower modulus value would be less also but the point is still that the author's simplified method should always be used with a realistic estimate of geofoam modulus which, in this type of problem, could allow for some material creep.

Nevertheless, there is clearly room for improvement of the simplified analytical methodology developed by the author. Further modifications to and improvement of this method should focus on developing and implementing empirical relationships for:

- estimating Δ_{MSEW} and Δ_{MSE}. It would be particularly useful if more-detailed relationships for estimating Δ_{MSEW} could be developed that explicitly incorporate key parameters such as reinforcement and soil stiffnesses. At present, using a single empirical relationship for all types of polymeric reinforcement with no regard for type of reinforcement or soil; vertical spacing of reinforcement layers; and other key details likely produces a significant degree of conservatism for many applications.

- approximating the possible curved relationship for a reinforced soil mass between β = 1 and β = 0 in Figure 3.43.

- approximating the curved distribution of lateral pressures in lieu of resorting to the traditional but incorrect triangular distribution.

3.3.3.11 First Thermal Contraction Peak (Case 2b and Case 2a/2b Comparison).
The lateral pressures at the first thermal contraction peak are shown in Figure 3.44. Corresponding results from the reference Case 2aii without reinforcement are shown together with the usual theoretical pressures. Significant additional reductions in the overall lateral pressures from the end of construction condition occurred (β = 0.28 and 0.09 for the polymeric and metallic reinforcements respectively), especially along the upper portion of the abutment where pressures dropped to zero and a small separation between the abutment and geofoam was calculated. This is due to the fact that contraction of the bridge superstructure pulled the top of the abutment outward approximately 9 mm (0.4 in) as expected from theoretical calculations. As in Case 1, the mode of abutment displacement during thermal contraction is primarily rotation about its bottom with a small translation component. Overall, the use of reinforcement provided a significant benefit compared to Case 2aii (compressible inclusion alone, β = 0.42) and the baseline Case 1a (no geosynthetics, β = 0.68).

Horizontal deformations of the geofoam compressible inclusion are shown in Figure 3.45. As expected, the inclusion expanded from the end of construction (Figure 3.41), especially along the upper portion of the abutment. Note also that compression of the inclusion exists even along the upper portion of the abutment where the back of the abutment separated from the inclusion and no lateral pressure against the abutment exists. This is possible because the geofoam is a true solid material with an inherent, stress-independent shear strength (unlike soil) and thus able to partially support the soil by itself and compress as a result.

An important observation is that the calculated settlement of the ground surface immediately behind the abutment was approximately zero for both Case 2b subcases which is less than any of the preceding Case 1 and Case 2a subcases. For both Case 2b subcases there was again indication of a slight (of the order of 1 mm) net upward movement of the abutment out of the ground as calculated for the preceding Case 1a and Case 2a subcases.
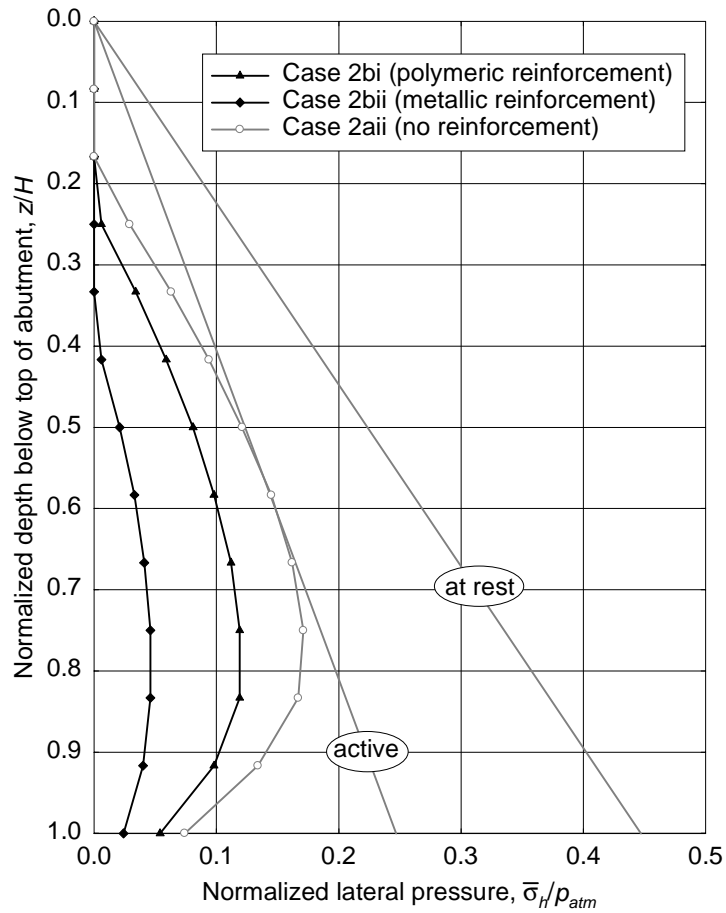
Figure 3.44. Case 2b:
Lateral Pressures at First Thermal Contraction Peak
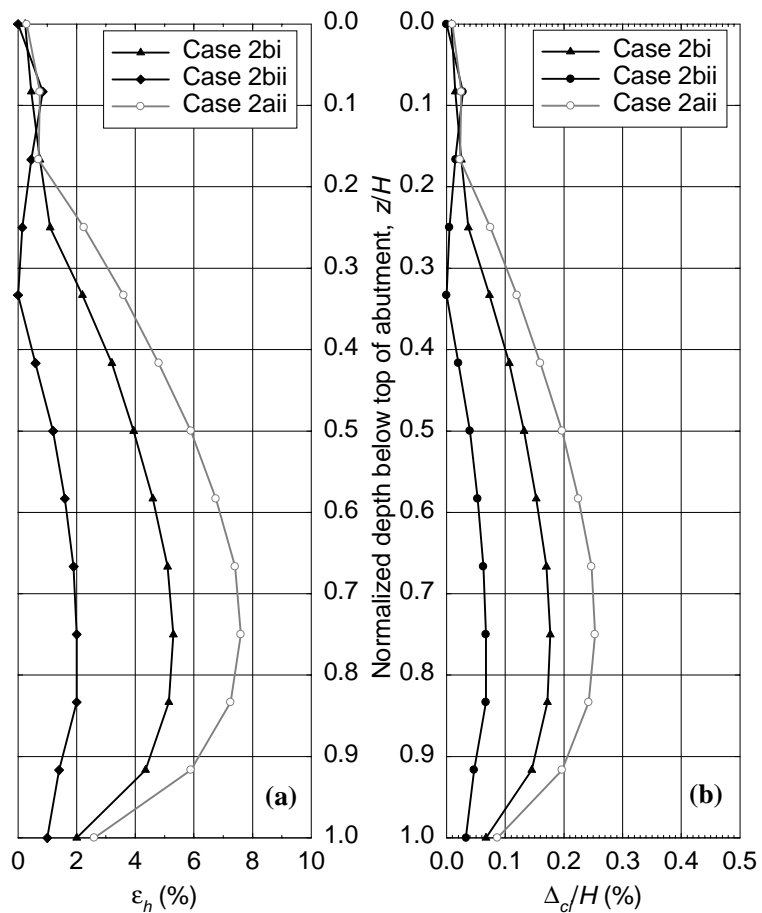
Figure 3.45. Case 2b: Horizontal Deformation of Geofoam Compressible Inclusion at First Thermal Contraction Peak

3.3.3.12 First Thermal Expansion Peak (Case 2b and Case 2a/2b Comparison).
The calculated lateral pressures at the first thermal expansion peak are shown in Figure 3.46 together with the results from the reference Case 2aii and the theoretical active, normally consolidated at-rest and passive states. Overall, the normalized horizontal resultant forces are β = 0.59 and 0.44 for the polymeric (Case 2bi) and metallic (Case 2bii) reinforcements respectively. These are below the reference Case 2aii without reinforcement (β = 0.76) and well below the Case 1a baseline value (β = 1.5) suggesting that the use of reinforcement together with the geofoam compressible inclusion has some benefit (at least along the lower two thirds of the abutment) even though reinforcement alone would have no theoretical benefit when a reinforced soil mass is loaded in compression parallel to the orientation of the reinforcements.
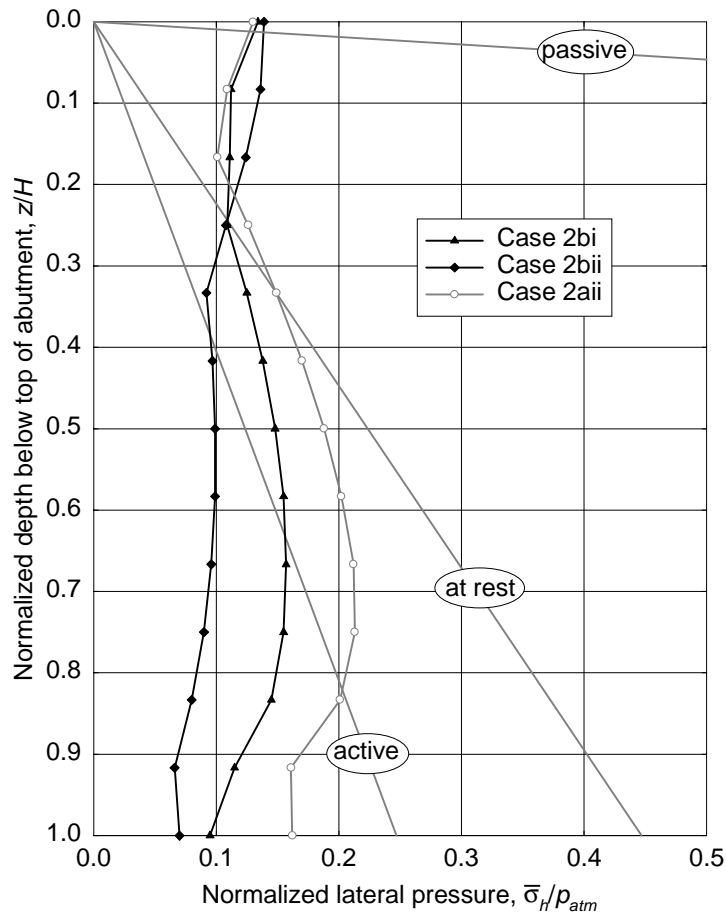
Figure 3.46. Case 2b:
Lateral Pressures at First Thermal Eexpansion Peak

The patterns of deformation within the compressible inclusion are shown in Figure 3.47. Although not apparent from the figure, most of the horizontal movement of the abutment (a maximum of approximately 10 mm (0.4 in) at the top) was accommodated by compression within the geofoam. Very little horizontal movement of the geofoam-soil interface occurred and what little did occur was limited to the area near the top of the abutment. In addition, the ground surface immediately behind the abutment rose upward approximately 2 mm (0.1 in) relative to its position immediately after construction and prior to any thermal loading.
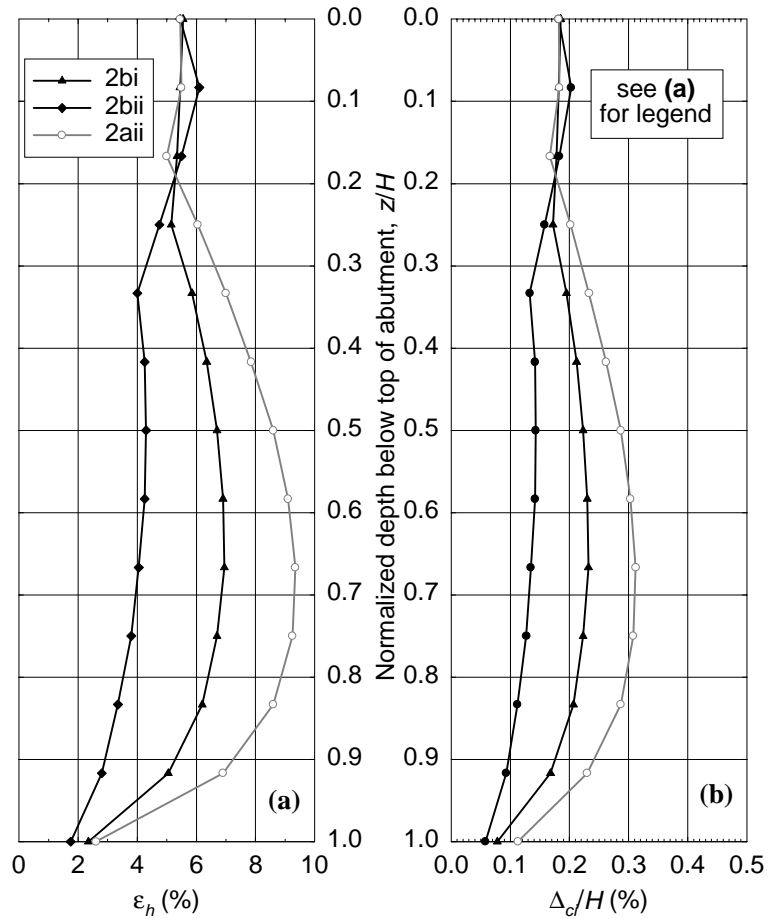
Figure 3.47. Case 2b: Horizontal Deformation of Geofoam Compressible Inclusion at First Thermal Expansion Peak

3.3.3.13 End of First Thermal Cycle (Case 2b and Case 2a/2b Comparison). The calculated lateral pressures at the end of the first full cycle of thermal loading are shown in Figure 3.48 together with the results from the reference Case 2aii and all three theoretical states. Overall, the normalized horizontal resultant forces are $\beta = 0.41$ and 0.23 for the polymeric (Case 2bi) and metallic (Case 2bii) reinforcements respectively. These are essentially the same values obtained immediately after construction (Figure 3.40).
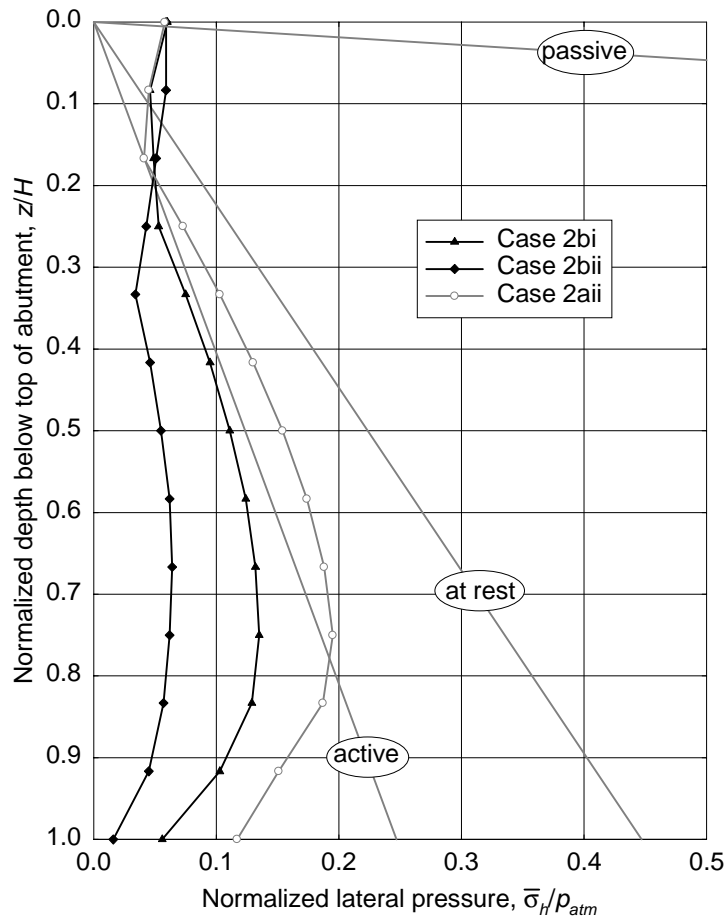
Figure 3.48. Case 2b:
Lateral Pressures at End of First Thermal Cycle

However, comparing resultant forces alone is deceptive in this case as there is a noticeable difference in the distribution of lateral pressures before any thermal loads are applied (Figure 3.40) and after one full thermal cycle (Figure 3.48) even though the resultant forces are the same. The buildup of lateral pressures near the top of the abutment after one thermal-load cycle is noteworthy as is the fact that the presence of the reinforcement apparently has no effect in this regard as the Case 2b (with reinforcement) and Case 2aii (no reinforcement) lateral pressures are essentially the same near the upper portion of the abutment as is apparent in Figure 3.48.

The patterns of horizontal deformation within the compressible inclusion are shown in Figure 3.49.
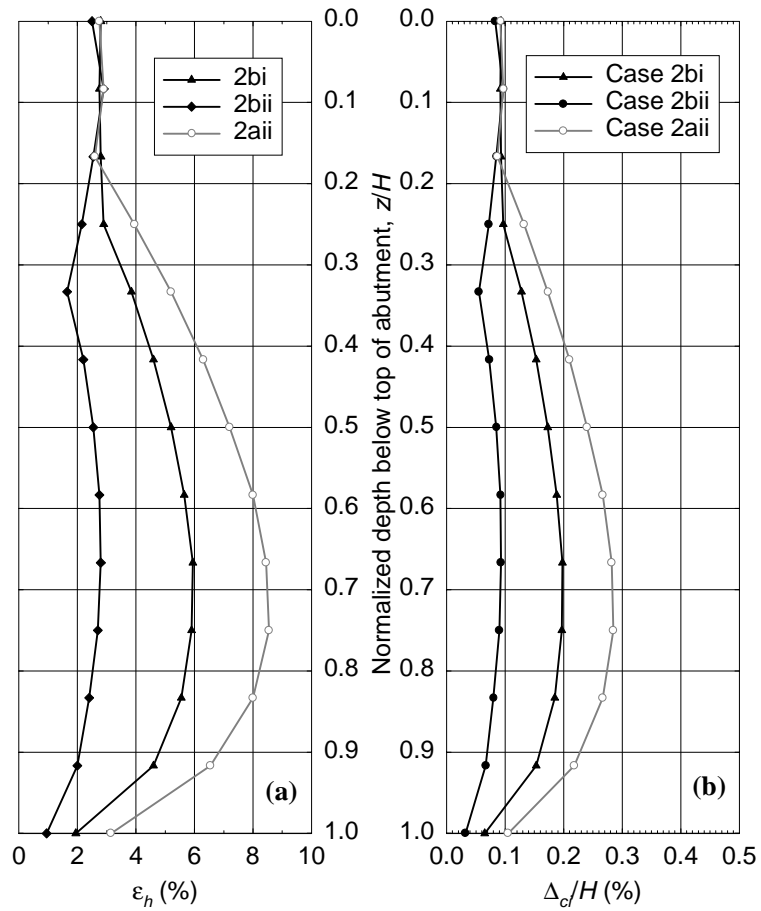
**Figure 3.49. Case 2b: Horizontal Deformation of Geofoam
Compressible Inclusion at End of First Thermal Cycle**

3.3.3.14 Fourth (Final) Thermal Expansion Peak (Case 2b and Case 2a/2b Comparison). The calculated lateral pressures at the fourth and final thermal expansion peak are shown in Figure 3.50 together with the results from the reference Case 2aii and all three theoretical states. Overall, the normalized horizontal resultant forces are β = 0.62 and 0.41 for the polymeric (Case 2bi) and metallic (Case 2bii) reinforcements respectively. These are essentially the same values obtained at the first expansion peak (Figure 3.46) and with a similar distribution of lateral pressures, i.e. roughly uniform in magnitude with depth.

The results for Case 2bii with metallic reinforcement were judged to be somewhat questionable because the distribution of lateral pressures exhibited some qualitative differences from Case 2bi as well as a somewhat erratic pattern. As discussed in Section 3.3.2.5, this may reflect an accumulation of problems with the way in which the nodal-link elements used to model the reinforcements were activated and deactivated during thermal cycling in an attempt to prevent the reinforcements from acting in compression during thermal expansion load applications.
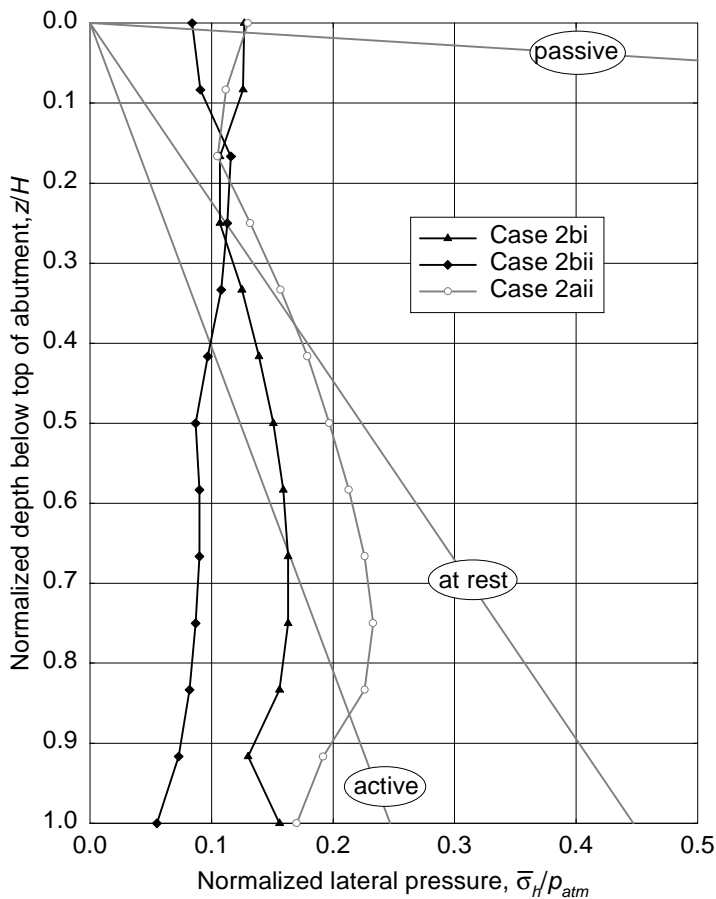
Figure 3.50. Case 2b:
Lateral Pressures at Fourth Thermal Expansion Peak

The patterns of horizontal deformation within the compressible inclusion are shown in Figure 3.51. It is of interest to note that the ground surface immediately behind the abutment rose upward relative to its as-built position, especially for the metallic reinforcement case where approximately 10 mm (0.4 in) of net upward movement was calculated.
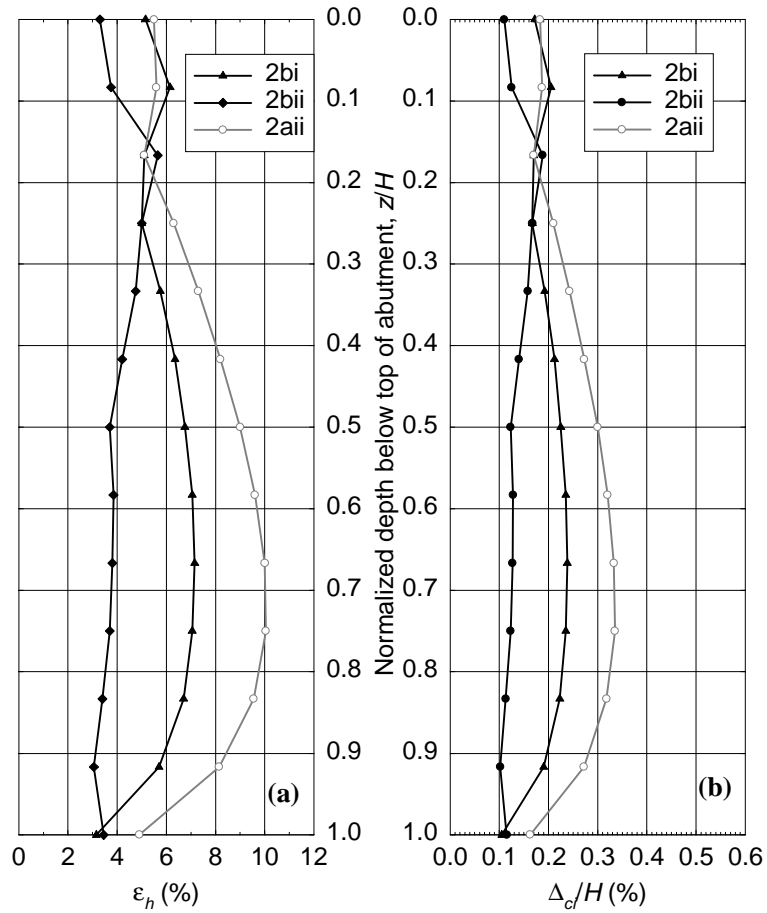
**Figure 3.51. Case 2b: Horizontal Deformation of Geofoam
Compressible Inclusion at Fourth Thermal Expansion Peak**

3.3.3.15 End of Fourth (Final) Thermal Cycle (Case 2b and Case 2a/2b Comparison). The final distribution of calculated lateral pressures after four thermal cycles is shown in Figure 3.52 together with the corresponding results from the reference Case 2aii and all three theoretical states. Overall, the normalized horizontal resultant forces are β = 0.40 and 0.15 for the polymeric (Case 2bi) and metallic (Case 2bii) reinforcements respectively.

The resultant force for Case 2bi (polymeric reinforcement) is essentially the same as at the end of construction. However, the distribution of lateral pressures is noticeably different between the end of construction (Figure 3.40) and the end of the fourth thermal cycle (Figure 3.52). There has been a redistribution of lateral pressures with an increase in pressures near the upper portion of the abutment just behind the superstructure that is compensated by decreases in pressure with depth. This is the same trend that was noted previously in Section 3.3.3.13 after just one thermal cycle. Qualitatively, this overall behavior is the same as that calculated previously for Case 2aii without reinforcement.
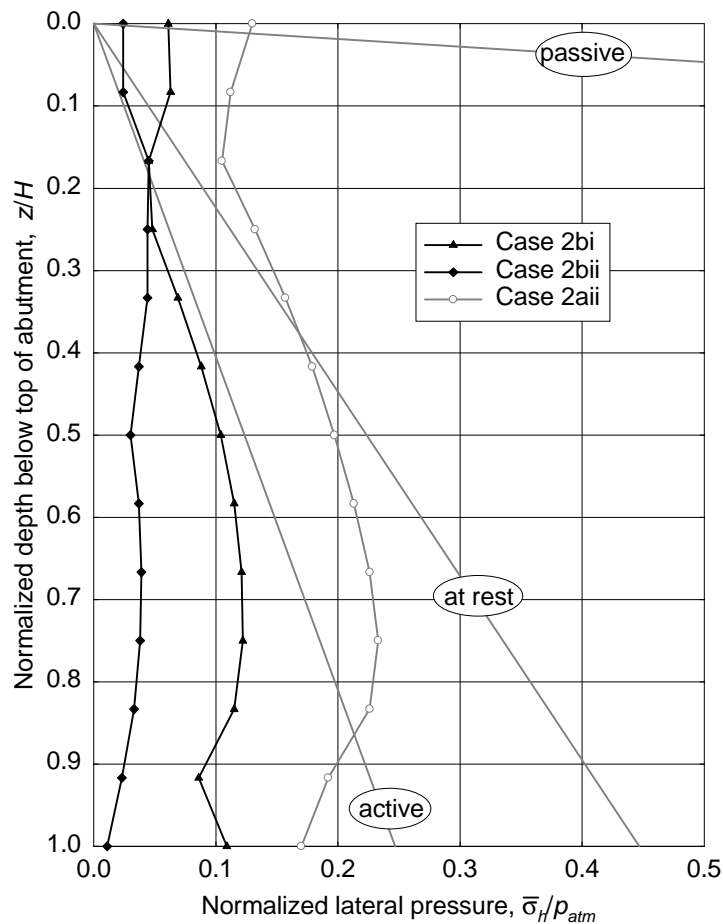
Figure 3.52. Case 2b:
Lateral Pressures at End of Fourth Thermal Cycle

The calculated result (β = 0.15) for Case 2bii (metallic reinforcement) is less than that at both the end of construction and after one complete thermal-load cycle (β = 0.23 in both cases). This fact together with the qualitatively different and somewhat erratic distribution of lateral pressures for this subcase suggests that there may have been problems with the model used and numerical solution. Hence the results for this subcase are considered questionable.

With regard to displacements, at the top of the abutment there was no residual net horizontal movement relative to the end of construction position. The top of the abutment exhibited a net upward movement of 4 to 5 mm (0.2 in). The surface of the soil immediately behind the abutment also moved upward relative to its as-built position. The calculated magnitude of movement was only about 1 mm (0.04 in) for Case 2bi (polymeric reinforcement) but approximately 8 mm (0.3 in) for Case 2bii (metallic reinforcement). The latter results are considered questionable in view of possible modeling problems for this subcase.

Depending on the subcase, the bottom of the abutment had a net outward (toward the left in Figure 3.21) movement of approximately 3 to 4 mm (0.1 in). The final distributions of deformation within the geofoam compression inclusion are shown in Figure 3.53.
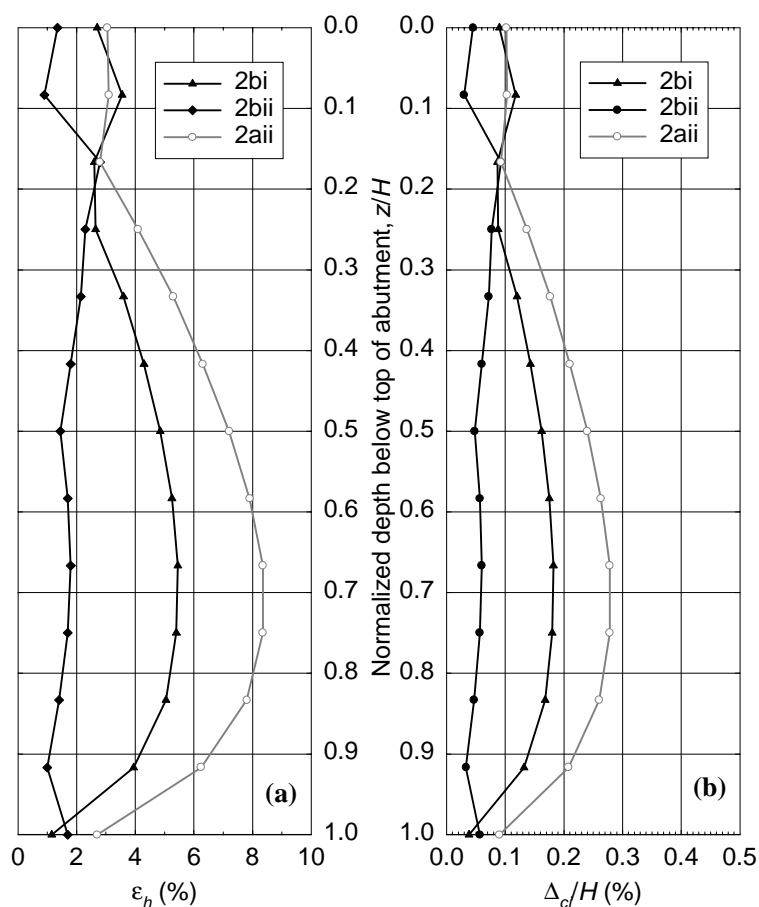
Figure 3.53. Case 2b: Horizontal Deformation of Geofoam Compressible Inclusion at End of Fourth Thermal Cycle

3.3.4 Case 2: Supplemental Analyses

3.3.4.1 Introduction. A series of supplemental analyses was also performed as part of Case 2. These supplemental analyses were not part of the original scope of work that was developed at the beginning of this study. The need for these additional analyses became apparent only after the original Case 2 analyses were performed and analyzed.

The reason for the supplemental analyses was based on the unanticipated result of a physical separation between the geofoam compressible inclusion and the upper portion of the back of the abutment during thermal contraction loading when the bridge superstructure pulled the top of the abutment away from the retained soil. Essentially, the geofoam compressible inclusion acted as a vertical cantilever wall supporting the upper portion of retained soil. Referring to Figure 3.21, this could occur because:

- The 2-D solid elements comprising the geofoam compressible inclusion were fully connected so that the geofoam effectively acted as a continuous vertical wall 6 m (20 ft) high.

- The geofoam was modeled as an elastic solid with stress-independent strength (cohesion within the context of the Mohr-Coulomb failure criterion) so could carry load without limit.

- A continuous vertical column of 1-D interface elements was used between the back of the abutment and compressible inclusion. These elements allow tension in a direction normal (perpendicular) to the element and concomitant separation to occur although the calculated magnitude of separation is of questionable accuracy.

The author's opinion is that such behavior as calculated in the original Case 2 analyses is not realistic. This is primarily because:

- The resilient-EPS geofoam products used in compressible inclusion applications typically come in panel-shaped pieces that are of the order of 1200 mm (4 ft) square. Although panels are butted against adjacent ones as they are placed, they is always a physical discontinuity between panels. Thus there is no structural continuity to provide flexural resistance as was implied by the model used in this study. Therefore, in the particular problem examined for this study it would be physically impossible for an actual geofoam compressible inclusion to act as a continuous cantilever wall 6 m (20 ft) high.

- Resilient-EPS geofoam panels used as a compressible inclusion behind an earth retaining structure are often lightly glued[25] to the exposed face of the earth retaining structure (back of the abutment in this case) so that they stay in place prior to backfilling/filling. Thus in an actual application it is unlikely that the geofoam compressible inclusion would physically separate from the abutment as the abutment moved outward during thermal contraction cycles. If anything, the geofoam panels would tend to move with the abutment and physically pull away from the retained soil.

Thus the conclusion reached after analyzing the original Case 2 analyses was that because the FEM model used originally did not reflect the way most geofoam compressible inclusions are currently installed using products that are currently available, certain behavior that deviated from

---

[25] In practice, the type of glue used must be selected with care so as not to dissolve or otherwise attack the EPS.

that which would likely occur in reality was calculated. Because this erroneous behavior could have an impact on overall results and conclusions drawn from these results, a series of additional, supplemental analyses was performed. In these supplemental analyses (only cases 2aii, 2bi and 2bii for the 200 mm (8 in) compressible inclusion with no reinforcement, polymeric reinforcement and metallic reinforcement respectively were rerun), the geofoam compressible inclusion was assumed to be perfectly attached to the back of the abutment. This was felt to overcome the most serious defect of the original model wherein separation between abutment and geofoam could occur.

One might wonder why this revised model was not used originally as it better reflects reality. There are several reasons:

- The original model was used intentionally to keep things as simple and generic as possible. There is no reason conceptually why relatively long, continuous panels of EPS geofoam could not be used and left unattached to the abutment. There are, in fact, EPS block molds in use worldwide that produce EPS blocks 6 m (20 ft) long.

- The author was unaware of any prior FEM analyses of a geofoam compressible inclusion with IABs. Thus the result of calculating separation between abutment and geofoam compressible inclusion was not anticipated.

- For both absolute and relative comparison purposes, it is desirable to have calculated horizontal stresses (lateral pressures) directly at the back of the abutment. Use of 1-D interface elements along the back of the abutment directly provides the desired calculated results at that location. If the interface elements are fixed to the back of the abutment (to simulate gluing the geofoam panels to the abutment), no slippage can occur and their calculated results are meaningless. As a result, the closest calculated horizontal stresses are for the first column of 2-D solid elements adjacent to (and to the right for the particular mesh used in this study) the interface elements. In the problem studied, this column of 2-D elements is the geofoam compressible inclusion. Because solid-element stresses are always an average value calculated at the geometric centroid of the element, they are not exactly the same as those acting along the interface (back of the abutment in this case).

The comparison between results from the original and supplemental analyses is presented in the following sections. Comparisons were made only at loading intervals that were judged to be significant from the perspective of evaluating the sensitivity of calculated results to the FEM model details used.

3.3.4.2 Results at Maximum Thermal Contraction. The first set of comparisons are at the maxima of thermal contraction. Both the first and fourth (final) contraction peaks were evaluated. Note that in the prior assessments of both the Case 1 (Section 3.3.2) and original Case 2 (Section 3.3.3) results only the first thermal contraction peak was discussed. This is because thermal contraction of IABs is of relatively less interest geotechnically compared to the thermal expansion and the full-cycle results. However, because of the calculated tendency of the abutment to physically separate from the retained soil it was judged of interest to examine both the first and fourth contraction peaks to see if there was any difference in results.

The first subcase examined is Case 2aii which is the reference case of a geofoam compressible inclusion without tensile reinforcement within the retained soil. Figure 3.54 shows the calculated lateral pressures acting on the abutment for both the original and revised analyses as well as the theoretical active state. Note that the plotted lateral pressures for the revised analyses are actually

the average horizontal stress within the 2-D elements modeling the geofoam compressible inclusion and are 200 mm (8 in) away from the actual abutment-geofoam interface. Thus the comparison with the original results, which used the stresses from the 1-D interface elements at the actual interface, is not quite exact but is as close as can be in this study. Nevertheless, the results in Figure 3.54 indicate good agreement between both the original and revised analyses, as well as agreement between results from the first and fourth contraction peaks.
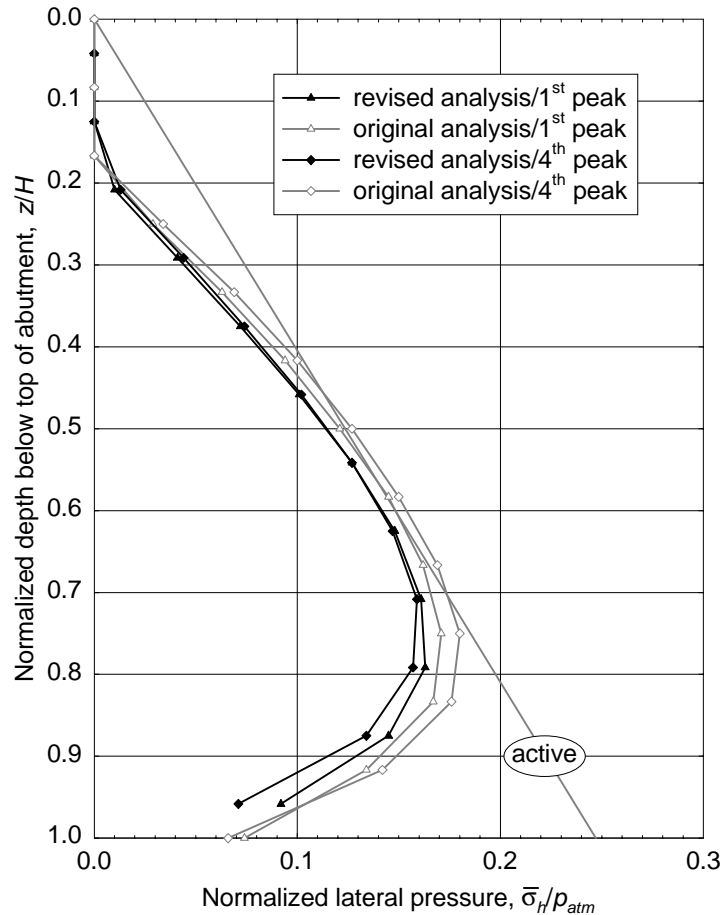
Figure 3.54. Case 2aii: Effect of FEM Model on Calculated Lateral Pressures at Thermal Contraction Peaks

These results suggest that:

- The calculated lateral pressures acting on the back of the abutment are not significantly influenced by the assumed interface (frictional versus fixed) between the abutment and geofoam compressible inclusion.

- There is no significant change in calculated lateral pressures between the first and fourth contraction peaks.

However, the latter conclusion may be influenced by inherent limitations of the analytical software used for this study. Specifically, the revised analyses indicated that a physical separation (gap) of the order of several millimetres between the geofoam compressible inclusion and retained soil occurs near the top of the abutment at thermal contraction peaks. This is not unexpected as in the original analyses a similar gap was calculated between the back of the abutment and the geofoam compressible inclusion. This suggests that in an actual IAB the soil in that region would tend to fail and slough downward to fill the gap. This would lead to both a progressive buildup of lateral pressures due to progressive soil wedging as well as surface settlement immediately behind the abutment (the latter was actually observed in large-scale 1-g model testing by Reeves and Filz (2000)). This probable behavior is not well modeled by the 1-D interface elements and constitutive soil model used for the 2-D elements in this study. Thus the effects of actual behavior may not have been adequately approximated in this study.

Figures 3.55 and 3.56 show the calculated lateral pressures acting on the back of the abutment for Case 2bi (polymeric reinforcement) and Case 2bii (metallic reinforcement) respectively. Again, results for both the original and revised analyses are shown together with the theoretical active state.
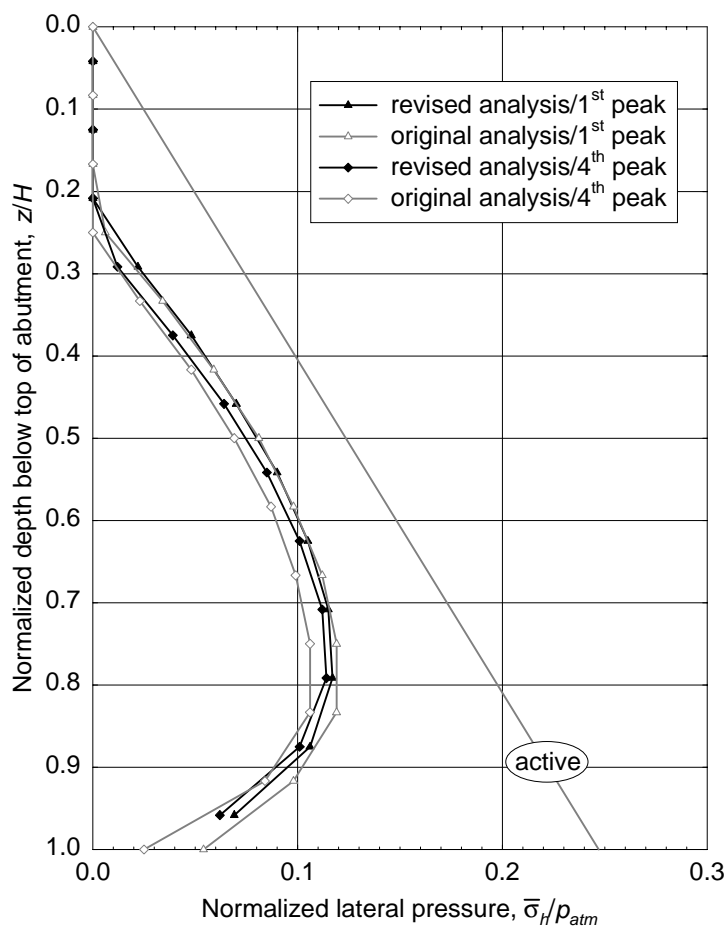
Figure 3.55. Case 2bi: Effect of FEM Model on Calculated Lateral Pressures at Thermal Contraction Peaks
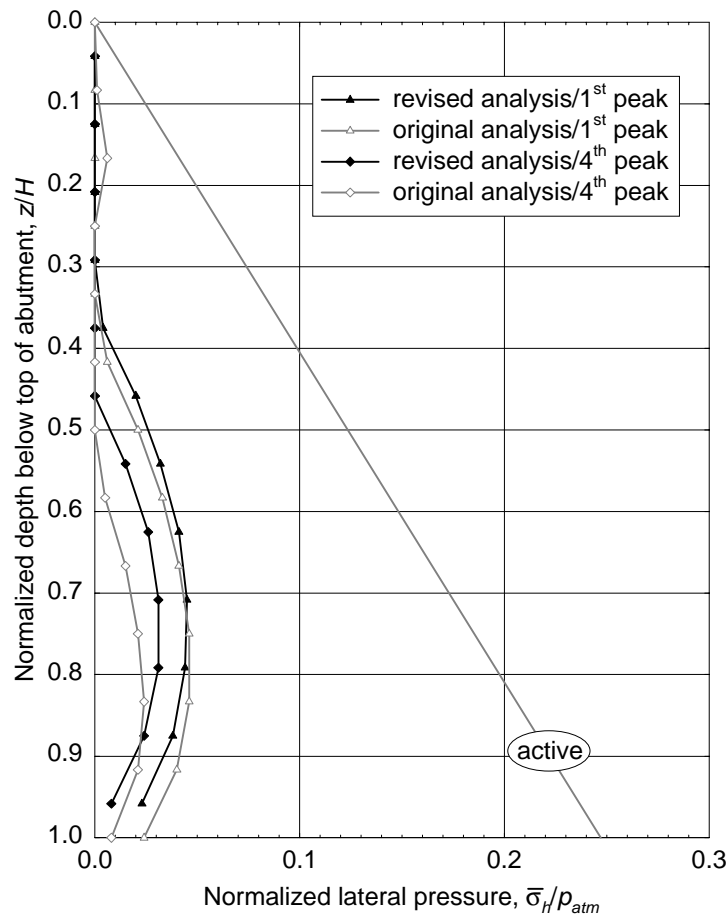
**Figure 3.56. Case 2bii: Effect of FEM Model on Calculated
Lateral Pressures at Thermal Contraction Peaks**

These results with tensile reinforcement are qualitatively similar to those observed for Case 2aii without reinforcement. Specifically:

- There is generally excellent agreement between each set of original and revised analyses in terms of lateral earth pressures acting on the back of the abutment.

- For a given type of reinforcement, there is relatively no difference in lateral earth pressures between the first and fourth contraction peaks.

- For the revised analyses, a gap of the order of several millimetres between the geofoam compressible inclusion and retained soil was calculated for both types of reinforcement and for both contraction peaks. Note that in this case, in an actual application this would not necessarily result in the soil slumping down to fill the gap. This is because the geosynthetic reinforcement could be designed to include a wrapped face (a benefit of using polymeric products) that would prevent this sloughing from occurring.

3.3.4.3 Results at Maximum Thermal Expansion. The next set of comparisons was for maximum thermal expansion. Again, the results at both the first and fourth (final) peaks were evaluated.

The lateral pressures acting on the back of the abutment are shown in figures 3.57 through 3.59 inclusive for Case 2aii (no reinforcement), Case 2bi (polymeric reinforcement) and Case 2bii (metallic reinforcement) respectively. Calculated results from both the original and revised analyses are shown together with the theoretical active, at-rest and passive states. The results are qualitatively consistent as a group in that the revised analyses produced results always somewhat lower (as gauged by values of the dimensionless horizontal resultant force, β) than those from the original analyses. This is different than what was observed for the maximum contraction conditions. The reason for this is unknown.
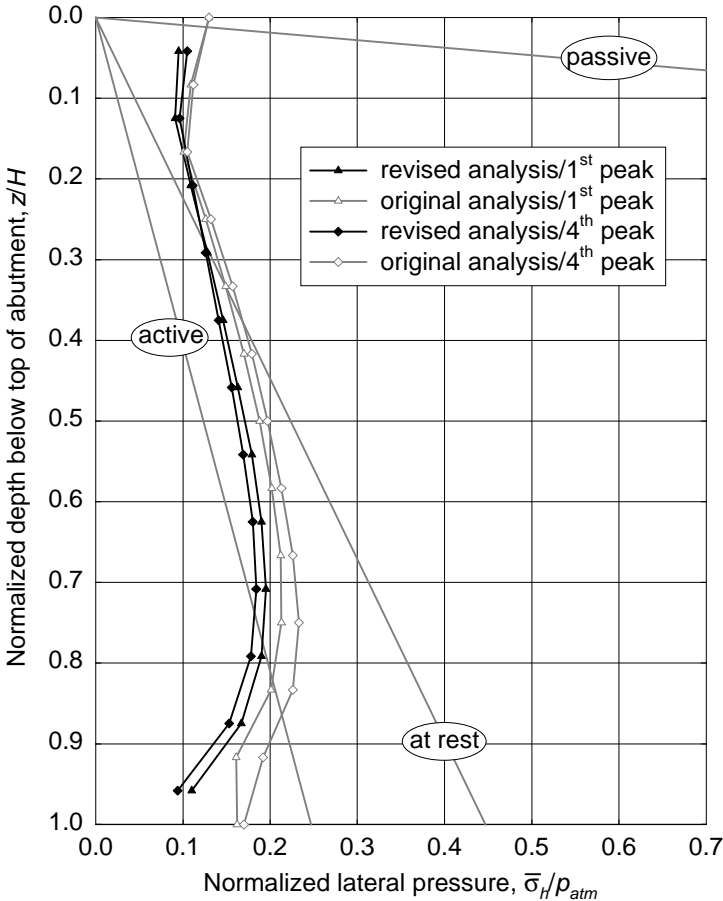
Figure 3.57. Case 2aii: Effect of FEM Model on Calculated Lateral Pressures at Thermal Expansion Peaks
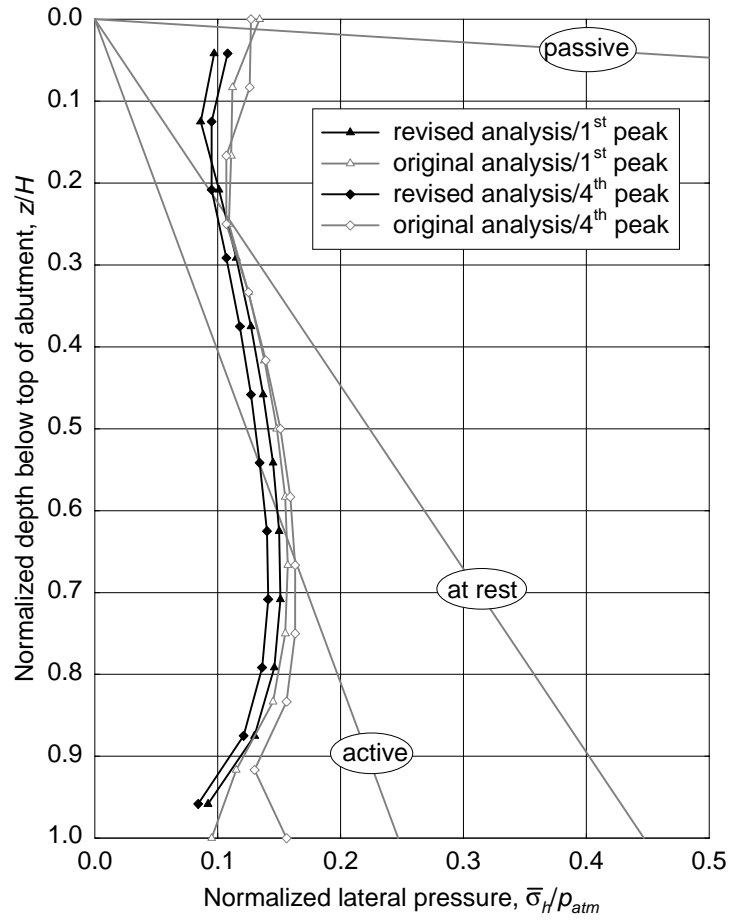
Figure 3.58. Case 2bi: Effect of FEM Model on Calculated Lateral Pressures at Thermal Expansion Peaks
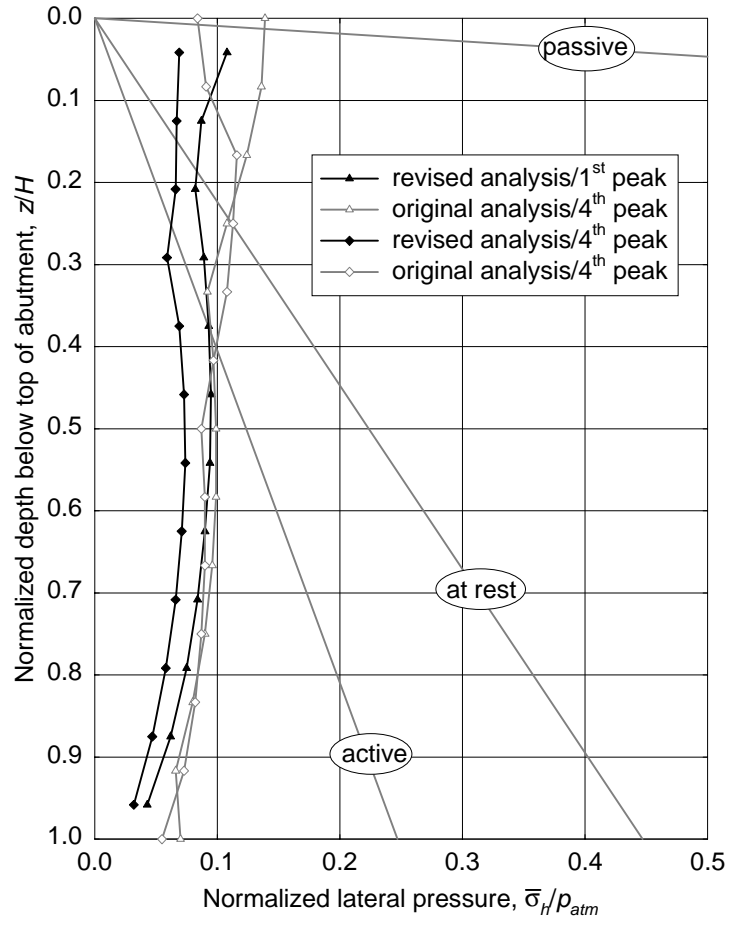
**Figure 3.59. Case 2bii: Effect of FEM Model on Calculated
Lateral Pressures at Thermal Expansion Peaks**

3.3.4.4 Results at Ends of Thermal Cycles. The final set of comparisons was for the neutral temperature condition that corresponds to complete cycles of thermal loading. Again, both the first and fourth (final) cycle results were evaluated.

The lateral pressures acting on the back of the abutment are shown in figures 3.60 through 3.62 inclusive for Case 2aii (no reinforcement), Case 2bi (polymeric reinforcement) and Case 2bii (metallic reinforcement) respectively. Calculated results from both the original and revised analyses are shown together with the theoretical active, at-rest and passive states. As with the thermal contraction maxima, the results from the revised analyses agree well with those from the original analyses although less so for Case 2bii with the metallic reinforcement. This may be due to errors with the way in which the reinforcement was modeled in this study.
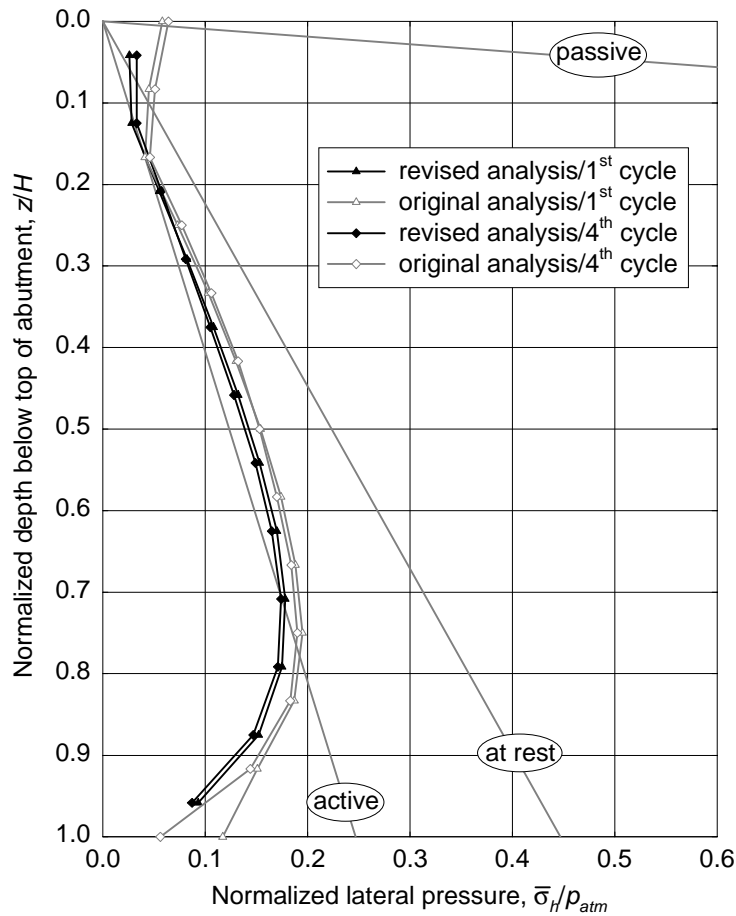
**Figure 3.60. Case 2aii: Effect of FEM Model on Calculated
Lateral Pressures at Ends of Thermal Cycles**
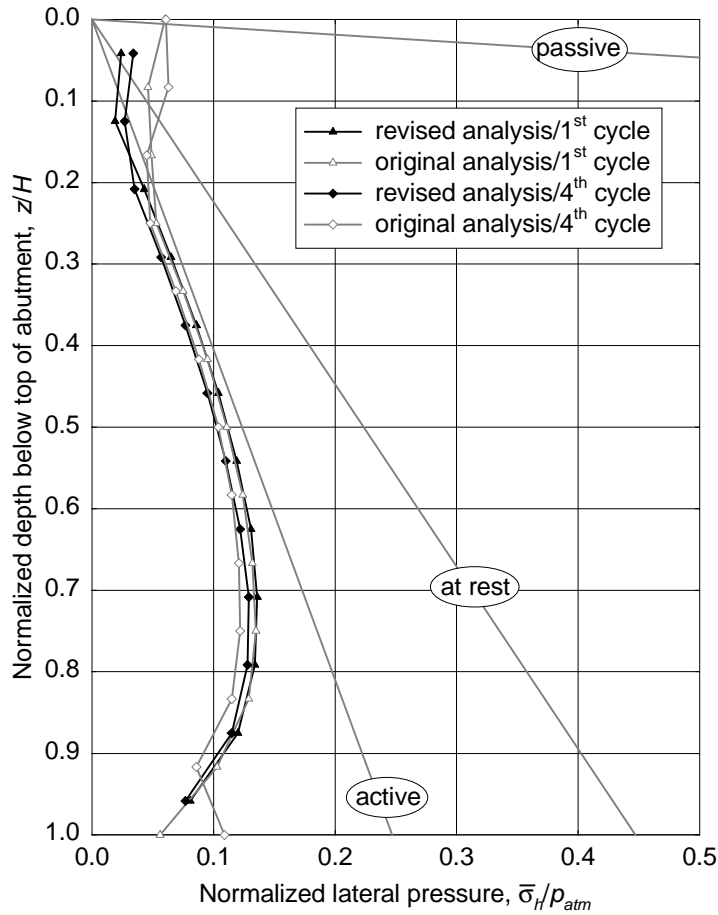
Figure 3.61. Case 2bi: Effect of FEM Model on Calculated Lateral Pressures at Ends of Thermal Cycles
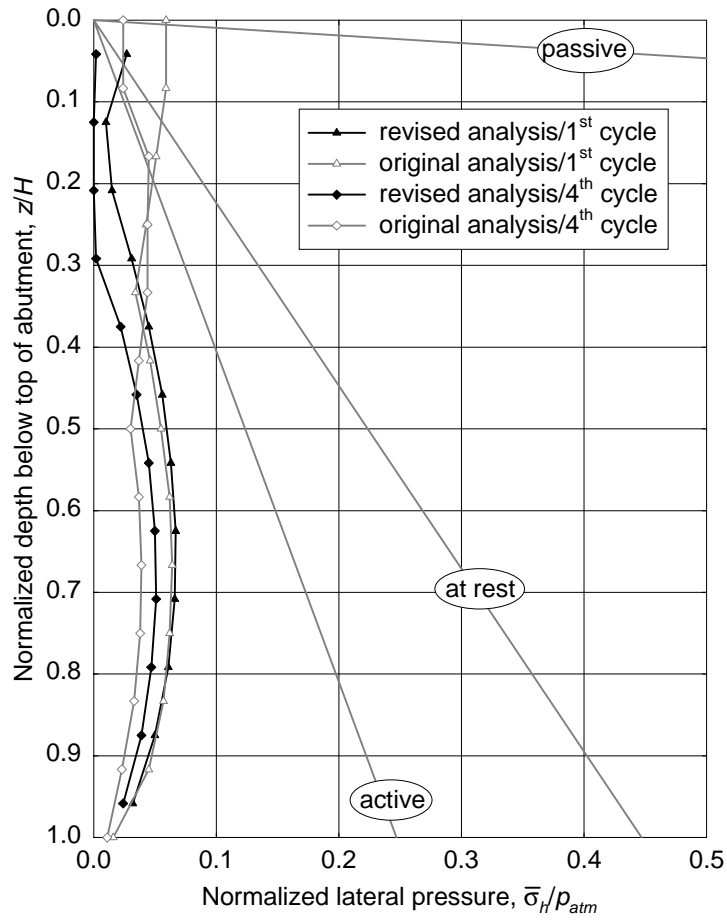
**Figure 3.62. Case 2bii: Effect of FEM Model on Calculated
Lateral Pressures at Ends of Thermal Cycles**

3.3.4.5 Conclusions. Comparing the original and revised Case 2 analyses overall, the conclusions drawn are:

- It is always important to model the actual physical relationship between the abutment and geofoam compressible inclusion as close to reality as possible. This relationship can vary depending on the specific geofoam material and product as well as construction details used.

- The overall lateral pressures are relatively insensitive to the two different models used for the abutment-geofoam compressible inclusion interface in the particular problem considered in this study.

- Horizontal displacements of the retained soil near the top of the abutment appear to be significantly affected by how the abutment, geofoam compressible inclusion and soil interact. The potential for gaps developing between these components and soil sloughing into these gaps has a significant effect on the recommendations made for practice as discussed in detail in Section 4 of this report.

3.3.5 Case 3: EPS-Block Geofoam as Lightweight Fill

3.3.5.1 Introduction. The primary focus of Case 3 was evaluating the benefit(s) of partial replacement of the retained soil with EPS-block geofoam acting as a lightweight fill. Two groups of analyses, Case 3a and Case 3b, were investigated, with two subcases (3ai and 3aii, 3bi and 3bii respectively) within each group for a total of four design alternatives investigated in Case 3.

The common element between all four subcases was that an assemblage of EPS blocks was assumed to be placed behind the abutment as shown conceptually in Figure 2.8(b). The only difference between the Case 3a and Case 3b analyses was in Case 3a the EPS blocks were assumed to be placed in direct contact with the back of the abutment. In Case 3b, a geofoam compressible inclusion composed of 200 mm (8 in) of resilient EPS was placed between the back of the abutment and the relatively stiffer "normal" EPS-block geofoam used as lightweight fill to see if this minor design variation had any significant effect on the calculated results. The rationale for using a geofoam compressible inclusion here is that EPS-block geofoam used as lightweight fill typically has mechanical (stress-strain-time) properties roughly equivalent to a medium-stiff clay. Consequently, during thermal expansion cycles of an IAB the lateral pressures acting on the EPS blocks might be sufficiently large so as to exceed the elastic-limit stress of the EPS and cause immediate plastic (non-recoverable) deformation as well as possibly excessive creep deformation. Thus a compressible inclusion composed of more-compressible EPS geofoam might be useful for preventing this.

Based on the experiences with the Case 2 analyses, all Case 3b analyses with a geofoam compressible inclusion were performed assuming the inclusion was physically attached to the back of the abutment. This decision was not as straightforward as it may seem. Although this models what would typically be done in current practice with currently available geofoam materials and products, and should predict any separation that may occur between the two different types of geofoam (resilient EPS comprising the compressible inclusion and normal EPS fill) during thermal contraction, the lateral pressures acting on the back of the abutment are somewhat less accurate because the average horizontal stress within the compressible inclusion (as opposed to the normal stresses in the 1-D interface elements) must be used for this purpose. However, it was judged better overall to use the revised FEM model with the geofoam compressible inclusion attached to the abutment to better capture any separation effects during thermal contraction. Note that the vertical interface between the geofoam compressible inclusion

and geofoam lightweight fill was retained as a 1-D element frictional interface using the parameters in Table 3.3.

Within each group (Case 3a and Case 3b) of analyses, the only difference between analyses (Case 3ai versus Case 3aii, Case 3bi versus Case 3bii) was the relative size of the triangular wedge of EPS blocks. Specifically, the variable was the assumed magnitude of the angle θ (see Figure 2.8(b)) formed by the geofoam lightweight fill-retained soil interface:

- Subcases 3ai and 3bi were called the "active wedge" alternatives that assumed only the theoretical Coulomb active wedge of soil was replaced. The angle, θ, that the planar intra-soil Coulomb failure surface makes with the horizontal is $45° + \phi/2 = 64°$ in this study. The theoretical Coulomb failure plane together with the actual mesh elements that were assumed to be composed of EPS-block geofoam lightweight fill are shown in Figure 3.63 (for Case 3ai) and Figure 3.64 (for Case 3bi).

- Subcases 3aii and 3bii were called the "full wedge" alternatives that assumed $\theta = \phi = 38°$ (i.e. the "angle of repose") based on the rationale, discussed in detail in Section 2.2.2.5, that the lateral earth pressure from the retained soil transmitted through the assemblage of EPS blocks to the abutment would be zero. The plane defined by this angle together with the actual mesh elements that were assumed to be composed of geofoam are shown in Figure 3.65 (Case 3aii) and Figure 3.66 (Case 3bii).
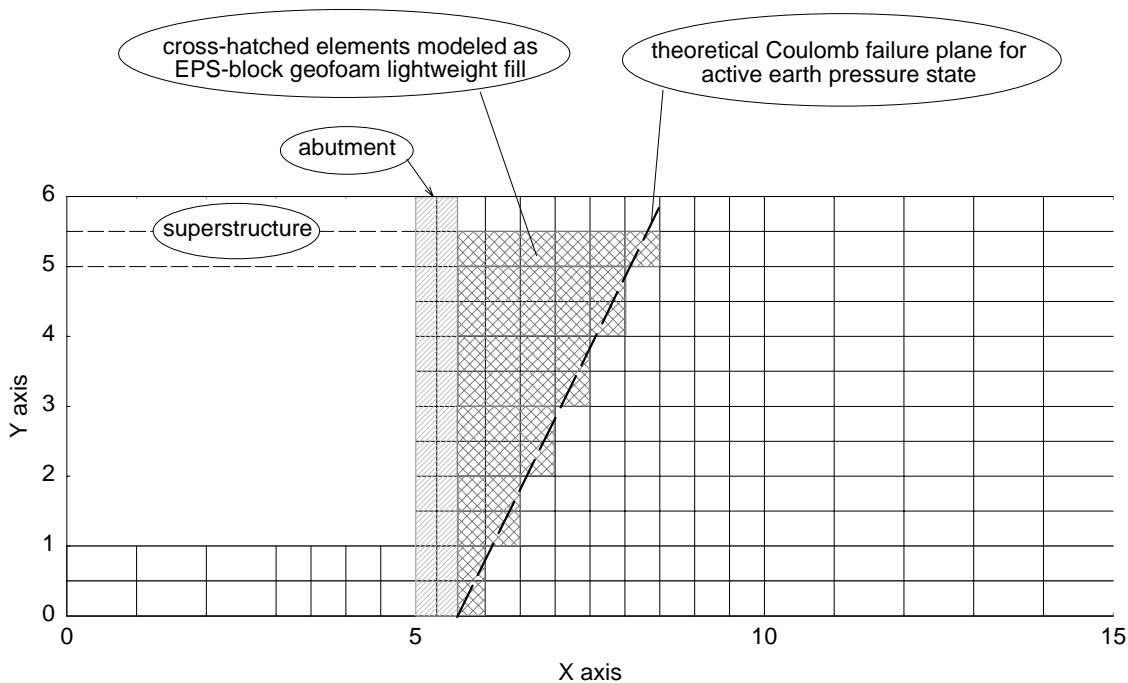
Note: Both axes scaled in metres (1 m = 0.305 ft).

Figure 3.63. Case 3ai: FEM Mesh (partial)

cross-hatched elements modeled as
EPS-block geofoam lightweight fill

theoretical Coulomb failure plane for
active earth pressure state

abutment

superstructure

resilient-EPS geofoam
compressible inclusion
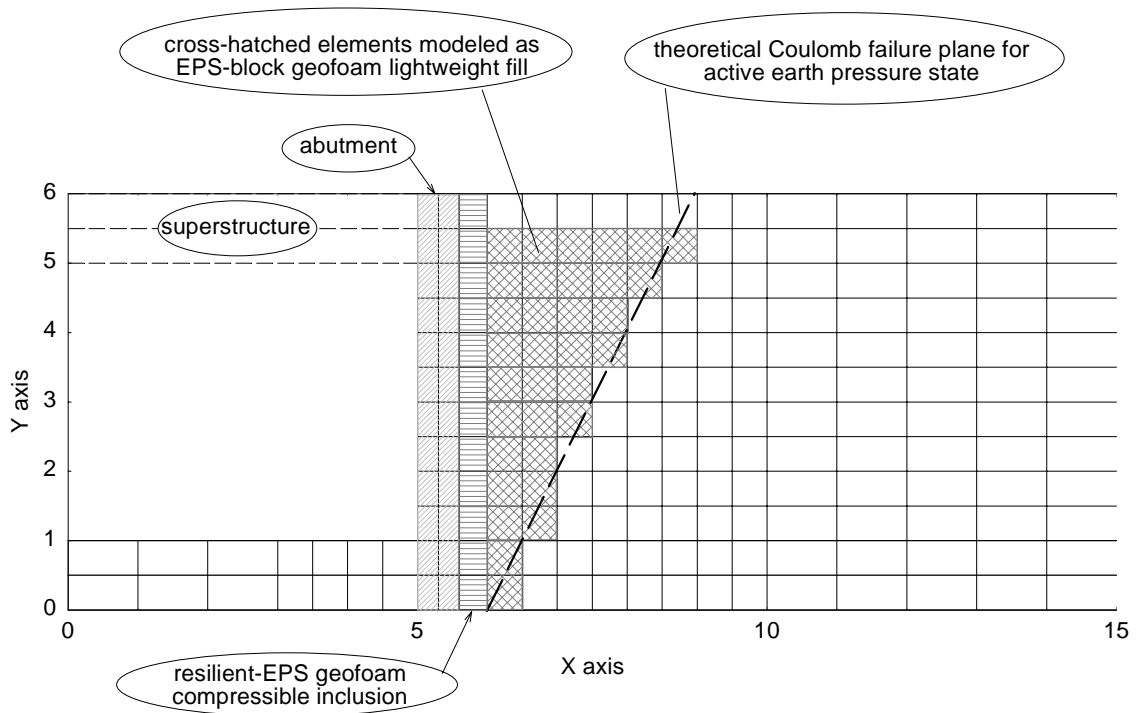
Note: Both axes scaled in metres (1 m = 0.305 ft).

Figure 3.64. Case 3bi: FEM Mesh (partial)
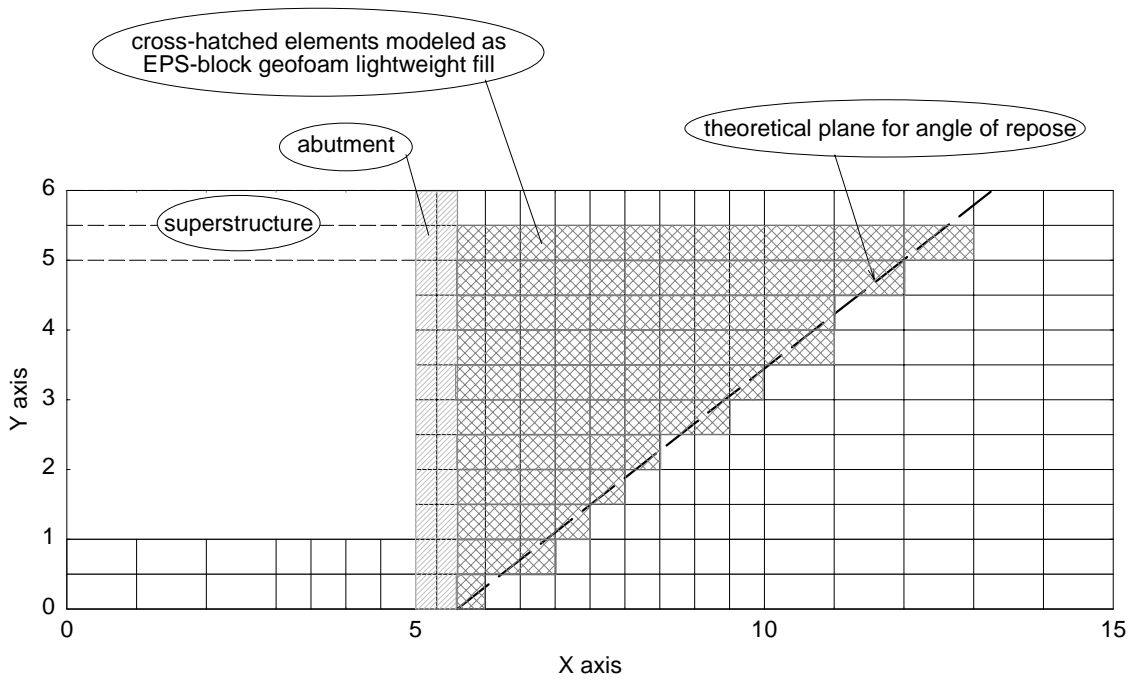
Figure 3.65. Case 3aii: FEM Mesh (partial)

cross-hatched elements modeled as
EPS-block geofoam lightweight fill

theoretical plane for angle of repose

abutment

superstructure

resilient-EPS geofoam
compressible inclusion

Note: Both axes scaled in metres (1 m = 0.305 ft).
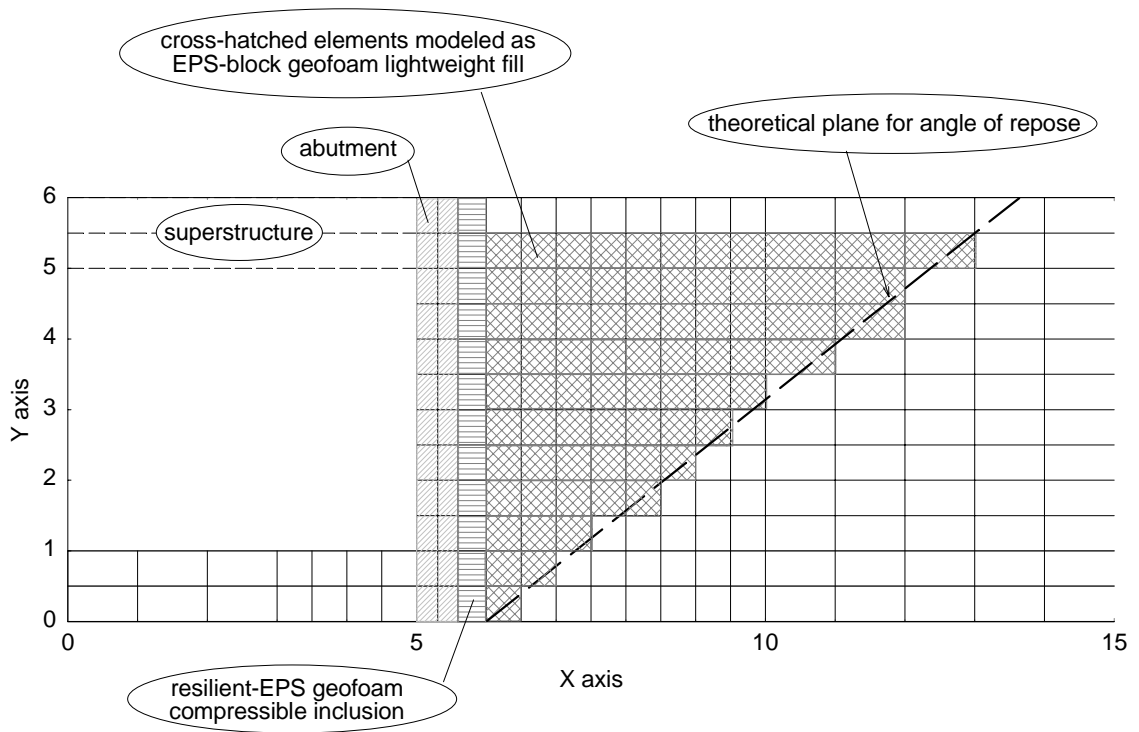
Figure 3.66. Case 3bii: FEM Mesh (partial)

It is of interest to note that the stepped interface between the simulated EPS block lightweight fill and retained soil shown in figures 3.63 to 3.66 is actually a realistic approximation of what would occur in practice. This is due to the geometry of EPS blocks which have thicknesses (vertical (*Y*-axis) dimension in these figures) that typically range from 500 mm (20 in) to 1000 mm (40 in) which is similar to the 500 mm (20 in) vertical dimension of the FEM elements used in this study. Note also that the interfaces between the EPS blocks and retained soil were assumed to be perfectly rough, i.e. no 1-D interface elements were used at these interfaces and the 2-D solid elements for the adjacent EPS blocks and soil had full connectivity at the common nodes. This was done primarily to keep the FEM mesh reasonably simple and was judged to be a suitable approximation in these analyses.

The various stages of the analyses at which the calculated Case 3 results were evaluated are the same as used previously for cases 1 and 2, and are discussed in the following sections. As for Case 2, separate presentations are made for cases 3a and 3b. Comparisons between cases 3a and 3b results are contained within the Case 3b sections.

Note that in all Case 3 plots of lateral pressure the values for the horizontal component of the theoretical active, normally consolidated at-rest and passive states were assumed to be the same as for Case 1. This was done to show a comparison to the baseline case of an all-soil backfill/fill retained by the abutment.

3.3.5.2 End of Construction (Case 3a).
The first set of results examined is at the completion of the simulated construction of the bridge and associated earthwork. The calculated lateral pressures acting on the back of the abutment are shown in Figure 3.67. Also shown in this figure for absolute comparative purposes are the theoretical active and normally consolidated at-rest state pressures for a soil backfill/fill (from Case 1) as well as the calculated results from the baseline Case 1a.

In both cases, the lateral pressures are reduced significantly from the baseline Case 1a (β = 0.99) reflecting the expected beneficial result from the use of the very low density EPS-block geofoam backfill/fill which has a density approximately 1% of that of soil. Quantitatively, β = 0.56 and 0.30 for cases 3ai (active wedge) and 3aii (full wedge) respectively.

However, the results for the full-wedge Case 3aii were unexpectedly high in magnitude. This is based on a comparison to the theoretical lateral pressure magnitude and distribution (shown as a dashed line in Figure 3.67) that would be expected based on the current state of practice which assumes:

- A normally consolidated at-rest lateral earth pressure exists within the upper 500 mm of soil that is in direct contact with the back of the abutment.

- The vertical effective overburden stress from the 500 mm of soil sitting on top of the EPS blocks (9.9 kPa in this case) creates a uniformly distributed lateral pressure within the zone where the EPS blocks are in contact within the back of the abutment. The magnitude of this uniform stress is typically taken to be one-tenth of the soil overburden stress or approximately 1 kPa in this case.

- The lateral pressure from the geofoam itself is very small in magnitude and negligible.

- With reference to the geometry shown in Figure 3.65, the soil to the right of the geofoam mass transmits no lateral earth pressure through the EPS blocks to the wall because the soil is theoretically self stable at its angle of repose.
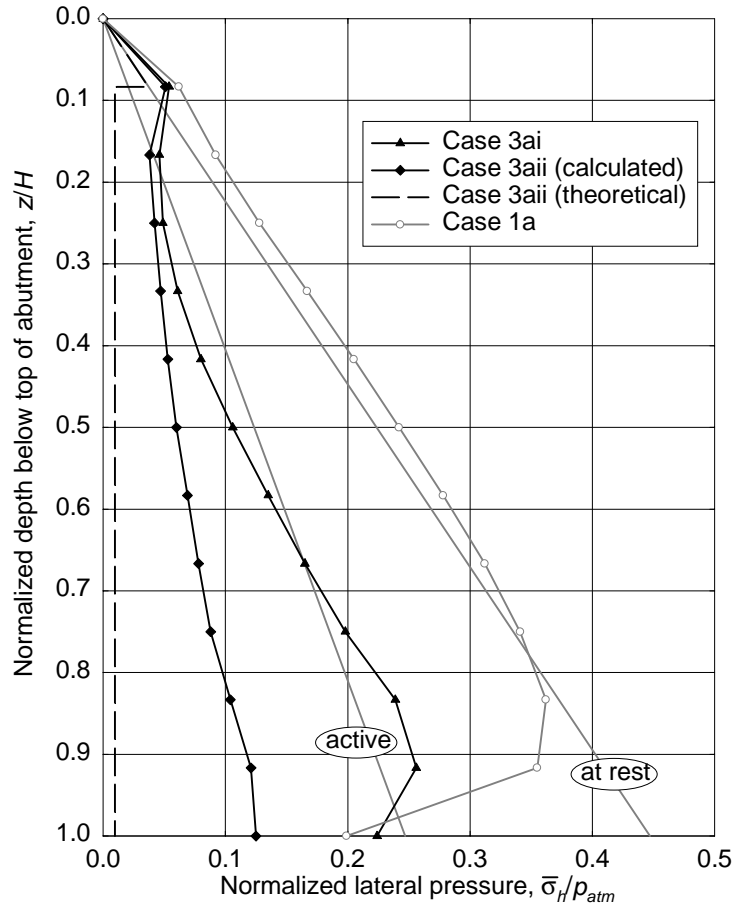
Figure 3.67. Case 3a:
Lateral Pressures at End of Construction

For these assumptions applied to the problem used in this study, $\beta = 0.05$ which is considerably less in magnitude than the $\beta = 0.30$ calculated.

The author's opinion is that the calculated FEM results are too high compared to what would actually occur in practice. This is based on several reasons:

- Actual construction practice differs in several important ways from the modeling used in the FEM analyses performed for this study. In particular, for simplicity a given layer of elements consisting of both EPS blocks and soil was placed horizontally across the entire mesh (see figures 3.3 and 3.65) in a given step of simulated construction. Thus each element in a given layer was perfectly tight against adjacent ones which had the effect of wedging horizontal stresses into the system (exacerbated to some extent by the assumed $K_o = 1$ within the soil elements at time of placement to simulate compaction effects). In practice, because the soil and EPS blocks would be placed separately horizontal stress relief would occur as each layer of material was placed.

- There is no convenient way in a FEM analysis to simulate the small gaps that will often exist between EPS blocks as they are placed. Such gaps also contribute to horizontal stress relief.

- Observations of actual EPS-block geofoam fills and structures support the theoretical lateral pressure diagram shown by the dashed line in Figure 3.67 (Horvath 1995b).

Despite the presumed errors in the calculated FEM results, the model used for this study was judged to be the best that could be used with a reasonable level of computational effort. Therefore, it was decided to proceed with the assessment of the Case 3 results based on the assumption that the results would at least provide insight into the relative changes that occur during thermal loading. However, it is clear that future numerical modeling of this and similar problems needs to address the issue of simulating construction more rigorously.

3.3.5.3 First Thermal Contraction Peak (Case 3a). The lateral pressures at the first thermal contraction peak are shown in Figure 3.68. Corresponding results from the baseline Case 1a are shown together with the theoretical pressures. Significant reductions overall from the end of construction condition occur (β = 0.33 and 0.12 for the active and full wedges respectively), especially along the upper portion of the abutment where pressures drop to zero and a small separation between the abutment and geofoam was calculated. This is due to the fact that contraction of the bridge superstructure pulled the top of the abutment outward approximately 9 mm (0.4 in) as expected from theoretical calculations.
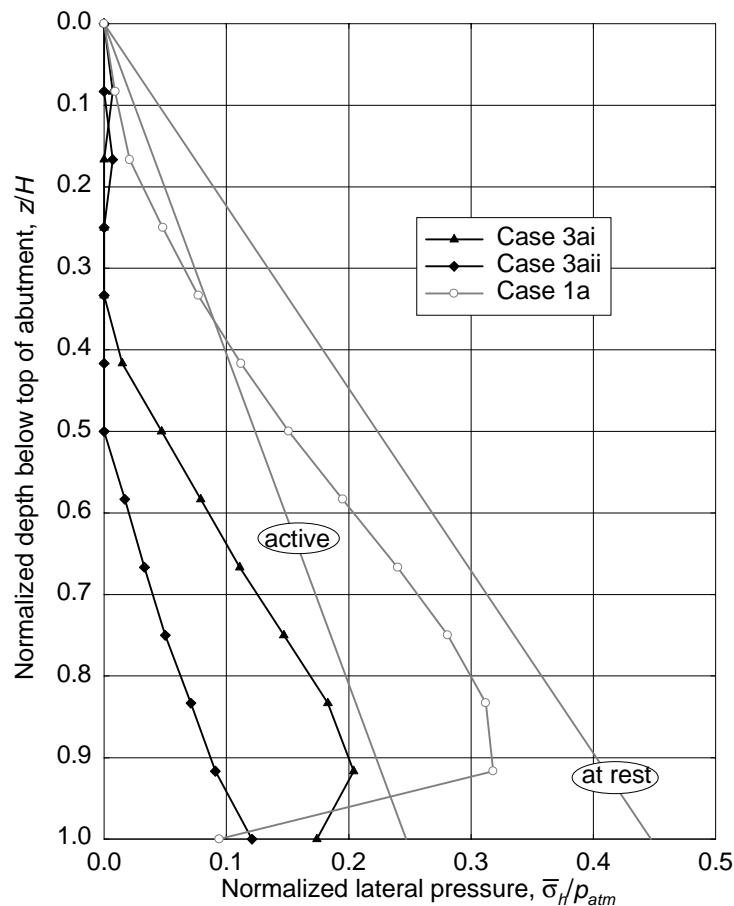
Figure 3.68. Case 3a:
Lateral Pressures at First Thermal Contraction Peak

The settlement of the ground surface immediately behind the abutment was small (approximately 3 mm (0.1 in)) for both Case 2a subcases.

3.3.5.4 First Thermal Expansion Peak (Case 3a). The calculated lateral earth pressures at the first thermal expansion peak are shown in Figure 3.69 together with the results from the baseline Case 1a and the theoretical active, normally consolidated at-rest and passive states. Overall, the normalized horizontal resultant forces are $\beta = 0.90$ and 0.56 for cases 3ai and 3aii respectively. These are well below the Case 1a baseline value ($\beta = 1.5$) indicating that the EPS blocks are quite effective in reducing lateral pressures even in the compressive loading induced by thermal expansion of the bridge superstructure.
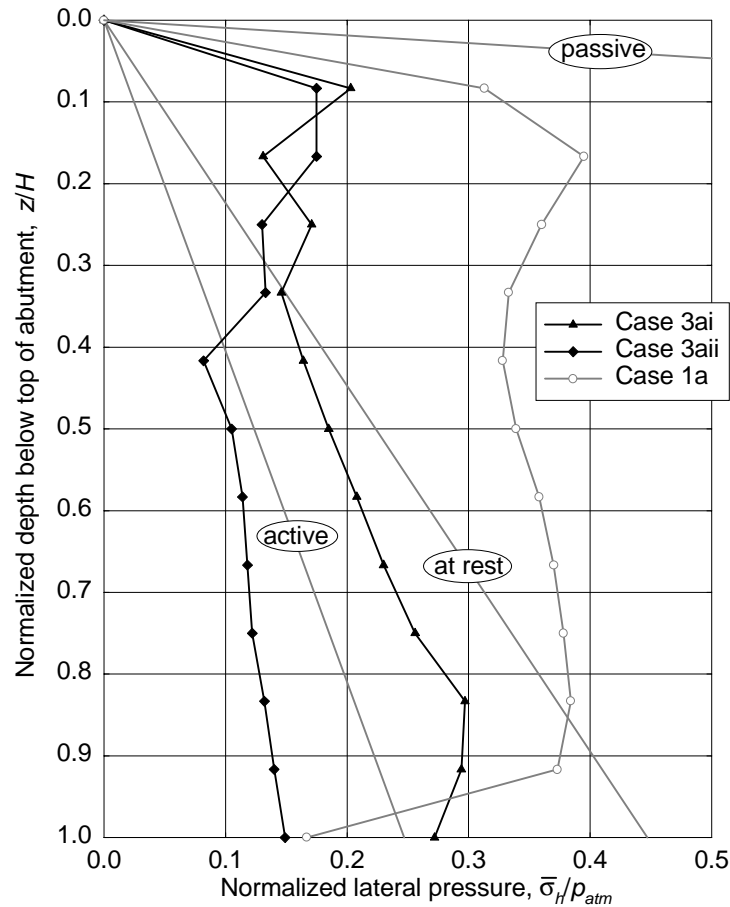
Figure 3.69. Case 3a:
Lateral Pressures at First Thermal Expansion Peak

As noted in Section 3.3.5.1, a concern when using EPS-block geofoam as lightweight fill with IABs is that the lateral pressures not exceed the elastic-limit stress of the EPS which is the de facto maximum allowable stress under service loads. The elastic limit stress for the 20 kg/m^3 (1.25 lb/ft^3) EPS assumed in this study is approximately 50 kPa (1000 lb/ft^2) which would be a lateral pressure, $\overline{\sigma}_h / p_{atm}$, $= 0.5$. Referring to Figure 3.69, the calculated lateral pressures for both the active wedge (Case 3ai) and full wedge (Case 3aii) subcases are well below this value.

3.3.5.5 End of First Thermal Cycle (Case 3a). The calculated lateral pressures at completion of the first full thermal cycle are shown in Figure 3.70. The corresponding results from the baseline Case 1a as well as the usual theoretical pressures are shown also for absolute comparison purposes. Overall, the resultant forces, β, = 0.57 and 0.32 for subcases 3ai and 3aii respectively which are approximately the same as at the end of construction.
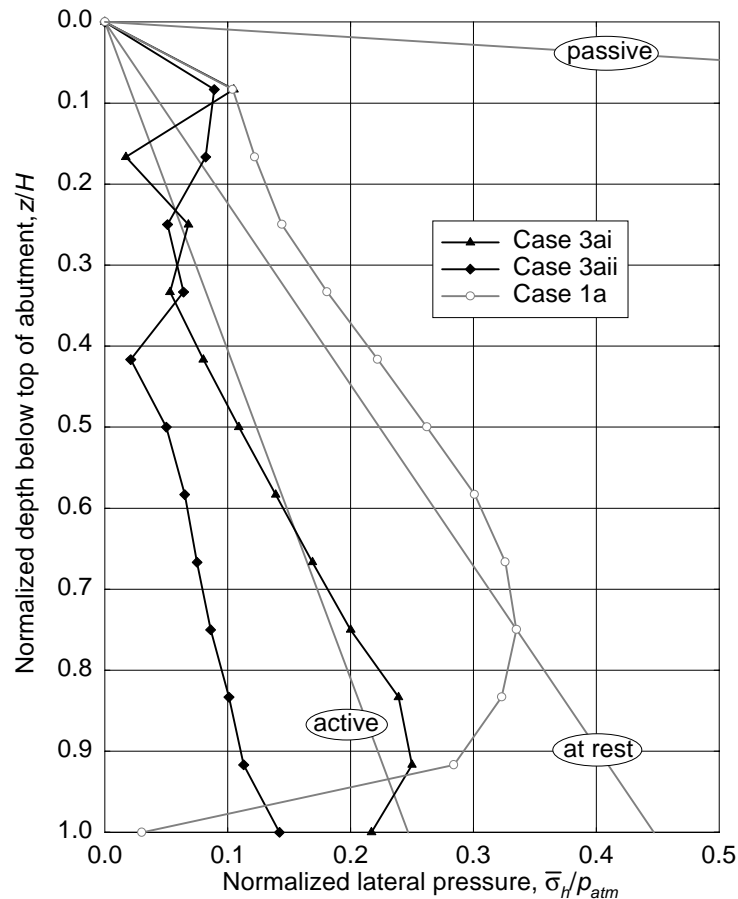
Figure 3.70. Case 3a:
Lateral Pressures at End of First Thermal Cycle

3.3.5.6 Fourth (Final) Thermal Expansion Peak (Case 3a). The calculated lateral pressures for this load are shown in Figure 3.71. The corresponding results from the baseline Case 1a as well as the usual theoretical pressures are shown also for absolute comparison purposes. The normalized resultant force, β, = 1.15 and 0.66 for subcases 3ai and 3aii respectively which are 28% and 18% greater respectively than at the first thermal expansion peak. However the lateral pressures are still significantly less than those for the baseline Case 1a (β = 1.8 at the fourth peak). Note that the lateral stresses for the active-wedge case (3ai) exceed the elastic-limit stress of the EPS-block geofoam ($\overline{\sigma}_h / p_{atm}$ = 0.5) at the bottom of the abutment.
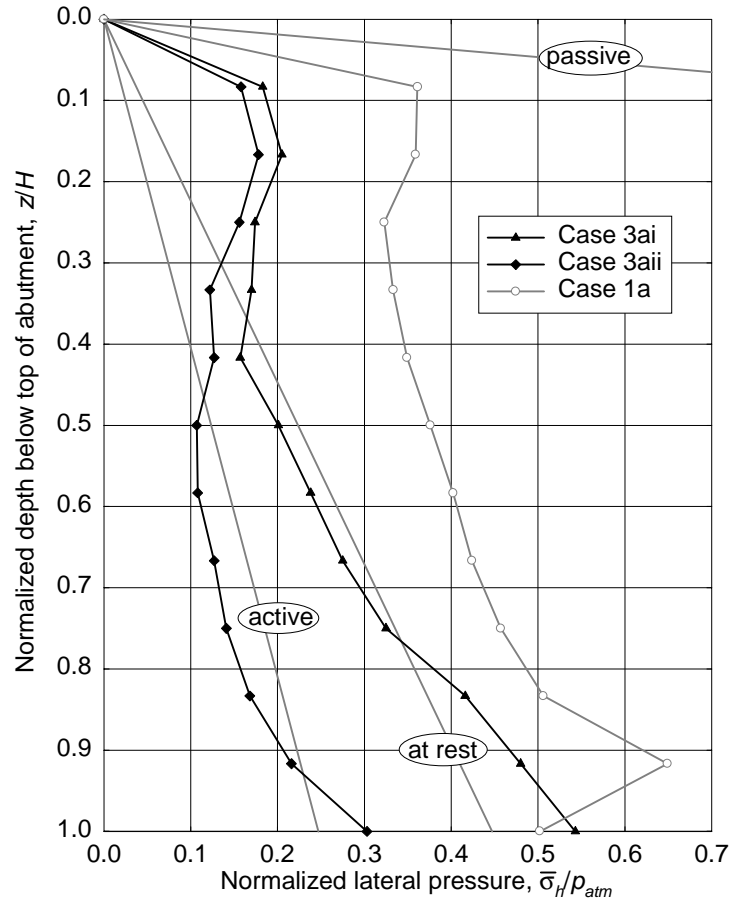
Figure 3.71. Case 3a:
Lateral Pressures at Fourth Thermal Expansion Peak

3.3.5.7 End of Fourth (Final) Thermal Cycle (Case 3a). The final distribution of calculated lateral pressures is shown in Figure 3.72. The corresponding results from the baseline Case 1a as well as the usual theoretical pressures are also shown for absolute comparison purposes. The normalized resultant forces, β, = 0.78 and 0.33 for subcases 3ai and 3aii respectively which are 39% and 10% greater respectively than at the end of construction. However, the lateral pressures are still significantly less than those for the baseline Case 1a (β = 1.3 after four thermal cycles).
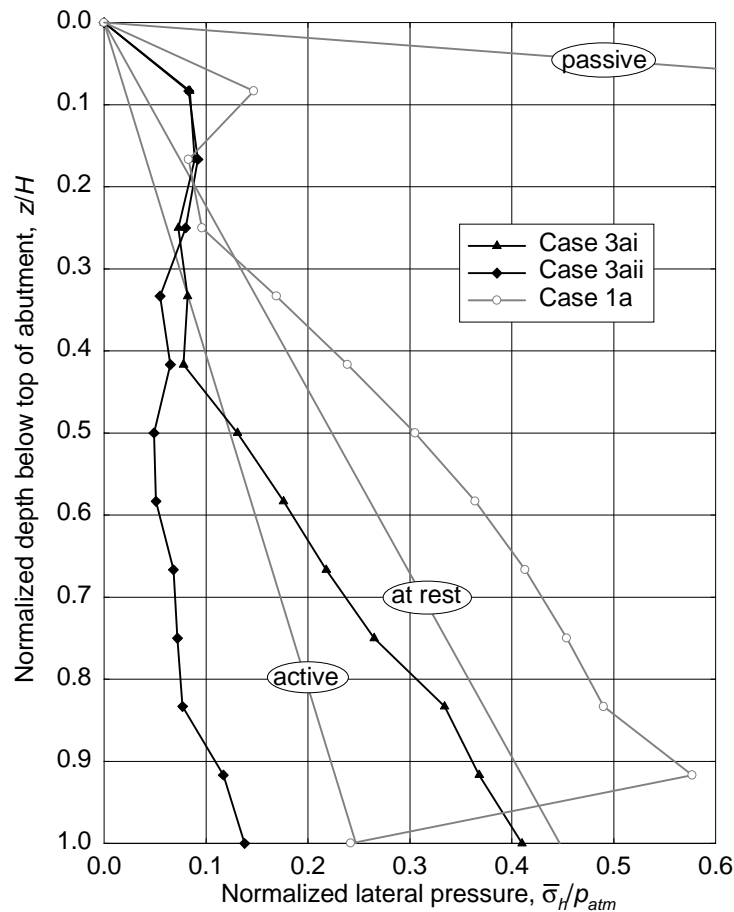
Figure 3.72. Case 3a:
Lateral Pressures at End of Fourth Thermal Cycle

With regard to displacements, the behavior of the two subcases (3ai and 3aii) was the same for all practical purposes. At the top of the abutment, there was essentially no net horizontal movement compared to the initial post-construction position. The bottom of the abutment moved outward 3 mm (0.1 in) relative its initial post-construction location.

With regard to vertical displacements, the top of the abutment exhibited a net upward movement of approximately 6 mm (0.2 in) while the surface of the soil immediately behind the abutment also had a net upward movement of 3 mm (0.1 in).

3.3.5.8 End of Construction (Case 3b and Case 3a/3b Comparison). The first set of results examined is at the completion of the simulated construction of the bridge and associated earthwork. The calculated lateral pressures acting on the back of the abutment for Case 3b with a geofoam compressible inclusion between the back of the abutment and the EPS-geofoam blocks are shown in Figure 3.73. Note that the calculated results shown for the Case 3b subcases are actually the stresses within the compressible inclusion, not along the back of the abutment, for the reasons discussed in sections 3.3.4.1 and 3.3.4.2. Also shown in this figure for absolute comparative purposes are the theoretical active and normally consolidated at-rest state pressures for a soil backfill/fill (from Case 1) as well as the calculated results from the baseline Case 1a.
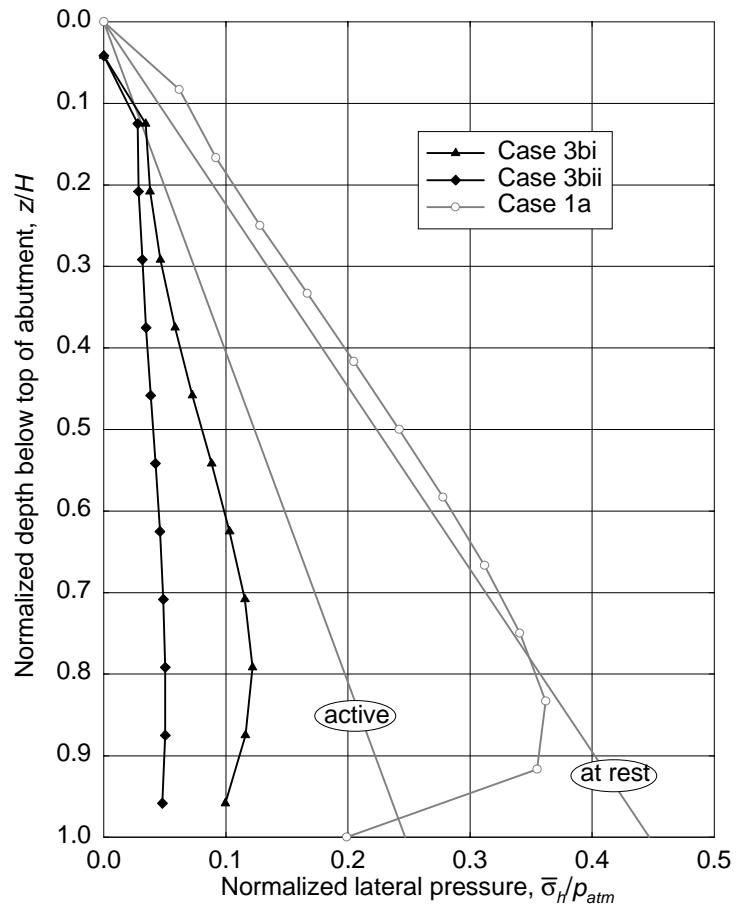
Figure 3.73. Case 3b:
Lateral Pressures at End of Construction

In both Case 3b subcases the horizontal resultant forces are reduced significantly (by approximately 40%) from the corresponding Case 3a subcases where no compressible inclusion was used (β = 0.33 and 0.17 for cases 3bi and 3bii respectively). This reduction can be seen graphically in Figure 3.74 where the results for comparable conditions with and without the compressible inclusion are shown for the active wedge (Figure 3.74(a)) and full wedge (Figure 3.74(b)). As can be seen, most of the resultant force reduction due to the use of the compressible inclusion is the result of lateral pressure reduction near the bottom of the abutment.
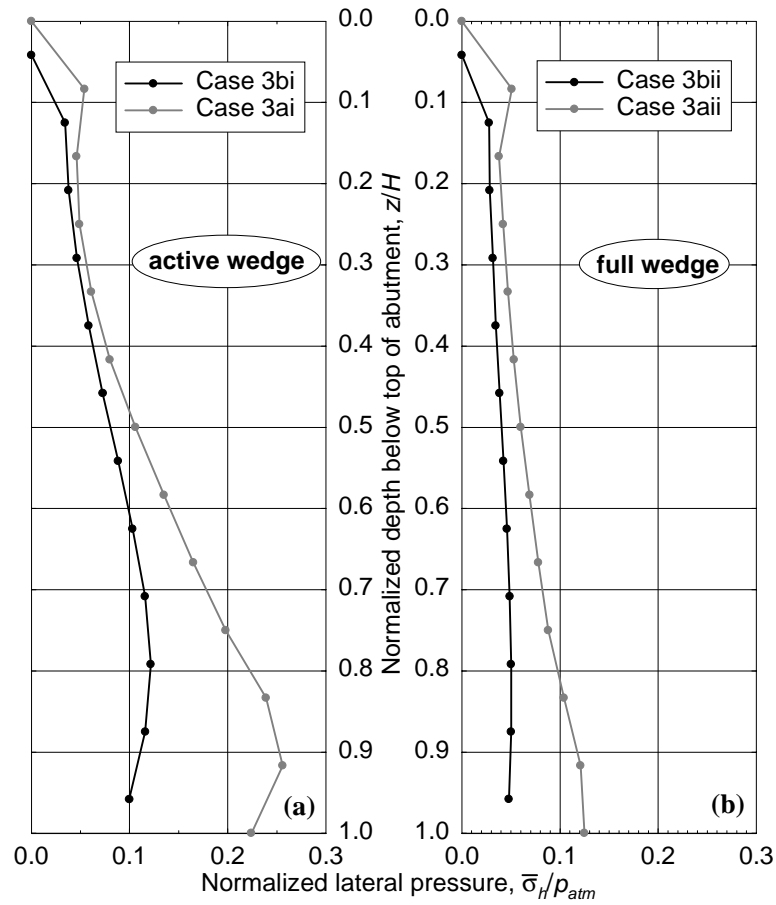
**Figure 3.74. Case 3: Comparison of 3a/3b Results
at End of Construction**

The patterns and magnitudes of compressive strain and displacement within the geofoam compressible inclusion are shown in Figure 3.75. They are both qualitatively and quantitatively different than those for an all-soil backfill under comparable loading (Figure 3.24). The deformation patterns in Figure 3.75 are both more uniform with depth and smaller in magnitude than for the all-soil cases considered in the various Case 2 problems.
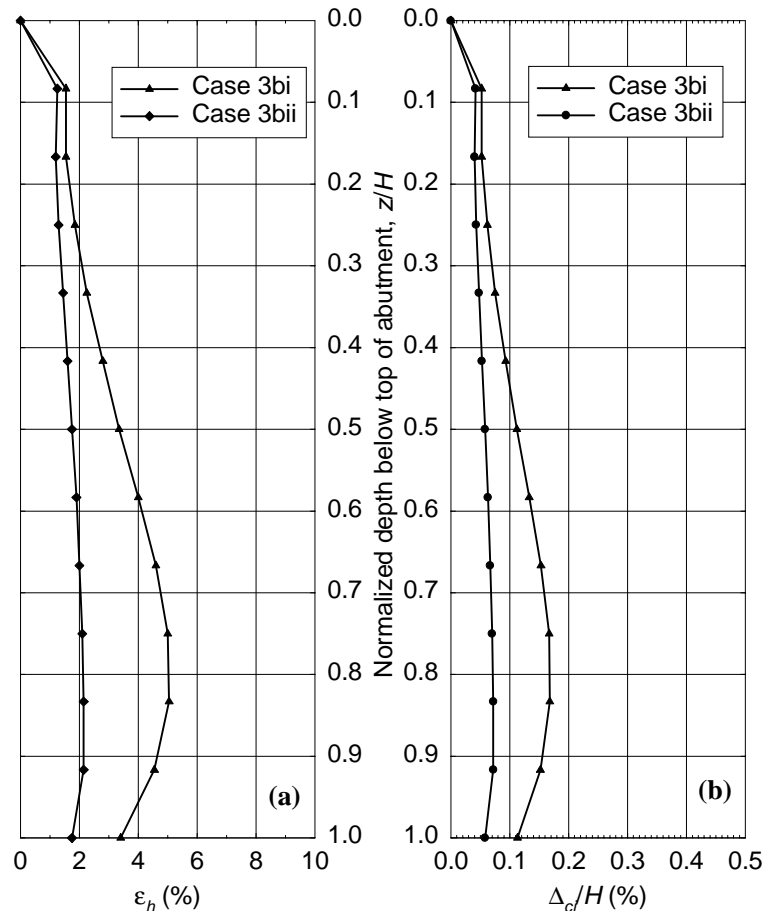
Figure 3.75. Case 3b: Horizontal Deformation of Geofoam Compressible Inclusion at End of Construction

3.3.5.9 First Thermal Contraction Peak (Case 3b and Case 3a/3b Comparison).

The lateral pressures on the back of the abutment for Case 3b at the first thermal contraction peak are shown in Figure 3.76. Also shown in this figure for absolute comparative purposes are the theoretical active and normally consolidated at-rest state pressures for a soil backfill/fill (from Case 1) as well as the calculated results from the baseline Case 1a.

In both Case 3b subcases the resultant forces are reduced significantly (by 50% or more) from the corresponding Case 3a subcases where no compressible inclusion was used ($\beta = 0.22$ and 0.06 for cases 3bi and 3bii respectively). The reduction can be seen graphically in Figure 3.77 where the results for comparable conditions with and without the compressible inclusion are shown for the active wedge (Figure 3.77(a)) and full wedge (Figure 3.77(b)). As can be seen in this figure, essentially all of the lateral stress reduction provided by the compressible inclusion occurs near the bottom of the abutment as it did for the end-of-construction condition.
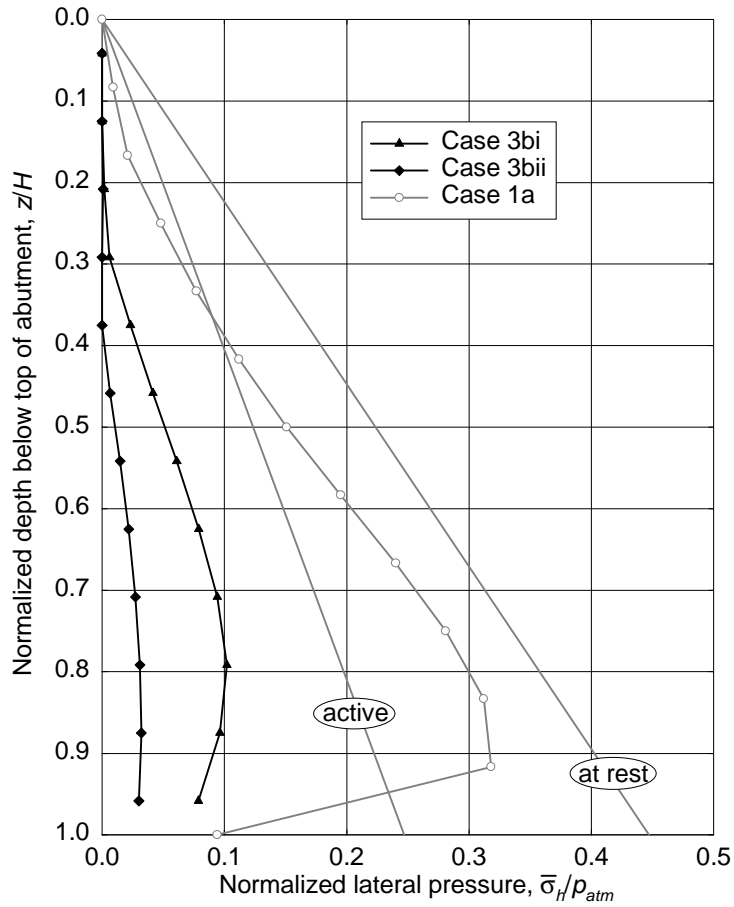
Figure 3.76. Case 3b:
Lateral Pressures at First Thermal Contraction Peak
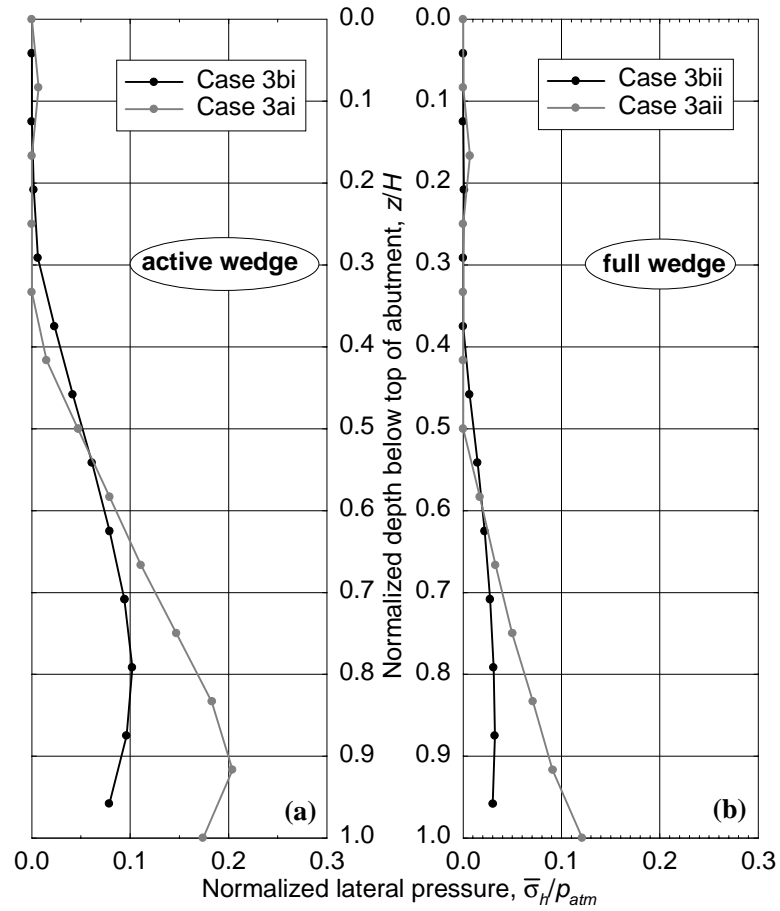
**Figure 3.77. Case 3: Comparison of 3a/3b Results
at First Thermal Contraction Peak**

The patterns and magnitudes of compressive strain and displacement within the compressible inclusion are shown in Figure 3.78. They are both qualitatively and quantitatively different than those for an all-soil backfill under comparable loading (Figure 3.27). The deformation pattern is both more uniform with depth and smaller in magnitude than for the all-soil cases considered in the various Case 2 problems.
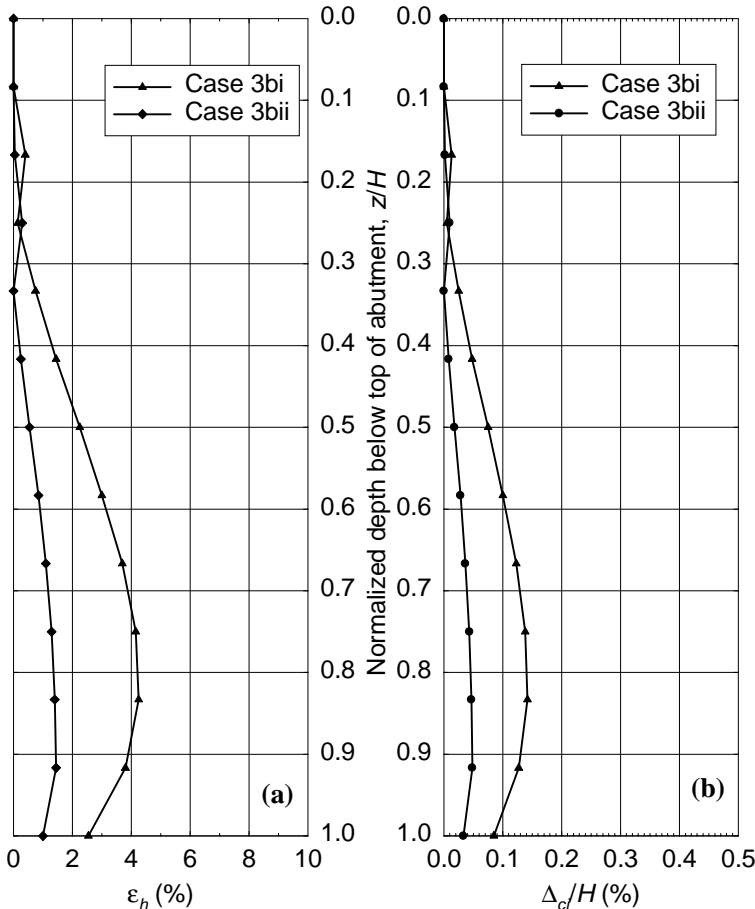
**Figure 3.78. Case 3b: Horizontal Deformation of Geofoam
Compressible Inclusion at First Thermal Contraction Peak**

The settlement of the ground surface immediately behind the abutment was approximately zero for both Case 3b subcases. In addition, there was no indication of upward movement of the abutment as observed for other cases.

3.3.5.10 First Thermal Expansion Peak (Case 3b and Case 3a/3b Comparison).
The lateral pressures on the back of the abutment for Case 3b at the first thermal expansion peak are shown in Figure 3.79. Also shown in this figure for absolute comparative purposes are the theoretical active, normally consolidated at-rest and passive state pressures for a soil backfill/fill (from Case 1) as well as the calculated results from the baseline Case 1a.
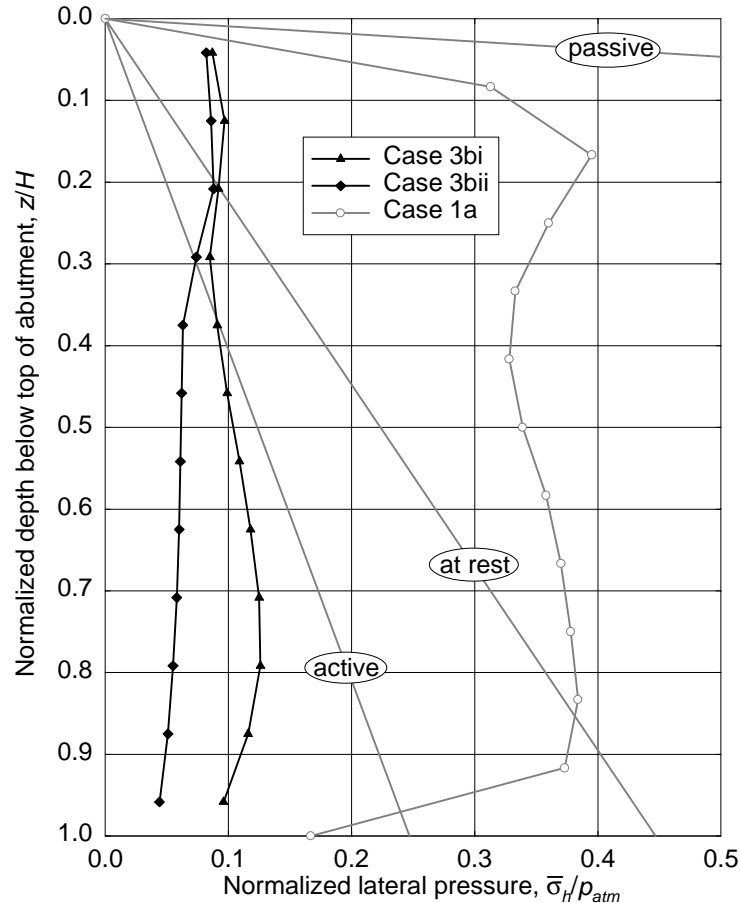
Figure 3.79. Case 3b:
Lateral Pressures at First Thermal Expansion Peak

In both Case 3b subcases the resultant forces are reduced significantly (by approximately 50%) from the corresponding Case 3a subcases where no compressible inclusion was used ($\beta = 0.46$ and 0.29 for cases 3bi and 3bii respectively). The reduction can be seen graphically in Figure 3.80 where the results for comparable conditions with and without the compressible inclusion are shown for the active wedge (Figure 3.80(a)) and full wedge (Figure 3.80(b)). Note that here the benefit of using a compressible inclusion occurs over the full height of the abutment, not just towards its bottom as was observed both after construction and at the first thermal contraction peak.

As noted previously in Section 3.3.5.4 for Case 3a, one concern when using EPS-block geofoam as lightweight fill with IABs is that the maximum compressive stresses in any direction not exceed the elastic-limit stress of the EPS which is essentially the maximum allowable stress under service loads. Although not shown in Figure 3.79, the elastic-limit stress for the 20 kg/m^3 (1.25 lb/ft^3) EPS assumed in this study would be approximately 50 kPa (1000 lb/ft^2) which would be a normalized lateral pressure, $\overline{\sigma}_h / p_{atm}$, = 0.5. As can be seen in Figure 3.79, the calculated lateral pressures for both the active (Case 3bi) and full (Case 3bii) wedge subcases are well less than this value.
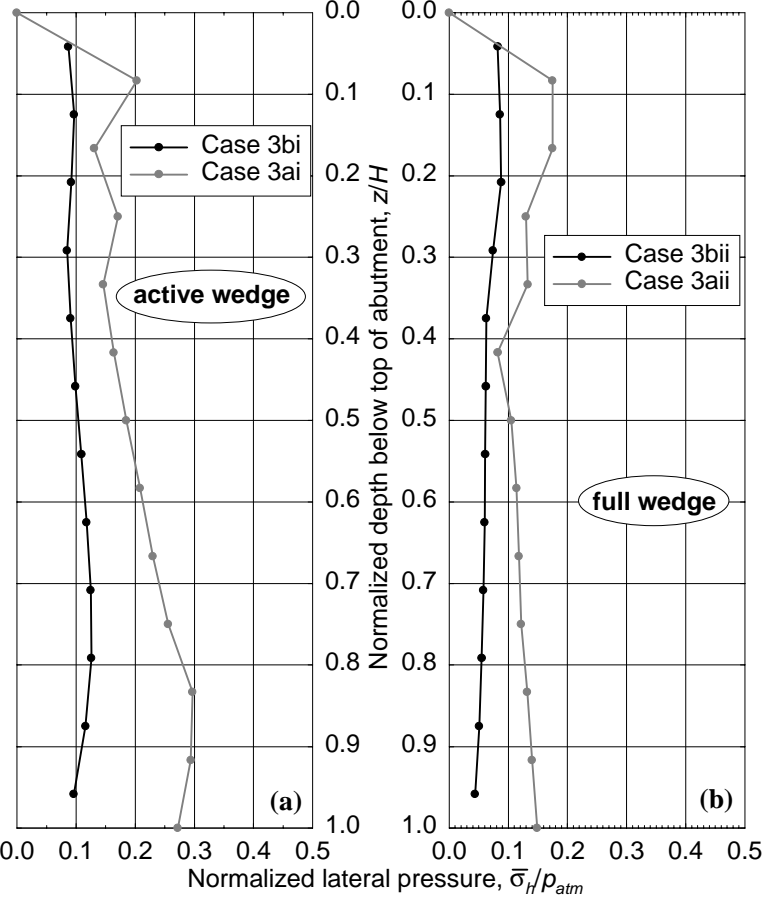
**Figure 3.80. Case 3: Comparison of 3a/3b Results
at First Thermal Expansion Peak**

The patterns and magnitudes of compressive strain and displacement within the geofoam compressible inclusion are shown in Figure 3.81. Although the strain/deformation patterns are nearly uniform with depth, the patterns are deceptively simple in appearance as the strains and deformations actually develop very differently at different depths along the back of the abutment. Specifically, the abutment rotates about its bottom into the EPS blocks and retained soil. Therefore, at and near the top of the abutment the geofoam compressible inclusion is compressed to accommodate the inward movement of the abutment. However, toward and at the bottom of the abutment it is the EPS blocks and retained soil that are pushing horizontally and compressing the compressible inclusion. Thus the compressible inclusion is simultaneously providing two benefits: accommodating the thermal movement of the upper portion of the abutment and relieving lateral stresses from the retained fill (EPS blocks plus soil).

3.3.5.11 End of First Thermal Cycle (Case 3b and Case 3a/3b Comparison). The lateral pressures on the back of the abutment for Case 3b at the completion of the first full thermal cycle are shown in Figure 3.82. Also shown in this figure for absolute comparative purposes are the theoretical active, normally consolidated at-rest and passive state pressures for a soil backfill/fill (from Case 1) as well as the calculated results from the baseline Case 1a.
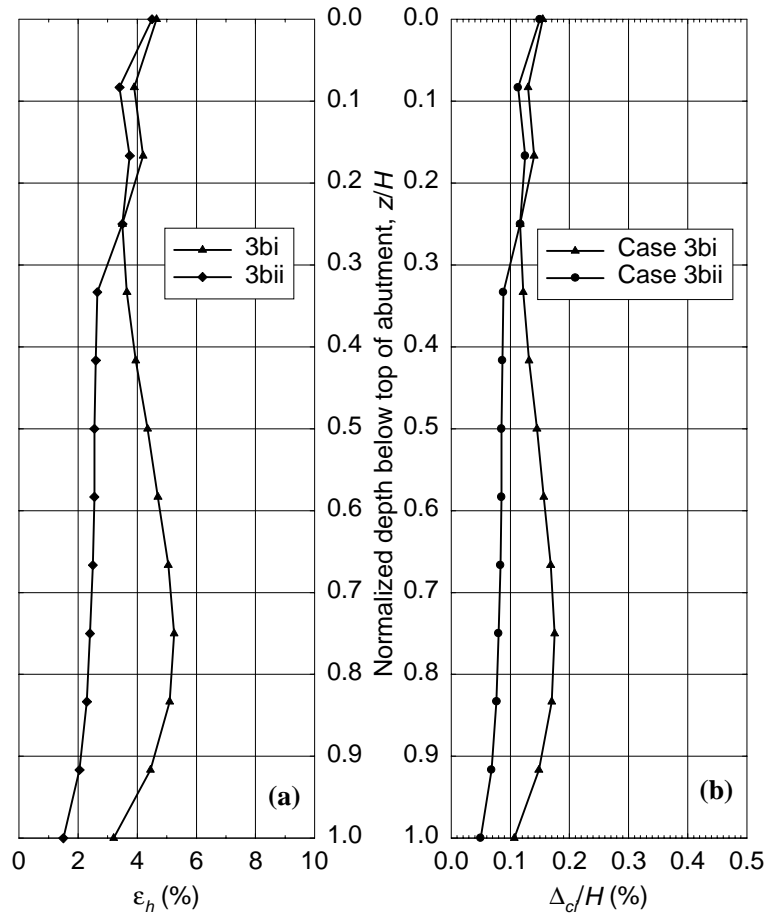
Figure 3.81. Case 3b: Horizontal Deformation of Geofoam Compressible Inclusion at First Thermal Expansion Peak
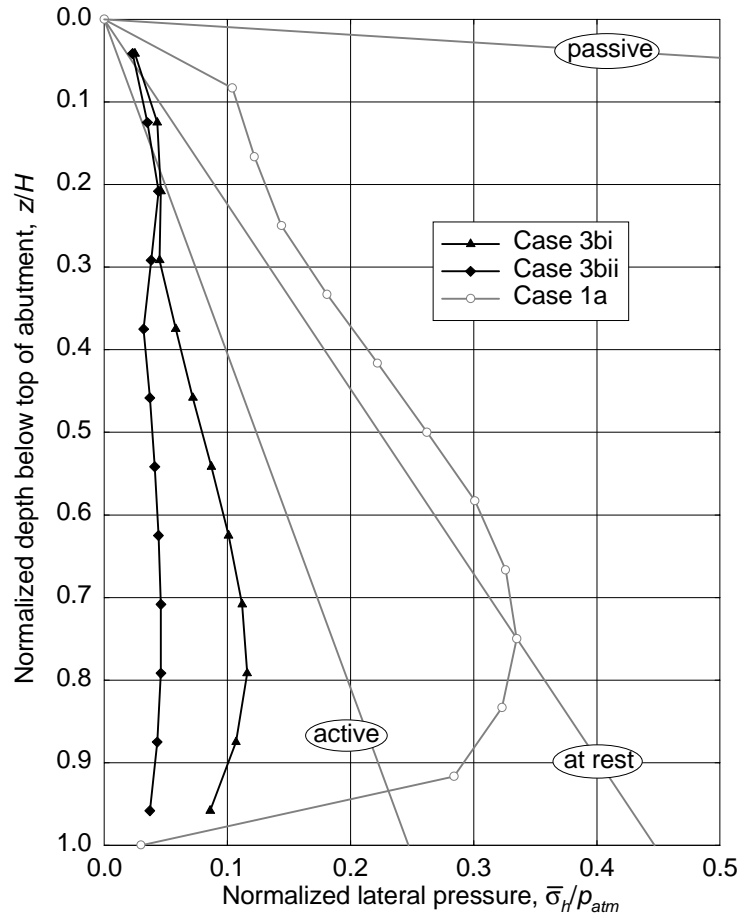
Figure 3.82. Case 3b:
Lateral Pressures at End of First Thermal Cycle

In both Case 3b subcases the resultant forces returned to those that existed at the end of construction ($\beta = 0.33$ and 0.17 for cases 3bi and 3bii respectively). By comparison, both Case 3a subcases (without the compressible inclusion) were not only significantly larger in magnitude than the Case 3b subcases but also exhibited slight increases in resultant forces after one complete thermal cycle.

3.3.5.12 Fourth (Final) Thermal Expansion Peak (Case 3b and Case 3a/3b Comparison). The lateral pressures on the back of the abutment for Case 3b at the fourth and final thermal expansion peak are shown in Figure 3.83. Also shown in this figure for absolute comparative purposes are the theoretical active, normally consolidated at-rest and passive state pressures for a soil backfill/fill (from Case 1) as well as the calculated results from the baseline Case 1a.
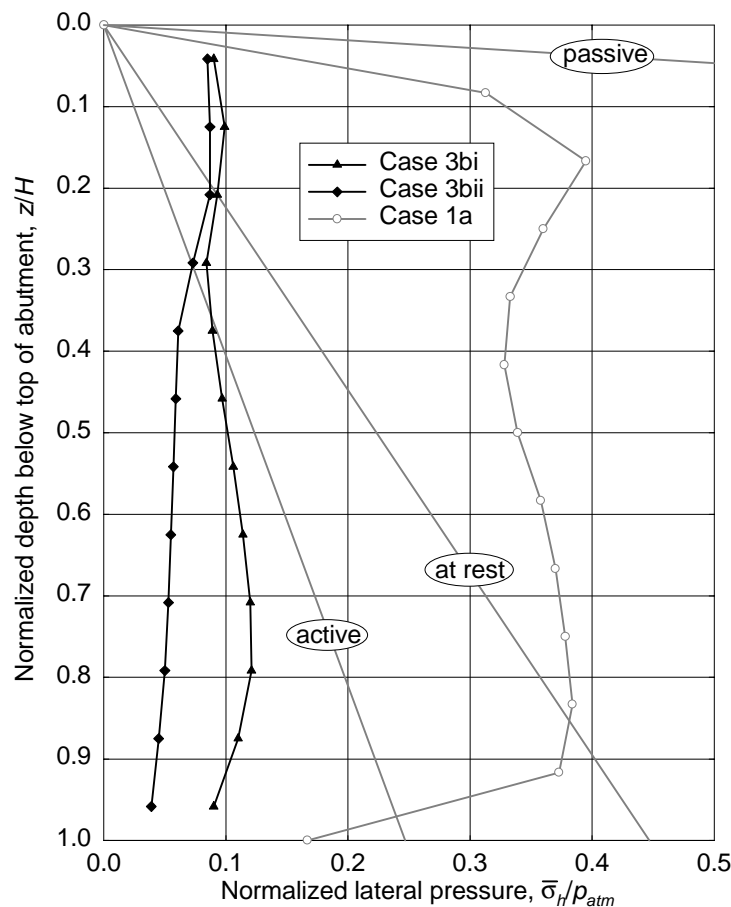
Figure 3.83. Case 3b:
Lateral Pressures at Fourth Thermal Expansion Peak

In both Case 3b subcases the resultant forces were essentially the same as at the first thermal expansion peak ($\beta = 0.45$ and 0.28 for cases 3bi and 3bii respectively). By comparison, both Case 3a subcases (without the compressible inclusion) exhibited significant increases in resultant forces between the first and fourth thermal expansion peaks, and were significantly larger in magnitude than the corresponding Case 3b subcases.

3.3.5.13 End of Fourth (Final) Thermal Cycle (Case 3b and Case 3a/3b Comparison). The lateral pressures on the back of the abutment for Case 3b at the end of the fourth and final thermal cycle are shown in Figure 3.84. Also shown in this figure for absolute comparative purposes are the theoretical active, normally consolidated at-rest and passive state pressures for a soil backfill/fill (from Case 1) as well as the calculated results from the baseline Case 1a.
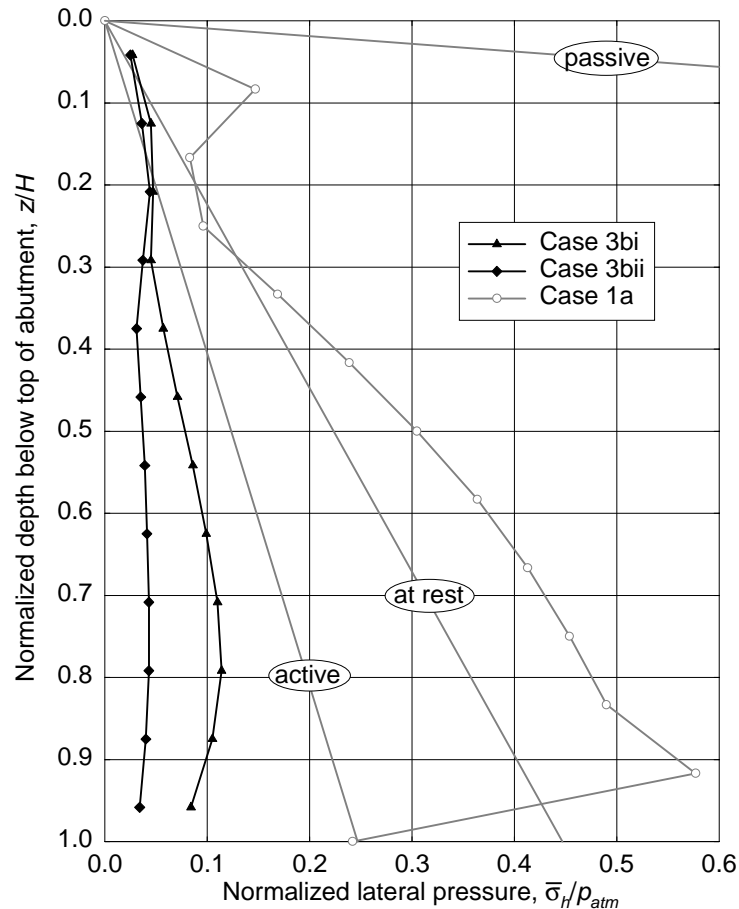
Figure 3.84. Case 3b:
Lateral Pressures at End of Fourth Thermal Cycle

In both Case 3b subcases the resultant forces were essentially the same as at the end of both the first thermal cycle as well as end of construction (β = 0.33 and 0.17 for cases 3bi and 3bii respectively). By comparison, both Case 3a subcases (without the compressible inclusion) were not only significantly larger in magnitude than the corresponding Case 3b subcases but exhibited increases in resultant forces between the end of construction and completion of four thermal cycles.

With regard to surface displacements, both the abutment and adjacent ground surface were essentially at the same level (i.e. no net settlement or heave) as at the end of construction.

Section 4
Conclusions and Recommendations

4.1 RESULTS FROM PRESENT STUDY

The broad goal of this study was to evaluate the efficacy of geosynthetics in eliminating or at least reducing several significant chronic problems exhibited by IABs:

- increases in lateral earth pressures on the abutments during seasonal summer expansion of the bridge superstructure;

- incremental, permanent buildup (ratcheting) of lateral earth pressures on the abutments as a result of annual thermal cycles of the bridge superstructure; and

- permanent settlement of the ground surface adjacent to the abutments as a result of annual thermal cycles of the bridge superstructure which will produce voids under approach slabs or settlement of the pavement surface on approach embankments.

An assessment of the various alternatives studied should take into account each of these issues. Clearly, however, control of lateral pressures acting on the abutments of IABs is the predominant issue so is used to provide an initial assessment of alternatives.

The relative efficiency of the alternatives considered in this study in addressing the lateral-pressure problem can be most easily compared by using the parameter of normalized horizontal resultant force, β. This comparison is facilitated by assembling the β values previously presented in Section 3 in tabular form as shown in Table 4.1. The values are given for each of the key load stages discussed in detail in Section 3. The baseline Case 1a is highlighted as this is the de facto reference standard for the other 11 alternatives. The values of β obtained using classical earth pressure theories for the active, normally consolidated at-rest and passive states are also noted at the bottom of Table 4.1 for comparative purposes.

Although 12 different alternatives were evaluated for this study, they can effectively be grouped into four categories of design strategies that would likely be considered in practice:

- Unreinforced soil backfill/fill (Case 1a). This is the current practice and baseline case.

- Geofoam compressible inclusion with unreinforced soil backfill/fill (Case 2a). This is the REP-Wall concept.

- Geofoam compressible inclusion with reinforced soil backfill/fill (Case 2b). This is the ZEP-Wall concept. It is likely that most applications in practice would use some type of face-wrapped polymeric reinforcement (geogrid or geotextile) which was Case 2bi in this study.

- Geofoam lightweight fill with a geofoam compressible inclusion (Case 3b). The full-wedge alternative, which was Case 3bii in this study, appears to be the more desirable.

Figure 4.1 shows the variation of β with load cycle for each of these four categories.

Table 4.1. Comparison of Normalized Horizontal Resultant Forces, β

analysis case		maximum contraction		neutral			maximum expansion	
		1st cycle	4th cycle	end of construction	1st cycle	4th cycle	1st cycle	4th cycle
1a	unreinforced soil (baseline)	0.68	-	0.99	0.98	1.3	1.5	1.8
1bi	reinforced soil · polymeric	0.60	-	0.92	0.86	?	1.4	?
1bii	reinforced soil · metallic	0.44	-	0.82	?	?	1.3	?
2ai	geofoam compressible inclusion · 100 mm (4 in)	0.46	-	0.61	0.66	0.65	0.94	1.0
2aii	geofoam compressible inclusion · 200 mm (8 in)	0.42 (0.40)	0.44 (0.38)	0.53 (-)	0.57 (0.50)	0.56 (0.50)	0.76 (0.66)	0.79 (0.63)
2aiii	geofoam compressible inclusion · 400 mm (16 in)	0.37	-	0.45	0.46	0.49	0.58	0.62
2bi	200 mm (8 in) geofoam compressible inclusion + reinforcement · polymeric	0.28 (0.28)	0.24 (0.26)	0.42 (-)	0.41 (0.40)	0.40 (0.38)	0.59 (0.55)	0.62 (0.52)
2bii	200 mm (8 in) geofoam compressible inclusion + reinforcement · metallic	0.09 (0.09)	0.03 (0.05)	0.23 (-)	0.23 (0.20)	0.15 (0.12)	0.44 (0.37)	0.41 (0.28)
3ai	geofoam wedge as lightweight fill · active	0.33	-	0.56	0.57	0.78	0.90	1.15
3aii	geofoam wedge as lightweight fill · full	0.12	-	0.30	0.32	0.33	0.56	0.66
3bi	geofoam fill wedge + 200 mm (8 in) inclusion · active	0.22	-	0.33	0.33	0.33	0.46	0.45
3bii	geofoam fill wedge + 200 mm (8 in) inclusion · full	0.06	-	0.17	0.17	0.17	0.29	0.28

Notes

1. For reference, β = 0.55, 1.0 and 24 for the theoretical active, normally consolidated at-rest and passive states respectively for an unreinforced soil backfill/fill.

2. All cases:
   - An entry of "-" indicates that β was not calculated for this combination of variables.
   - An entry of "?" indicates that the calculated result was omitted intentionally due to suspected error due to the approximate way in which the reinforcement was modeled in this study.

3. Case 2:
   - Values not in parentheses are for the original analyses with a frictional interface between the geofoam compressible inclusion and back of the abutment.
   - Values in parentheses are for the supplemental analyses with a fixed interface between the geofoam compressible inclusion and back of the abutment.

4. Case 3:
   - All Case 3b analyses assumed a fixed interface between the geofoam compressible inclusion and back of the abutment.
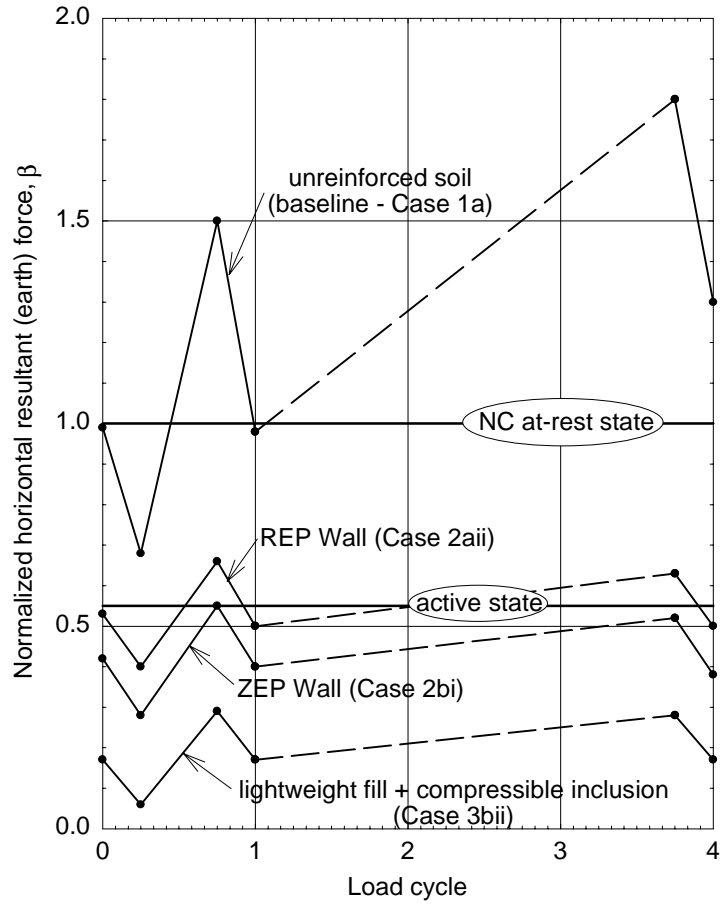
**Figure 4.1. Comparison of Normalized Horizontal
Resultant Forces for Various Design Alternatives**

However, with regard to the settlement problem it appears that only two of these four alternatives are effective at controlling settlements adjacent to the abutment:

- the ZEP Wall (Case 2bi) in which the synergistic combination of a face-wrapped reinforced soil mass plus resilient-EPS compressible inclusion effectively stiffens the soil against settlement. This is consistent with the findings of earlier independent research by Monley and Wu (1993).

- the use of a full wedge of EPS-block geofoam lightweight fill with a resilient-EPS geofoam compressible inclusion (Case 3bii). This is consistent with almost 30 years of experience with this material as a lightweight fill in which it has been found to be inherently self stable.

With reference to Figure 4.1, it is of interest to note that these two alternatives also produce the lowest horizontal forces on the abutment as well.

4.2 INTERIM SUGGESTIONS FOR PRACTICE

Overall, the results of this study confirm the author's original hypothesis that an effective, long-term design solution to integral abutment bridge problems must contain two complementary elements:

- a highly compressible filler (compressible inclusion) placed between the back of the abutment and backfill/fill material to:
  - accommodate the seasonal thermal movements of the structurally monolithic bridge superstructure and abutments,
  - reduce lateral pressures on the abutments under summer expansion of the superstructure and
  - prevent the long-term ratcheting upward of lateral pressures on the abutments in general; and

- an inherently self-stable fill mass behind the abutment to prevent the development of a settlement trough adjacent to the top of the abutment that can lead to failure of approach slabs or development of the "bump at the end of the bridge" on the approach embankment.

Of the alternatives considered in this study, there appear to be two viable means to achieve these goals simultaneously:

- the REP-Wall concept which uses a resilient-EPS geofoam compressible inclusion plus face-wrapped tensile reinforcement (most likely a geogrid or geotextile) of the soil backfill/fill or

- a full triangular wedge of EPS-block geofoam as lightweight fill with a resilient-EPS geofoam compressible inclusion between the EPS blocks and abutment.

The selection should be based on both technical and cost considerations. It is likely that the REP-Wall alternative will be the more economical in general and should be evaluated first for technical acceptability on a given project. It is likely that the wedge of EPS-block geofoam fill would be more expensive but more desirable for sites underlain with soft, compressible soils where it is necessary to limit global settlement and prevent deep-seated rotational failure of the

approach embankment as well as limit lateral squeeze of the underlying soft soil which can cause buckling of deep foundations supporting the abutments.

It is worth noting that the geofoam compressible inclusion in both cases can easily be designed to be multi-functional and act as a thermally insulated chimney drain for ground water control behind the abutment in addition to serving its primary function as a compressible inclusion (Horvath 1995a, 1995b).

4.3 RECOMMENDATIONS FOR FUTURE STUDY

There is a high degree of confidence in the concepts developed for this study because they utilize well-proven geosynthetic products in basic ways in which they are already known to be successful in practice. Nevertheless, good engineering practice dictates that these concepts should be validated by a comprehensive program consisting of physical testing as well as observation of instrumented IABs that utilize either of the two designs suggested in Section 4.2. Both large-scale 1-g and small-scale centrifuge testing have proven to be viable physical testing methodologies for IABs and there is no reason why both could not be utilized in future studies.

Development of reliable numerical models that better capture the hysteretic, ratcheting behavior of soil should also be investigated, developed if necessary and calibrated using the results of both the physical testing and case history observations. These numerical models, incorporated into appropriate finite-element or finite-difference computer software, should be used to develop simplified analytical methods that could be used in routine practice to determine the required stiffness of the geofoam compressible inclusion and tensile reinforcement (where used).

In the longer term, there are several additional geotechnical issues that should be studied. This includes basic study of the fundamental behavior of IABs incorporating the suggested design strategies discussed in Section 4.2 under seismic load and when fine-grain soils are used as a backfill/fill material. These studies should build on earlier work by Bathurst and Alfaro (1996) and Inglis et al. (1996) involving seismic loading with reinforced soil masses and EPS-geofoam compressible inclusions respectively, as well as the existing body of work (Aytekin et al. 1993, Aytekin 1997, Brookes et al. 1995, Carder et al. 1980, Clayton et al. 1991, O'Connor and Taylor 1994, Symons et al. 1989) involving fine-grain soil and earth retaining structures.

This page intentionally left blank.

Section 5
References

Aytekin, M., Wray, W. K. and Vallabhan, C. V. G. (1993). "Transmitted swelling pressures on retaining structures", *Unsaturated Soils*, S. L. Houston and W. K. Wray (eds.), American Society of Civil Engineers, New York, N.Y., U.S.A., pp. 32-43.

Aytekin, M. (1997). "Numerical modeling of EPS geofoam used with swelling soil", *Geotextiles and Geomembranes*, Elsevier Science Ltd., London, U.K., Vol. 15, Nos. 1-3, pp. 133-146.

Bathurst, R. J. and Alfaro, M. C. (1996). "Review of seismic design, analysis and performance of geosynthetic reinforced walls, slopes and embankments", *Proceedings of the Third International Symposium on Earth Reinforcement (IS-Kyushu '96)*, Fukuoka, Kyushu, Japan.

Boscardin, M. D., Selig, E. T., Lin, R.-S. and Yang, G.-R. (1990). "Hyperbolic parameters for compacted soil", *Journal of Geotechnical Engineering*, American Society of Civil Engineers, New York, N.Y., U.S.A., Vol. 116, No. 1, pp. 88-104.

Briaud, J.-L., James, R. W. and Hoffman, S. B. (1997). "*Settlement of bridge approaches (the bump at the end of the bridge)*", Synthesis of Highway Practice 234, National Academy Press, Washington, D.C., U.S.A., 75 pp.

Broms, B. B. and Ingleson, I. (1971). "Earth pressure against the abutments of a rigid frame bridge", *Géotechnique*, The Institution of Civil Engineers, London, U.K., Vol. 21, No. 1, pp. 15-28.

Brookes, A. H., Carder, D. R. and Darley, P. (1995). "*Earth pressures against an experimental retaining wall backfilled with Lias clay*", TRL Report 152, Transport Research Laboratory, Crowthorne, Berkshire, U.K.

Card, G. B. and Carder, D. R. (1993). "*A literature review of the geotechnical aspects of the design of integral bridge abutments*", Project Report 52, Transport Research Laboratory, Crowthorne, Berkshire, U.K.

Carder, D. R. and Card, G. B. (1997). "*Innovative structural backfills to integral bridge abutments*", Project Report 290, Transport Research Laboratory, Crowthorne, Berkshire, U.K.

Carder, D. R., Murray, R. T. and Krawczyk, J. V. (1980). "*Earth pressures against an experimental retaining wall backfilled with silty clay*", Laboratory Report 946, Transport and Road Research Laboratory, Crowthorne, Berkshire, U.K.

Clayton, C. R. I., Symons, I. F. and Hiedra-Cobo, J. C. (1991). "The pressure of clay backfill against retaining structures", *Canadian Geotechnical Journal*, Vol. 28, No. 2, pp. 282-297.

Clough, G. W. and Duncan, J. M. (1991). "Earth pressures", Chapter 6 in *Foundation Engineering Handbook*, H.-Y. Fang (ed.), Van Nostrand Reinhold, New York, N.Y., U.S.A., 2nd edition.

Duncan, J. M., Clough, G. W. and Ebeling, R. M. (1990). "Behavior and design of gravity earth retaining structures", *Design and Performance of Earth Retaining Structures*, P. C. Lambe and L. A. Hansen (eds.), American Society of Civil Engineers, New York, N.Y., U.S.A., pp. 251-277.

Duncan, J. M., Williams, G. W., Sehn, A. L. and Seed, R. B. (1991). "Estimating earth pressures due to compaction", *Journal of the Geotechnical Engineering Division*, American Society of Civil Engineers, New York, N.Y., U.S.A., Vol. 117, No. 12, pp. 1833-1847.

Ebeling, R. M., Peters, J. F. and Mosher, R. L. (1992). "Finite element analysis of slopes with layer reinforcement", *Stability and Performance of Slopes and Embankments-II*, R. B. Seed and R. W. Boulanger (eds.), American Society of Civil Engineers, New York, N.Y., U.S.A., pp. 1427-1443.

Edgar, T. V., Puckett, J. A. and D'Spain, R. B. (1989). "Effects of geotextiles on lateral pressure and deformation in highway embankments", *Geotextiles and Geomembranes*, Elsevier Science Ltd., London, U.K., Vol. 8, No. 4, pp. 275-292.

England, G. L. (1994). "The performance and behaviour of biological filter walls as affected by cyclic temperature changes", *Serviceability of Earth Retaining Structures*, R. J. Finno (ed.), American Society of Civil Engineers, New York, N.Y., U.S.A., pp. 57-76.

England, G. L. and Dunstan, T. (1994). "Shakedown solutions for soil containing structures as influenced by cyclic temperatures - integral bridge and biological filter", *Proceedings of the Third International Conference on Structural Engineering*, Singapore.

England, G. L., Dunstan, T., Tsang, C. M., Mihajlovic, N. and Bazaz, J. B. (1995). "Ratcheting flow of granular materials", *Static and Dynamic Properties of Gravelly Soils*, M. D. Evans and R. J. Fragaszy (eds.), American Society of Civil Engineers, New York, N.Y., U.S.A., pp. 64-76.

Fang, Y.-S. and Ishibashi, I. (1985). "Static earth pressures with various wall movements", *Journal of the Geotechnical Engineering Division*, American Society of Civil Engineers, New York, N.Y., U.S.A., Vol. 112, No. 3, pp. 317-333.

"*Foundations and earth structures*" (1982). U. S. Navy Design Manual 7.2, U.S. Government Printing Office, Washington, D.C., U.S.A.

Handy, R. L. (1985). "The arch in soil arching", *Journal of the Geotechnical Engineering Division*, American Society of Civil Engineers, New York, N.Y., U.S.A., Vol. 111, No. 3, pp. 302-318.

Harrop-Williams, K. O. (1989). "Geostatic wall pressures", *Journal of the Geotechnical Engineering Division*, American Society of Civil Engineers, New York, N.Y., U.S.A., Vol. 115, No. 9, pp. 1321-1325.

Horvath, J. S. (1990). "*The use of geosynthetics to reduce lateral earth pressures on rigid walls; phase I: concept evaluation*", Research Report No. CE/GE-90-2, Manhattan College, Civil Engineering Department, Bronx, N.Y., U.S.A.

Horvath, J. S. (1991a). "Using geosynthetics to reduce earth loads on rigid retaining structures", *Proceedings - Geosynthetics '91*, Industrial Fabrics Association International, St. Paul, Minn., U.S.A., pp. 409-424.

Horvath, J. S. (1991b). "Using geosynthetics to reduce surcharge-induced stresses on rigid earth retaining structures", *Transportation Research Record No. 1330*, Transportation Research Board, Washington, D.C., U.S.A., pp. 47-53.

Horvath, J. S. (1995a). "Geoinclusion™: a new, multi-functional geocomposite", *Geotechnical Fabrics Report*, Industrial Fabrics Association International, St. Paul, Minn., U.S.A., Vol. 13, No. 2, pp. 8-9.

Horvath, J. S. (1995b). "*Geofoam geosynthetic*", Horvath Engineering, P.C., Scarsdale, N.Y., U.S.A.

Horvath, J. S. (1996). "The compressible inclusion function of EPS geofoam: an overview", *Proceedings; International Symposium on EPS Construction Method (EPS Tokyo '96)*, EPS Construction Method Development Organization, Tokyo, Japan, pp. 71-81.

Horvath, J. S. (1997). "The compressible inclusion function of EPS geofoam", *Geotextiles and Geomembranes*, Elsevier Science Ltd., London, U.K., Vol. 15, Nos. 1-3, pp. 77-120.

Horvath, J. S. (1998a). "*The compressible-inclusion function of EPS geofoam: an overview of concepts, applications, and products*", Research Report No. CE/GE-98-1, Manhattan College, Civil Engineering Department, Bronx, N.Y., U.S.A.

Horvath, J. S. (1998b). "*The compressible-inclusion function of EPS geofoam: analysis and design methodologies*", Research Report No. CE/GE-98-2, Manhattan College, Civil Engineering Department, Bronx, N.Y., U.S.A.

Humphrey, D. N., Whetten, N., Weaver, J., Recker, K. and Cosgrove, T. A. (1998). "Tire shreds as lightweight fill for embankments and retaining walls", *Recycled Materials in Geotechnical Applications*, C. Viupulanandan and D. J. Elton (eds.), American Society of Civil Engineers, Reston, Va., U.S.A., pp. 51-65.

Inglis, D., Macleod, G., Naesgaard, E. and Zergoun, M. (1996). "Basement wall with seismic earth pressures and novel expanded polystyrene foam buffer layer", *Proceedings of the 10th Annual Symposium*, Vancouver Geotechnical Society, Vancouver, B.C., Canada.

Karpurapu, R. and Bathurst, R. J. (1992). "Numerical investigation of controlled yielding of soil retaining wall structures", *Geotextiles and Geomembranes*, Elsevier Science Publishers Ltd., London, U.K., Vol. 11, No. 2, pp. 115-131.

Koerner, R. M. (1998). "*Designing with geosynthetics*", Prentice Hall, Upper Saddle River, N.J., U.S.A., 4th edition.

McCarthy, D. F. (1988). "*Essentials of soil mechanics and foundations: basic geotechnics*", Prentice Hall, Englewood Cliffs, N. J., U.S.A., 3rd edition, 614 pp.

Monley, G. J. and Wu, J. T. H. (1993). "Tensile reinforcement effects on bridge-approach settlement", *Journal of Geotechnical Engineering*, American Society of Civil Engineers, New York, N.Y., U.S.A., Vol. 119, No. 4, pp. 749-762.

Murphy, G. (1997). "The influence of geofoam creep on the performance of a compressible inclusion", *Geotextiles and Geomembranes*, Elsevier Science Ltd., London, U.K., Vol. 15, Nos. 1-3, pp. 121-131.

Murray, R. T. and Farrar, D. M. (1988). "Temperature distribution in reinforced soil retaining walls", *Geotextiles and Geomembranes*, Elsevier Science Publishers Ltd., London, U.K., Vol. 7, Nos. 1 & 2, pp. 33-50.

Ng, C. W. W., Springman, S. and Norrish, A. R. M. (1998). "Centrifuge modeling of spread-base integral bridge abutments", *Journal of Geotechnical and Geoenvironmental Engineering*, American Society of Civil Engineers, Reston, Va., U.S.A., Vol. 124, No. 5, pp. 376-388.

O'Connor, K. and Taylor, R. N. (1994). "*The swelling pressure of compacted clayey fill*", Project Report 72, Transport Research Laboratory, Crowthorne, Berkshire, U.K.

Partos, A. M. and Kazaniwsky, P. M. (1987). "Geoboard reduces lateral earth pressures", *Proceedings - Geosynthetics '87*, Industrial Fabrics Association International, St. Paul, Minn., U.S.A., pp. 628-639.

Reeves, J. N. and Filz, G. M. (2000). "*Earth force reduction by a synthetic compressible inclusion*", report of research sponsored by GeoTech Systems Corporation and Virginia's Center for Innovative Technology, Virginia Tech, Department of Civil Engineering, Blacksburg, Va., U.S.A., 57 pp.

Reid, R. A., Soupir, S. P. and Schaefer, V. R. (1998a). "Use of fabric reinforced soil walls for integral abutment bridge end treatment", *Proceedings of the Sixth International Conference on Geosynthetics*, R. K. Rowe (ed.), Industrial Fabrics Association International, Roseville, Minn., U.S.A., pp. 573-576.

Reid, R. A., Soupir, S. P. and Schaefer, V. R. (1998b). "Mitigation of void development under bridge approach slabs using rubber tire chips", *Recycled Materials in Geotechnical Applications*, C. Viupulanandan and D. J. Elton (eds.), American Society of Civil Engineers, Reston, Va., U.S.A., pp. 37-50.

Sandford, T. C. and Elgaaly, M. (1993). "Skew effects on backfill pressures at frame bridge abutments", *Transportation Research Record No. 1415*, National Academy Press, Washington, D.C., U.S.A., pp. 1-11.

Segrestin, P. and Jailloux, J.-M. (1988). "Temperature in soils and its effect on the aging of synthetic materials", *Geotextiles and Geomembranes*, Elsevier Science Publishers Ltd., London, U.K., Vol. 7, Nos. 1 & 2, pp. 51-69.

Spangler, M. G. and Handy, R. L. (1982). "*Soil engineering*", Harper & Row, New York, N,Y., U.S.A., 4th edition.

Symons, I. F., Clayton, C. R. I., and Darley, P. (1989). "*Earth pressures against an experimental retaining wall backfilled with heavy clay*", Research Report 192, Transport and Road Research Laboratory, Crowthorne, Berkshire, U.K.

Timoshenko, S. P. and Gere, J. M. (1972). "*Mechanics of materials*", D. Van Nostrand Co., New York, N.Y., U.S.A.

Tscebotarioff, G. P. (1973). "*Foundations, retaining and earth structures*", McGraw-Hill, New York, N.Y., U.S.A., 2nd edition.

Ulrich, E. J. (1991). "Subgrade reaction in mat foundation design", *Concrete International*, American Concrete Institute, Detroit, Mich. U.S.A., April, pp. 41-50.

This page intentionally left blank.

Section 6
Notation

6.1 DEFINITIONS

A_r = cross-sectional area of geosynthetic tensile reinforcement
A_s = cross-sectional area of bridge superstructure or a structural element in general

B = bulk modulus of a solid material
c = Mohr-Coulomb shear-strength parameter (cohesion)

c_a = Mohr-Coulomb shear-strength parameter (adhesion) at interface of dissimilar materials

E_{ci} = Young's modulus of compressible inclusion material or product
E_r = Young's modulus of geosynthetic tensile reinforcement
E_s = Young's modulus of bridge superstructure or a structural material in general
E_{ti} = initial tangent Young's modulus (hyperbolic constitutive model parameter for a solid material)
E_t = tangent Young's modulus (hyperbolic constitutive model parameter for a solid material)

$f_c^{'}$ = unconfined compressive strength of Portland-cement concrete

H = geotechnical height of a bridge abutment or earth retaining structure in general

K = hyperbolic constitutive model parameter for a solid material

K_a = coefficient of lateral earth pressure for the active state
K_b = hyperbolic constitutive model parameter for a solid material
K_h = coefficient of lateral earth pressure (general)
K_{hh} = horizontal component of the coefficient of lateral earth pressure, K_h
K_n = interface constitutive model parameter
K_{ni} = interface constitutive model parameter
K_o = coefficient of lateral earth pressure for the at-rest state
K_{onc} = coefficient of lateral earth pressure at rest, K_o, for the normally consolidated case
K_p = coefficient of lateral earth pressure for the passive state
$K_{s,i}$ = interface constitutive model parameter
K_{si} = interface constitutive model parameter
$K_{s,u}$ = interface constitutive model parameter
K_{su} = interface constitutive model parameter
K_{tn} = interface constitutive model parameter
K_{tsi} = interface constitutive model parameter
K_{tsu} = interface constitutive model parameter

L_o = original length of bridge superstructure or a structural element in general
L_r = embedded length of geosynthetic tensile reinforcement/length of reinforced zone

m = hyperbolic constitutive model parameter for a solid material
n = hyperbolic constitutive model parameter for a solid material

p_{atm} = atmospheric pressure
P_{ah} = horizontal resultant (earth) force, P_h, for the active state
P_h = horizontal resultant (earth) force
$P_h^{'}$ = horizontal resultant (earth) force, P_h, mobilized in ZEP-Wall applications
$P_{h(MAX)}$ = maximum horizontal resultant (earth) force, P_h
P_o^{*} = reference horizontal earth force, P_h, for the normally consolidated at-rest state
P_s = force in a structural element

R_f = hyperbolic constitutive model parameter for a solid material

S = stress level

t_{ci} = thickness of compressible inclusion

X = horizontal axis for the FEM mesh

Y = vertical axis for the FEM mesh

z = depth relative to top of abutment

α = coefficient of thermal expansion of a solid material

β = normalized horizontal resultant (earth) force
β' = normalized horizontal resultant (earth) force, β, mobilized in ZEP-Wall applications
β_a = normalized horizontal resultant (earth) force, β, at the active state

δ = Mohr-Coulomb strength parameter (friction angle) at interface of dissimilar materials
δ_1 = δ at a normal stress of one atmosphere
Δ = horizontal displacement (general)
Δ' = horizontal displacement, Δ, of the compressible inclusion-reinforced soil mass interface in ZEP-Wall applications
Δ_{ci} = horizontal compression of compressible inclusion
Δ_{MSE} = horizontal displacement, Δ, of a reinforced soil mass necessary to fully mobilize reinforcements
Δ_{MSEW} = maximum free-field horizontal displacement, Δ, of a mechanically stabilized earth wall
Δ_s = horizontal displacement of retained soil mass
$(\Delta_s/H)_a$ = minimum normalized horizontal displacement, Δ_s, of soil necessary to achieve the active earth pressure state
Δ_{sa} = minimum horizontal displacement, Δ_s, of retained soil mass necessary to mobilize the active earth pressure state
ΔL = change in length of bridge superstructure or a structural element in general
ΔT = change in temperature of bridge superstructure or a structural element in general
$\Delta \delta$ = change in δ for a ten-fold change in atmospheric pressure
$\Delta \phi$ = change in ϕ for a ten-fold change in atmospheric pressure

ε_h = horizontal strain of compressible inclusion

ϕ = Mohr-Coulomb strength parameter (angle of internal friction; a.k.a. "angle of repose" of soil)
ϕ_1 = ϕ at a confining stress of one atmosphere

γ_t = total unit weight of a material
γ_w = unit weight of water

λ = normalized compressible inclusion stiffness

σ = normal stress (general)
$\overline{\sigma}_h$ = effective horizontal earth stress ("lateral earth pressure")
$\overline{\sigma}_{vo}$ = effective vertical stress under gravity (overburden) conditions
$\overline{\sigma}_n$ = normal effective stress at an interface between dissimilar materials
$\overline{\sigma}_1$ = major principal effective stress
$\overline{\sigma}_3$ = minor principal effective stress
$\left(\overline{\sigma}_1 - \overline{\sigma}_3\right)_f$ = principal effective stress difference (deviatoric stress) at failure

θ = angle of assumed planar interface between EPS-block geofoam lightweight fill and soil

τ = shear stress at interface between dissimilar materials

6.2 CONSTITUTIVE MODEL EQUATIONS

6.2.1 Two-Dimensional Solid Elements

$$E_{ti} = K \cdot p_{atm} \cdot \left(\frac{\overline{\sigma}_3}{p_{atm}}\right)^n \qquad (6.1)$$

$$E_t = E_{ti} \cdot \left\{1 - \left[\frac{R_f \cdot (1 - \sin\phi) \cdot (\overline{\sigma}_1 - \overline{\sigma}_3)}{(2 \cdot c \cdot \cos\phi) + (2 \cdot \overline{\sigma}_3 \cdot \sin\phi)}\right]\right\}^2 \qquad (6.2)$$

$$\phi = \phi_1 - \left[\Delta\phi \cdot \log_{10} \cdot \left(\frac{\overline{\sigma}_3}{p_{atm}}\right)\right] \qquad (6.3)$$

$$B = K_b \cdot p_{atm} \cdot \left(\frac{\overline{\sigma}_3}{p_{atm}}\right)^m \qquad (6.4)$$

6.2.2 One-Dimensional Interface Elements

initial loading/reloading in shear: $\quad K_{si} = K_{s,i} \cdot \gamma_w \cdot \left(\frac{\overline{\sigma}_n}{p_{atm}}\right)^n \qquad$ (6.5a)

$$K_{tsi} = K_{si} \cdot \left\{ 1 - \left[\frac{\left(R_f \cdot \tau \right)}{\left(\overline{\sigma}_n \cdot \tan \delta \right)} \right] \right\}^2 \tag{6.5b}$$

unloading in shear:
$$K_{su} = K_{s,u} \cdot \gamma_w \cdot \left(\frac{\overline{\sigma}_n}{p_{atm}} \right)^n \tag{6.6a}$$

$$K_{tsi} = K_{su} \cdot \left\{ 1 - \left[\frac{\left(R_f \cdot \tau \right)}{\left(\overline{\sigma}_n \cdot \tan \delta \right)} \right] \right\}^2 \tag{6.6b}$$

$$\delta = \delta_1 - \left[\Delta\delta \cdot \log_{10} \cdot \left(\frac{\overline{\sigma}_n}{p_{atm}} \right) \right] \tag{6.7}$$

normal compressive loading:
$$K_{tn} = K_{ni} = K_n \cdot \gamma_w \cdot \left(\frac{\overline{\sigma}_n}{p_{atm}} \right) \tag{6.8}$$

normal tensile loading: K_{tn} is reduced to a small value

Section 7
Bibliography

7.1 MISCELLANEOUS LATERAL EARTH PRESSURE STUDIES

Aytekin, M., Wray, W. K., and Vallabhan, C. V. G., "Transmitted swelling pressures on retaining structures", *Unsaturated Soils*, S. L. Houston and W. K. Wray (eds.), American Society of Civil Engineers, New York, N.Y., U.S.A., 1993, pp. 32-43.

Bathurst, R. J., "Instrumentation of geogrid reinforced soil walls", preprint paper No. 90-0453, Transportation Research Board 69th Annual Meeting, Washington, D.C., U.S.A., January 1990.

Brookes, A. H., Carder, D. R. and Darley, P., "*Earth pressures against an experimental retaining wall backfilled with Lias clay*", TRL Report 152, Transport Research Laboratory, Crowthorne, Berkshire, U.K., 1995.

Carder, D. R., Murray, R. T. and Krawczyk, J. V., "*Earth pressures against an experimental retaining wall backfilled with silty clay*", Laboratory Report 946, Transport and Road Research Laboratory, Crowthorne, Berkshire, U.K., 1980.

Carder, D. R., Pocock, R. G. and Murray, R. T., "*Experimental retaining wall facility - lateral stress measurements with sand backfill*", Laboratory Report 766, Transport and Road Research Laboratory, Crowthorne, Berkshire U.K., 1977.

Clayton, C. R. I., Symons, I. F. and Hiedra-Cobo, J. C., "The pressure of clay backfill against retaining structures", *Canadian Geotechnical Journal*, Vol. 28, No. 2, 1991, pp. 282-297.

Day, R. W., discussion of "Estimating earth pressures due to compaction" by J. M. Duncan, G. W. Williams, A. L. Sehn and R. B. Seed, *Journal of the Geotechnical Engineering Division*, American Society of Civil Engineers, New York, N.Y., U.S.A., Vol. 119, No. 7, 1993, pp. 1162.

Duncan, J. M., Clough, G. W. and Ebeling, R. M., "Behavior and design of gravity earth retaining structures", *Design and Performance of Earth Retaining Structures*, P. C. Lambe and L. A. Hansen (eds.), American Society of Civil Engineers, New York, N.Y., U.S.A., 1990, pp. 251-277.

Duncan, J. M. and Seed, R. B., "Compaction-induced earth pressures under K_o-conditions", *Journal of the Geotechnical Engineering Division*, American Society of Civil Engineers, New York, N.Y., U.S.A., Vol. 112, No. 1, 1986, pp. 1-22.

Duncan, J. M., Williams, G. W., Sehn, A. L. and Seed, R. B., "Estimating earth pressures due to compaction", *Journal of the Geotechnical Engineering Division*, American Society of Civil Engineers, New York, N.Y., U.S.A., Vol. 117, No. 12, 1991, pp. 1833-1847.

Duncan, J. M., Williams, G. W., Sehn, A. L. and Seed, R. B., closure to "Estimating earth pressures due to compaction", *Journal of the Geotechnical Engineering Division*, American Society of Civil Engineers, New York, N.Y., U.S.A., Vol. 119, No. 7, 1993, pp. 1172-1177.

Fang, Y.-S. and Ishibashi, I., "Static earth pressures with various wall movements", *Journal of the Geotechnical Engineering Division*, American Society of Civil Engineers, New York, N.Y., U.S.A., Vol. 112, No. 3, 1985, pp. 317-333.

Filz, G. M. and Duncan, J. M., "*An experimental and analytic study of earth loads on rigid retaining walls*", research report, The Virginia Polytechnic Institute and State University, Department of Civil Engineering, Blacksburg, Va., U.S.A., 1992.

Filz, G. M. and Duncan, J. M., "Earth pressures due to compaction: comparison of theory with laboratory and field behavior", *Transportation Research Record No. 1526*, Transportation Research Board, Washington, D.C., U.S.A., 1996, pp. 28-37.

Ghaly, A., discussion of "Estimating earth pressures due to compaction" by J. M. Duncan, G. W. Williams, A. L. Sehn and R. B. Seed, *Journal of the Geotechnical Engineering Division*, American Society of Civil Engineers, New York, N.Y., U.S.A., Vol. 119, No. 7, 1993, pp. 1162-1165.

Handy, R. L., "The arch in soil arching", *Journal of the Geotechnical Engineering Division*, American Society of Civil Engineers, New York, N.Y., U.S.A., Vol. 111, No. 3, 1985, pp. 302-318.

Harrop-Williams, K. O., "Geostatic wall pressures", *Journal of the Geotechnical Engineering Division*, American Society of Civil Engineers, New York, N.Y., U.S.A., Vol. 115, No. 9, 1989, pp. 1321-1325.

Ishihara, K. and Duncan, J. M., "*At-rest and compaction-induced earth pressures of moist soils*", research report, The Virginia Polytechnic Institute and State University, Department of Civil Engineering, Blacksburg, Va., U.S.A., 1993.

Mesri, G. and Hayat, T. M., discussion of "Estimating earth pressures due to compaction" by J. M. Duncan, G. W. Williams, A. L. Sehn and R. B. Seed, *Journal of the Geotechnical Engineering Division*, American Society of Civil Engineers, New York, N.Y., U.S.A., Vol. 119, No. 7, 1993, pp. 1165-1168.

Mesri, G., Hayat, T. M. and Shahien, M., discussion of "Estimating earth pressures due to compaction" by J. M. Duncan, G. W. Williams, A. L. Sehn and R. B. Seed, *Journal of the Geotechnical Engineering Division*, American Society of Civil Engineers, New York, N.Y., U.S.A., Vol. 119, No. 7, 1993, pp. 1168-1171.

O'Connor, K. and Taylor, R. N., "*The swelling pressure of compacted clayey fill*", Project Report 72, Transport Research Laboratory, Crowthorne, Berkshire, U.K., 1994.

Peck, R. B., discussion of "Estimating earth pressures due to compaction" by J. M. Duncan, G. W. Williams, A. L. Sehn and R. B. Seed, *Journal of the Geotechnical Engineering Division*, American Society of Civil Engineers, New York, N.Y., U.S.A., Vol. 119, No. 7, 1993, pp. 1171-1172.

Sehn, A. L. and Duncan, J. M., "*Experimental study of earth pressures on retaining structures*", research report, The Virginia Polytechnic Institute and State University, Department of Civil Engineering, Blacksburg, Va., U.S.A., 1990.

Symons, I. F. and Clayton, C. R. I., "Earth pressures on backfilled retaining walls", *Ground Engineering*, Thomas Telford Ltd., London, U.K., April 1992, pp. 26-34.

Symons, I. F., Clayton, C. R. I., and Darley, P., "*Earth pressures against an experimental retaining wall backfilled with heavy clay*", Research Report 192, Transport and Road Research Laboratory, Crowthorne, Berkshire, U.K., 1989.

Yeh, S.-T. and Su, C. K., "*EPS flow fill and structure fill for bridge abutment backfill*", Report No. CDOT-R-SM-95-15, Colorado Department of Transportation, Denver, Colo., U.S.A., 1995, 17 pp.

7.2 GENERAL CONCEPT OF CONTROLLED YIELDING

Ahmad, F., supplemental comments to "Influence of lateral boundary movements on earth pressure" by K. Z. Andrawes, A. McGown and F. Ahmad, *Performance of Reinforced Soil Structures*, A. McGown, K. Yeo, and K. Z. Andrawes (eds.), Thomas Telford Ltd., London, U.K., 1991, p. 381.

Andrawes, K. Z, supplemental comments to "Application of boundary yielding concept to full scale reinforced and unreinforced soil walls" by K. Z. Andrawes, K. H. Loke, K. C. Yeo and R. T. Murray, *Performance of Reinforced Soil Structures*, A. McGown, K. Yeo, and K. Z. Andrawes (eds.), Thomas Telford Ltd., London, U.K., 1991, p. 93.

Andrawes, K. Z., Loke, K. H. and Murray, R. T., "The behaviour of reinforced soil walls constructed by different techniques", *Grouting, Soil Improvement and Geosynthetics*, R. H. Borden, R. D. Holtz, and I. Juran (eds.), American Society of Civil Engineers, New York, N.Y., U.S.A., 1992, pp. 1237-1248.

Andrawes, K. Z., Loke, K. H., Yeo, K. C. and Murray, R. T., "Application of boundary yielding concept to full scale reinforced and unreinforced soil walls", *Performance of Reinforced Soil Structures*, A. McGown, K. Yeo, and K. Z. Andrawes (eds.), Thomas Telford Ltd., London, U.K., 1991, pp. 79-83.

Andrawes, K. Z., McGown, A. and Ahmad, F., "Influence of lateral boundary movements on earth pressure", *Performance of Reinforced Soil Structures*, A. McGown, K. Yeo, and K. Z. Andrawes (eds.), Thomas Telford Ltd., London, U.K., 1991, pp. 359-364.

Andrawes, K. Z., Yeo, K. C. and Loke, K. H., "Behaviour of geogrid reinforced soil walls subjected to lateral boundary yielding", *Retaining Structures*, C. R. I. Clayton (ed.), Thomas Telford Ltd., London, U.K., 1993, pp. 549-558.

McGown, A., Andrawes, K. Z. and Murray, R. T., "Controlled yielding of the lateral boundaries of soil retaining structures", *Geosynthetics for Soil Improvement*, R. D. Holtz (ed.), American Society of Civil Engineers, New York, N.Y., U.S.A., 1988, pp. 193-210.

McGown, A., Murray, R. T. and Andrawes, K. Z., "*Influence of wall yielding on lateral stresses in unreinforced and reinforced fills*", Research Report 113, Transport and Road Research Laboratory, Crowthorne, Berkshire, U.K., 1987.

Murray, R. T. and Farrar, D. M., "*Reduction in lateral forces in retaining walls by controlled yielding*", Project Report 242, Transport Research Laboratory, Crowthorne, Berkshire, U.K., 1997, 30 pp.

7.3 COMPRESSIBLE-INCLUSION APPLICATIONS

Aytekin, M., "Use of geofoam with expansive soil", *Proceedings of the Second International Conference in Civil Engineering on Computer Applications, Research and Practice- ICCE-96*, Vol. 2, University of Bahrain, Bahrain, 1996, pp. 541-546.

Aytekin, M., "Numerical modeling of EPS geofoam used with swelling soil", *Geotextiles and Geomembranes*, Elsevier Science Ltd., London, U.K., Vol. 15, Nos. 1-3, 1997, pp. 133-146.

Ebeling, R. M., Peters, J. F. and Mosher, R. L., "Finite element analysis of slopes with layer reinforcement", *Stability and Performance of Slopes and Embankments-II*, R. B. Seed and R. W. Boulanger (eds.), American Society of Civil Engineers, New York, N.Y., U.S.A., 1992, pp. 1427-1443.

Ebeling, R. M., Peters, J. F. and Mosher, R. L., "The role of non-linear deformation in the design of a reinforced soil berm at Red River u-frame lock no. 1", *International Journal for Numerical and Analytical Methods in Geomechanics*, Vol. 21, 1997, pp. 756-787.

Edgar, T. V., Puckett, J. A. and D'Spain, R. B., "Effects of geotextiles on lateral pressure and deformation in highway embankments", *Geotextiles and Geomembranes*, Elsevier Science Ltd., London, U.K., Vol. 8, No. 4, 1989, pp. 275-292.

Horvath, J. S., "*The use of geosynthetics to reduce lateral earth pressures on rigid walls; phase I: concept evaluation*", Research Report No. CE/GE-90-2, Manhattan College, Civil Engineering Department, Bronx, N.Y., U.S.A., 1990.

Horvath, J. S., "Using geosynthetics to reduce surcharge-induced stresses on rigid earth retaining structures", preprint paper No. 910096, Transportation Research Board 70th Annual Meeting, Washington, D.C., U.S.A., January 1991.

Horvath, J. S., "Using geosynthetics to reduce earth loads on rigid retaining structures", *Proceedings - Geosynthetics '91*, Industrial Fabrics Association International, St. Paul, Minn., U.S.A., 1991, pp. 409-424.

Horvath, J. S., "*Developments in thick-geosynthetics technology: 1991 update*", Research Report No. CE/GE-91-1, Manhattan College, Civil Engineering Department, Bronx, N.Y., U.S.A., 1991.

Horvath, J. S., "Using geosynthetics to reduce surcharge-induced stresses on rigid earth retaining structures", *Transportation Research Record No. 1330*, Transportation Research Board, Washington, D.C., U.S.A., 1991, pp. 47-53.

Horvath, J. S., discussion of "Tensile reinforcement effects on bridge-approach settlement" by G. J. Monley and J. T. H. Wu, *Journal of Geotechnical Engineering*, American Society of Civil Engineers, New York, N.Y., U.S.A., Vol. 121, No. 1, 1995, pp. 93-94.

Horvath, J. S., "*Geofoam geosynthetic*", Horvath Engineering, P.C., Scarsdale, N.Y., U.S.A., 1995.

Horvath, J. S., "The compressible inclusion function of EPS geofoam: an overview", *Proceedings; International Symposium on EPS Construction Method (EPS Tokyo '96)*, EPS Construction Method Development Organization, Tokyo, Japan, 1996, pp. 71-81.

Horvath, J. S., discussion of "Numerical study of parameters influencing the response of flexible retaining walls" by H. H. Vaziri, *Canadian Geotechnical Journal*, Vol. 34, No. 1, 1997, p. 166.

Horvath, J. S., "The compressible inclusion function of EPS geofoam", *Geotextiles and Geomembranes*, Elsevier Science Ltd., London, U.K., Vol. 15, Nos. 1-3, 1997, pp. 77-120.

Horvath, J. S., discussion of "Analyses of active earth pressure against rigid retaining wall subjected to different modes of movement" by H. Matsuzawa and H. Hazarika, *Soils and Foundations*, Japanese Geotechnical Society, Tokyo, Japan, Vol. 37, No. 4, 1997, p. 133.

Horvath, J. S., "*The compressible-inclusion function of EPS geofoam: an overview of concepts, applications, and products*", Research Report No. CE/GE-98-1, Manhattan College, Civil Engineering Department, Bronx, N.Y., U.S.A., 1998.

Horvath, J. S., "*The compressible-inclusion function of EPS geofoam: analysis and design methodologies*", Research Report No. CE/GE-98-2, Manhattan College, Civil Engineering Department, Bronx, N.Y., U.S.A., 1998.

Karpurapu, R. and Bathurst, R. J., "Numerical investigation of controlled yielding of soil retaining wall structures", *Geotextiles and Geomembranes*, Elsevier Science Publishers Ltd., London, U.K., Vol. 11, No. 2, 1992, pp. 115-131.

Monley, G. J. and Wu, J. T. H., "Tensile reinforcement effects on bridge-approach settlement", *Journal of Geotechnical Engineering*, American Society of Civil Engineers, New York, N.Y., U.S.A., Vol. 119, No. 4, 1993, pp. 749-762.

Monley, G. J. and Wu, J. T. H., closure to "Tensile reinforcement effects on bridge-approach settlement", *Journal of Geotechnical Engineering*, American Society of Civil Engineers, New York, N.Y., U.S.A., Vol. 121, No. 1, 1995, pp. 96-97.

Murphy, G., "The influence of geofoam creep on the performance of a compressible inclusion", *Geotextiles and Geomembranes*, Elsevier Science Ltd., London, U.K., Vol. 15, Nos. 1-3, 1997, pp. 121-131.

Partos, A. M. and Kazaniwsky, P. M., "Geoboard reduces lateral earth pressures", *Proceedings - Geosynthetics '87*, Industrial Fabrics Association International, St. Paul, Minn., U.S.A., 1987, pp. 628-639.

Reeves, J. N. and Filz, G. M., "*Earth force reduction by a synthetic compressible inclusion*", report of research sponsored by GeoTech Systems Corporation and Virginia's Center for Innovative Technology, Virginia Tech, Department of Civil Engineering, Blacksburg, Va., U.S.A., January 2000, 57 pp.

Rehnman, S. E. and Broms, B. B., "Lateral pressures on basement wall; results from full-scale tests", *Proceedings of the Fifth European Conference on Soil Mechanics and Foundation Engineering*, 1972, pp. 189-197.

Vaziri, H. H., closure to "Numerical study of parameters influencing the response of flexible retaining walls", *Canadian Geotechnical Journal*, Vol. 34, No. 1, 1997, p. 167.

7.4 INTEGRAL-ABUTMENT BRIDGES

Bellin, J., "Bridge end panels on jointless bridges", Oregon Department of Transportation, Bridge Section, Salem, Ore., 1994, 2 pp.

Broms, B. B. and Ingleson, I., "Earth pressure against the abutments of a rigid frame bridge", *Géotechnique*, Vol. 21, No. 1, 1971, pp. 15-28.

Burke, M. P., "Bridge approach pavements, integral bridges, and cycle-control joints", *Transportation Research Record No. 1113*, Transportation Research Board, Washington, D.C., U.S.A., 1987, pp. 54-65.

Burke, M. P., "Integral bridges", *Transportation Research Record No. 1275*, Transportation Research Board, Washington, D.C., U.S.A., 1990, pp. 53-61.

Burke, M. P., "Semi-integral bridge: a concept whose time has come?", *Proceedings of the Henderson Colloquium - Towards Joint-Free Bridge Decks*, International Association for Bridge and Structural Engineering, Pembroke College of Cambridge University, Cambridge, U.K., 1993.

Burke, M. P., "Integral bridges: attributes and limitations", *Transportation Research Record No. 1393*, Transportation Research Board, Washington, D.C., U.S.A., 1993, pp. 1-8.

Cabrera, F. M. Y., "Italian joint free bridge decks", *Proceedings of the Henderson Colloquium - Towards Joint-Free Bridge Decks*, International Association for Bridge and Structural Engineering, Pembroke College of Cambridge University, Cambridge, U.K., 1993.

Card, G. B. and Carder, D. R., "*A literature review of the geotechnical aspects of the design of integral bridge abutments*", Project Report 52, Transport Research Laboratory, Crowthorne, Berkshire, U.K., 1993.

Carder, D. R. and Card, G. B., "*Innovative structural backfills to integral bridge abutments*", Project Report 290, Transport Research Laboratory, Crowthorne, Berkshire, U.K., 1997.

Darley, P. and Carder, D. R., "*Consultation document on suitability tests for stress absorbing layers behind integral bridge abutments*", Project Report 328, Transport Research Laboratory, Crowthorne, Berkshire, U.K., 1998.

Darley, P., Carder, D. R. and Alderman, G. H., "*Seasonal thermal effects on the shallow abutment of an integral bridge in Glasgow*", Project Report 178, Transport Research Laboratory, Crowthorne, Berkshire, U.K., 1995.

Darley, P., Carder, D. R. and Barker, K. J., "*Seasonal thermal effects over three years on the shallow abutment of an integral bridge in Glasgow*", Project Report 344, Transport Research Laboratory, Crowthorne, Berkshire, U.K., 1998, 22 pp.

Emerson, M., "*Bridge temperatures estimated from the shade temperature*", TRRL Report 696, Transport and Road Research Laboratory, Crowthorne, Berkshire, U.K., 1976.

England, G. L., "The performance and behaviour of biological filter walls as affected by cyclic temperature changes", *Serviceability of Earth Retaining Structures*, R. J. Finno (ed.), American Society of Civil Engineers, New York, N.Y., U.S.A., 1994, pp. 57-76.

England, G. L. and Dunstan, T., "Shakedown solutions for soil containing structures as influenced by cyclic temperatures - integral bridge and biological filter", *Proceedings of the Third International Conference on Structural Engineering*, Singapore, 1994.

England, G. L., Dunstan, T., Tsang, C. M., Mihajlovic, N. and Bazaz, J. B., "Ratcheting flow of granular materials", *Static and Dynamic Properties of Gravelly Soils*, M. D. Evans and R. J. Fragaszy (eds.), American Society of Civil Engineers, New York, N.Y., U.S.A., 1995, pp. 64-76.

Greimann, L. F., Abendroth, R. E., Johnson, D. E. and Ebner, P. B., "Pile design and tests for integral abutment bridges", report to Iowa Department of Transportation Project HR-273, Iowa Department of Transportation, Ames, Ia., U.S.A., 1987, 302 pp.

Hambly, E. C., "*Integral bridge abutment details in practice and theory*", Technical Paper PA2138/92, Transport and Road Research Laboratory, Crowthorne, Berkshire, U.K., 1992.

Hearn, G., "*Faulted pavements at bridge abutments*", Colorado Transportation Institute Synthesis, University of Colorado, Boulder, Colo., U.S.A., 1995, 181 pp.

Humphrey, D. N., Whetten, N., Weaver, J., Recker, K. and Cosgrove, T. A., "Tire shreds as lightweight fill for embankments and retaining walls", *Recycled Materials in Geotechnical Applications*, C. Viupulanandan and D. J. Elton (eds.), American Society of Civil Engineers, Reston, Va., U.S.A., 1998, pp. 51-65.

Ng, C. W. W., "*Cyclic loading of a sand behind a spread-base integral bridge abutment*", TRL Data Report IV & V, Transport Research Laboratory, Crowthorne, Berkshire, U.K., 1995.

Ng, C., Springman, S. and Norrish, A., "Soil-structure interaction of spread-base integral bridge abutments", *Soils and Foundations*, Japanese Geotechnical Society, Tokyo, Japan, Vol. 38, No. 1, 1998, pp. 145-162.

Ng, C. W. W., Springman, S. and Norrish, A. R. M., "Centrifuge modeling of spread-base integral bridge abutments", *Journal of Geotechnical and Geoenvironmental Engineering*, American Society of Civil Engineers, Reston, Va., U.S.A., Vol. 124, No. 5, 1998, pp. 376-388.

Norrish, A. R. M., "*Cyclic loading of cohesiveless soil behind bridge abutment*", Ph.D. thesis, Cambridge University, Cambridge, U.K., 1998.

Porter, J. C., Morvant, M. J. and Moon, R. J., "Back to the future for abutment design", *Concrete International*, Vol. 14, June 1992, pp. 29-35.

Reid, R. A., Soupir, S. P. and Schaefer, V. R., "Use of fabric reinforced soil walls for integral abutment bridge end treatment", *Proceedings of the Sixth International Conference on Geosynthetics*, R. K. Rowe (ed.), Industrial Fabrics Association International, Roseville, Minn., U.S.A., 1998, pp. 573-576.

Reid, R. A., Soupir, S. P. and Schaefer, V. R., "Mitigation of void development under bridge approach slabs using rubber tire chips", *Recycled Materials in Geotechnical Applications*, C. Viupulanandan and D. J. Elton (eds.), American Society of Civil Engineers, Reston, Va., U.S.A., 1998, pp. 37-50.

Sandford, T. C. and Elgaaly, M., "Skew effects on backfill pressures at frame bridge abutments", *Transportation Research Record No. 1415*, National Academy Press, Washington, D.C., U.S.A., 1993, pp. 1-11.

Schaefer, V. R. and Koch, J. C., "Void development under bridge approaches", Report No. SD90-03, South Dakota Department of Transportation, Pierre, S.D., U.S.A., 1992, 147 pp.

Springman, S. M., Norrish, A. R. M. and Ng, C. W. W., "*Cyclic loading of sand behind integral bridge abutments*", Project Report 146, Transport Research Laboratory, Crowthorne, Berkshire, U.K., 1996.

Wasserman, E. P., "Jointless bridges", *Engineering Journal*, Vol. 24, No. 3, 1987, pp. 93-100.

Appendix A
Reduced Earth Pressure (REP) Wall Analysis: Version 2.0

A.1 BACKGROUND

As discussed in Section 3.3.3.3, a simplified analytical model was developed for solving the REP-Wall problem where a compressible inclusion (not limited to geofoam) is placed between a rigid, non-yielding earth retaining structure and its retained soil. The conceptual basis for this model involves using the maximum lateral earth pressure. Version 1.0 of this model was first developed by Partos and Kazaniwsky (1987) based on the normally consolidated at-rest earth pressure at the base of the structure and culminated with author's Version 1.2 suggested in this present study based on the active state at a depth of three-quarters of the geotechnical height of the structure.

Although Version 1.2 produced results that were in good agreement with the numerical results of the present study (see Table 3.5), an alternative conceptual basis for deriving a model was felt to be desirable. This alternative basis, referred to as Version 2.0, involves using the horizontal resultant earth force or, more specifically, the normalized horizontal resultant earth force, β, instead of lateral earth pressure. The reason for preferring this alternative was to provide a model whose conceptual basis was the same as that for the simplified analytical model for the ZEP-Wall problem that was developed in Section 3.3.3.10. It was felt to be better for both the long-term development of simplified analytical models for REP- and ZEP-Wall problems as well as end-user understanding of such models to have a unified conceptual basis for model development.

A.2 MODEL DERIVATION

A.2.1 Concept

The model concept for Version 2.0 of the simplified analytical method for the REP-Wall problem is basically the same as that shown in Figure 3.42 for the ZEP-Wall problem with the obvious difference that the retained soil is unreinforced. As a result, the spring stiffnesses for the REP-Wall problem as shown in Figure A.1 have a very different qualitative relationship than those for the ZEP-Wall problem (see Figure 3.43). Most importantly, this means there is a unique solution to the REP-Wall problem, i.e. a single value of compressible inclusion thickness, t_{ci}, that is required to achieve the minimum lateral pressure (assumed to be the horizontal component of the active earth pressure state). The required value of t_{ci} is obtained by equating the equivalent model spring stiffnesses of the compressible inclusion and soil at the desired solution point of $\beta = \beta_a$ and $\Delta = \Delta_a$ which correspond to the active state. This is developed in the following section.

Note that the existence of a unique solution to the REP-Wall problem is significantly different than for the ZEP-Wall problem where there is no unique solution. As can be seen in Figure 3.43, there are, theoretically, an infinite number of combinations of compressible inclusion thickness and reinforcement stiffness that could be chosen to produce a normalized horizontal resultant force, β, between one and zero. Note also that it is theoretically impossible to achieve a condition of no horizontal force ($\beta = 0$) in reality as there is no perfectly compressible inclusion nor infinitely rigid reinforcement. However, it is possible to achieve a value of β that is very close to zero for all practical purposes using realistic combinations of compressible-inclusion and reinforcement stiffness (Horvath 1991a).
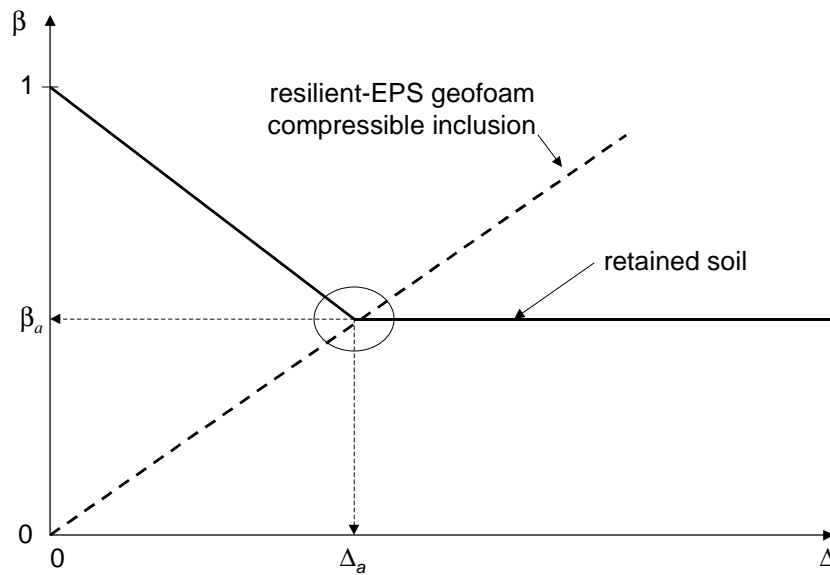
Figure A.1. Approximate REP-Wall Analysis Method: Spring Stiffnesses

A.2.2 Theory

A.2.2.1 Compressible-Inclusion Stiffness. Assuming one-dimensional compression conditions exist within the compressible inclusion (reasonable for most materials used for this purpose)

$$\overline{\sigma}_h = E_{ci} \cdot \varepsilon_h \tag{A.1}$$

where

    E_{ci} = Young's modulus of the compressible-inclusion material,
    ε_h = horizontal normal strain of the compressible inclusion and
    $\overline{\sigma}_h$ = horizontal normal stress within the compressible inclusion.

Based on the results presented in Section 3.3.3.2 and Figure 3.24 in particular, the average strain within the compressible inclusion is assumed to be two-thirds of the maximum value. Therefore, ε_h in Equation A.1 is taken to be

$$\varepsilon_h = \frac{2 \cdot \Delta_{ci}}{3 \cdot t_{ci}} \tag{A.2}$$

where

    t_{ci} = thickness of the compressible inclusion and
    Δ_{ci} = horizontal compression of the compressible inclusion.

Combining equations A.1 and A.2 produces the average stress within the compressible inclusion:

$$\sigma_h = \frac{2 \cdot E_{ci} \cdot \Delta_{ci}}{3 \cdot t_{ci}} \tag{A.3}$$

The horizontal resultant force, P_h, is

$$P_h = \sigma_h \cdot H = \frac{2 \cdot E_{ci} \cdot \Delta_{ci} \cdot H}{3 \cdot t_{ci}} \tag{A.4}$$

The normalized horizontal resultant force, β, is

$$\beta = \frac{P_h}{P_o^*} = \frac{2 \cdot E_{ci} \cdot \Delta_{ci} \cdot H}{3 \cdot t_{ci} \cdot P_o^*} \tag{A.5}$$

The special case of Equation A.5 for the normalized horizontal resultant force, β_a, at the active state ($\Delta_{ci} = \Delta_a$) is

$$\beta_a = \frac{2 \cdot E_{ci} \cdot \Delta_a \cdot H}{3 \cdot t_{ci} \cdot P_o^*} \tag{A.6}$$

A.2.2.2 Soil Stiffness. Referring to Figure A.1, the equation of the line that is assumed to define the soil behavior between $\beta = 1$ and $\beta = \beta_a$ is

$$\beta = \frac{P_h}{P_o^*} = \left[1 - \left(\frac{\Delta_s}{\Delta_a} \right) \right] + \left[\beta \cdot \left(\frac{\Delta_s}{\Delta_a} \right) \right] \tag{A.7}$$

where Δ_s = horizontal displacement of the retained soil.
  But

$$\beta_a = \frac{P_{ah}}{P_o^*} \tag{A.8}$$

where P_{ah} = horizontal component of the active earth pressure force. Using the classical triangular distribution of the active earth pressure shown in Figure 3.6 and used throughout this report

$$P_{ah} = 0.5 \cdot K_a \cdot \cos \delta \cdot \gamma_t \cdot H^2 \tag{A.9}$$

where
  H = the geotechnical height of the earth retaining structure,
  K_a = the coefficient of active earth pressure from either Coulomb or exact theory,
  δ = the soil-compressible inclusion interface friction angle and
  γ_t = total unit weight of the retained soil.

Combining equations A.7 through A.9 yields

$$\beta = \left(1 - \frac{\Delta_s}{\Delta_a}\right) + \left[\left(\frac{0.5 \cdot K_a \cdot \cos\delta \cdot \gamma_t \cdot H^2}{P_o^*}\right) \cdot \left(\frac{\Delta_s}{\Delta_a}\right)\right] \qquad \textbf{(A.10)}$$

The special case of Equation A.10 for the normalized horizontal resultant force, β_a, at the active state ($\Delta_s = \Delta_a$) is

$$\beta_a = \left(\frac{0.5 \cdot K_a \cdot \cos\delta \cdot \gamma_t \cdot H^2}{P_o^*}\right) \qquad \textbf{(A.11)}$$

A.2.2.3 Solution. The solution is obtained by equating equations A.6 and A.11 which produces

$$\frac{2 \cdot E_{ci} \cdot \Delta_a \cdot H}{3 \cdot t_{ci} \cdot P_o^*} = \frac{0.5 \cdot K_a \cdot \cos\delta \cdot \gamma_t \cdot H^2}{P_o^*} \qquad \textbf{(A.12)}$$

Recognizing that

$$\Delta_a = \left(\Delta_s / H\right)_a \cdot H \qquad \textbf{(A.13)}$$

where $(\Delta_s/H)_a$ is the minimum normalized horizontal displacement of the soil mass necessary to mobilize the active earth pressure state, then simplifying and rearranging to solve for the required thickness of the compressible inclusion, t_{ci}, yields the desired final result:

$$t_{ci} = \frac{E_{ci} \cdot \left(\Delta_s / H\right)_a}{0.75 \cdot K_a \cdot \cos\delta \cdot \gamma_t} \qquad \textbf{(A.14)}$$

Note that Equation A.14 is the same as Equation 3.11 for Version 1.2 of the simplified REP-Wall analysis method.